CHAPTER III

RESULTS AND DTSCUSSION

3. Electrochemical Characterization of AOT and C_{18}DMB Micelles and Microemulsion Systems.

This section presents some results from the electrochemical measurements to provide some information about micelles and the structure of microemulsions containing octadecyldimethyl betaine (C_{18}DMB) and bis (2-ethylhexyl) sulfosuccinate (AOT). C_{18}DMB and AOT were used as model zwitterionic and nonionic surfactants, respectively. The microemulsions formulated from these two surfactant types will be used as media for electrochemical reactions investigations in the next section. Before the degression into the details of the electrochemical experiments, there are some requirements for a suitable probe, which is the key to the success of any electrochemical characterization. The requirements for a suitable probe are:

1- Electroactive.

2- Reversible behaviour.

3- Hydrophobic in nature, i.e, very low solubility in the aqueous external phase.

4- The half-wave potential within the potential range allowed in the microemulsion medium or not too positive or too negative preferably between 400 mV to -200 mV.

5- Negligible or no adsorption on the electrode surface.

6- No effect on the chemical properties of the surfactant solution.

The probe that was found to be most suitable for this research is ferrocene (Fc). Other probes which were tested include vinglferrocene, methyl viologen and tetrathiafulvalene (TTF). But ferrocene was found most efficient.

3.1 Electrochemical Characterization of AOT Micelles

3.1.1 Voltammetric Detection of Micelles

The electrochemical techniques are successfully used for the determinations of the critical micelles concentration (CMC) of anionic surfactant AOT as well as solublization studies. Three different electro-chemical techniques were used. Such techniques used are cyclic voltammetry (CV), rotating disk voltammetry (RDV) and chronocoulametry (CC).

A. Cyclic voltammetry (CV)

Cyclic voltammetric behaviour of $7x10^{-5}$ M of ferrocene as hydrophobic probe was recorded in anionic AOT surfactant of different concentrations containing indifferent amounts of supporting electrolyte, 0.1 M NaCl. The surfactant concentration was varied from $1x10^{-4}$ to $2x10^{-3}$ M. The voltammograms were recorded in the potential window from 0.0 to 500 mV versus SCE at different potential sweep rates varying from 20 to 500 mV/sec. The voltammograms obtained showed one anodic and one cathodic peaks on the anodic and cathodic sweeps as represented in Fig. (1). The anodic peak current, $I_{p,a}$ and the cathodic peak current, $I_{p,c}$ are almost of equal heights and the ratio of $I_{p,a}/I_{p,c}$ does not exceed 1.076 at different sweeps in all media, Table (4). The peak potential separation $\Delta E_p = (E_{p,a} - E_{p,c})$ is almost around the theoretical value for one-electron transfer in AOT micelles (56-62 mV). These results indicate that the electrochemical oxidation of ferrocene (Fc) is a reversible one electron transfer process forming ferrocenium ion as Following

$$Fe \quad \Leftrightarrow \quad Fc^{+} + e$$

The voltammograms recorded at different sweep rates are essentially similar and showed one reversible peak.

On using Randless-Sevcik equation [140] which has given as following:

$$I_p = 0.4463\ (n^{3/2} F^{3/2})\ (R^{1/2} T^{1/2})\ D^{1/2} AC\upsilon^{1/2} \qquad \text{(III.1)}$$

The plots of anodic peak current ($I_{p,a}$) versus square root of sweep rate ($\upsilon^{1/2}$) gives straight lines intersecting the origin at all surfactant concentrations, Fig. (2). These results indicate that the electrode process is diffusion controlled [117].

The plots of $I_{p,a}$ versus surfactant concentration showed linear correlation consisting of two segments, Fig (3a). The CMC of AOT is determined at the point at which the breaks occur. At CMC the solution changes from surfactant solution (true solution) to aggregates (micelles). The CMC was obtained at 5.05×10^{-4} M of AOT in 0.1 M NaCl at 25°C.

The CMC was further confirmed from the plots of the peak potential shift $E_{p,a}$ versus surfactant concentration, where variations are attributed to structural changes, Fig. (3b).

B- Rotating disk voltammetry (RDV)

On using the RDV method, a known concentration of the electroactive probe was added to a series of the monomeric surfactant solution, AOT, containing indifferent supporting electrolyte, 0.1 M NaCl. The surfactant concentration was varied in the range from 1×10^{-4} to 1×10^{-3} M, Fig. (4). The effect of rotation speed on the voltammograms of 7×10^{-5} M electroactive ferrocene was recorded at rotation speeds 250, 500, 750,1000,1250,1500 and 2000 RPM in such surfactant solutions. The scan rate used was 5 mV/sec in these experiments at all rotation speeds. The limiting current (i_l) measured from the current-potential response at the steady state was found to be linearly increased on increasing the rotation speed. Fig. (5) showed that, on increasing the surfactant concentration, the limiting current is slightly decreased up to a concentration 6×10^{-4} M followed by sharp decrease.

The decreasing behaviour of the limiting diffusion current in rotating disk experiments by increasing surfactant concentration is not attributed to surfactant adsorption, because chronocoulometry showed that there is a negligible adsorption at all surfactant concentrations. Therefore, this can be only attributed to structural changes of surfactant and a transition from true surfactant solution to aggregates (micelles).

On using Levich equation [133]:

$$i_l = 0.62nFACD_l^{2/3}\nu^{-1/6}\,\omega^{1/2} \qquad \text{(III.2)}$$

where i_l is the limiting diffusion current (amp), n is the number of electrons transferred, F is the faraday's constant, A is the area of the electrode, C is the concentration of the electroactive probe (moles), ν is the kinematic viscosity of the solution, cm^2/sec and ω is the angular velocity (rad s^{-1}). The plots of i_l versus $\omega^{1/2}$ for the electrochemical oxidation of ferrocene at different AOT concentrations give linear correlations passing through the origin, confirming the diffusion nature of the electrochemical reactions Fig. (5). The slope values were used to estimate the apparent diffusion coefficient.

On increasing the rotation speed (ω), the half wave potential ($E_{1/2}$) of the rotating disk voltammograms was held constant indicating the reversibility of ferrocene oxidations. Furthermore, on using the following relationship [117].

$$E = E_{1/2} + \frac{RT}{nF} \ln (i_l - i)/i \qquad \text{(III.3)}$$

The logarithmic analysis of the rotating disk voltammograms were used for testing the thermodynamic reversibility. On plotting $\log[i/(i_l - i)]$ versus E at rotation speed 1000 RPM a straight line of slope amounting to 0.053 is obtained which corresponds to a one electron transfer process as shown in Fig.(6).

The corresponding micellar sizes were calculated from the diffusion coefficient values using the Stokes-Einstein equation [151] which states that:

$$D = KT/6\pi\eta R_h \qquad \text{(III.4)}$$

where D is the diffusion coefficient in cm^2/sec, K is the Boltzman constant in erg/K, η is the viscosity coefficient of the continuous medium in centipoise (cp), and R_h is the radius of micelle droplet in cm, and since the electroactive probe is distributed between the continuous aqueous phase and micelles, the Levich equation (III.2) may be written in the pseudophase approximation as:

$$i_l = 0.62\, nFA\{D^{2/3}(C_1 - C_2) + D_2^{2/3} C_2\}\, \nu^{-1/6}\, \omega^{1/2} \qquad \text{(III.5)}$$

where C_1 and D_1 are the total concentration of the probe and aqueous phase diffusion coefficient, respectively; C_2 is the concentration (relative to the total volume) of the probe in the micelles and D_2 is the micelle diffusion coefficient.

At Kinematic viscosities common to moderately dilute equeous solutions, the root-angular velocity dependence of the Levich-equation allows to extract a slope

$$S_0 = \partial i_l/\partial\omega^{1/2} = i_l/\omega^{1/2} \qquad \text{(III.6)}$$

The analogous quantity derived from equation (III.5) when divided by equation (III.6) gives

$$S/S_o = [(C_1 - C_2)/C_1 + (D_2/D_1)^{2/3}(C_2/C_1)]x\,(\nu/\nu_o)^{-1/6} \qquad \text{(III.7)}$$

The slope of the i_l versus $\omega^{1/2}$ of ferrocone in aqueous solution containing 0.1M NaCl is considered as (S_0). On plotting the ratio of slopes (S/So) against the logarithm of surfactant concentration, an S-shapped curve was obtained as shown in Fig.(7). The use of the ratio of slope in rotating disk method provides an exact method of determining the critical micelle concentration by avoiding the fluctuation in the probe concentration, the inflection point on the curve indicated the critical micelle concentration (CMC) and it was found to equal 5.05×10^{-4} M which was found in a good agreement with those obtained from CV experiments.

3.1.2 Solubility of Ferrocene in AOT Micelles

The rotating disk voltammetry experiments were used to determine the diffusion coefficients of AOT micelles in 0.1M NaCl solution, in the range from 6×10^{-4} to 1×10^{-2} M of surfactant, by using ferrocene as the hydrophobic electroactive probe, Fig. (8). The concentrations of ferrocene used were very close to the saturation concentration in each micellar solution. The amount of ferrocene solubilized in AOT micelles were determined via spectrophotometric technique. The spectral measurements were performed in the UV-visible range at wavelengths λ = 350 and 440 nm using Perkin Elmer Spectrophotometry model JASCO V-530. The absorbance values (measured at λ = 440 nm) obtained for ferrocene solubilized at different surfactant concentrations were compared with the calibration graph of ferrocene in pure ethanol, Fig. (9a,9b). Using Beer's-lambet law which states that:

$$A = \epsilon b C \qquad \text{(III.8)}$$

where A is absorbance, ϵ is molar extinction coefficient, b is bath length (=1cm) and c is the molar concentration. The concentration of ferrocene solubilized surfactant was determined at ϵ = 92.3 and listed in Table (5).

Under these conditions, ferrocene was also present in the aqueous phase and was assumed to be present to the extent of its solubility in the electrolyte 0.1 M NaCl. The solubility and the diffusion coefficient of ferrocene in 0.1 M NaCl are $5x10^{-5}$ M and $6.7x10^{-6}$ cm^2 respectively [34]. This diffusion coefficient is an order of magnitude higher than the diffusion coefficients of micelles. The diffusion coefficients obtained directly from the experiment represent apparent values. These apparent diffusion coefficients of ferrocene are sum of diffusion coefficients of ferrocene present in the aqueous phase and that present in micelles. So correction can be made to obtain a better estimate of the actual micelle diffusion coefficient by knowing the relative concentrations of probe in the aqueous phase and in the micelles. Fig (10) showed the plots of the limiting currents of ferrocene in AOT micelles against the square root of angular velocity ($\omega^{1/2}$). Straight lines intersecting the origin were obtained. The slopes of these plots were used to estimate the apparent diffusion coefficient values (D_a) using the Levich equation [133]. The redox behaviour of ferrocene as the hydrophobic probe was treated depending on the exit-entrance rate using two methods of treatments slow rate which termed as zero-kinetics and fast-rate.

First, the corrections of these values of diffusion coefficient were made using the procedure and the zero-kinetics limiting equation [38] developed for partitioning solutes using RDV technique:

$$D_d = [D_a^{2/3} C/C_d - D_c^{2/3} C_c/C_d]^{3/2} \qquad \text{(III.9)}$$

where C is the total concentration of the probe, C_c is the concentration of the probe in the aqueous (continuous) phase and C_d is diffusion coefficient of probe in the micellar discontinuous pseudophase. D_c is the diffusion coefficient for the probe in the aqueous phase, D_a is the apparent diffusion

coefficient and D_d is the corrected micellar diffusion coefficient. The values of the diffusion coefficients in the discontinuous pseudo-phase (D_d) were calculated at different AOT concentrations using equation (III.9) and listed in Table (5).

Second, the apparent diffusion coefficient (D_a) obtained from Levich equation was corrected using the following equation of fast-kinetics approximation [152], depending on the respective mole fractions in both aqueous and discontinuous phases:

$$D_d = [D_aC/C_d - D_cC_c/C_d] \qquad \text{(III.10)}$$

The D_d values calculated in the fast-kinetics approximation are smaller than the zero-kinetics (slow) values.

The plots of D_a and D_d "obtained by the above two mentioned methods" against the surfactant concentration is represented in Fig. (11). The plots showed that, the diffusion coefficients D_a and D_d were sharply decreased before the critical micelles concentration then becomes nearly constant as the surfactant concentration is increased. Inspection of the values of D_d indicated that the micellar sizes become nearly constant by increasing the surfactant concentration and the morphological features revealed that AOT is spherical in shape and not rod-like.

3.1.3 Effect of salt concentration

The effect of salt concentration on the diffusion coefficient of AOT micellar solutions was studied at 0.10, 0.16, 0.62 and 1.0 M of NaCl, by using 0.5 mM ferrocene as eletroactive probe solubilized in $8x10^{-4}$ M AOT. The cyclic voltammograms were recorded at different scan rates varying from 20 to 500 mV/sec. The cyclic voltammograms obtained at different

concentrations of NaCl indicate decreasing in the peak current on increasing NaCl concentration in miceller solutions as shown in Fig.(12). The increase in NaCl concentration induced a positive shift of the peak potentials as shown from Table (6).

The plots of anodic peak current ($I_{p,a}$) versus square root of sweep rate ($\upsilon^{1/2}$) of AOT micellar solutions for 0.16 M , 0.62 M and 1.0 M NaCl concentrations, were obtained and showed linear correlations passing through the origin, in Fig.(13). On using The Randless-Sevcik equation [140] and the slopes of the linear plots, the diffusion coefficients were estimated. The data listed in Table (7) showed that the micellar diffusion coefficient (D_d) is gradually decreases while the half-wave potential $E_{1/2}$ for the oxidation of ferrocene in micellar solutions increases linearly, Fig. (14).

First, the reason for the decrease in D_d with NaCl concentration is the increase in the solution viscosity with NaCl concentration, the ratio of the solution viscosity to that of pure water at 25°C is obtained as 1.02, 1.06, 1.10 for 0.16 M, 0.62M and 1.0 M NaCl solutions, respectively [153]. Since the diffusion of AOT micelles is simply obeys the Stokes-Einstein equation [151], D_d should be in proportion to the inverse of the solution viscosity. Secondly, the change in $E_{1/2}$ with NaCl concentration is discussed in terms of the thermodynamics of micelles formation.

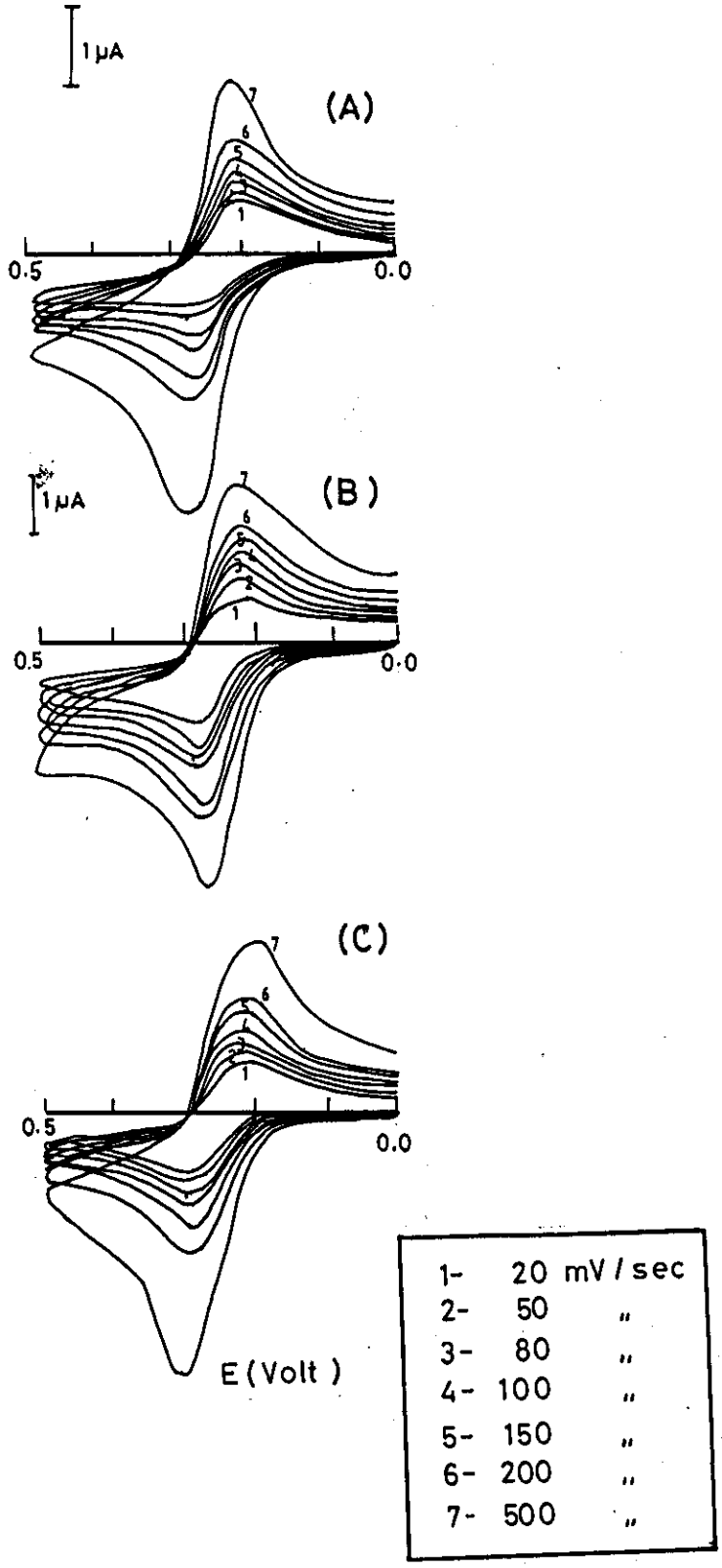

Figure 1: Cyclic volltammograms of $7x10^{-5}$ ferrocene in AOT micellar solutions containing (a) $1x10^{-4}$M AOT, (b) $2x10^{-4}$M AOT, (c) $4x10^{-4}$M AOT, (d) $6x10^{-4}$M AOT, (e) $8x10^{-4}$M AOT, (f) $1x10^{-3}$M AOT and (g) $2x10^{-3}$M AOT, at 25°C. The sweep rates are 20,50,80,100,150,200 and 500 mV/sec.

Follow:

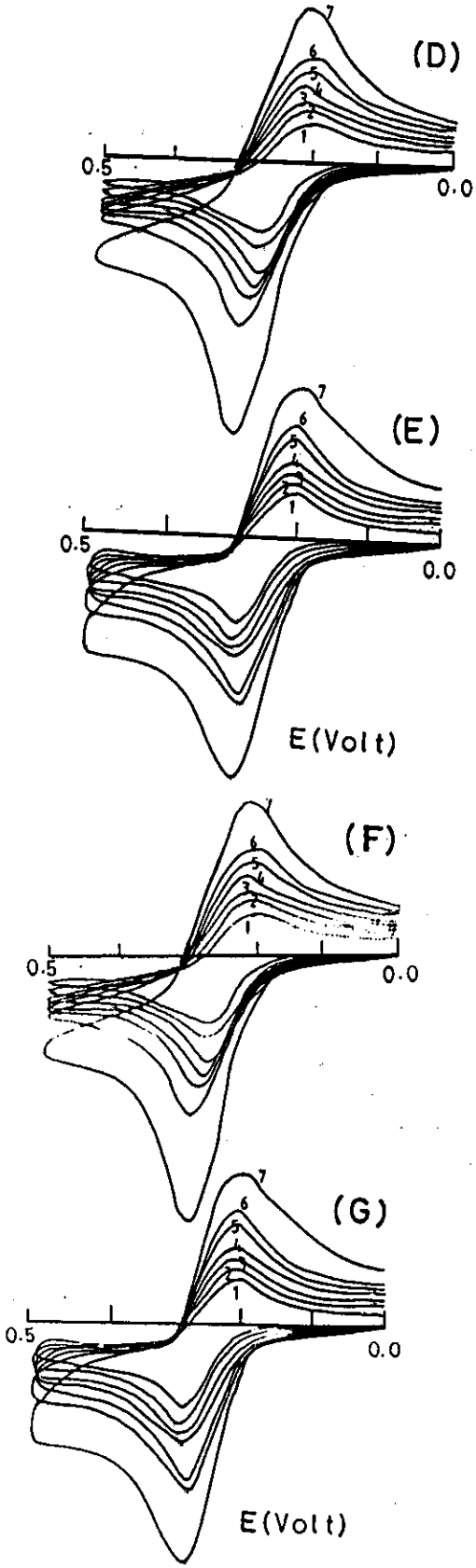

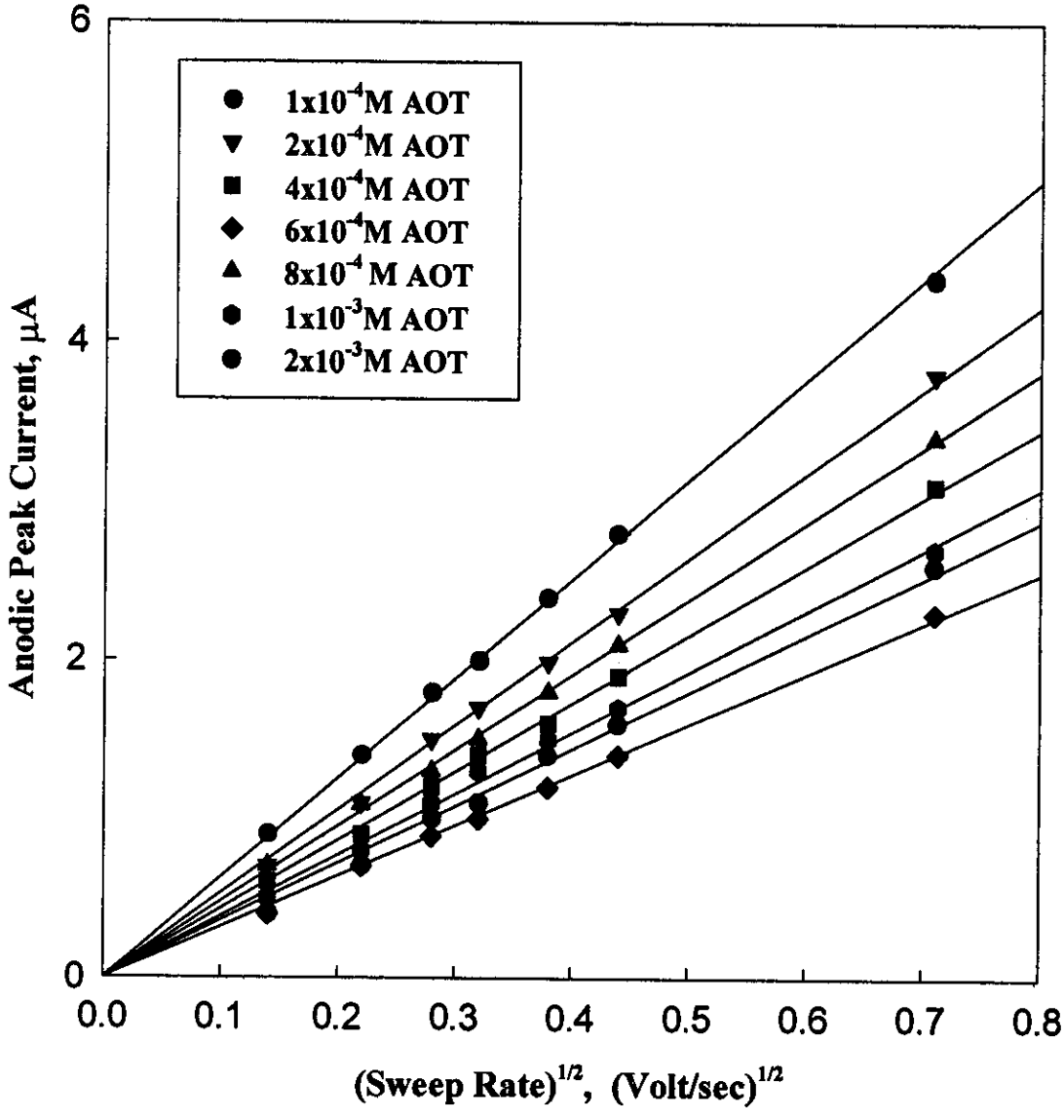

Figure 2: The plots of anodic peak currents versus ($\upsilon^{1/2}$) of $7x10^{-5}$ M ferrocene in AOT micellar solutions at 25°C.

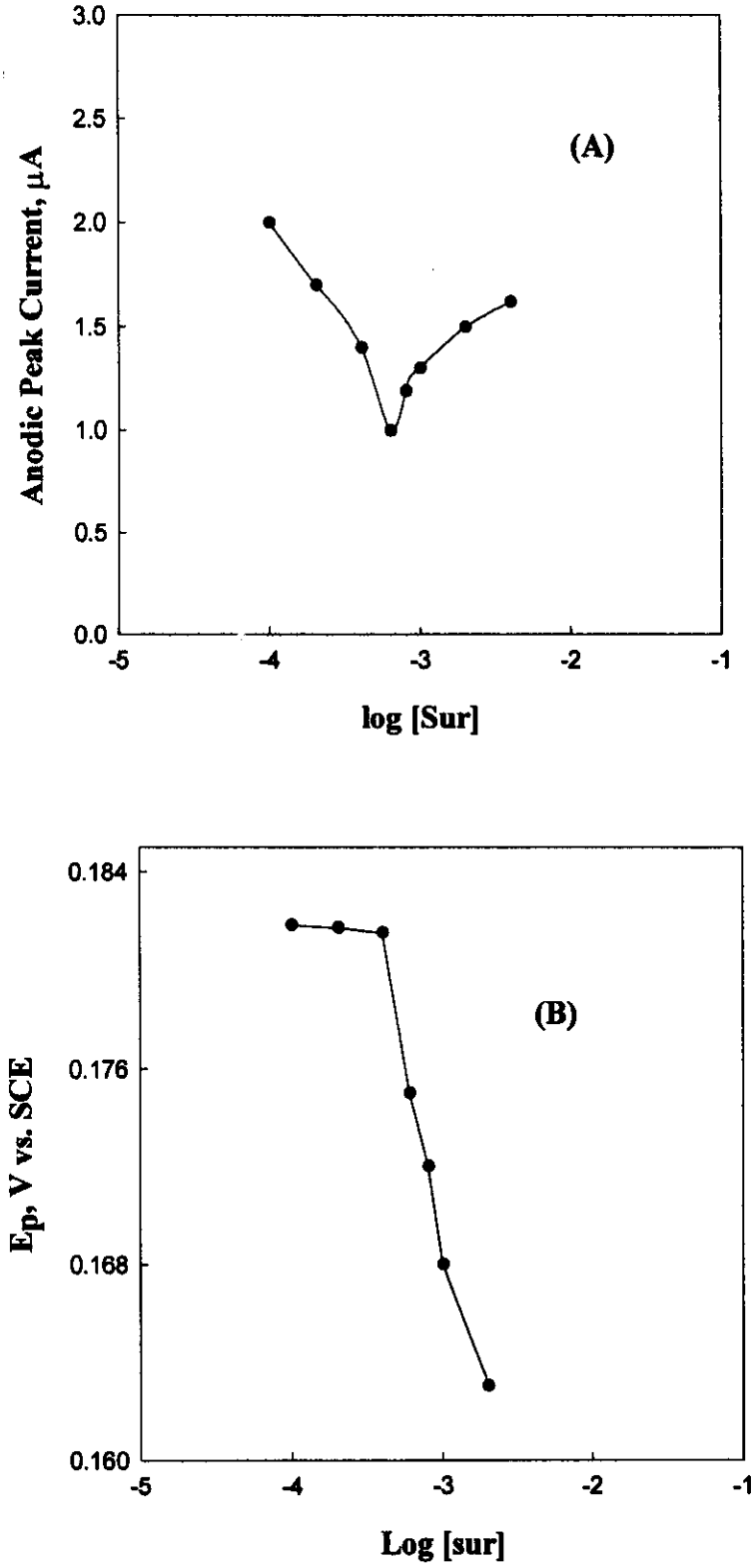

gure 3: The plots of (a) anodic peak currents (b) peak potentials of $7x10^{-5}$ M ferrocene AOT micellar solutions at 100 mV/sec againts the logarithm of surfactant concentration.

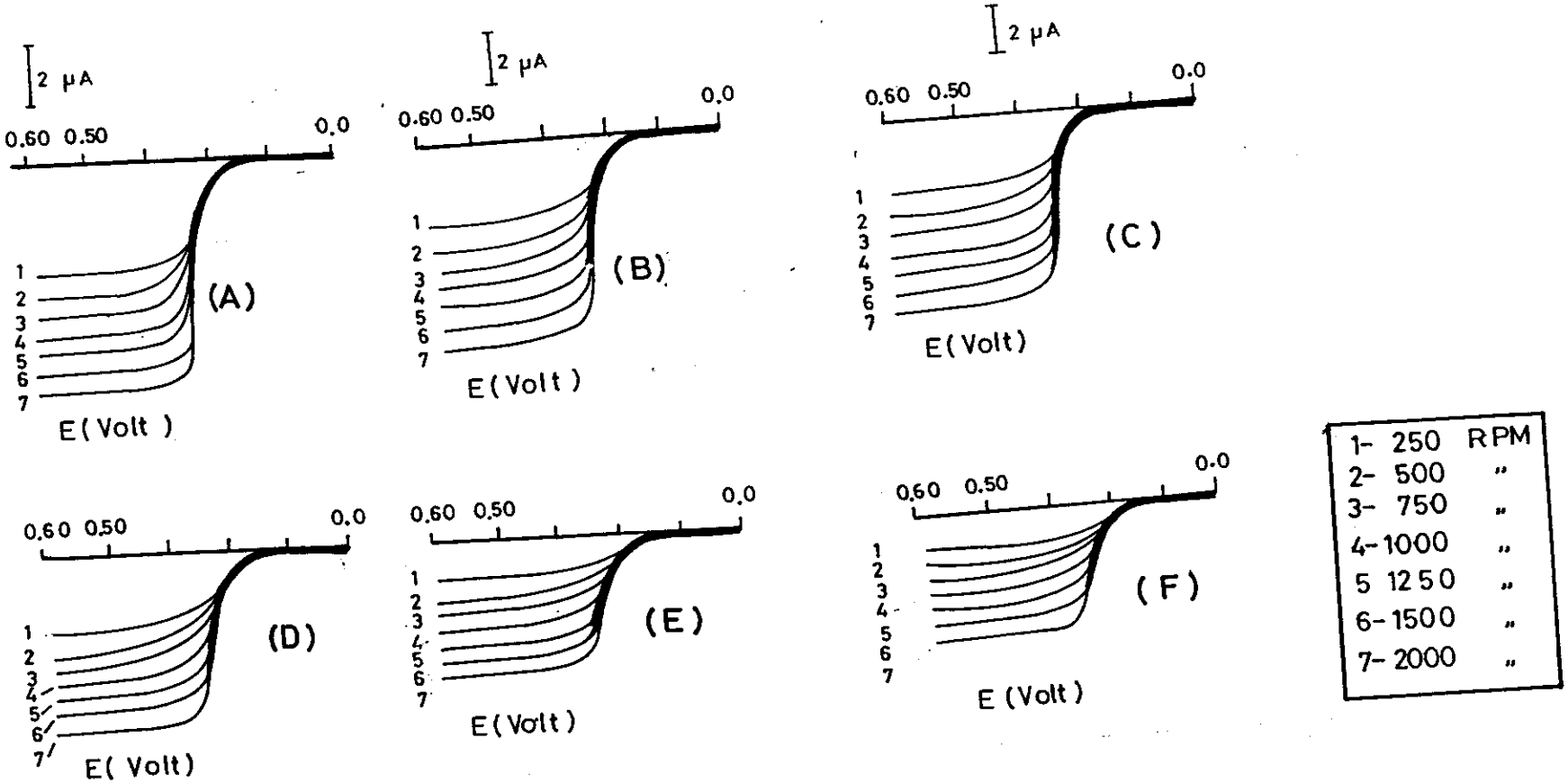

Figure 4: The effect of rotation speed of glassy carbon electrode on the linear sweep voltammograms obtained for $7x10^{-5}$ M ferrocene in AOT micellar solutions containing (a) $1x10^{-4}$ M AOT, (b) $2x10^{-4}$ M AOT, (C) $4x10^{-4}$ M AOT, (d) $6x10^{-4}$ M AOT, (e) $8x10^{-4}$M AOT and (f) $1x10^{-3}$ M AOT. The rotation speed are 250,500,750,1000,1250,1500 and 2000 RPM .

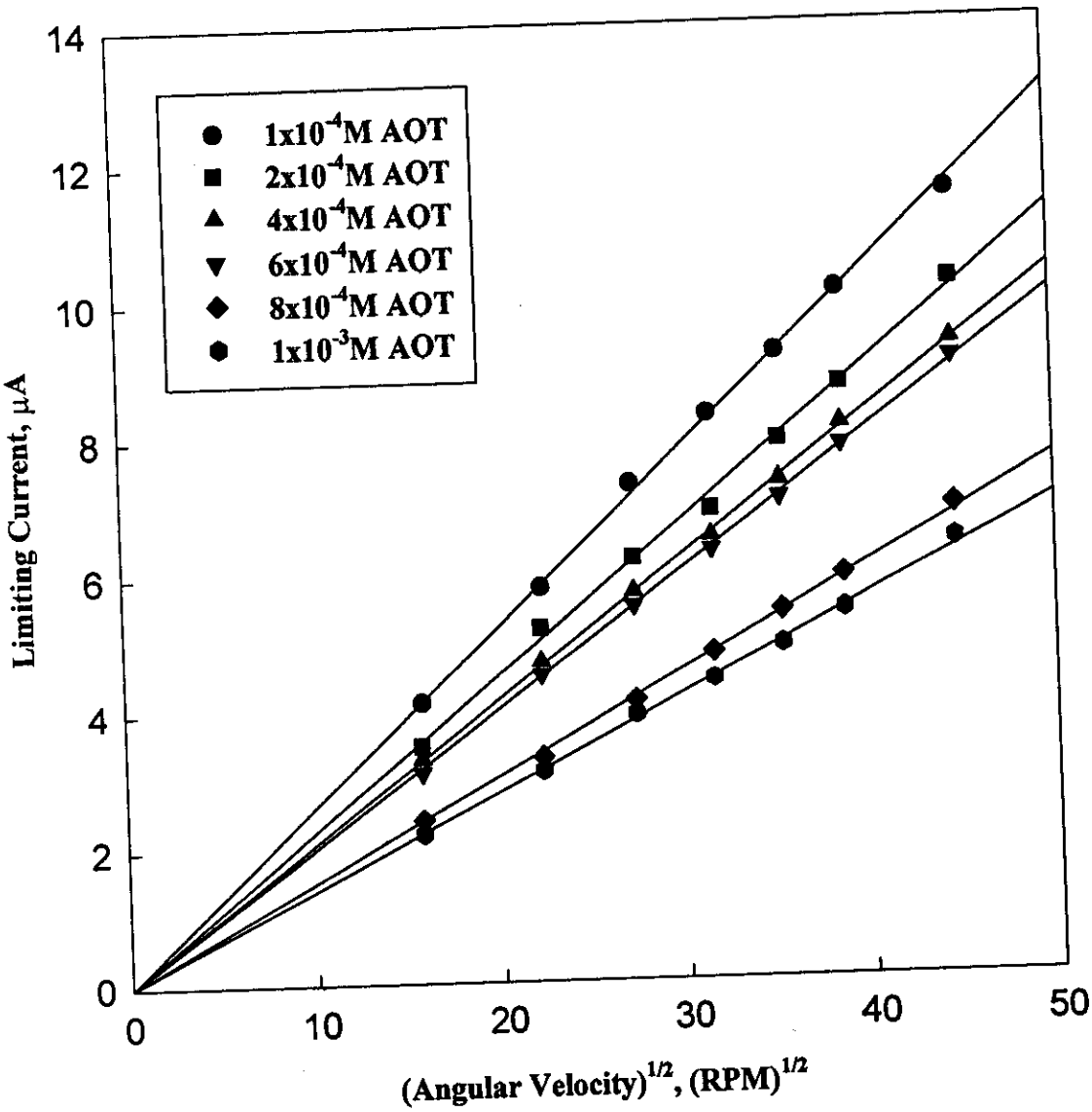

Figure 5: The plots of the limiting current (i_l) versus the square root of angular velocity ($\omega^{1/2}$) for $7x10^{-5}$M ferrocene in AOT micellar solutions.

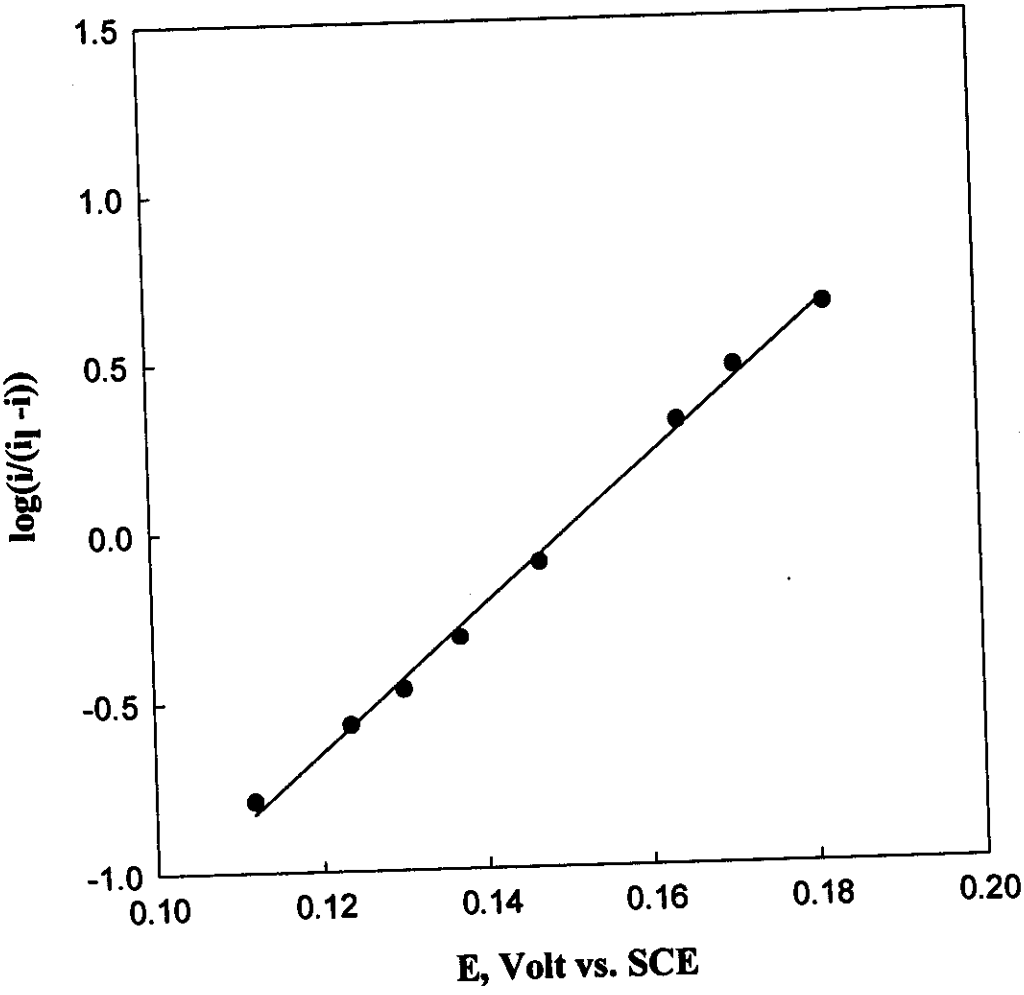

Figure 6: RDV - Logarithmic analysis of $7x10^{-5}$ M ferrocene in $8x10^{-4}$ M AOT micellar solution at 1000 RPM.

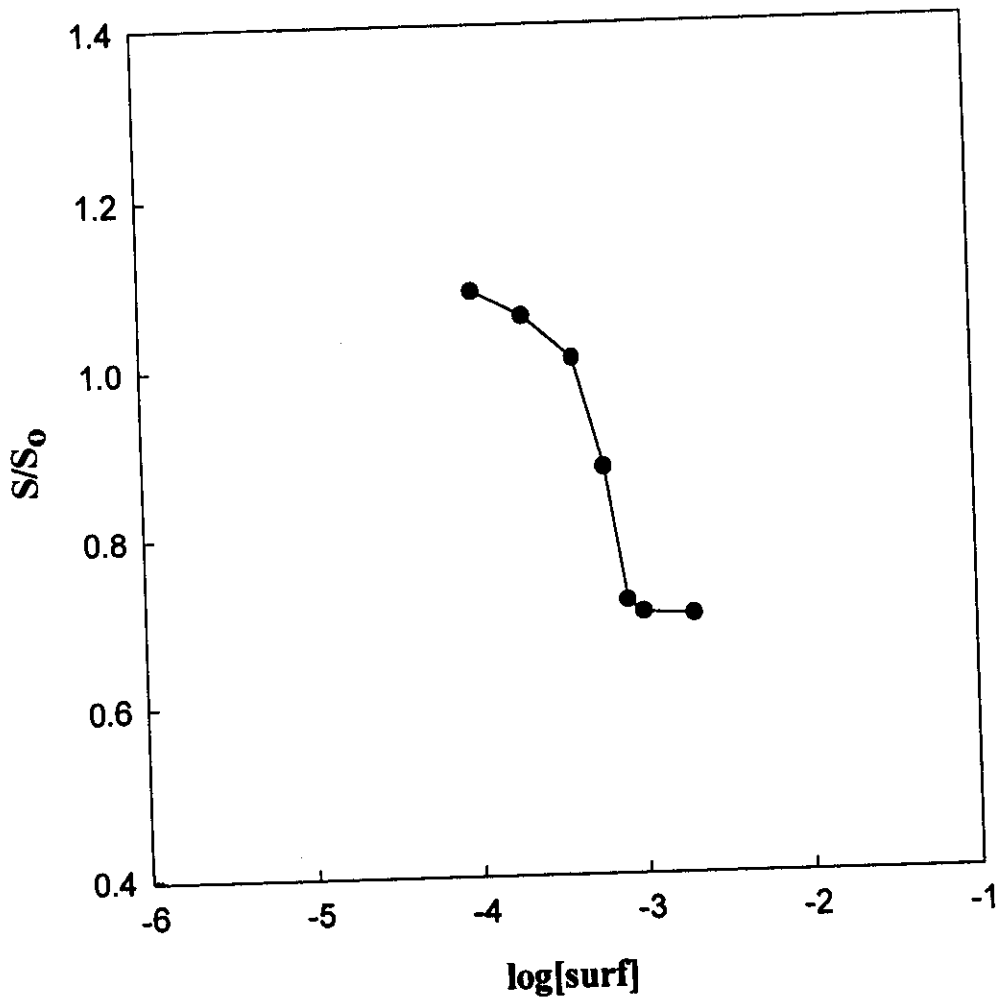

Figure 7: The plots of the ratio of slopes of (i_l) versus $\omega^{1/2}$ obtained from aqueous and in AOT micellar solutions (S/S_o) against the logarithm surfactant concentration.

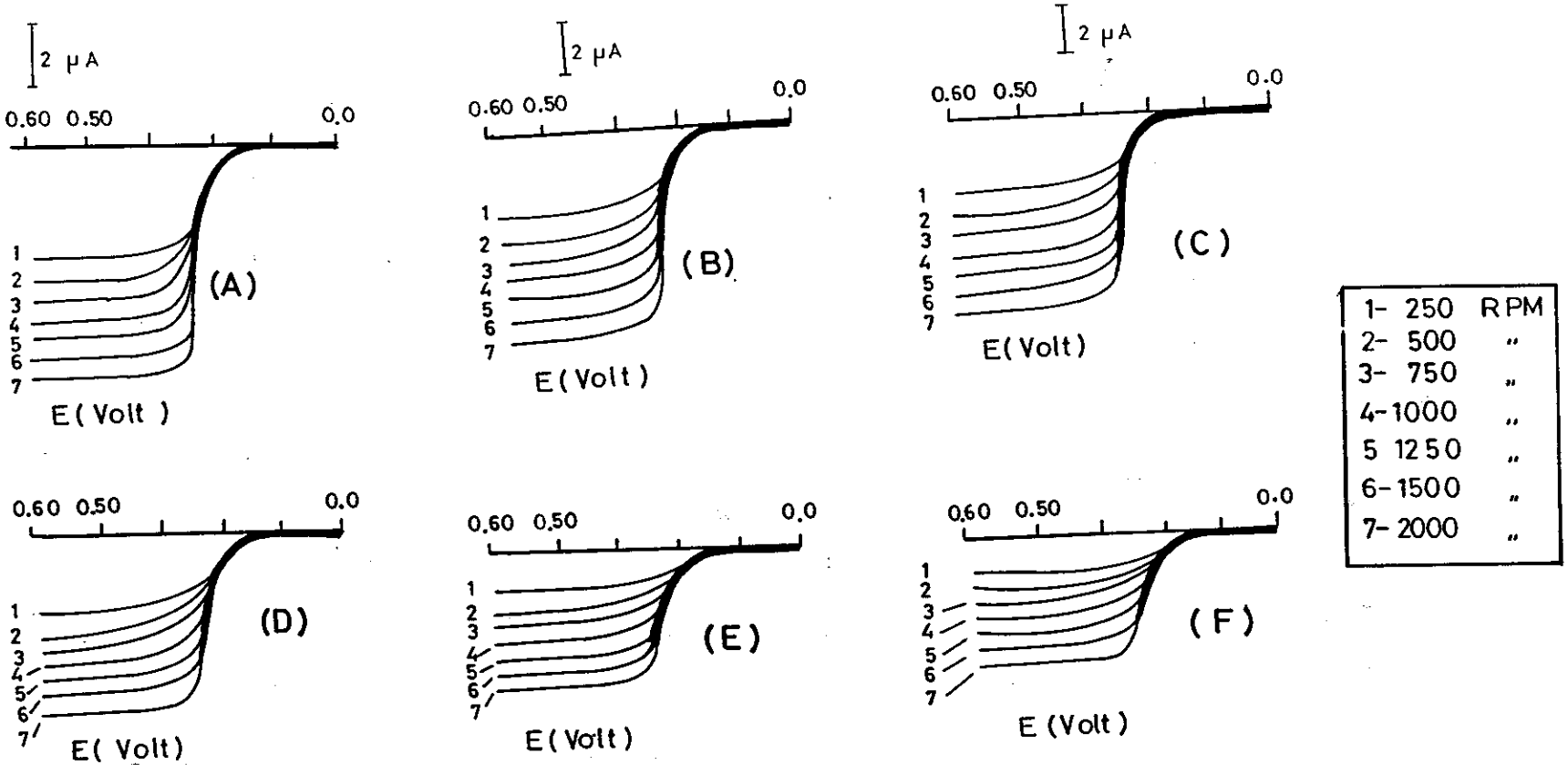

Figure 8: The effect of rotation speed of glassy carbon electrode on the linear sweep voltammograms obtained for solubilized ferrocene in AOT micellar solutions containing, (a) $6x10^{-4}$ M AOT, (b) $8x10^{-4}$ M AOT, (c)$1x10^{-3}$ M AOT, (d) $2x10^{-3}$ M AOT, (e) $4x10^{-3}$ M AOT and (f)$1x10^{-2}$ M AOT. The rotation speed are 250,500,750,1000,1250,1500 and 2000 RPM.

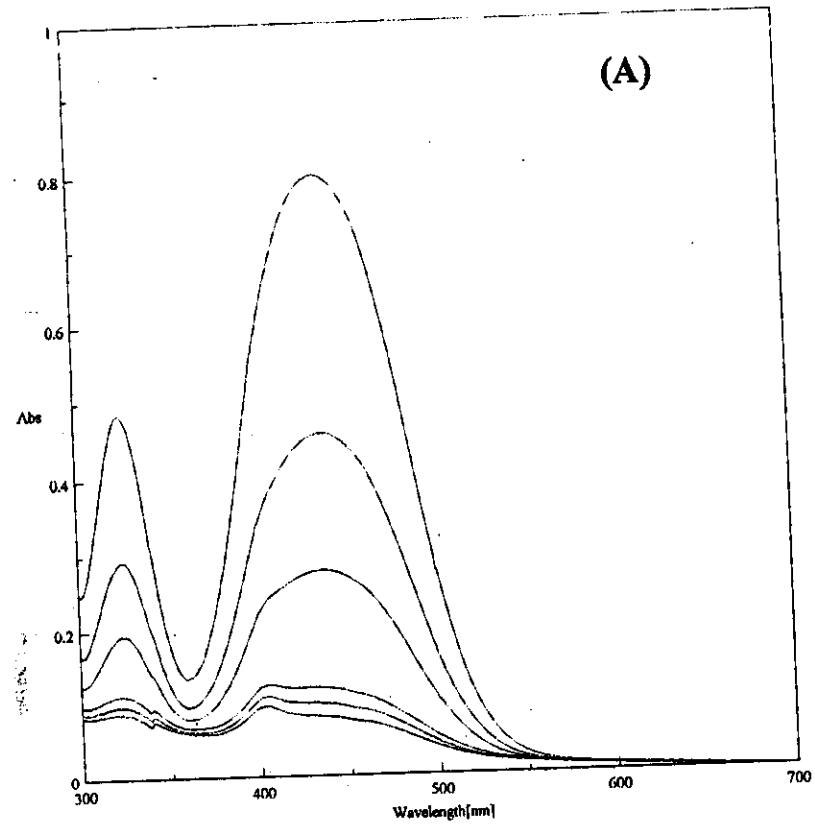

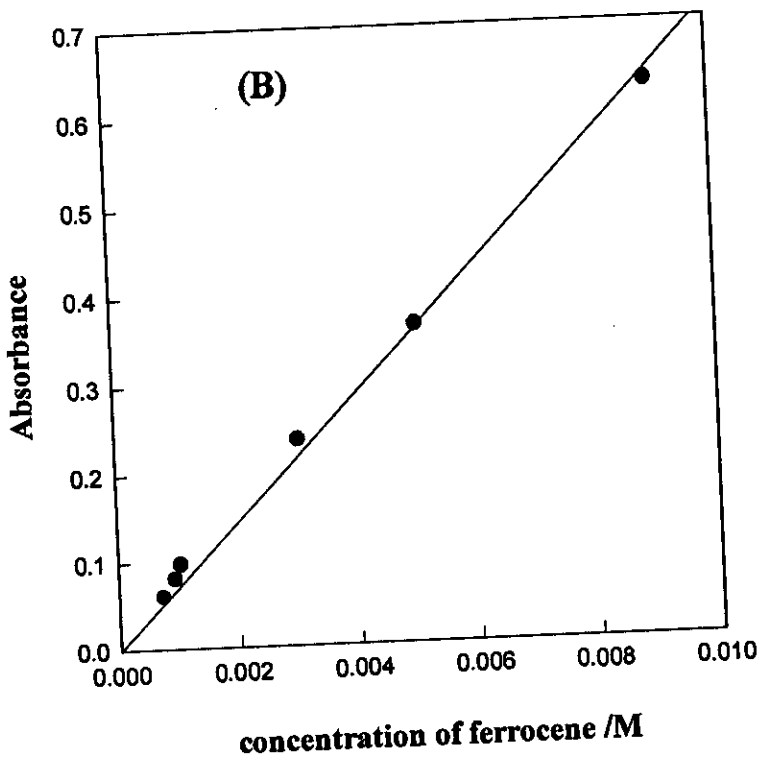

Figure 9: (a) UV-visible absorption spectra of ferrocene in pure ethanol and (b) its calibration curve (absorbance measured at λ=400 nm).

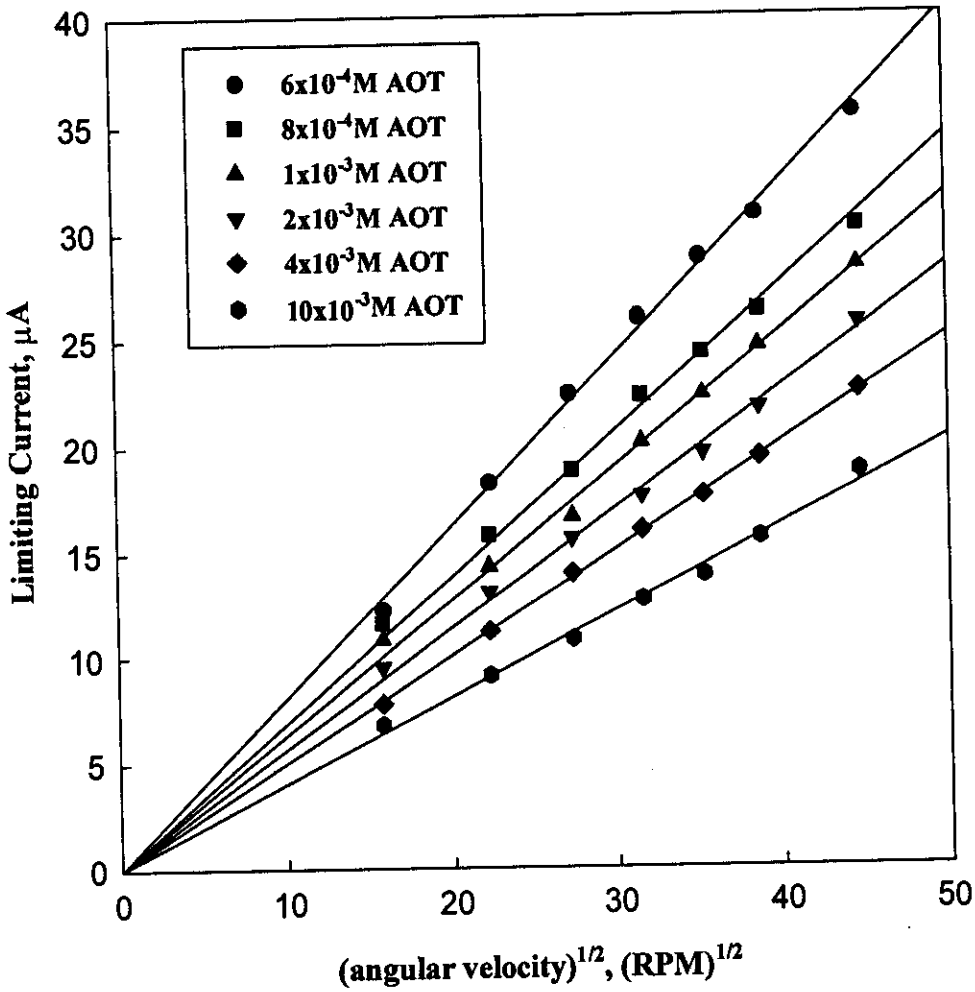

Figure 10: The plots of limiting currents (i_l) versus square root of angular velocity ($\omega^{1/2}$) for solubilized ferrocene in AOT micellar solutions.

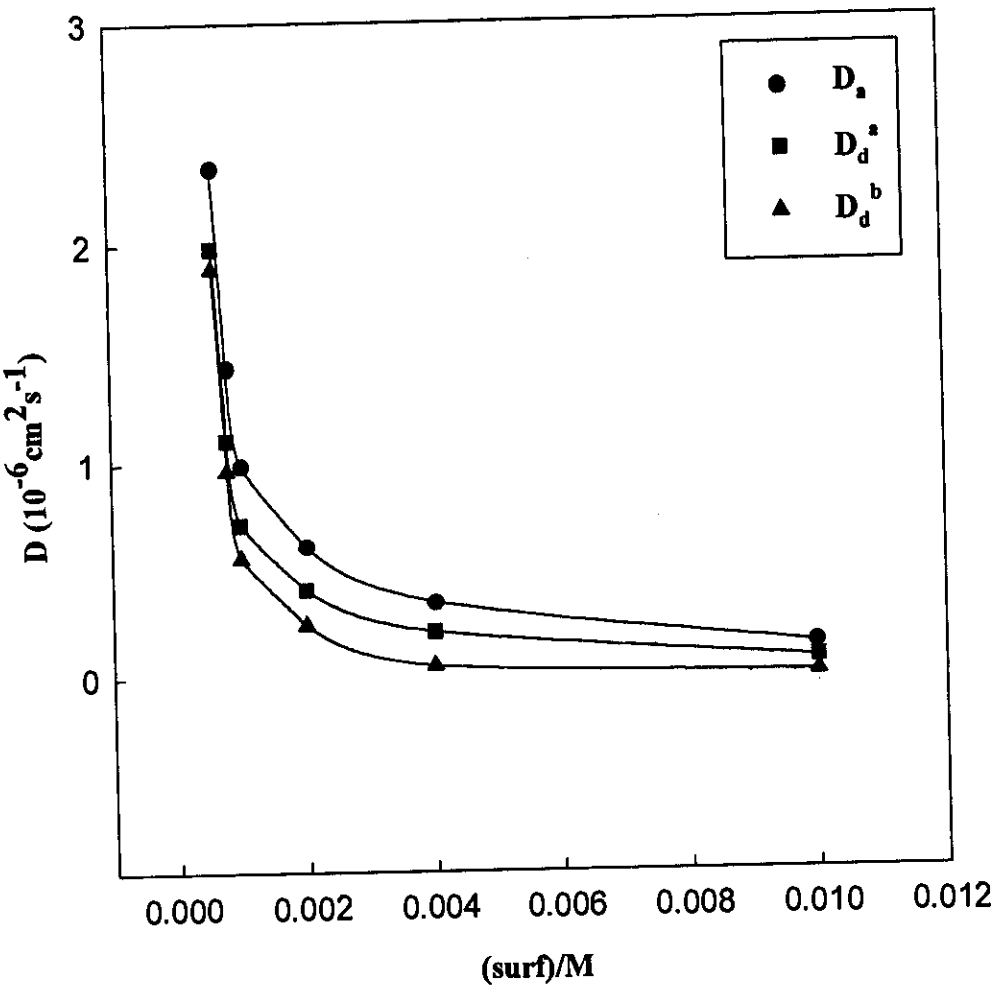

Figure 11: Diffusion coefficients of AOT micelles, (D_a) is the apparent diffusion coefficient, (D_d^a) and (D_d^b) are the corrected diffusion coefficients calculated in zero-kinetics approximation and in fast-kinetic limit, respectively.

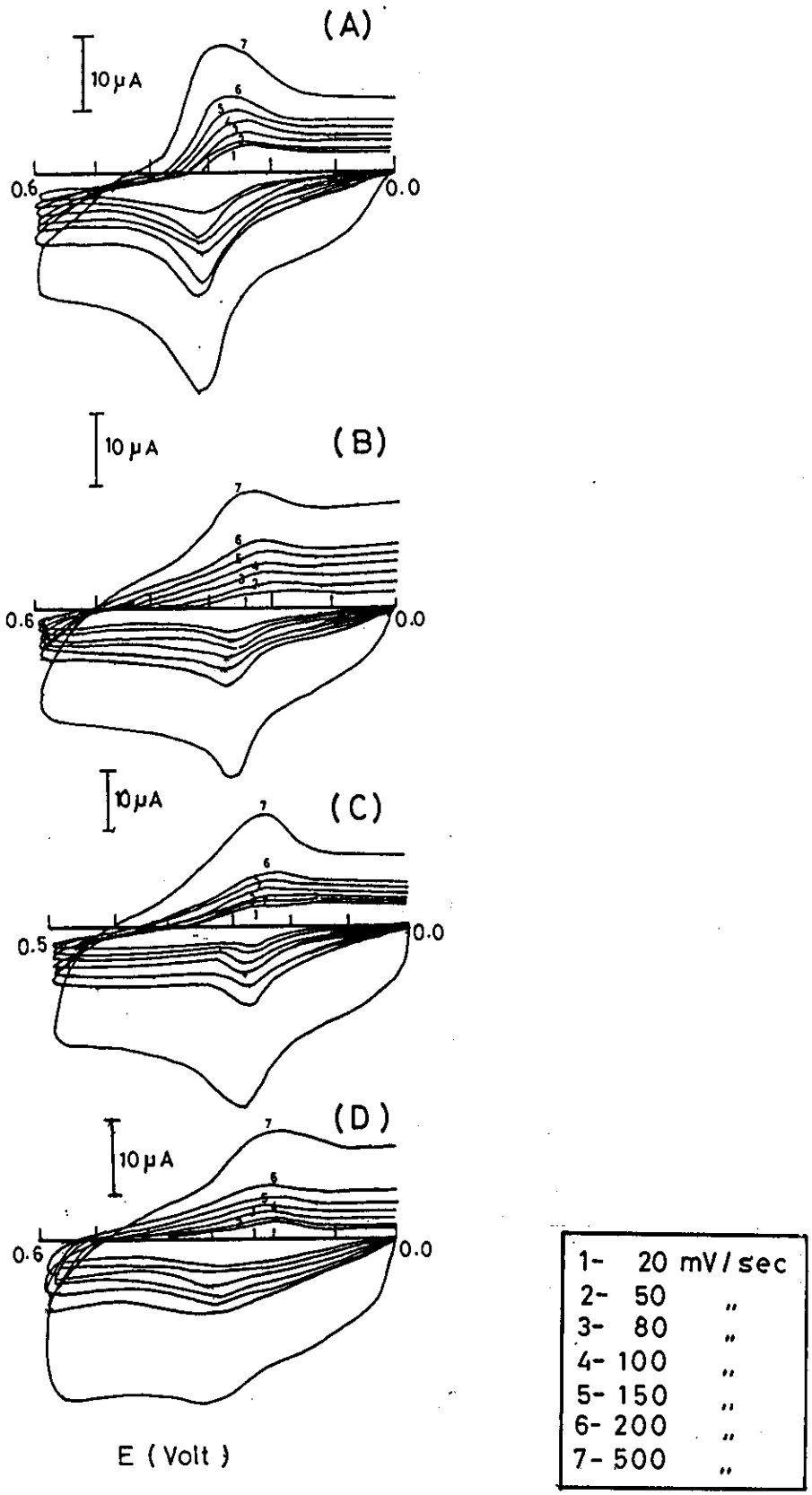

gure 12: Cyclic volltammograms of 0.5 mM ferrocene in $8x10^{-4}$ M AOT micellar lutions containing, (a) 0.05 M NaCl, (b) 0.16 M NaCl, (c) 0.62 M NaCl, and (d) 0 M NaCl, at 25°C. The sweep rates are 20,50,80,100,150,200 and 500 mV/sec.

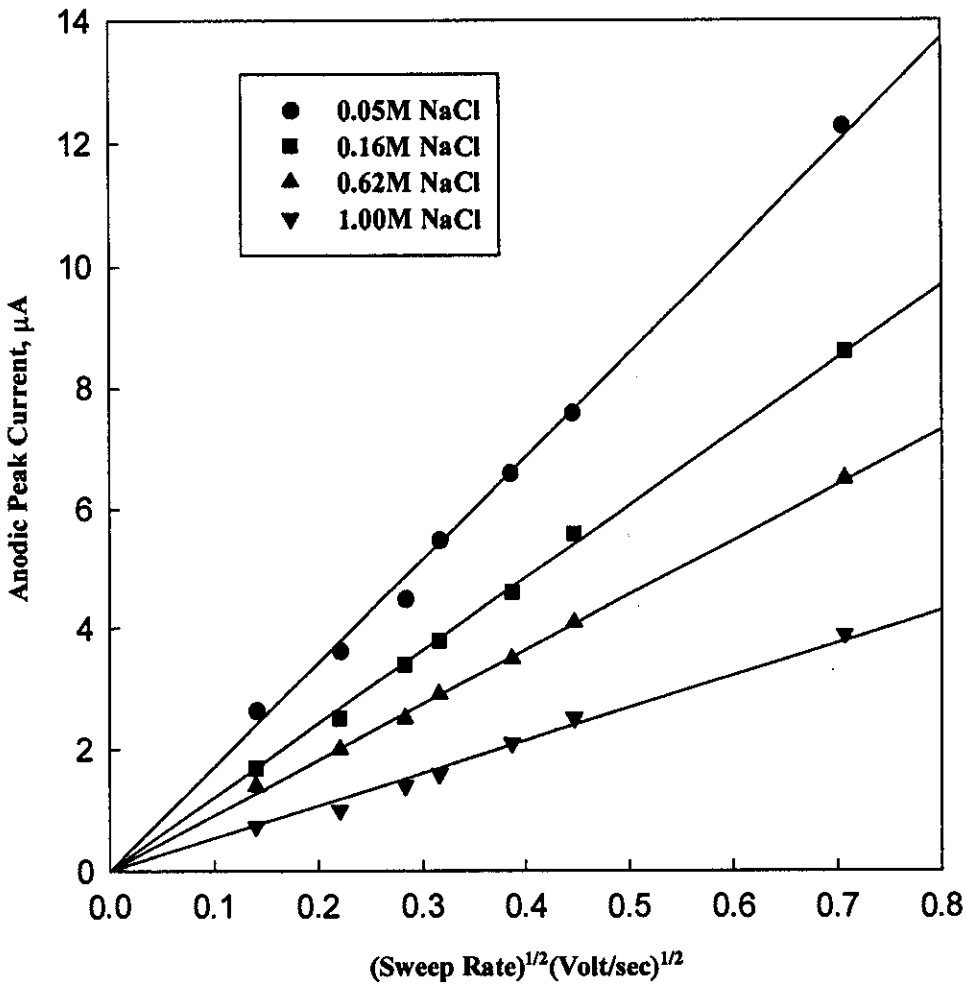

Figure 13: The plots of anodic peak currents versus ($\upsilon^{1/2}$) of 0.5 mM ferrocene in $8x10^{-4}$ M AOT micellar solutions at differernt concentrations of NaCl

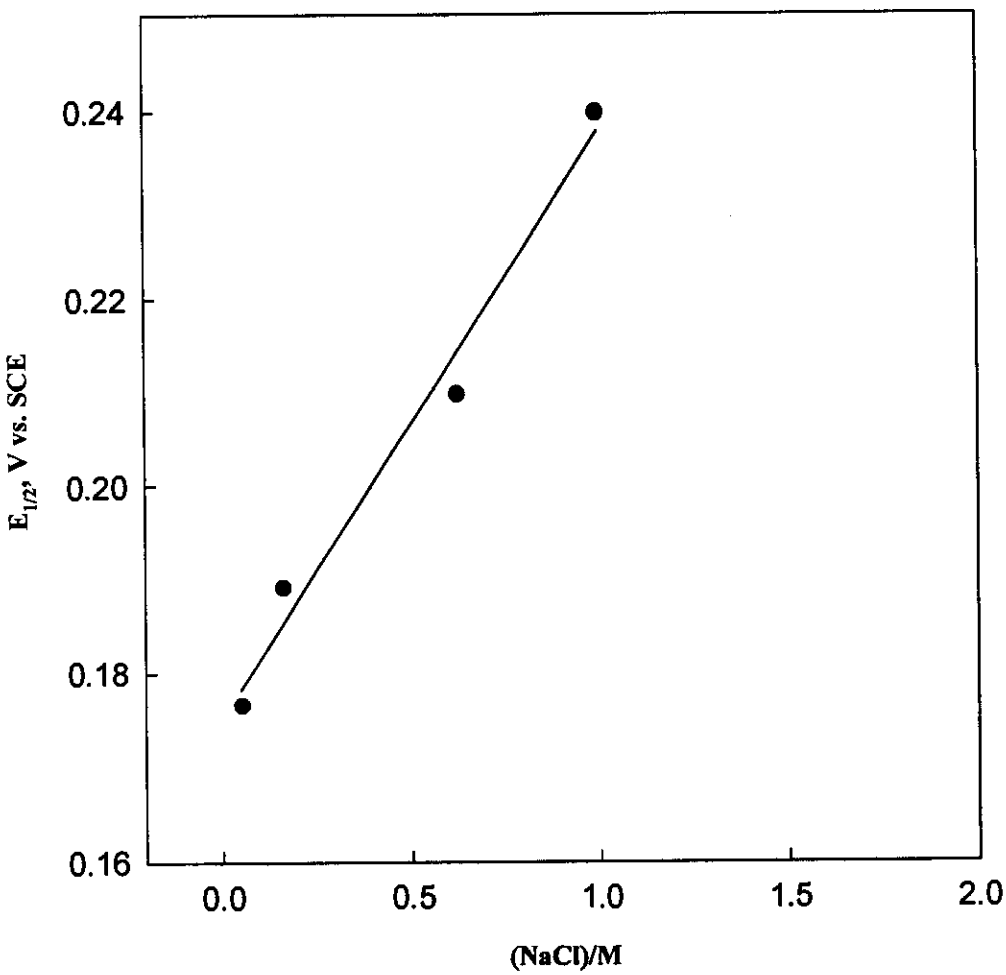

Figure 14: Half-wave potential ($E_{1/2}$) of AOT micellar solutions plotted versus NaCl concentration.

Table 4 : Cyclic voltammetric data obtained for $7x10^{-5}$ M ferrocene in AOT micellar solutions.

Sweep Rate	$E_{p,a}$	$E_{p,c}$	$I_{p,a}$	$I_{p,c}$	$I_{p,a}/I_{p,c}$	ΔE_p	$E_{1/2}$	$E_{1/2}$(average)
mV/sec	mV	mV	µA	µA	-	mV	mV	mV
(A) $1x10^{-4}$ M AOT								
20	180	121	1.30	1.29	1.007	59	150	
50	180	122	1.50	1.48	1.013	58	151	
80	181	122	1.60	1.62	0.987	59	151	
100	182	123	1.80	1.80	1.000	59	152	151
150	182	123	2.20	2.10	1.047	59	152	
200	181	122	2.60	2.61	0.996	59	151	
500	183	121	4.08	4.07	1.001	62	152	
(B) $2x10^{-4}$ M AOT								
20	180	121	1.20	1.22	0.983	59	150	
50	180	122	1.40	1.41	0.992	58	151	
80	181	122	1.54	1.52	1.013	59	151	
100	182	123	1.70	1.70	1.000	59	152	151
150	182	123	2.10	2.00	1.050	59	152	
200	181	122	2.50	2.51	0.996	59	151	
500	183	121	3.90	3.95	0.987	62	152	
(C) $4x10^{-4}$ M AOT								
20	180	121	1.22	1.21	1.008	59	150	
50	180	122	1.10	1.12	0.987	58	151	
80	181	122	1.29	1.28	1.007	59	151	
100	180	121	1.46	1.43	1.020	59	150	151
150	180	120	1.80	1.81	0.994	60	150	
200	180	120	2.10	2.11	0.995	60	150	
500	181	122	3.40	3.42	0.994	59	151	

Follow:

Sweep Rate	$E_{p,a}$	$E_{p,c}$	$I_{p,a}$	$I_{p,c}$	$I_{p,a}/I_{p,c}$	ΔE_p	$E_{1/2}$	$E_{1/2}$(average)
mV/sec	mV	mV	μA	μA	-	mV	mV	mV
(D) $6x10^{-4}$ M AOT								
20	172	115	0.91	0.90	1.007	57	143	
50	173	116	1.04	1.03	1.013	57	144	
80	174	116	1.14	1.12	0.987	58	145	
100	175	114	1.25	1.24	1.000	61	144	144
150	175	114	1.58	1.57	1.047	61	144	
200	176	117	1.80	1.74	0.996	59	146	
500	176	118	2.90	2.85	1.001	58	147	
(E) $8x10^{-4}$ M AOT								
20	170	112	0.74	0.71	1.042	58	141	
50	170	112	0.87	0.85	1.023	58	141	
80	171	114	1.02	1.02	1.000	57	142	
100	172	114	1.10	1.11	0.990	58	143	142
150	172	114	1.40	1.34	1.044	58	143	
200	172	115	1.60	1.59	1.006	57	143	
500	173	116	2.60	2.57	1.011	57	144	
(F) $1x10^{-3}$ M AOT								
20	167	111	0.61	0.60	1.016	56	139	
50	167	110	0.72	0.71	1.014	57	138	
80	168	111	0.85	0.84	1.011	57	139	
100	168	111	0.98	0.96	1.020	57	139	139
150	169	112	1.20	1.21	0.991	57	140	
200	169	113	1.40	1.38	1.014	56	141	
500	170	114	2.19	2.13	1.028	56	142	

Follow:

Sweep Rate	$E_{p,a}$	$E_{p,c}$	$I_{p,a}$	$I_{p,c}$	$I_{p,a}/I_{p,c}$	ΔE_p	$E_{1/2}$	$E_{1/2}$(average)
mV/sec	mV	mV	μA	μA	-	mV	mV	mV
(G) $2x10^{-3}$ M AOT								
20	162	106	0.43	0.42	1.023	56	134	
50	163	106	0.56	0.52	1.076	57	134	
80	163	106	0.76	0.71	1.070	57	134	
100	163	105	0.94	0.90	1.040	58	134	134
150	165	104	1.11	1.06	1.047	61	134	
200	165	104	1.30	1.32	0.986	61	134	
500	166	108	2.01	1.99	1.030	58	137	

Table 5 : Diffusion coefficient values of solubilized ferrocene in AOT micellar solutions obtained from RDV measurements.

Concentration of		Diffusion coefficient (10^{-6} cm^2 s^{-1})		
		Electrochemical		
		D_a	D_d	
Surfactant mM	Ferrocene M		Slow[a]	Fast[b]
0.6	$5.25x10^{-4}$	1.985	1.892	2.350
0.8	$6.00x10^{-4}$	1.103	0.962	1.440
1.0	$7.07x10^{-4}$	0.715	0.558	0.992
2.0	$8.68x10^{-4}$	0.409	0.245	0.617
4.0	$1.13x10^{-3}$	0.208	0.052	0.346
10.0	$2.50x10^{-3}$	0.077	0.010	0.139

. : calculated in zero-kinetics approximation using Eq. (III.9)

ɔ : calculated in fast-kinetic limit using the linear mole fraction weighting Eq. (III.10)

Table 6 : Cyclic voltammetric data obtained for 1mM ferrocene in AOT micellar solutions containing different amounts of NaCl at 25°C.

Sweep Rate	$E_{p,a}$	$E_{p,c}$	$I_{p,a}$	$I_{p,c}$	$I_{p,a}/I_{p,c}$	ΔE_p	$E_{1/2}$
mV/sec	mV	mV	μA	μA	-	mV	mV
(A) 0.05M NaCl							
20	203	149	5.90	5.80	1.017	54	176
50	204	149	6.20	6.10	1.016	55	176
80	204	149	6.50	6.45	1.007	55	176
100	204	149	7.50	7.49	1.001	55	176
150	198	150	8.80	8.83	0.996	48	174
200	198	150	9.87	9.84	1.003	48	174
500	207	156	16.20	15.98	1.013	51	181
						$E_{1/2}$(average) = 176	
(B) 0.16M NaCl							
20	220	162	2.80	2.81	0.996	58	191
50	221	163	2.90	2.92	0.993	58	192
80	220	162	3.10	3.11	0.996	58	191
100	220	162	3.60	3.65	0.986	58	191
150	220	162	4.20	4.30	0.976	58	191
200	220	171	4.70	4.64	1.010	49	195
500	225	171	8.20	8.17	1.003	54	198
						$E_{1/2}$(average) = 192	

Follow:

Sweep Rate	$E_{p,a}$	$E_{p,c}$	$I_{p,a}$	$I_{p,c}$	$I_{p,a}/I_{p,c}$	ΔE_p	$E_{1/2}$
mV/sec	mV	mV	μA	μA	-	mV	mV
(C) 0.62M NaCl							
20	234	177	2.10	2.03	1.034	57	205
50	234	177	2.50	2.52	0.992	57	205
80	235	176	2.70	2.68	1.007	59	205
100	235	176	2.90	2.91	0.996	59	205
150	235	177	3.50	3.48	1.005	58	206
200	235	179	4.10	4.05	1.012	56	207
500	235	179	5.90	5.84	1.010	56	207
						$E_{1/2}$(average) =	205
(D) 1M NaCl							
20	285	232	0.73	0.71	1.028	53	259
50	285	232	0.77	0.76	1.013	53	259
80	285	232	0.83	0.82	1.012	53	259
100	286	232	0.87	0.86	1.011	54	259
150	286	232	1.18	1.15	1.026	54	259
200	286	229	1.69	1.67	1.011	57	257
500	287	229	2.90	2.80	1.035	58	258
						$E_{1/2}$(average) =	258

Table 7 : Effect of salt concentrations on the diffusion coefficient and the radius of micelle droplets of 0.5 mM ferrocene in $8x10^{-4}$ M AOT micellar solution using cyclic voltammetry.

NaCl Concentration M	$D_a x10^{-7}$ cm^2/sec	R_h A^o
0.10	6.03	40.8
0.16	3.79	64.9
0.62	1.97	125.0
1.00	0.40	559.0

3.2 Electrochemical Characterization of AOT Microemulsion System

The voltammograms of 1mM ferrocene (Fc) were recorded in AOT microcemulsion containing 6% AOT as the surfactant, 3% n-decane as the oil and 4.5% n-butanol as the cosurfactant in 0.10 M NaCl supporting electrolyte. The voltammograms were recorded in the potential window from 0.0 to + 500 mV (versus SCE) and at potential sweep rates between 20 and 500 mV/sec. Well defined voltammograms were obtained in micro-emulsion media as represented in Fig. (15). The voltammograms show one anodic and one cathodic peak on the anodic and cathodic sweeps. The anodic peak current, $I_{p,a}$, and cathodic peak current, $I_{p,c}$, are almost of equal heights as shown from Table (8). The anodic to cathodic peak current ratios ($I_{p,a}/I_{p,c}$) does not exceed 1.095, which indicate the reversibility of the electrode process and confirmed that, there is no adsorption contribution to the electrode surface. The peak potential separation $\Delta E_p = (E_{p,a} - E_{p,c})$ is almost around the theoretical value for one-electron transfer ~ 60 mV in AOT microemulsion system. These results indicate that the electrochemical oxidation of ferrocene (Fc) is a one-electron transfer process.

The voltammograms recorded at different sweep rates varying from 20 to 500 mV/sec are essentially similar and show one anodic and one cathodic peak. The constancy of the cathodic and anodic peak potentials, $E_{p,a}$ and $E_{p,c}$ respectively, confirms the reversible nature of the electrode reaction. Also the peak potential separation ΔE_p values fall within the rang from 56 - 60 in AOT microemulsions, within the experimental error of ~5 mV as given in Table (8). On using Randless-Sevcik equation [140], the plots of anodic peak current ($I_{p,a}$) versus square root of sweep rate ($\upsilon^{1/2}$), straight lines intersecting the origin were obtained for AOT microemulsion and shown in Fig. (16). These results indicate that the electrode process is diffusion controlled [117].

The slopes of $I_{p,a}$ vs. $\upsilon^{1/2}$ were used to estimate the apparent diffusion coefficient of the reductant (D_a). The apparent diffusion coefficient values for ferrocene in AOT microemulsion were determined and listed in Table (9).

Therefore, cyclic voltamograms of ferrocene in AOT microemulsion system are well-behaved in the sense that they yielded linear $I_{p,a}$ versus $\upsilon^{1/2}$ plots, nearly unity of $I_{p,a}/I_{p,c}$ ratios and constancy values for $(E_{p,a} + E_{p,c})/2$ at sweep rates of 20 to 500 mV/sec. Ferrocene (Fc) is hydrophobic in nature, its solubility in water is 5×10^{-5} M [34] and of solubility 0.15 M in dodecane [154]. Singly charged Fc^+ cation is water soluble, thus $Fc^{0/+}$ couple represents the limiting case where one form of the probe is oil soluble (Fc^0) and the other (Fc^+) is water soluble.

By using Stokes-Einstein equation (III.4) the radius of microemulsion droplets were determined by using the values of the apparent diffusion coefficients, Table (9).

3.2.1 Effect of probe concentration

The effect of probe concentration on cyclic voltammetry experiments was studied using both ferrocene and potassium ferrocyanide as hydrophobic and water-soluble electoactive probes, respectively. Cyclic voltammagrams obtained at different concentrations of ferrocene and potassium ferrocyanide in the range from 2×10^{-4} to 3×10^{-3} M, indicate increase in peak current on increasing the probe concentration in microemulsion system, as shown in Fig. (15, 17). The results obtained are listed in Tables (8,10). The value of the half-wave potential was constant in the range of this probe concentration. The plots of anodic peak current ($I_{p,a}$) versus square root of sweep rate ($\upsilon^{1/2}$) for AOT microemulsion solutions at both different ferrocene and potassium ferrocyanide concentrations give linear correlations passing through the origin, Figs.(16,18), confirming the diffusion nature of the electrochemical

reactions. The slope values were used to estimate the apparent diffusion coefficient as shown in Table (9,11).

3.2.2 Effect of hydrocarbon

The effect of oil content on the diffusion coefficient and the radius of microemulsion system of AOT was studied in the range from 2.00 to 3.50% (wt./wt.) of n-decane, using ferrocene as electroactive probe. Cyclic voltammograms obtained at different percentages of oil content indicate the slight decrease in peak current on increasing the oil content in microemulsion system, as shown in Fig.(19). Results shown in Table (12) indicate that as the oil content increased, the heterogeneity of microemulsion system is increased, this reflects the increased size of the droplets. Size obtained indicate the microstructure of microemulsion. The plots of the half-wave potential ($E_{1/2}$) versus the weight percent of n-decane (oil) showed a positive shift of $E_{1/2}$ as the oil content is increased as represented by Fig.(20). Therefore the half-wave potential of the electroactive probe was found dependent on the composition of microemulsion system.

3.2.3 Effect of salt concentration

The effect of salt concentration on the diffusion coefficient of AOT microemulsion was studied at 0.08, 0.10 and 0.12 M of NaCl. The effect of salt concentrations on the voltammetric behaviour of ferrocene in micro-emulsion represented in Fig.(21). The results obtained from cyclic voltammetry were listed in Table (13), and showed a decrease of peak current as NaCl concentration is increased. Fig.(22) show the plots of anodic peak currents versus ($\upsilon^{1/2}$) at different NaCl concentrations. In general the diffusion coefficients calculated were found to decrease with increasing

salinity as represent in Table (14). This behaviour could be attributed to the increased viscosity of the medium.

3.2.4 Effect of surfactant concentration

The effect of surfactant concentration on the diffusion coefficient of AOT microemulsion was checked using cyclic voltammetry. The surfactant concentration was varied in the range from 5.0% to 6.5% (wt./wt.). The other components of microemulsion system were held constant. The recorded voltammograms of 1 mM ferrocene at different percentages of surfactant indicate the increase of peak current on increasing the surfactant concentration in microemulsion system, as shown in Fig.(23). Fig.(24) shows the plot of anodic peak current versus ($\upsilon^{1/2}$). There is increase in the diffusion coefficients as the surfactant concentration is increased at a constant oil concentration, Table (15).

3.2.5 Rotating disk voltammetry (RDV)

The rotating disk voltammetry experiments were carried out successfully in AOT microemulsion system in the range from $2x10^{-4}$ to $3x10^{-3}$ M of ferrocene electroactive probe. The microemulsion composition was held constant at 6% AOT as the surfactant, 3% n-decane as the oil and 4.5% n-butanol as the cosurfactant containing 0.10 M NaCl. The effect of rotation speed of the glassy carbon electrode was carried out using linear sweep voltammetry. The voltammograms were recorded at small sweep rate, 5 mV/sec to obtain a steady state plateau and avoiding peaked shape. The voltammograms recorded in AOT microemulsion showing the one step oxidation-plateau. The effect of rotation speed on the voltammograms was recorded at angular velocities varying from 250 to 2000 RPM, Fig. (25). On increasing the angular velocity (ω) the limiting current (i_l) is increased

whereas the half-wave potential ($E_{1/2}$) is constant and not affected by the electrode rotation. This behaviour of constancy of $E_{1/2}$-values revealed the reversibility of ferrocene oxidations in these systems.

On employing the Levich equation [133]:

$$i_l = 0.62nFACD^{2/3} v^{-1/6} \omega^{1/2} \qquad \text{(III.2)}$$

where i_l is the limiting current in amp., ω is the angular velocity in rad/sec, v is the kinematic viscosity in cm^2/sec and other terms have their usual meanings. The plots of the limiting current (i_l) versus square root of the angular velocity ($\omega^{1/2}$) for ferrocene in AOT microemulsion systems showed linear correlations intersecting the origin, Fig. (26). The limiting current was measured at the steady state at 400 mV. These typical results indicating that the electrode process is under mass transfer control. The slopes of these linear plots were used to estimate the apparent diffusion coefficients of microemulsion droplets using Levich equation. Generally, a good agreement for the diffusion coefficient values obtained from rotating disk voltammetry with those obtained from cyclic voltammetry, Table (9).

The half-wave potential and the number of electrons consumed in the oxidation process were determined from the logarithmic analysis of the oxidation waves of 1mM ferrocene in AOT microemulsion at 1000 RPM.

On using the following relationship [117]:

$$E = E_{1/2} - 2.303\ RT/\ nF.\log [i/(i_l - i)] \qquad \text{(III.3)}$$

and on plotting $\log[i/(i_l - i)]$ versus E straight line is obtained as shown in Fig.(27). The half- wave potential ($E_{1/2}$) of the system was determined from the potential axis at $\log[i/(i_l - i)]$ value equal to zero where $i = i_l/2$ at the $E_{1/2}$

value. The half-wave potentials were determined and found to be 243 mV for ferrocene in AOT microemulsion. The reciprocal slope of that plot was found to be 62 mV which is consistent with a one electron transfer process.

3.2.6 Chronocoulometry (CC)

Chronocoulometry is an extremely valuable technique for the direct measurement of adsorption of electroactive species [143-149]. Double-potential step chronocoulometry used to get information about the adsorption in the electrochemical system, also the net potential change is zero on using the double-potential step chronocoulometric experiments. The chronocoulometric responses of ferrocene in AOT micelles and microemulsion systems were recorded by plotting the charge versus time after taking the cyclic voltammograms in the same potential widow. The stepping time was 250 m sec and the potential widow was from 0.0 to 500 mV, which pre-selected from cyclic voltammetric behaviour of ferrocene recorded in both AOT micelles and microemulsion. Typical chronocoulograms of the forward step in these systems were obtained by plotting the total amount of diffusional charge (Q_{tot}) versus time (t), as represented in Fig. (28a,28b). Also, the Anson plots were tested by plotting the charge Q versus $t^{1/2}$ and versus θ for the forward and reverse steps by using the following two equations [144-145]

$$Q_{tot} = [2nFAD_o^{1/2}C_o t^{1/2}]/\pi^{1/2} + Q_c + Q_{ads} \qquad \text{(III.11)}$$

where $Q_{ads} = nF\Gamma_o$

$$Q_r = [2nFAD_o^{1/2}C_o \theta^{1/2}]/\pi^{1/2} + Q_c + nF\Gamma_o \qquad \text{(III.12)}$$

These typical plots of Q_{tot} versus $t^{1/2}$ and Q_r versus θ called Anson plots.

From the difference of intercepts of the forward and reverse steps of the Anson plots, the capacitive component in Q_{tot} is cancelled out. The amount of

adsorbed reactant species (Γ_o) then can be obtained quantitatively in general form as following:

$$\text{Intercept 1} - \text{Intercept 2} = nF(\Gamma_o - \Gamma_R) \qquad \text{(III.13)}$$

The typical valuse of Γ_o of ferrocene in AOT micelles and microemulsion system is in the range of 10^{-12} to 10^{-13} moles. Inspection of the values indicating a negligible surfactant adsorption at the electrode surface compared to the bulk concentration of the reactant molecules (0.5 mM,1 mM) for micelles and microemulsion systems, respectively.

3.3 Partitioning of Ferrocene in AOT

The partioning effect of ferrocene between the hydrophobic core and the hydrophilic medium is discussed for AOT micelles and AOT microemulsion systems. By considering that both the reductant Fc and oxidant Fc^+ exist in the aqueous and micellar phases, respectively. The redox reaction may be written as :

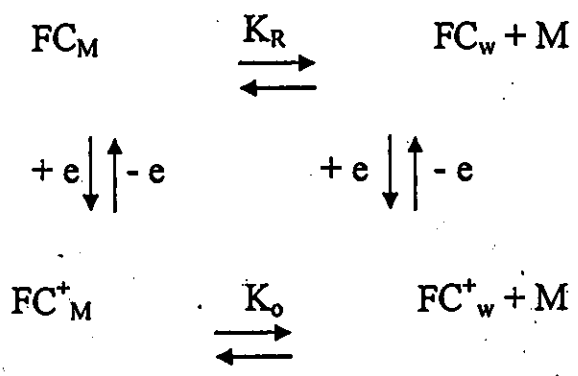

where K is a coefficient which represents the partition of the solubilizate between water (W) and micelles or microemulsion (M) phases. The subscript O) and (R) being the oxidant Fc^+ and the reductant Fc; respectively. Where

$$K_R = [Fc_w]/[Fc_M]$$

and

$$K_O = [Fc^+_w]/[Fc^+_M]$$

and the total concentration of the solubilizates are expressed as follows :

$$[Fc] = [Fc_w] + [Fc_M]$$

and

$$[Fc^+] = [Fc^+_w] + [Fc^+_M]$$

The diffusion coefficient of ferrocene can be written as,

$$D_{Fc} = (D_m + D_w K_{Fc})/(1 + K_{Fc}) \qquad \text{(III.14)}$$

where:

D_{Fc} is the diffusion coefficient of ferrocene in micelles or microemulsion ,

D_m is the diffusion coefficient of micelle or microemulsion droplet,

D_w is the diffusion coefficient of probe in water, and

$K_{Fc} = [Fc]_w / [Fc]_m$

where $[Fc]_w$ and $[Fc]_m$ are the concentrations in water and micelles or microemulsion droplet, respectively in moles per liter.

Since the hydrophobic core of microemulsion droplet contains hydrocarbon, the solubility of ferrocene in microemulsion is much higher than in micelles. Assuming $[Fc]_w = 5x10^{-5}$ M and $[Fc]_m = 1x10^{-2}$ M, the value of K_{Fc} is approximated equal to $5x10^{-3}$. It is implied from these values and equation (III.14) that $D_{Fc} \simeq D_m$.

The half-wave potential from CV and RDV are given by [117]

$$E_{1/2,CV} = E^{0} - \frac{RT}{nF} \ln \left(\frac{D_{Fc}^{+}}{D_{Fc}}\right)^{1/2} \quad \text{(III.15)}$$

$$E_{1/2,RDV} = E^{0} - \frac{RT}{nF} \ln \left(\frac{D_{Fc}^{+}}{D_{Fc}}\right)^{1/2} \quad \text{(III.16)}$$

hence by combining the above equations, the ratio of D_{Fc}^{+}/D_{Fc} can be obtained as follows:

$$\frac{D_{Fc}^{+}}{D_{Fc}} = \left[\mathrm{Exp}\left(\frac{nF}{RT}\Delta E_{1/2}\right)\right]^2 \quad \text{(III.17)}$$

A typical ratio for micelles was found to be 1.46×10^{2}, 1.54×10^{2} using CV and RDV, respectively. The D_{Fc+}/D_{Fc} in AOT microemulsion were found to be 1.06×10^{3}, and 3.36×10^{3} using CV and RDV, respectively.

Since microemulsion droplets are significantly larger in volume than micelles, the partitioning of ferrocene between the aqueous phase and the organic phase may be neglected. where ferrocene is predominately solubilized in the droplets.

When Fc and Fc^{+} both predominately exist in the microemulsion droplets, the half-wave potential obtained from CV can be written as:

$$E_{1/2} = E^{o}_{w} + RT/nF \ln K_{Fc+}/K_{Fc} - RT/nF \ln D_{Fc+}/D_{Fc} \quad \text{(III.18)}$$

where $E_{1/2}$ is the half- wave potential of Fc^{+}/Fc redox reaction and E^{o}_{w} is the formal potential of Fc in the aqueous phase. The value of E^{o}_{w} was calculated to be 0.160 ± 0.005 V versus SCE. The half-wave potential value for microemulsions containing 6% AOT, 3% n-decane, 4.5% n-butanol and 0.1M NaCl was 206 mV, hence $K_{Fc+}/K_{Fc} = 70.49$

It can be concluded from this discussion that ferrocene was predominately solubilized in droplets and $D_{Fc} \simeq D_{m}$ and the partitioning effect of ferrocene in AOT microemulsion can be neglected.

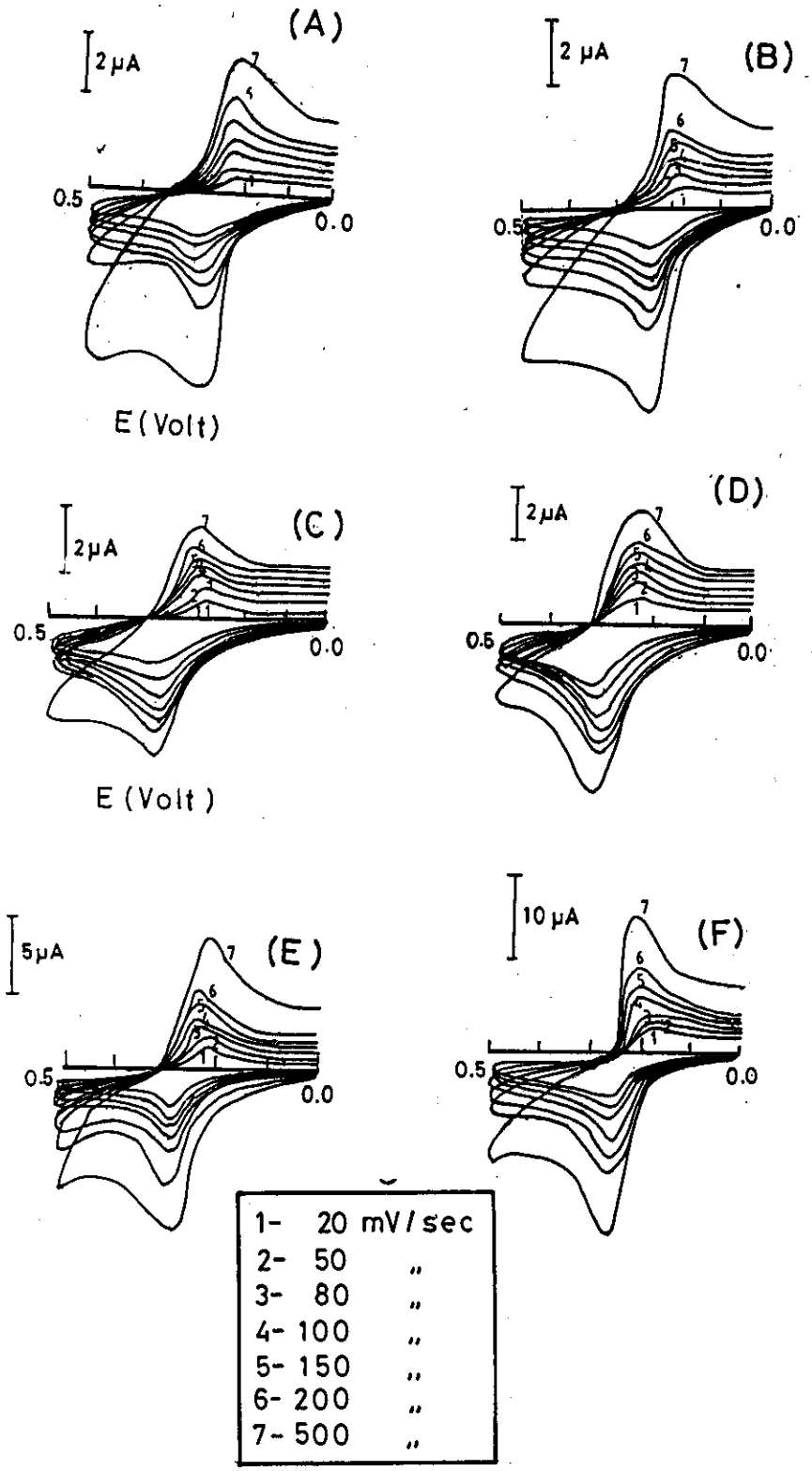

Figure 15: Cyclic voltammograms of ferrocene recorded in AOT microemulsion systems containing (a) $2x10^{-4}$ M ferrocene (b) $4x10^{-4}$ M ferrocene, (c) $8x10^{-4}$ M ferrocene, (d) $1x10^{-3}$ M ferrocene (e) $2x10^{-3}$ M ferrocene and (f) $3x10^{-3}$ M ferrocene. The sweep rates are 20,50,80,100,150,200 and 500 mV/sec.

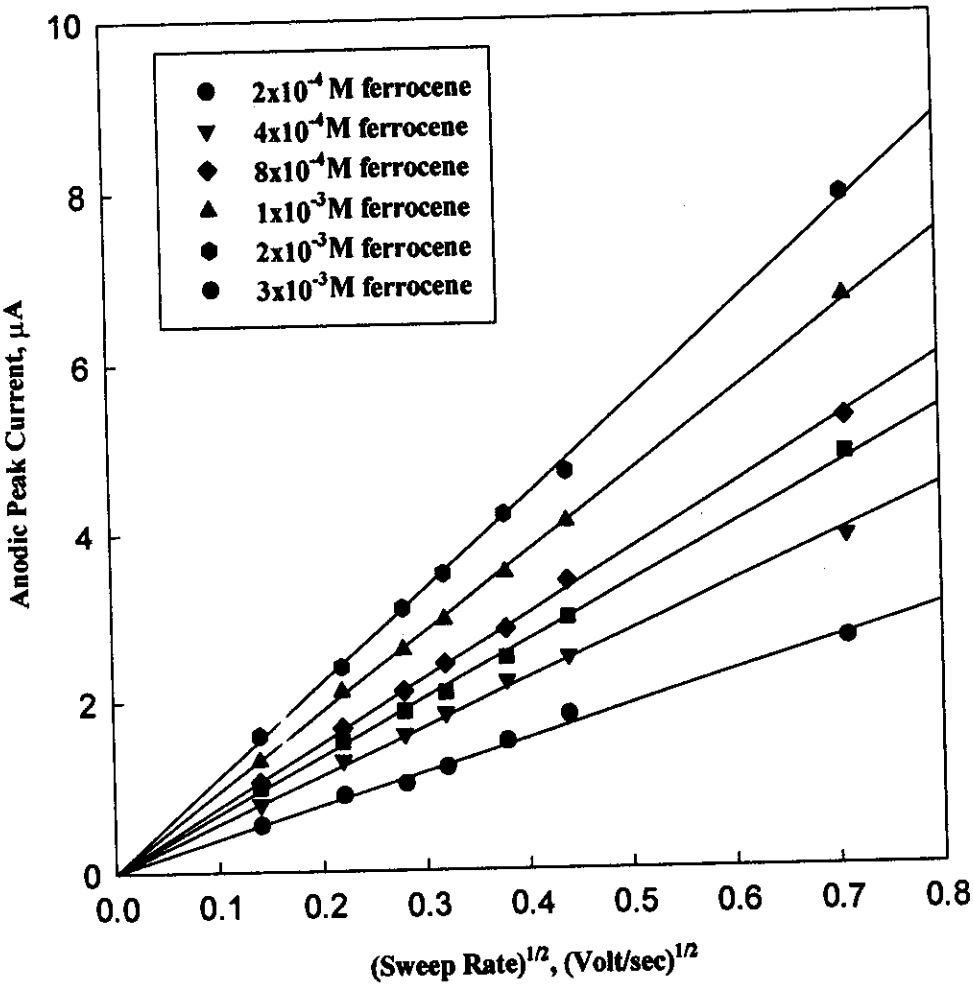

Figure 16: The plots of anodic peak currents versus ($\upsilon^{1/2}$) of ferrocene in AOT microemulsion.

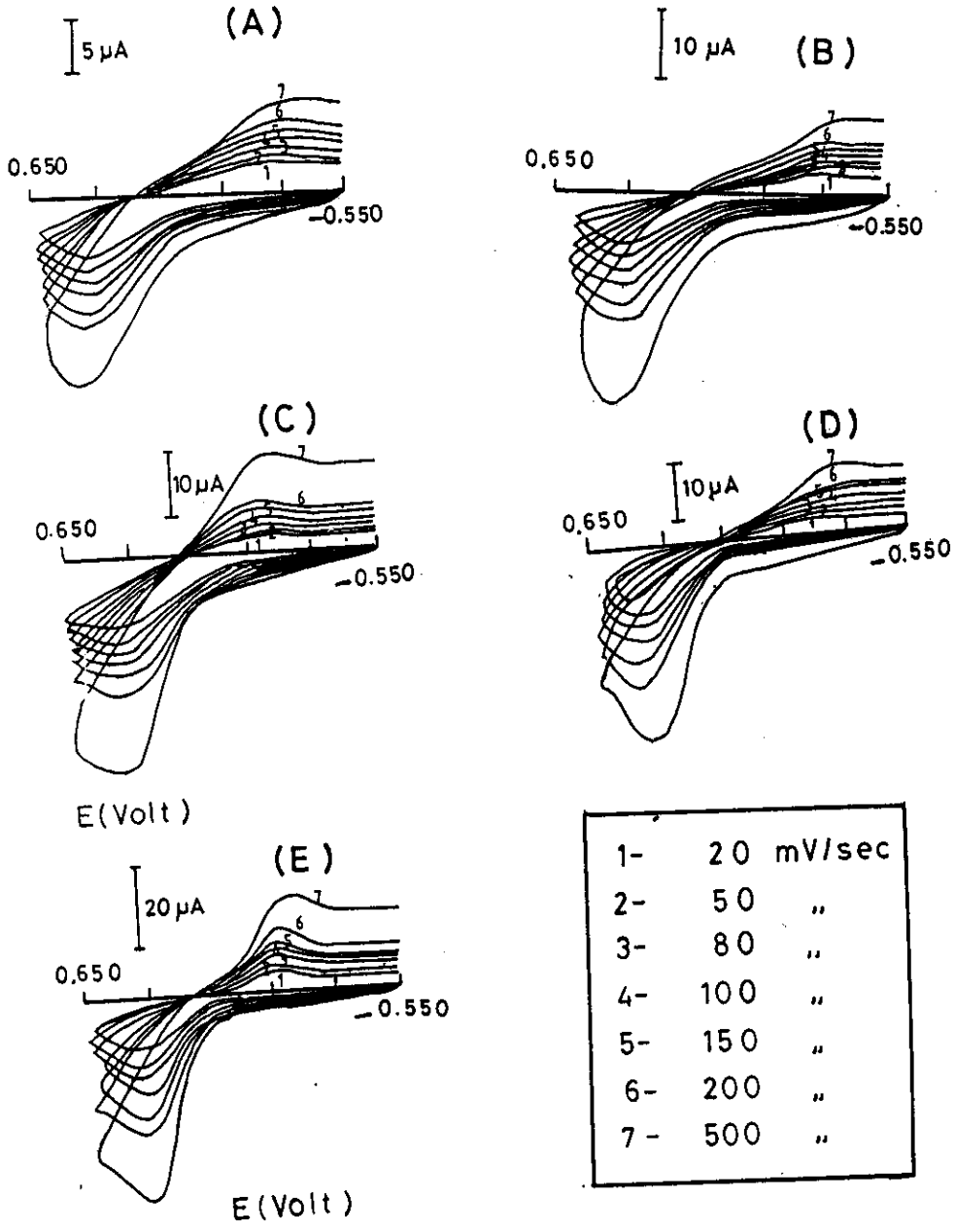

Figure 17: Cyclic voltammograms of potassium ferrocyainde recorded in AOT microemulsion systems containing (a) $2x10^{-4}$ M potassium ferrocyainde, (b) $8x10^{-4}$ M potassium ferrocyainde, (c) $1x10^{-3}$ M potassium ferrocyainde, (d) $2x10^{-3}$ M potassium ferrocyainde and (e). $3x10^{-3}$ M potassium ferrocyainde. The sweep rates are 20,50,80,100,150,200 and 500 mV/sec.

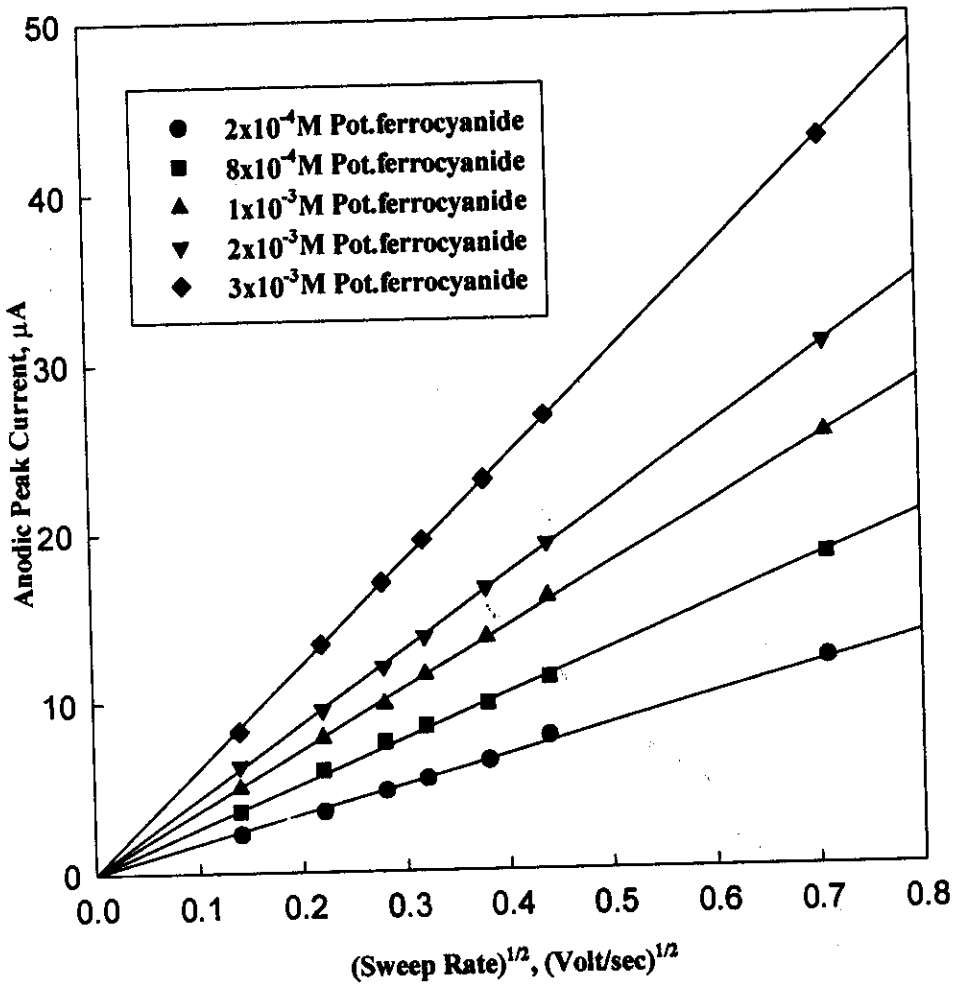

Figure 18: The plots of anodic peak currents versus ($\upsilon^{1/2}$) of potassium ferrocyanide in AOT microemulsion.

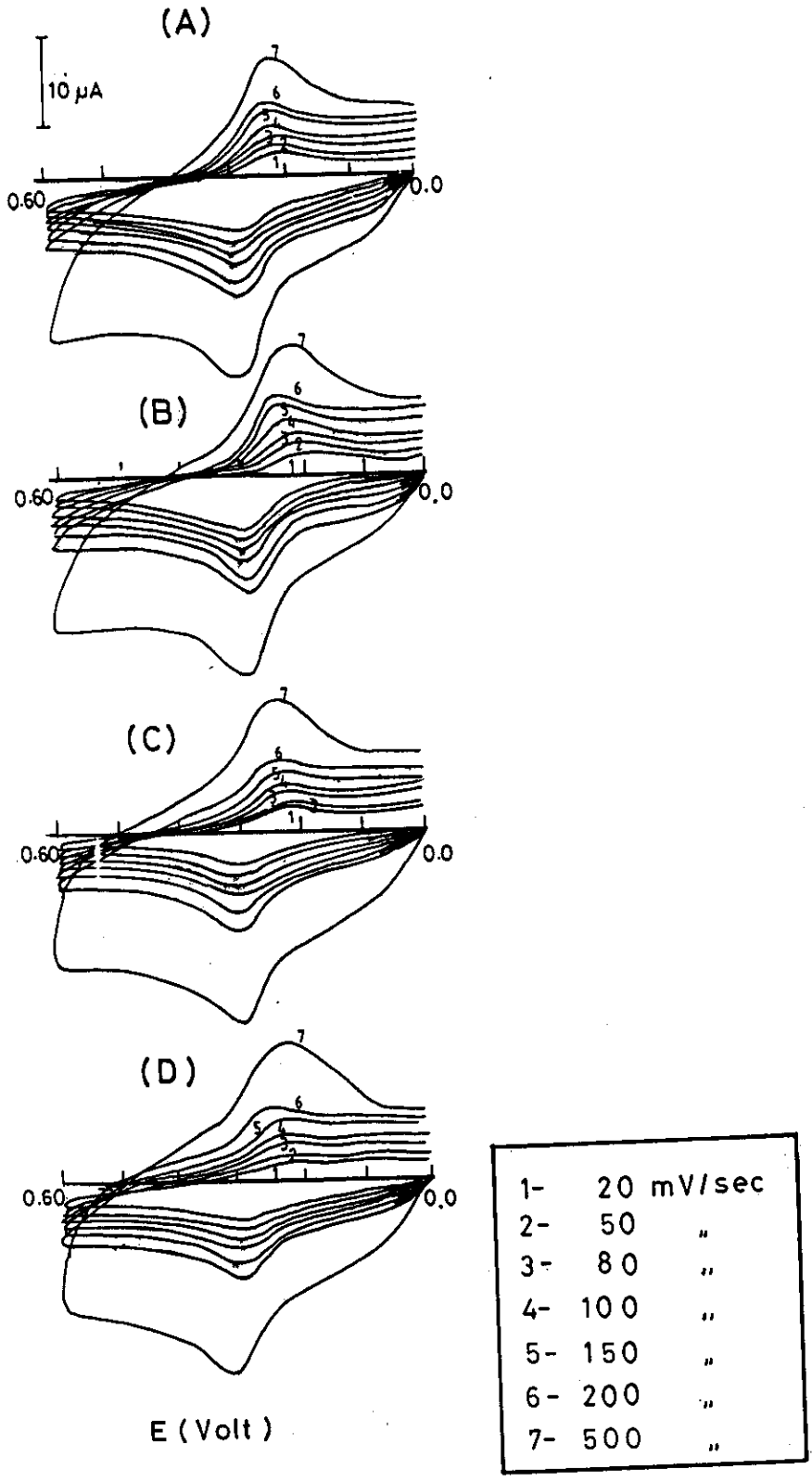

Figure 19: Cyclic voltammograms of 1mM ferrocene recorded in AOT microemulsion systems containing (a) 2.0% n-decane, (b) 2.5% n-decane, (c) 3.0% n-decane and (d) 3.5% n-decane. The sweep rates are 20,50,80,100,150,200 and 500 mV/sec.

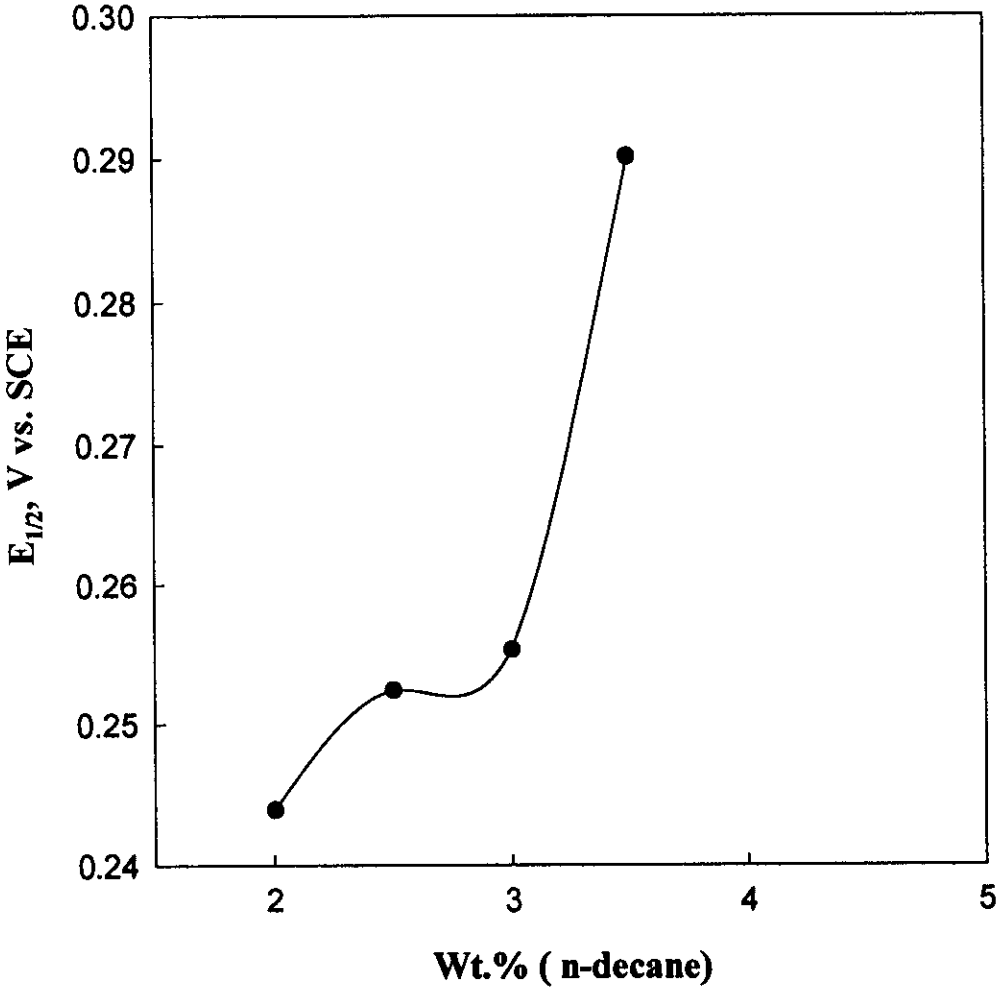

Figure 20: The dependence of half-wave potential ($E_{1/2}$) of 1mM ferrocene in AOT microemulsion on the hydrocarbon contents.

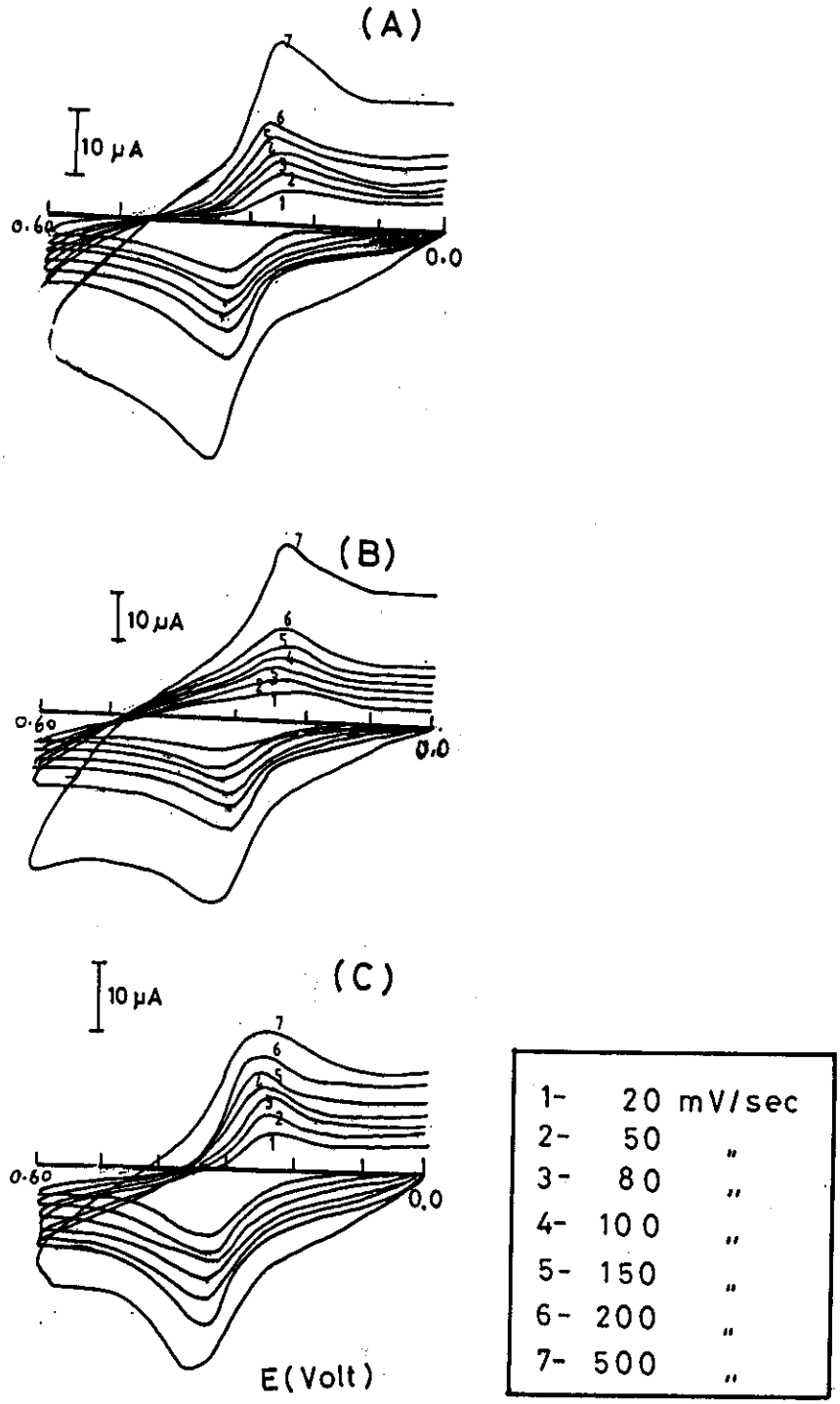

Figure 21: Cyclic voltammograms of 1mM ferrocene recorded in AOT microemulsion systems containing (a) 0.08 M NaCl, (b) 0.10 M NaCl and (c) 0.12 M NaCl at 25°C. The sweep rates are 20,50,80,100,150,200 and 500 mV/sec.

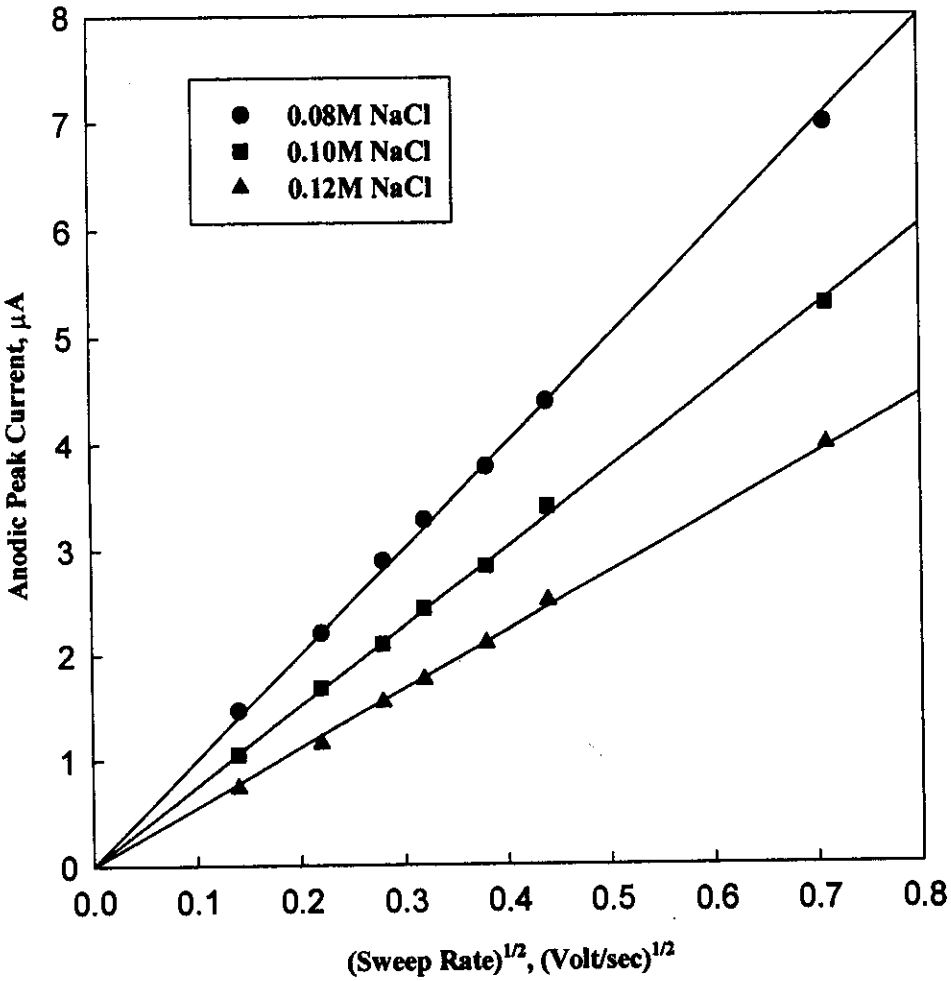

Figure 22: The plots of anodic peak currents versus ($\upsilon^{1/2}$) of 1mM ferrocene in AOT microemulsion systems at different concentrations of NaCl.

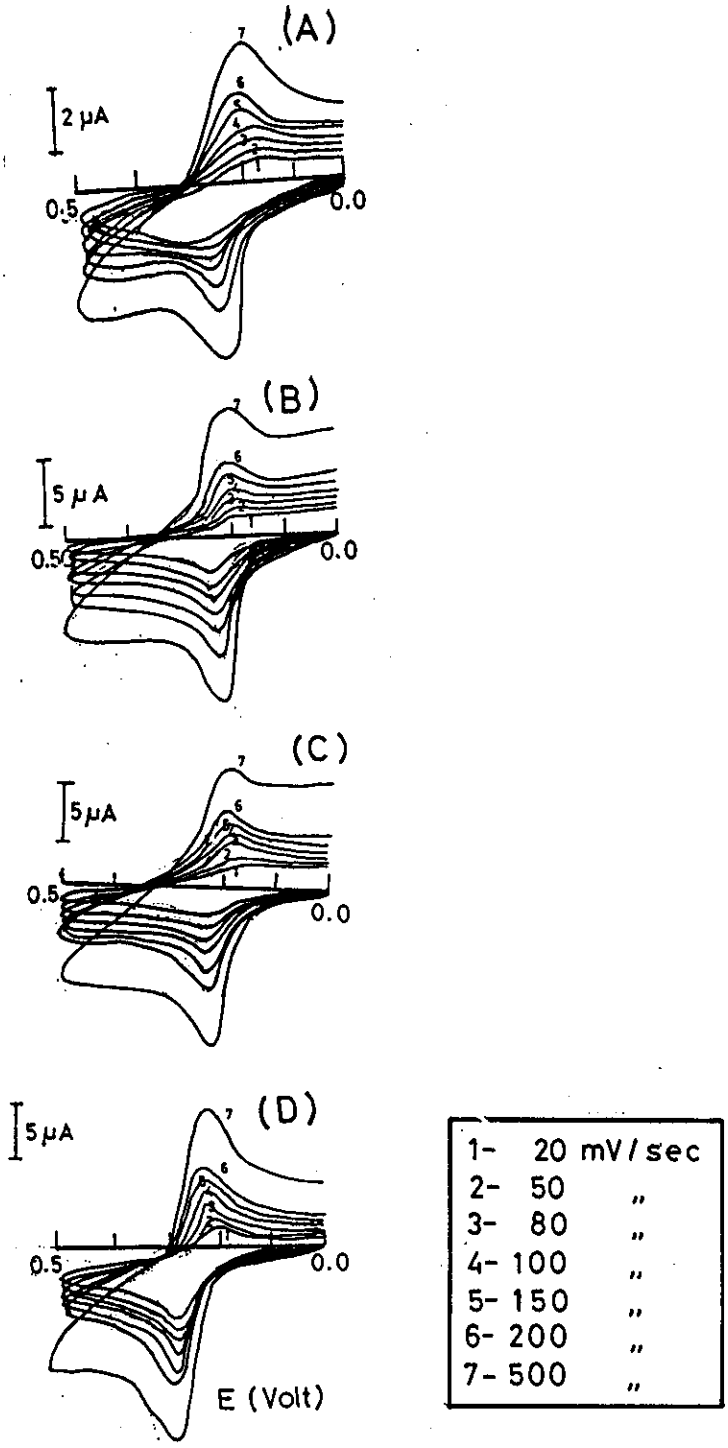

Figure 23: Cyclic voltammograms of 1mM ferrocene recorded in AOT microemulsion systems containing (a) 5.0% AOT, (b) 5.5% AOT, (c) 6.0% AOT and (d) 6.5% AOT at 25°C. The sweep rates are 20,50,80,100,150,200 and 500 mV/sec.

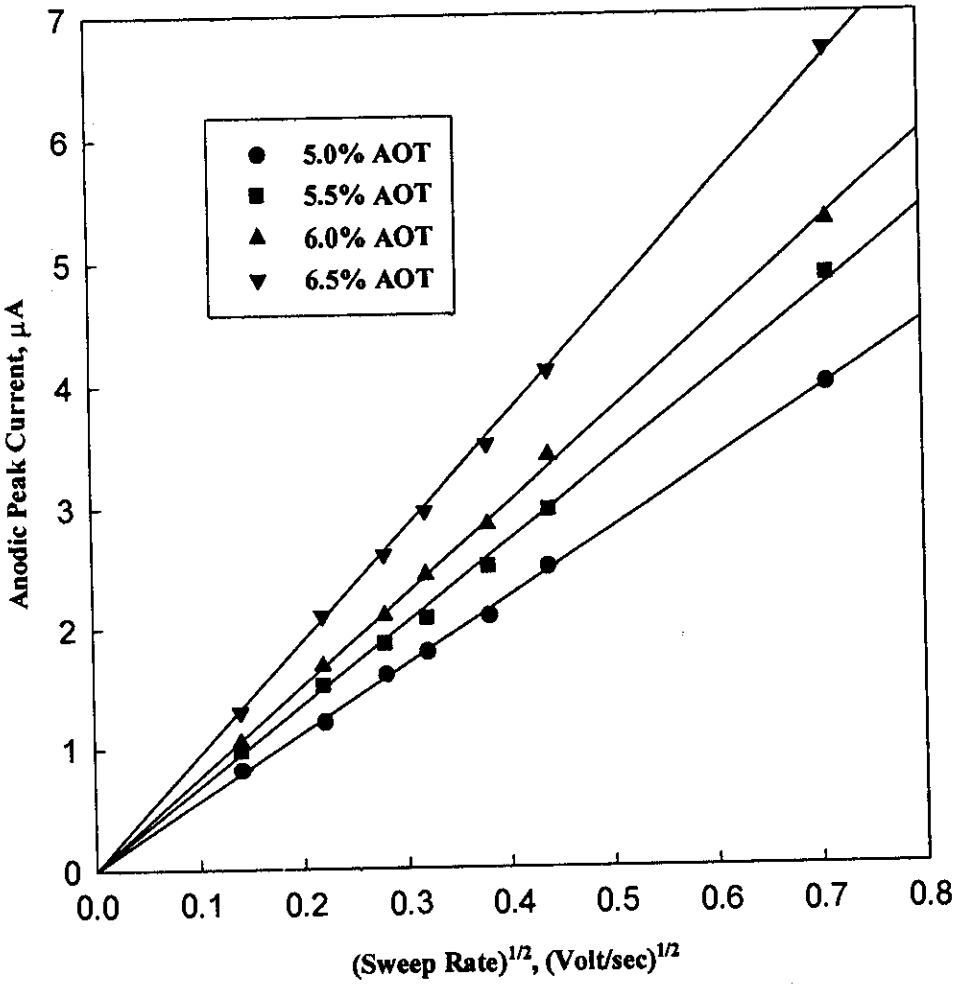

Figure 24: The plots of anodic peak currents versus ($\upsilon^{1/2}$) of 1mM ferrocene in AOT microemulsion systems containing different amounts of surfactant at a constant oil content.

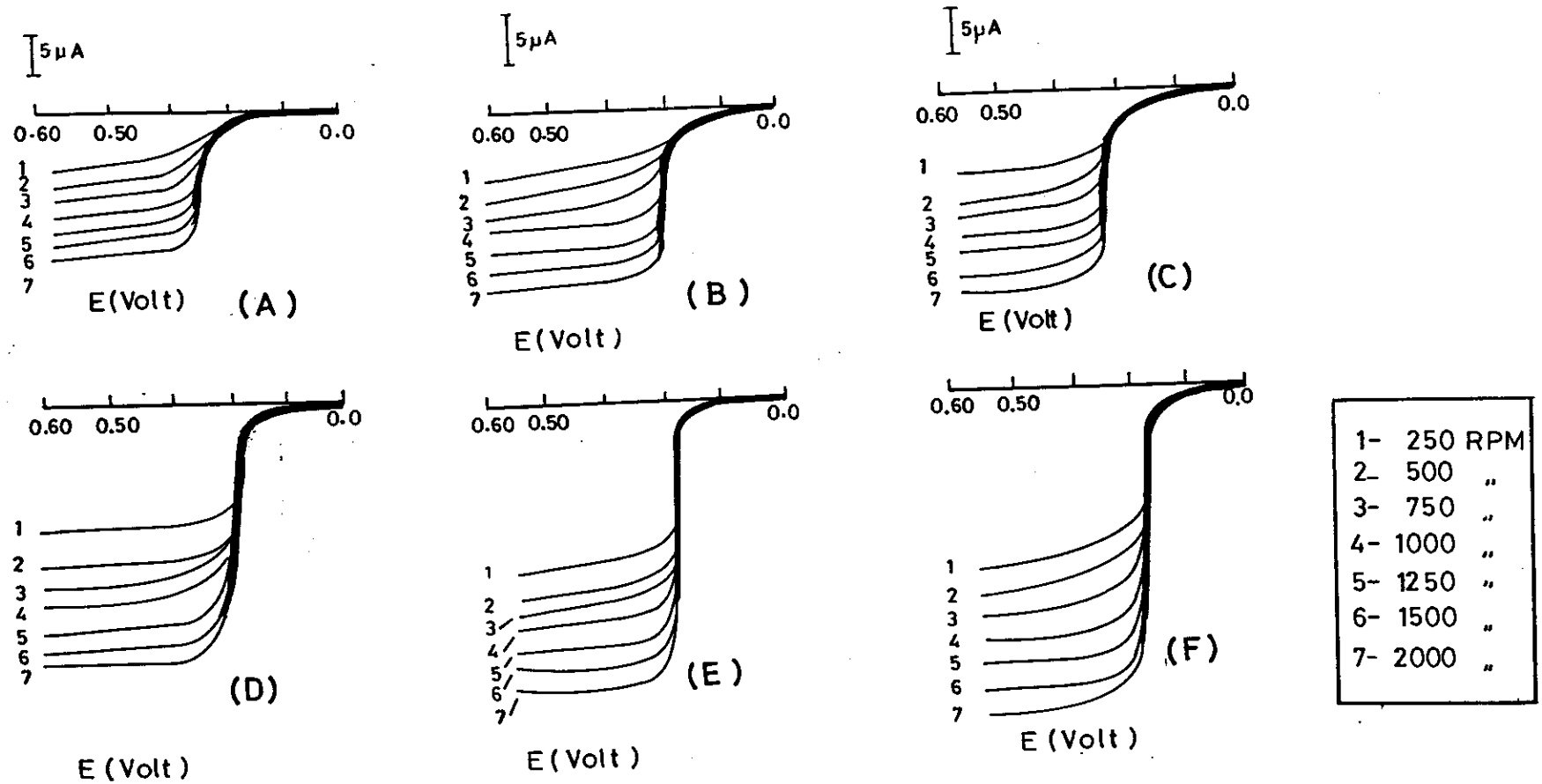

Figure 25: The effect of rotation speed of glassy carbon electrode on the linear sweep voltammograms obtained for AOT microemulsion systems containing (a) $2x10^{-4}$ M ferrocene, (b) $4x10^{-4}$ M ferrocene, (c) $8x10^{-4}$ M ferrocene, (d) $1x10^{-3}$ M ferrocene (e) $2x10^{-3}$ M ferrocene and (f) $3x10^{-3}$ M ferrocene. The rotation speeds are 250,500,750, 1000,1250,1500, and 2000 RPM.

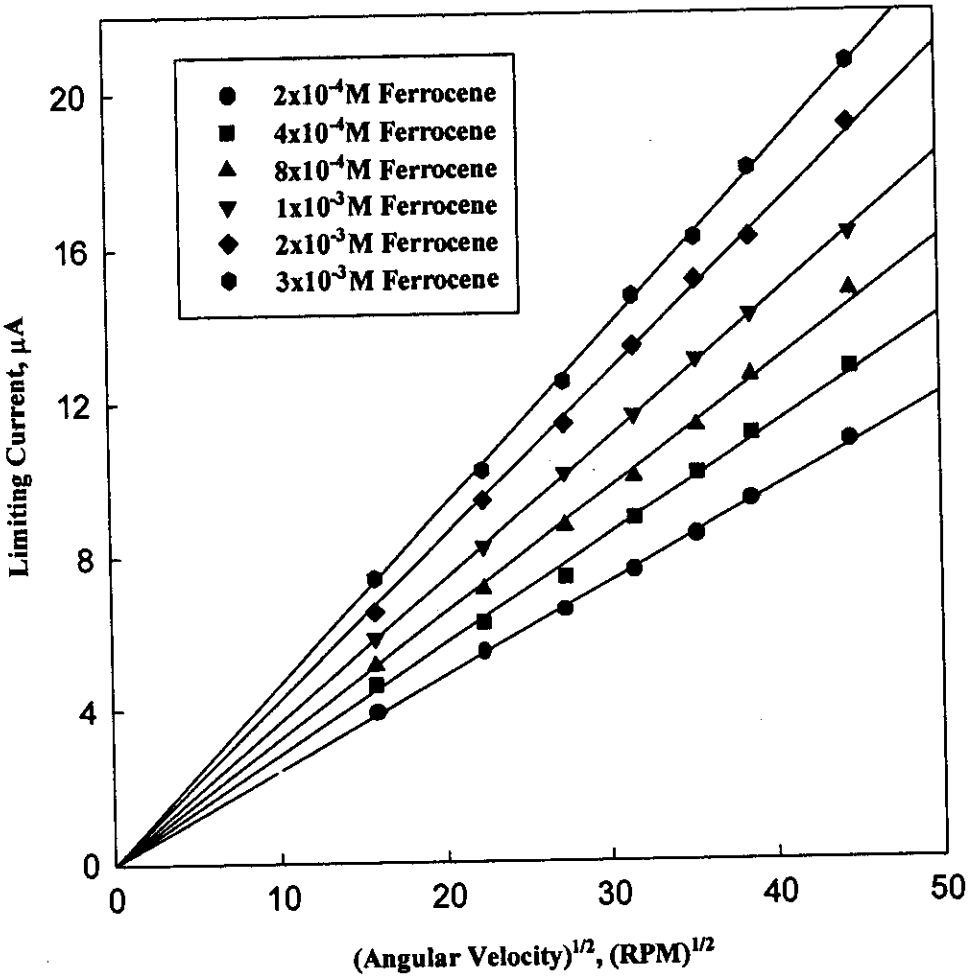

Figure 26: The plots of the limmiting current (i_l) versus the square root of angular velocity ($\omega^{1/2}$) for ferrocene in AOT microemulsion.

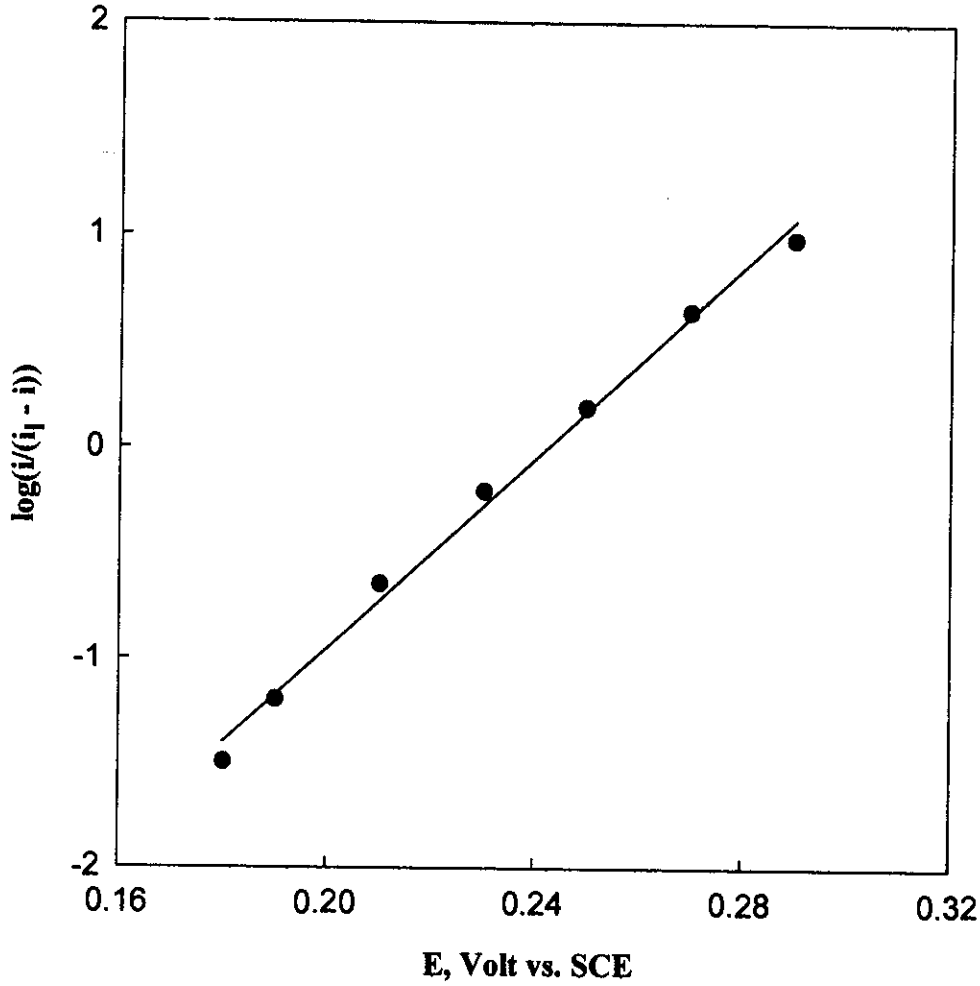

Figure 27: RDV-Logarithmic analysis of 1mM ferrocene in AOT microemulsion at 1000 RPM.

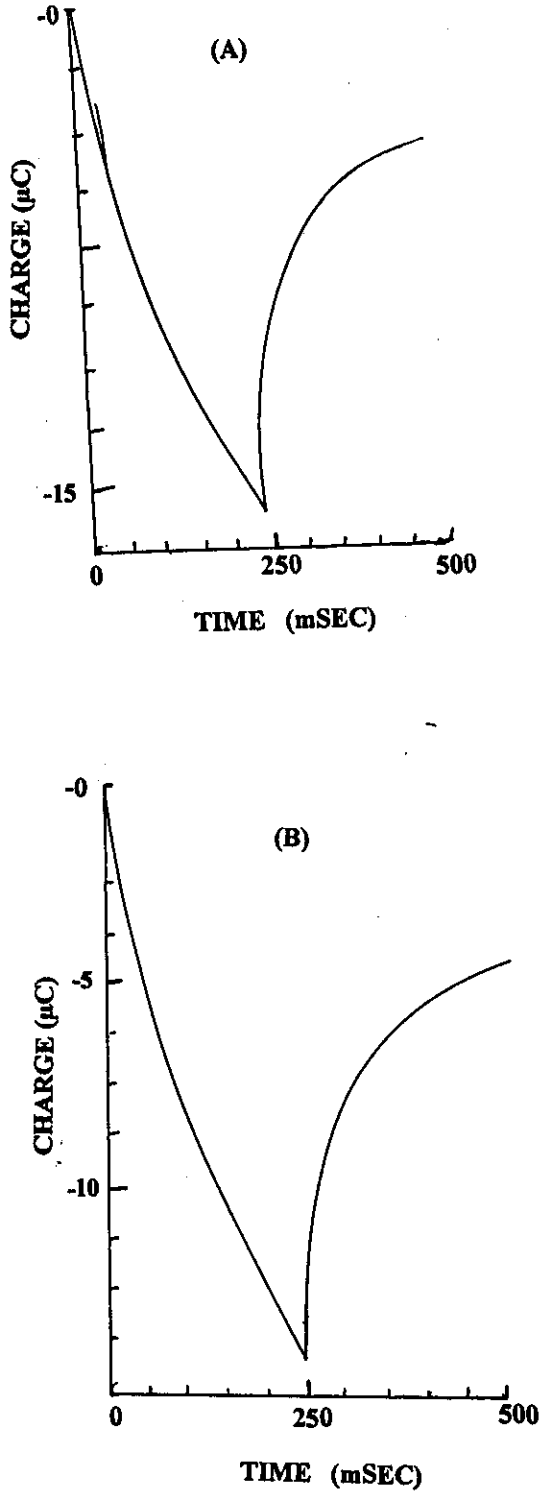

Figure 28 : Chronocoulometric responses of (a) 0.5 mM ferrocene in AOT micelle and (b) 1.0 mM ferrocene in AOT microemulsion. Charge versus time

Table 8 : Cyclic voltammetric data obtained for different concentrations of ferrocene in AOT microemulsion system at 25°C.

Sweep Rate	$E_{p,a}$	$E_{p,c}$	$I_{p,a}$	$I_{p,c}$	$I_{p,a}/I_{p,c}$	ΔE_p	$E_{1/2}$	$E_{1/2}$(average)
mV/sec	mV	mV	μA	μA	-	mV	mV	mV
(A) $2x10^{-4}$ M Ferrocene								
20	233	176	0.54	0.56	0.960	57	204	
50	233	176	0.88	0.91	0.967	57	204	
80	234	176	1.01	1.09	0.926	58	204	
100	235	177	1.20	1.30	0.923	58	206	205
150	235	177	1.50	1.70	0.882	58	206	
200	237	176	1.80	1.90	0.947	61	206	
500	244	175	2.70	2.90	0.931	61	205	
(B) $4x10^{-4}$ M Ferrocene								
20	273	181	0.79	0.80	0.989	56	209	
50	238	180	1.20	1.30	0.923	58	209	
80	238	180	1.60	1.70	0.941	58	209	
100	239	180	1.90	1.80	1.055	59	209	210
150	240	182	2.30	2.10	1.095	58	211	
200	241	184	2.50	2.60	0.961	57	212	
500	242	183	3.80	3.90	0.923	59	212	
(C) $8x10^{-4}$ M Ferrocene								
20	238	181	0.98	1.02	0.960	57	209	
50	238	181	1.40	1.40	1.000	57	209	
80	238	181	1.55	1.70	0.911	57	209	
100	240	182	2.08	2.10	0.990	58	211	211
150	241	182	2.70	2.70	1.000	59	211	
200	242	183	2.97	3.10	0.958	59	212	
500	244	185	4.87	4.80	1.014	59	214	

Follow:

Sweep Rate mV/sec	$E_{p,a}$ mV	$E_{p,c}$ mV	$I_{p,a}$ µA	$I_{p,c}$ µA	$I_{p,a}/I_{p,c}$ -	ΔE_p mV	$E_{1/2}$ mV	$E_{1/2}$(average) mV
(D) $1x10^{-3}$ M Ferrocene								
20	232	175	1.05	1.02	1.029	58	203	
50	233	177	1.60	1.85	0.864	56	205	
80	234	176	2.10	2.30	0.913	58	205	
100	235	177	2.40	2.30	1.043	58	206	206
150	237	177	2.70	2.90	0.931	60	207	
200	238	179	3.30	3.60	0.916	59	208	
500	239	180	5.30	5.60	0.946	59	209	
(E) $2x10^{-3}$ M Ferrocene								
20	245	185	1.30	1.30	1.000	60	215	
50	246	186	2.10	2.07	1.014	60	216	
80	247	188	2.60	2.70	0.962	59	217	
100	248	190	2.96	2.99	0.989	58	219	218
150	250	192	3.50	3.68	0.951	58	221	
200	251	192	4.10	4.30	0.953	59	221	
500	252	193	6.70	6.80	0.985	59	222	
(F) $3x10^{-3}$ M Ferrocene								
20	247	189	1.60	1.70	0.941	58	218	
50	248	190	2.40	2.50	0.960	58	219	
80	249	192	3.10	3.30	0.939	57	220	
100	251	191	3.50	3.60	0.972	60	221	221
150	252	193	4.20	4.30	0.976	59	222	
200	254	195	4.70	4.90	0.959	59	223	
500	255	197	7.90	8.10	0.975	58	226	

Table 9 : Diffusion coefficient and the radius of microemulsion droplets values of ferrocene in AOT microemulsion system containing 6% AOT, 3% n-decane, 4.5% n-butanol and 0.1 M NaCl.

ferrocene	(CV)		(RDV)	
Concentration	$D_a x10^{-7}$	R_b	$D_a x10^{-7}$	R_b
mM	cm^2/sec	A^o	cm^2/sec	A^o
0.2	11.70	21	10.50	23
0.4	5.56	44	5.36	34
0.8	2.13	115	2.03	114
1.0	1.85	133	1.71	130
2.0	1.30	188	1.42	172
3.0	0.94	260	1.01	242

Table 10: Cyclic voltammetric data obtained for different concentrations of Potassium ferrocyanide in AOT micremulsion system at 25°C.

Sweep Rate	$E_{p,a}$	$-E_{p,c}$	$I_{p,a}$	$I_{p,c}$	$I_{p,a}/I_{p,c}$	ΔE_p	$E_{1/2}$	$E_{1/2}$(average)
mV/sec	mV	mV	µA	µA	-	mV	mV	mV
(A) $2x10^{-4}$ M Potassium ferrocyanide								
20	521	172	2.20	2.40	0.916	693	174	
50	521	172	3.50	3.70	0.945	693	174	
80	522	171	4.70	4.50	1.044	693	175	
100	523	172	5.40	5.60	0.964	695	175	175
150	520	173	6.40	6.90	0.927	693	173	
200	524	174	7.80	8.10	0.962	698	175	
500	524	174	12.20	12.90	0.945	698	175	
(B) $8x10^{-4}$ M Potassium ferrocyanide								
20	523	174	3.60	3.88	0.927	697	174	
50	523	174	6.00	6.20	0.967	697	174	
80	524	173	7.60	7.80	0.974	697	175	
100	524	173	8.50	8.90	0.955	697	175	175
150	525	174	9.80	9.10	0.970	699	175	
200	525	174	11.26	11.90	0.946	699	175	
500	524	174	18.40	18.50	0.994	698	175	
(C) $1x10^{-3}$ M Potassium ferrocyanide								
20	526	175	4.86	4.95	0.981	701	175	
50	526	175	7.88	7.88	1.000	701	175	
80	527	178	9.80	10.40	0.942	705	175	
100	528	178	11.80	11.10	1.060	705	174	174
150	528	179	13.70	13.90	0.985	705	174	
200	527	179	16.01	16.20	0.988	706	174	
500	529	179	25.50	25.70	0.992	708	175	

Follow:

Sweep Rate	$E_{p,a}$	$-E_{p,c}$	$I_{p,a}$	$I_{p,c}$	$I_{p,a}/I_{p,c}$	ΔE_p	$E_{1/2}$	$E_{1/2}$(average)
mV/sec	mV	mV	µA	µA	-	mV	mV	mV
(D) $2x10^{-3}$ M Potassium ferrocyanide								
20	530	180	6.30	6.50	0.969	710	175	
50	530	180	9.50	9.60	0.989	710	175	
80	531	181	12.01	12.30	0.976	712	175	
100	532	181	13.80	13.90	0.992	713	175	175
150	532	182	16.60	16.70	0.994	714	175	
200	533	182	19.20	19.10	1.005	715	175	
500	533	183	30.80	31.10	0.990	716	175	
(E) $3x10^{-3}$ M Potassium ferrocyanide								
20	535	184	8.30	8.40	0.988	719	175	
50	535	184	13.40	13.60	0.985	719	175	
80	534	185	16.90	17.10	0.988	719	174	
100	534	185	19.50	19.60	0.994	719	174	174
150	536	187	23.01	23.20	0.991	723	174	
200	536	188	26.75	26.80	0.998	724	174	
500	536	189	42.85	42.92	0.998	725	173	

Table 11 : Diffusion coefficient and the radius of microemulsion droplets values of potassium ferrocyanide in AOT microemulsion system containing 6% AOT, 3% n-decane, 4.5% n-butanol and 0.1 M NaCl using cyclic voltammetry.

$K_4[Fe(CN)_6]$ Concentration mM	$D_a x10^{-7}$ cm^2/sec	R_h A°
0.2	13.70	17.9
0.8	19.90	12.3
1.0	15.10	16.2
2.0	14.10	17.4
3.0	9.97	24.6

Table12: Cyclic voltammetric data obtained for 1mM ferrocene in AOT microemulsion systems contaning different amounts of n-Decane at 25°C.

Sweep Rate	$E_{p,a}$	$E_{p,c}$	$I_{p,a}$	$I_{p,c}$	$I_{p,a}/I_{p,c}$	ΔE_p	$E_{1/2}$
mV/sec	mV	mV	μA	μA	-	mV	mV
(A) 2.0% n-Decane							
20	277	217	2.89	2.87	1.006	60	247
50	277	217	3.45	3.51	0.982	60	247
80	277	217	3.65	3.96	0.921	60	247
100	277	217	4.59	4.57	1.004	60	247
150	274	214	6.40	6.50	0.984	60	244
200	274	214	7.68	7.50	1.024	60	244
500	271	204	11.30	11.24	1.005	67	237
(B) 2.5% n-Decane							
20	277	218	2.82	2.74	1.029	59	247
50	278	221	3.39	3.41	0.994	57	249
80	278	221	3.68	3.91	0.941	57	249
100	278	222	4.58	4.59	0.997	56	250
150	282	225	6.43	6.54	0.983	57	253
200	283	225	7.67	7.52	1.019	58	254
500	284	226	11.32	11.26	1.005	58	255

Follow:

Sweep Rate	$E_{p,a}$	$E_{p,c}$	$I_{p,a}$	$I_{p,c}$	$I_{p,a}/I_{p,c}$	ΔE_p	$E_{1/2}$
mV/sec	mV	mV	μA	μA	-	mV	mV
(A) 3.0% n-Decane							
20	283	221	2.72	2.77	0.978	62	252
50	283	222	3.31	3.21	1.031	61	252
80	284	221	3.51	3.56	0.985	63	252
100	287	224	4.43	4.37	1.013	63	255
150	287	224	6.21	6.10	1.018	63	255
200	287	221	7.54	7.50	1.005	66	254
500	297	221	11.12	11.04	1.007	76	259
(B) 3.5% n-Decane							
20	326	256	2.65	2.64	1.003	70	291
50	326	256	3.30	3.34	0.988	70	291
80	327	257	3.48	3.47	1.002	70	292
100	327	257	4.39	4.35	1.009	70	292
150	324	257	6.10	6.14	0.993	67	290
200	324	254	7.42	7.41	1.001	70	289
500	331	244	11.02	11.08	0.994	87	287

Table13: Cyclic voltammetric data obtained for 1mM ferrocene in AOT microemulsion system contaning different concentrations of NaCl at 25°C.

Sweep Rate	$E_{p,a}$	$E_{p,c}$	$I_{p,a}$	$I_{p,c}$	$I_{p,a}/I_{p,c}$	ΔE_p	$E_{1/2}$	$E_{1/2}$(average)
mV/sec	mV	mV	µA	µA	-	mV	mV	mV
(A) 0.08M NaCl								
20	203	149	1.46	1.50	0.973	54	176	
50	204	149	2.20	2.40	0.916	55	176	
80	204	149	2.90	2.90	1.000	55	176	
100	204	149	3.29	3.49	0.942	55	176	176
150	198	150	3.79	3.83	0.989	48	174	
200	198	150	4.40	4.84	0.909	48	174	
500	207	156	6.99	6.98	1.001	51	181	
(B) 0.10M NaCl								
20	220	162	1.05	1.08	0.972	58	191	
50	221	163	1.66	1.92	0.864	58	192	
80	220	162	2.10	2.11	0.990	58	191	
100	220	162	2.43	2.65	0.916	58	191	192
150	220	162	2.84	2.80	1.014	58	191	
200	220	171	3.40	3.64	0.934	49	195	
500	225	171	5.30	5.17	1.025	54	198	
(C) 0.12M NaCl								
20	234	177	0.74	0.83	0.891	57	205	
50	234	177	1.15	1.20	0.958	57	205	
80	235	176	1.54	1.68	0.916	59	205	
100	235	176	1.76	1.91	0.921	59	205	205
150	235	177	2.10	2.18	0.963	58	206	
200	235	179	2.50	2.52	0.992	56	207	
500	235	179	3.90	3.84	1.015	56	207	

Table 14 : Diffusion coefficients and the radius of microemulsion droplets of 1 mM ferrocene in AOT microemulsion system containing 6% AOT, 3% n-decane, 4.5% n-butanol at different concentrations of NaCl using CV.

NaCl Concentration mM	$D_a x10^{-7}$ cm^2/sec	R_h A°
0.08	3.07	80
0.10	1.85	133
0.12	1.36	181

Table 15 : Diffusion coefficients and the radius of microemulsion droplets of 1 mM ferrocene in AOT microemulsion system containing 6% AOT, 3% n-decane, 4.5% n-butanol at different concentrations of surfactant using CV.

%AOT	$D_a x10^{-7}$ cm^2/sec	R_h A°
5.0	1.14	215
5.5	1.36	181
6.0	1.85	133
6.5	2.43	101

3.4 Electrochemical Characterization of C_{18}DMB Surfactant

3.4.1 Voltammetric Detection of Micelles

The electrochemical techniques are successfully used for the determinations of the critical micelles concentration (CMC) of zwitterionic surfactant octadecyldimethyl betaine (C_{18}DMB) as well as solublization studies. Three different electrochemical techniques were used. Such techniques used are cyclic voltammetry (CV), rotating disk voltammetry (RDV) and chronocoulametry (CC).

A. Cyclic voltammetry (CV)

Cyclic voltammetric behaviour of $7x10^{-5}$ M of ferrocene as hydrophobic probe was recorded in zwitterionic C_{18}DMB surfactant of different concentrations containing indifferent supporting electrolyte, 0.1M NaCI. The surfactant concentration was varied from 0.05% to 1.2% (wt./wt.). The voltammograms were recorded in the potential window from 0.0 to 500 mV versus SCE at different potential sweep rates varying from 20 to 500 mV/sec. The voltammograms obtained showed one anodic and one cathodic peaks on the anodic and cathodic sweeps as represented in Fig (29). The anodic peak current, $I_{p,a}$ and the cathodic peak current, $I_{p,c}$ are almost of equal heights and the ratio of $I_{p,a}/I_{p,c}$ does not exceed 1.040 at different sweep rates in all media, Table (16). The peak potential separation $\Delta E_p = (E_{p,a} - E_{p,c})$ is almost around the theoretical value for one-electron transfer in C_{18}DMB micelles ~ (56-60) mV. These results indicate that the electrochemical oxidation of ferrocene (Fc) is a reversible one electron transfer process forming ferrocenium ion (Fc^+). The voltammograms recorded at different sweep rates are essentially similar and showed one reversible peak. The constancy of peak potential

separation (ΔE_p) on inceasing the sweep rate is further confirmed the reversible one-electrone transfer process.

On using Randless-Sevcik equation [140] the plots of anodic peak current ($I_{p,a}$) versus square root of sweep rate ($\upsilon^{1/2}$) gives straight lines intersecting the origin at all surfactant concentrations Fig. (30). These results indicate that the electrode process is diffusion controlled [117].

The plots of $I_{p,a}$ versus surfactant concentration showed linear correlation consisting of two segments, Fig. (31a). The CMC of C_{18}DMB is determined at the point at which the breaks occur. At CMC the solution changes from surfactant solution (true solution) to aggregates (micelles). The CMC was then obtained at 0.2% of C_{18}DMB in 0.1 M NaCl.

The CMC was further confirmed from the plots of the peak potential shift ($E_{p,a}$)versus surfactant concentration, where variations are attributed to structural changes and found to equal 0.2% of C_{18}DMB, as represented from Fig. (31b).

B. Rotating disk voltammetry (RDV)

On using RDV method, $7x10^{-5}$ M ferrocene electroactive probe was added to a series of surfactant solutions of different concentrations containing 0.1M NaCl as supporting electrolyte at 40°C. The concentration of C_{18}DMB was varied in the range from 0.05% to 1.2% (wt./wt.). The effect of rotation speed (ω) on the voltammograms of ferrocene was recorded at angular velocity varying from 250 to 2000 RPM at small sweep rate, 5 mV/sec. The rotating disk voltammograms that recorded at different C_{18}DMB concentrations showed decrease in the limiting current (i_l) values, Fig. (32). The limiting current (i_l) was measured at the steady state at 400 mV.

On using Levich equation [133], the plots of i_l versus $\omega^{1/2}$ of ferrocene at different C_{18}DMB concentrations showed linear correlations passing through the origin were obtained as represented in Fig.(33). This behaviour confirming that the oxidation process is under mass transfer control. The slope values were used to estimate the apparent diffusion coefficients (D_a).

On increasing the rotation speed (ω), the half wave potential ($E_{1/2}$) of the rotating disk voltammograms was constant indicating the reversibility of ferrocene oxidations. Furthermore, on using the following relationship [117].

$$E = E_{1/2} + \frac{RT}{nF} \ln \frac{(i_l - i)}{i}$$

The logarithmic analysis of the RDV voltammograms were used for testing the thermodynamic reversibility. By plotting log (i/i_l-i) versus E at 1000 RPM and different surfactant concentrations, linear correlations were obtained, Fig. (34). The slopes of the linear plots were found amounting to 58 mV indicating the single electron transfer process.

Generally, it was found that on increasing the C_{18}DMB concentration the limiting current is slightly decreased up to concentration 0.2% a significant decrease was observed on the limiting current values. At concentrations beyond that point, i_l is slightly decreased again. From equation (III.7), the CMC was determined from the plots of the ratio of slopes (S/S_o) against the logarithm of surfactant concentration. Where S_o is the slope of the i_l versus $\omega^{1/2}$ of ferrocene at zero surfactant concentration " i.e pure aqueous solution" and S is the slope of i_l versus $\omega^{1/2}$ at different concentrations of C_{18}DMB surfactant. An S-shapped curve was obtained as shown in Fig.(35). The use of the ratio (S/S_o) is to avoid the fluctuation in the probe concentration. The

inflection point on the curve indicate the critical micelle concentration and it was found to equal 0.2% C_{18}DMB.

3.4.2 Solubilization Studies of Ferrocene in C_{18}DMB Micelles

The rotating disk voltammograms of ferrocene in C_{18}DMB micelles were recorded at different concentrations of surfactant containing 0.1M NaCl at 40°C. The surfactant concentration was varied in the range from 0.2% to 2.0% (wt./wt.) where beyond this concentration it becomes gel. Ferrocene was used as the hydrophobic electroactive probe, its concentration used is very close to the saturation concentration in each micellar solution. The amount of ferrocene solubilized in C_{18}DMB micelles were determined via spectrophotometric technique. The spectral measurements were performed in the UV-visible range at wavelengths λ = 350 and 440 nm. The absorbance values obtained for ferrocene solubilized at different surfactant concentrations were compared with the calibration graph of ferrocene in pure ethanol, Fig. (9a,9b). Using Beer's-lamber law, the concentration of ferrocene solubilized surfactant was determined at ϵ = 92.3 and listed in Table (17).

The recorded voltammograms at ferrocene saturated solutions in different C_{18}DMB concentrations were given in Fig. (36). Since ferrocene is hydrophobic in nature and its solubility in the aqueous phase at 0.1M NaCl is $5x10^{-5}$ M with diffusion coefficient equal to $6.7x10^{-6}$ cm^2s^{-1} [34], this diffusion coefficient is higher than the real diffusion coefficients of micelles. The diffusion coefficients obtained directly from the electrochemical experiments represent apparent values. Where the diffusion current for the electrooxidation of ferrocene measured in micellar solutions has significant contribution due to the oxidation of fast diffusing ferrocene present in the aqueous phase apart from the oxidation of ferrocene present in the more

slowly diffusing micelles. Fig.(37) showed the plots of limiting currents (i_l) of ferrocene in C_{18}DMB micelles versus ($\omega^{1/2}$). It showed straight lines intersecting the origin. The apparent diffusion coefficients (D_a) were estimated from the RDV measurements using Levich equation [133] and the values were given in Table (17). Inspection of the values of D_a is therfore higher than the real micelles diffusion coefficients. Corrections could be made to obtain a better estimate of the actual micelle diffusion coefficient as well as its real size by knowing the relative concentrations of ferrocene in the aqueous phase and in the micellar pseudo-phase. The redox behaviour of ferrocene as the hydrophobic probe was treated depending on the exit-entrance rate using two methods of treatments [38,152] slow rate which termed as zero-kinetics and fast-rate.

The corrections were made using the procedure of zero-kinetics limiting equation developed for partitioning of solutes from rotating disk voltammetry [38]. The values of the diffusion coefficients in the discontinuous pseudo-phase (D_d) were calculated at different C_{18}DMB concentrations using equation (III.9) and listed in Table (17) .

On using equation (III.10) treating the mode of exit-entrance rate of ferrocene-surfactant solution at the electrode surface as fast-kinetic approximation [152], the apparent diffusion coefficient (D_a) obtained from Levich equation was then corrected. The corrected values according to this approximation was found to be smaller than the zero-kinetics. The measured (D_a) and the corrected (D_d) diffusion coefficient values for C_{18}DMB micelles obtained by both methods are summarized in Table (17).

The plots of D_a and D_d "obtained by the above two mentioned methods" against the surfactant concentration is represented in Fig. (38). The plots showed that, the diffusion coefficients D_a and D_d were sharply decreased

before the critical micelles concentration then becomes nearly constant as the surfactant concentration is increased. Inspection of the values of D_d indicated that the micellar size is becomes nearly constant by increasing the surfactant concentration and the morphological features revealed that C_{18}DMB is spherical in shape and not rod-like.

3.4.3 Effect of salt on C_{18}DMB micelles

The effect of salt concentration on the voltammetric behaviour of 0.5 mM ferrocene solubilized in 1.2% C_{18}DMB zwitterionic surfactant was recorded using cyclic voltammetry at 40°C. The cyclic voltammograms were recorded at different scan rates varying from 20 to 500 mV/sec. The voltammograms were recorded in surfactant solutions of different NaCl concentrations at 0.10, 0.16, 0.62 and 1.00 M and represent in Fig. (39). The voltammetric data obtained at different salinity concentrations were listed in Table (18). The obtained results showed decrease in the peak current whereas the peak potentials were shifted to more positive values on increasing NaCl concentration.

The plots of anodic peak current ($I_{p,a}$) versus square root of sweep rate ($\upsilon^{1/2}$) of 0.5 mM ferrocene in 1.2% (wt./wt.) C_{18}DMB micelles at different NaCl concentrations showed linear correlations passing through the origin, Fig. (40). The slopes of the linear plots were used to estimate the apparent diffusion coefficients using Randless-Sevcik equation [140]. The data listed in Table (19) showed that the micellar diffusion coefficient (D_d) is gradually decreases while the half-wave potential $E_{1/2}$ for the oxidation of ferrocene in micellar solutions increases linearly, Fig. (41). This behaviour could be explained from the reversible behaviour of ferrocene in these media using

Nernst equation [117] for reversible electrochemical reactions which was given as following:

$$E_{1/2} = E^{o} + RT/nF \ln (D_O/D_R)^{1/2} \qquad \text{(III.18)}$$

The rotating disk voltammetry (RDV) gave the same result obtained from cyclic voltammetry. The voltammograms showed a decrease in the limiting currents on increasing NaCl concentration as represented in Fig.(42) Fig. (43) showed the plots of limiting current (i_l) versus square root of angular velocity ($\omega^{1/2}$). The measured diffusion coefficients estimated from RDV measurements using the Levich equation are in agreement with those obtained from CV, Table (19).

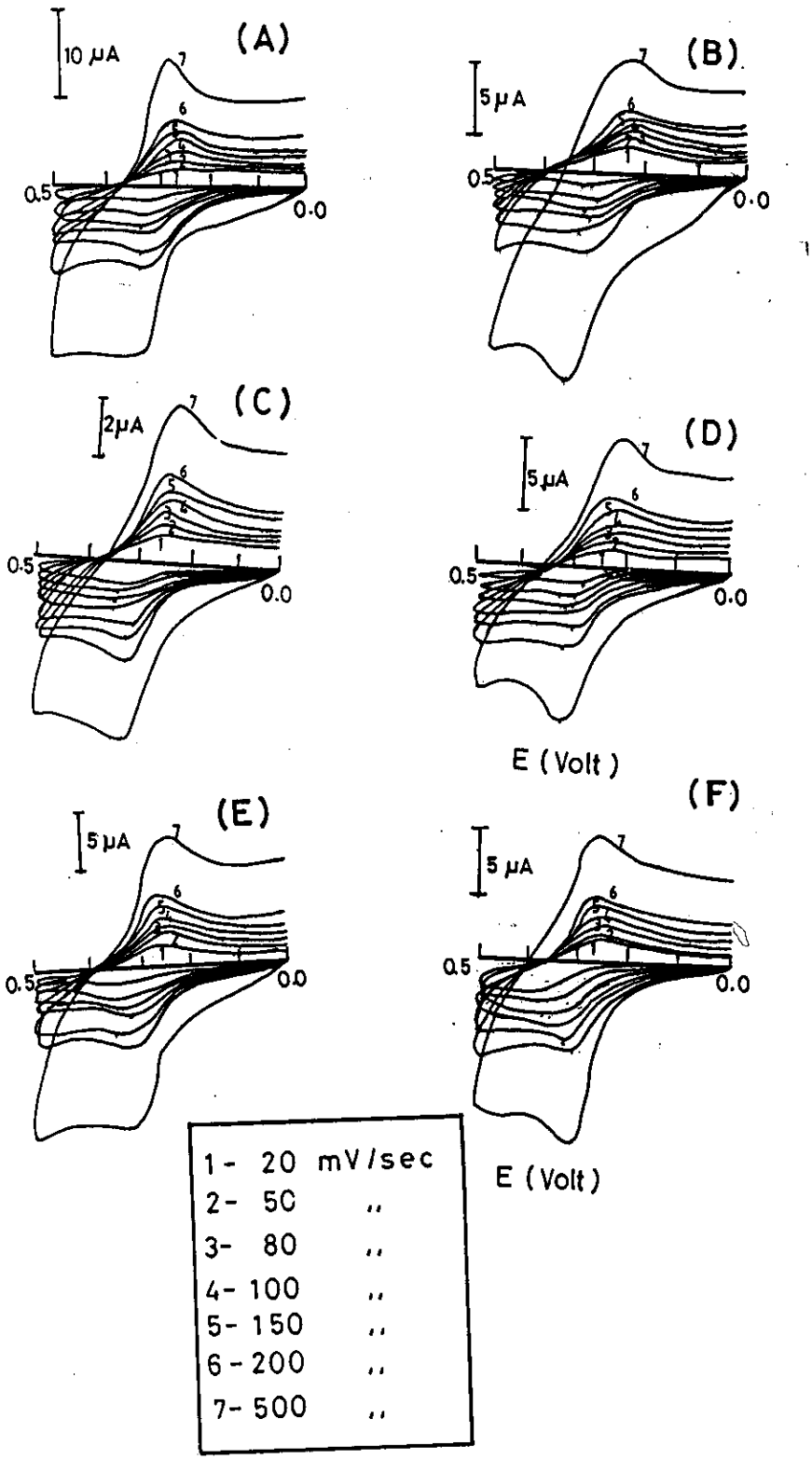

igure 29: Cyclic volltammograms of $7x10^{-5}$ M ferrocene in C_{18}DMB micellar olutions containing (a) 0.05% C_{18}DMB, (b) 0.10% C_{18}DMB, (c) 0.20% C_{18}DMB, (d) 0.50% C_{18}DMB, (e) 0.70% C_{18}DMB and (f) 1.20% C_{18}DMB, at 5°C. The sweep rates are 20,50,80,100,150,200 and 500 mV/sec.

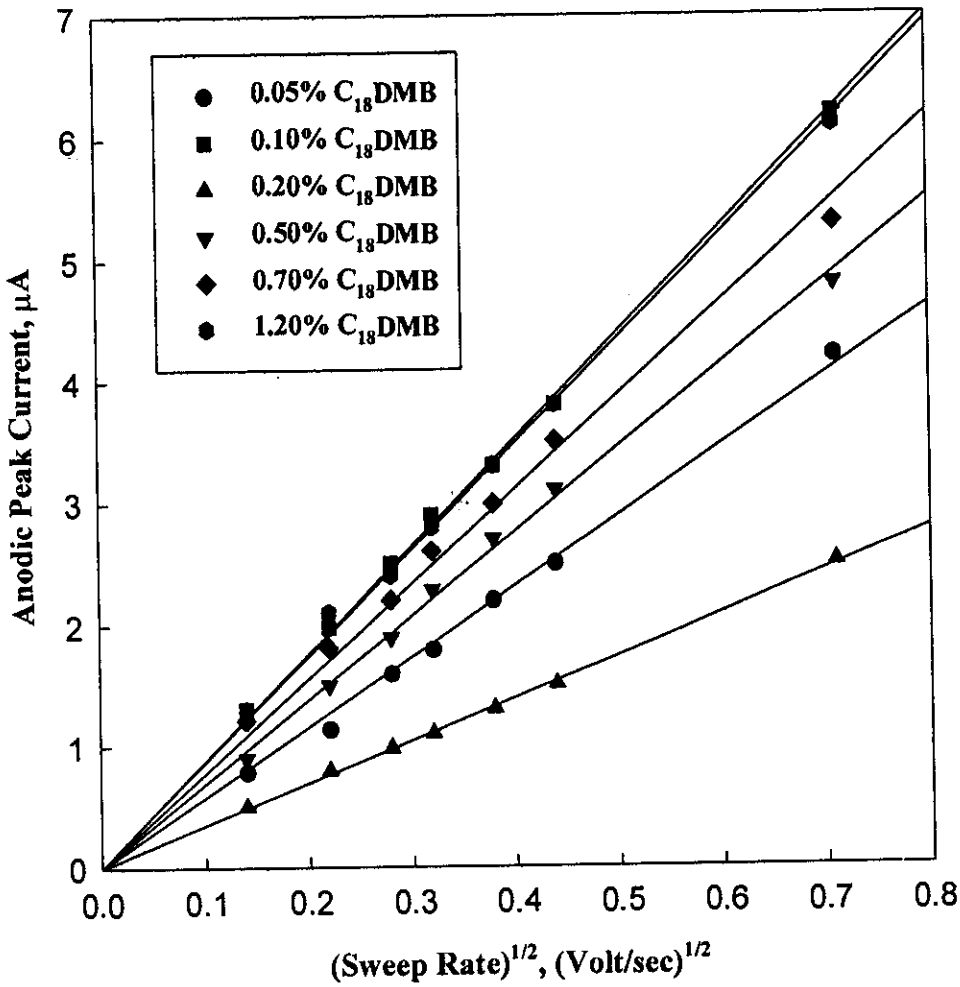

Figure 30: The plots of anodic peak currents versus ($\upsilon^{1/2}$) of $7x10^{-5}$ M ferrocene in C_{18}DMB micellar solutions at $40^{o}C$.

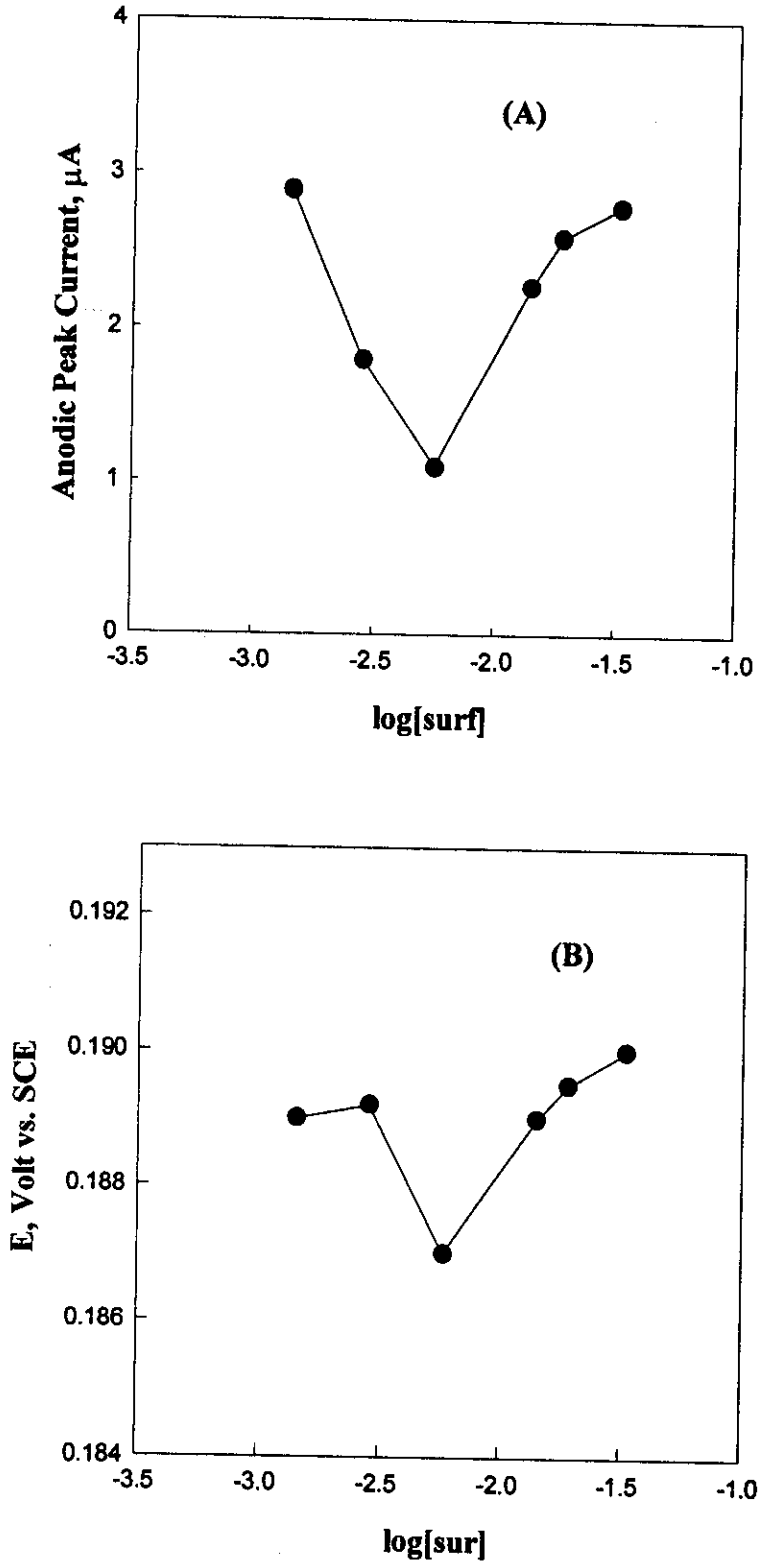

Figure 31 :The plots of (a) anodic peak currents (b) anodic peak potentials of ferrocene in C_{18}DMB micellar solutions at 100 mV/sec againts the logarithm of surfactant concentration at 40^{o}C.

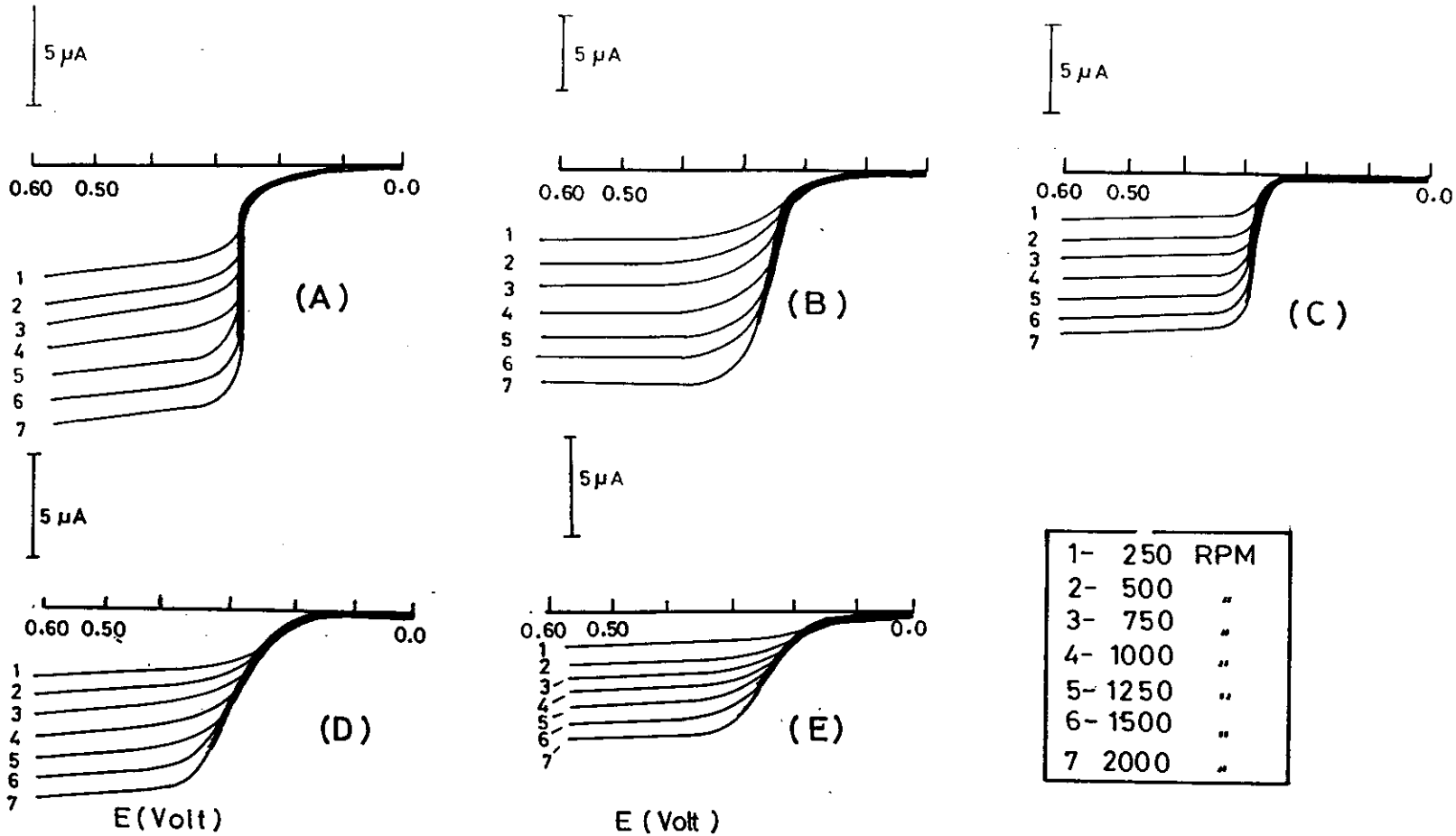

Figure 32: The effect of rotation speed of glassy carbon electrode on the linear sweep voltammograms obtained for $7x10^{-5}$ M ferrocene in C_{18}DMB micellar solutions containing (a) 0.05% C_{18}DMB, (b) 0.10% C_{18}DMB, (c) 0.20% C_{18}DMB, (d) 0.50% C_{18}DMB, and (e) 1.20% C_{18}DMB. The rotation speed are 250,500,750,1000,1250,1500 and 2000 RPM .

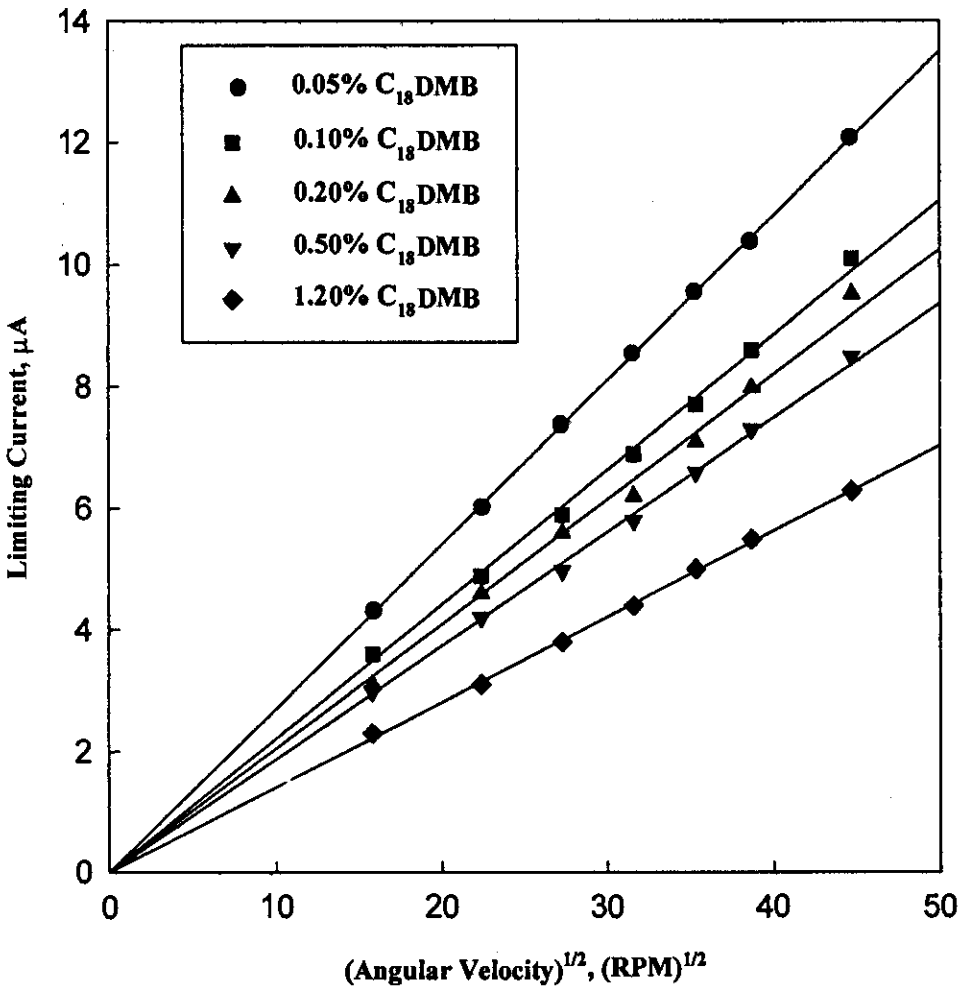

Figure33: The plots of limiting current (i_l) versus the square root of angular velocity ($\omega^{1/2}$) for $7x10^{-5}$ M ferrocene in C_{18}DMB micellar solutions of different surfactant concentrations at 40^{o}C.

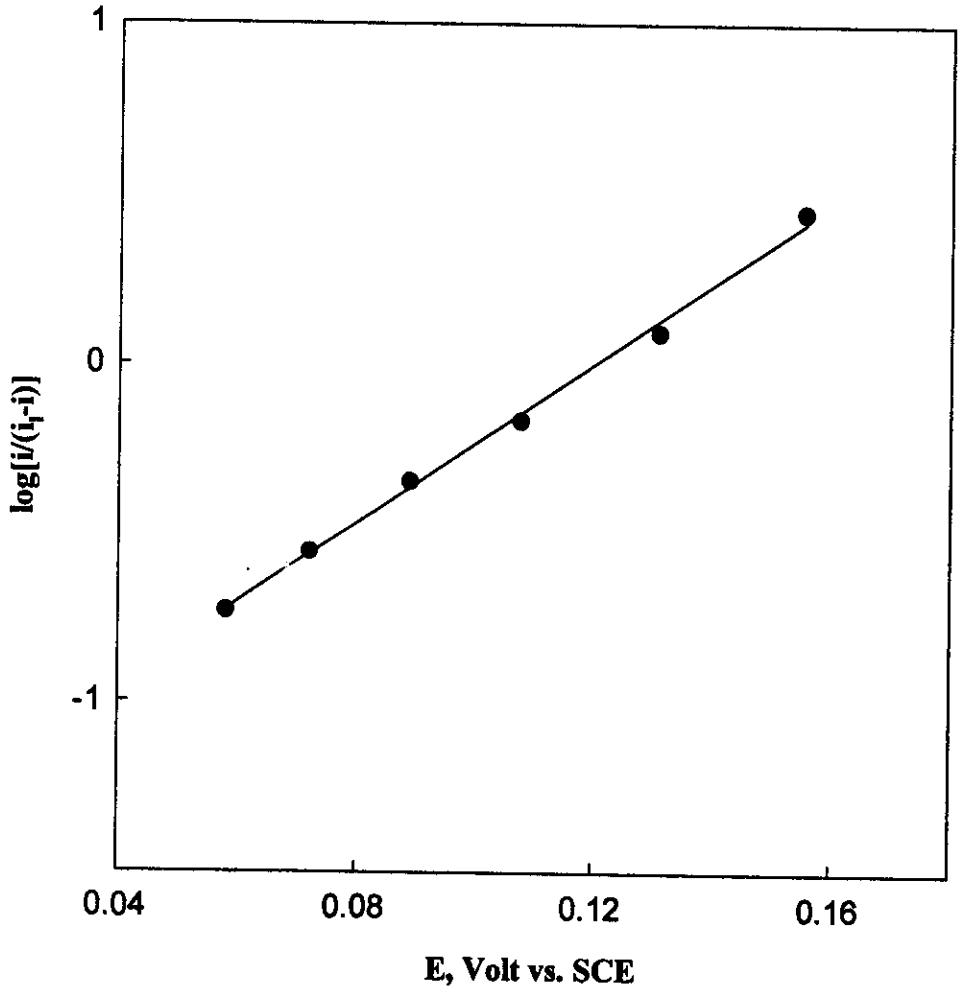

Figure 34: RDV-Logarithmic analysis of $7x10^{-5}$ M ferrocene in 0.20% C_{18}DMB micellar solution at 1000 RPM.

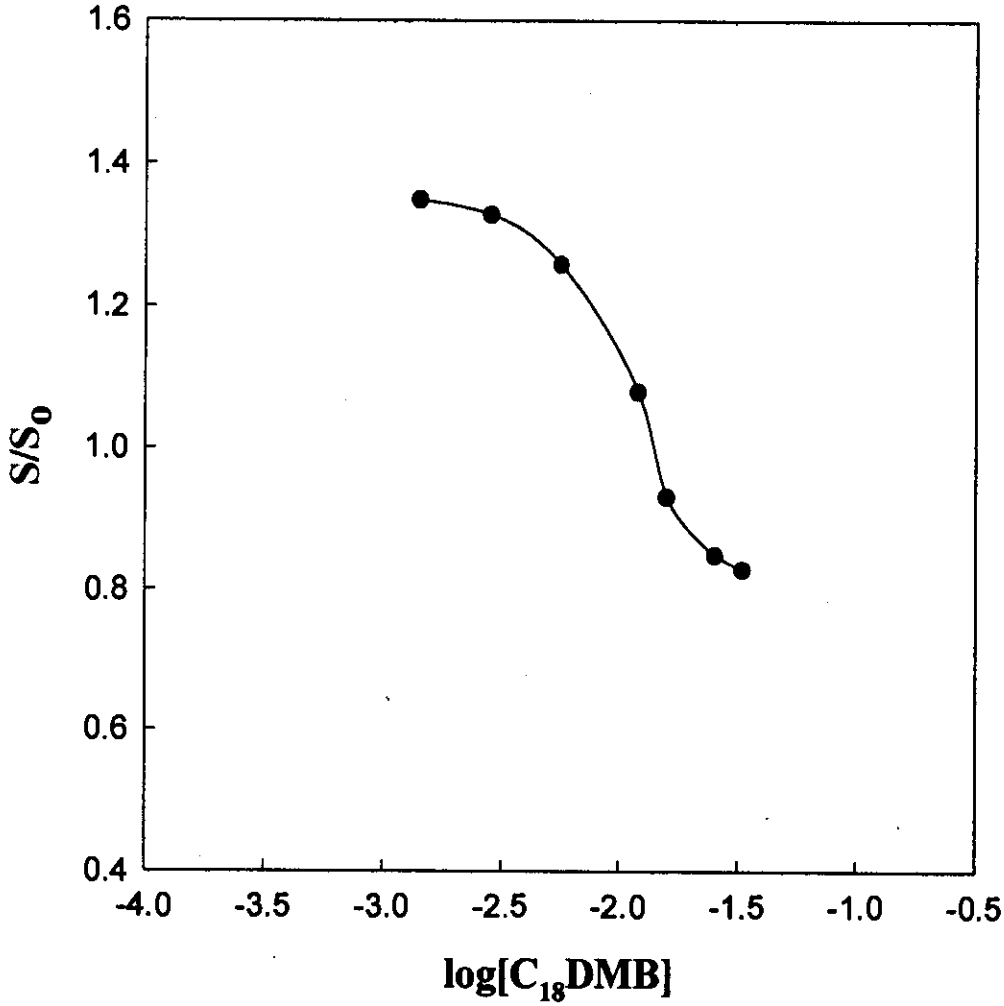

Figure 35: The plots of the ratio of slopes of i_l versus $\omega^{1/2}$ obtained from aqueous and in C_{18}DMB micellar solutions (S/S_O) againts the logarithm of surfactant concentration.

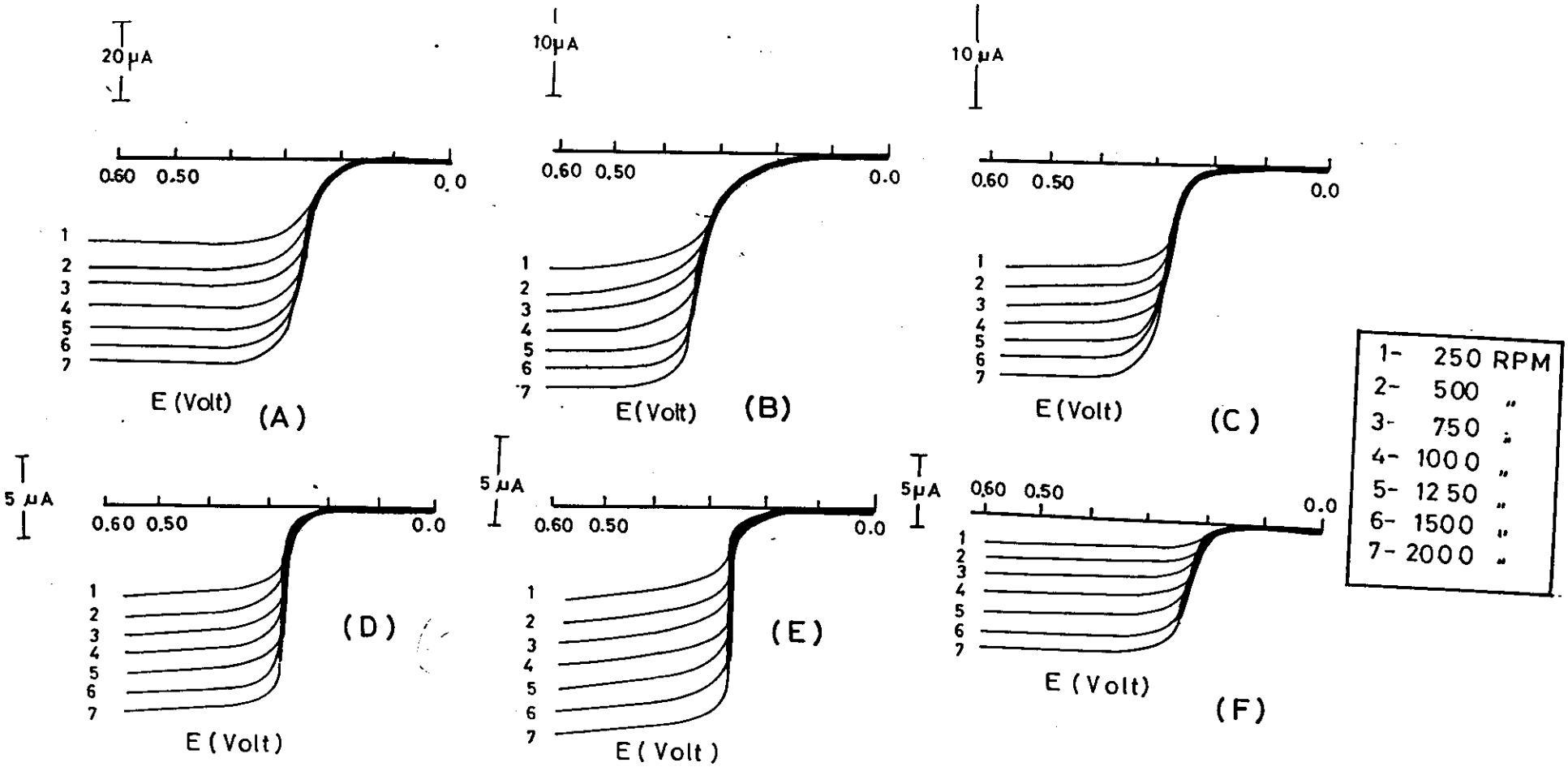

Figure 36: The effect of rotation speed of glassy carbon electrode on the linear sweep voltammograms obtained for solubilized ferrocene in C_{18}DMB micellar solutions containing, (a) 0.20% C_{18}DMB, (b) 0.70% C_{18}DMB, (c) 0.90% C_{18}DMB, (d) 1.20% C_{18}DMB, (e) 1.50% C_{18}DMB and (f) 2.00% C_{18}DMB. The rotation speed are 250,500,750, 1000,1250,1500 and 2000 RPM.

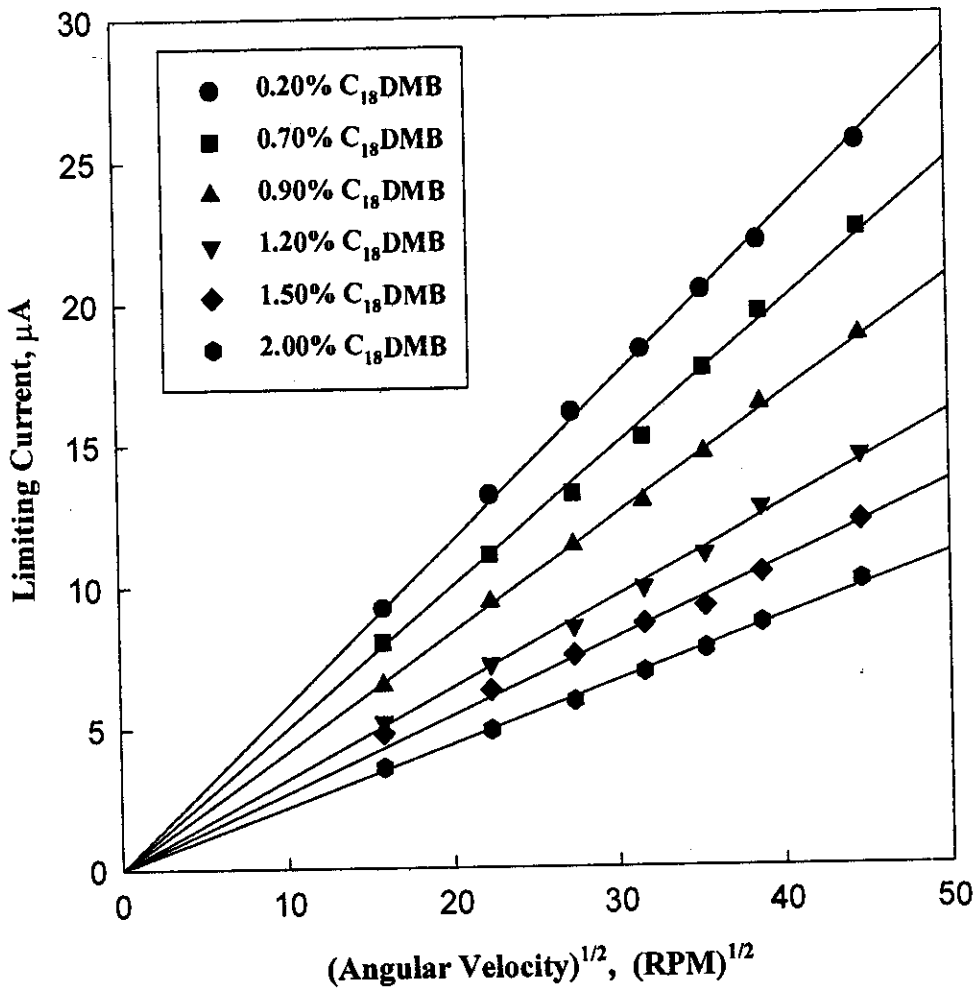

Figure 37: The plots of limiting currents (i_l) versus square root of angular velocity ($\omega^{1/2}$) of solubilized ferrocene in C_{18}DMB micellar solutions at 40^{o}C.

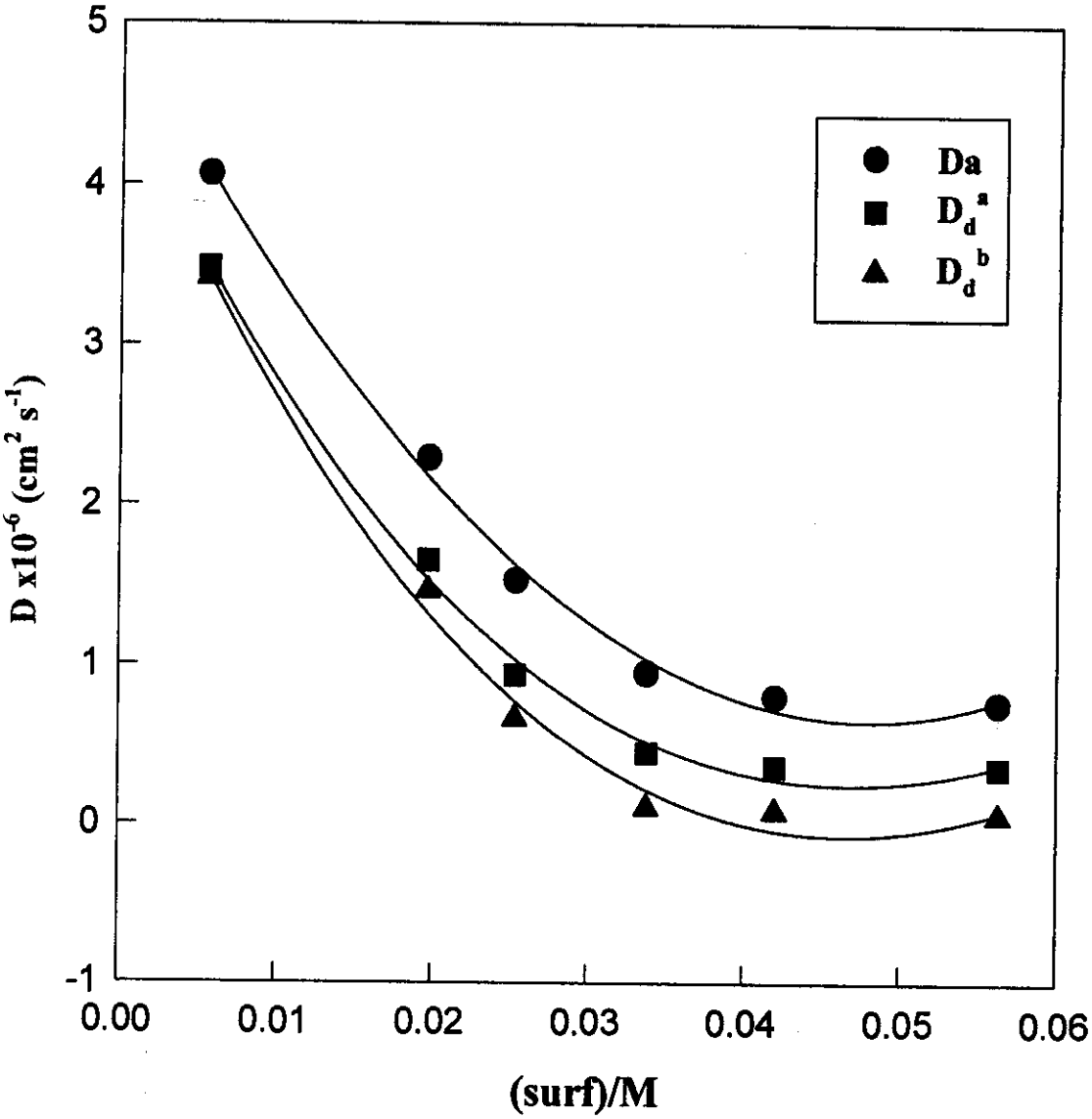

Figure 38: The plots of diffusion coefficients of solubilized ferrocene in C_{18}DMB micellar solutions againts surfactant concentrations, where (D_a) is the apparent diffusion coefficient, (D_d^a) and (D_d^b) are the corrected diffusion coefficients calculated in zero-kinetics approximation and in fast-kinetic limit, respectively.

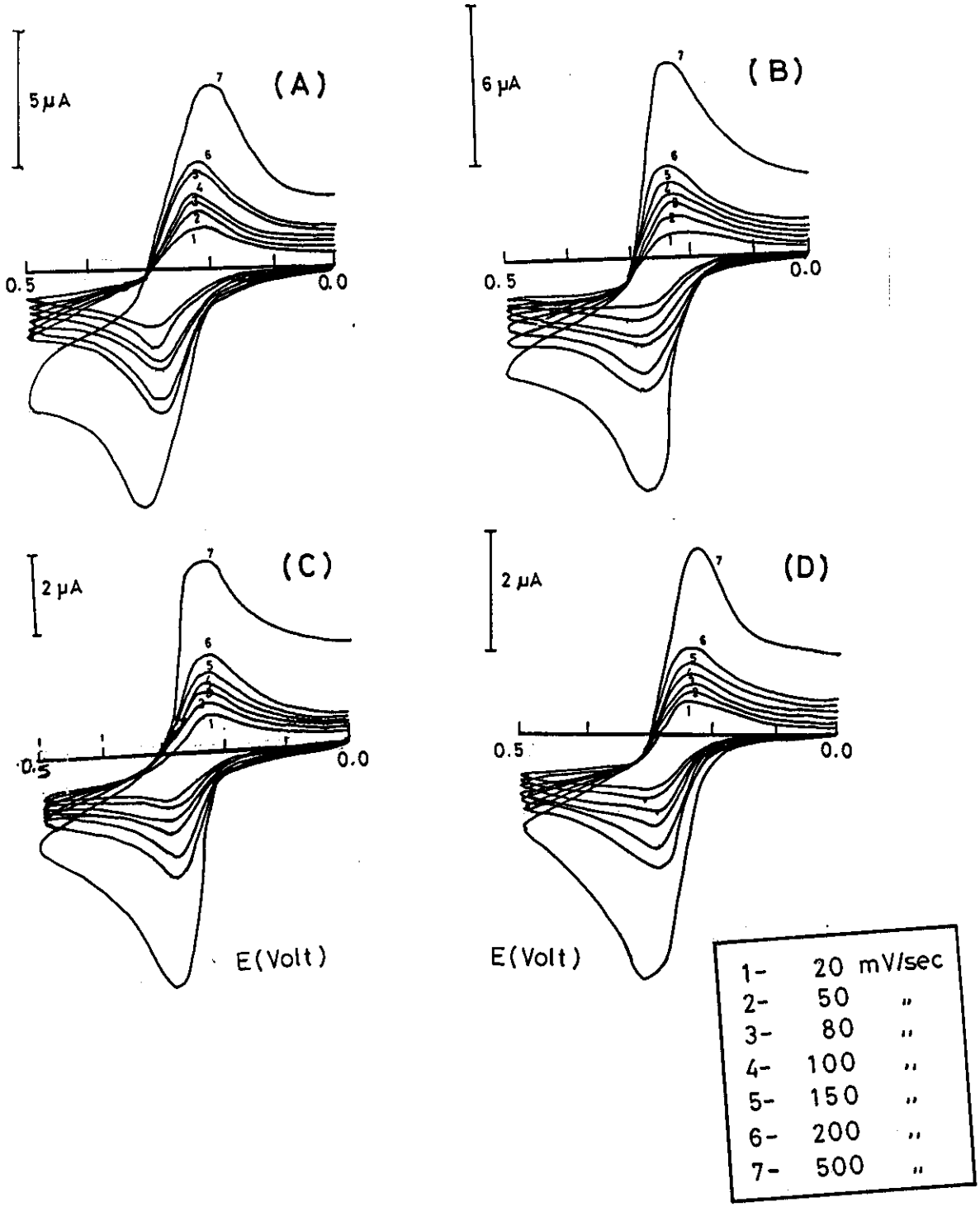

gure 39: Cyclic volltammograms of 0.5 mM ferrocene in 1.2% C_{18}DMB icellar solutions containing, (a) 0.10 M NaCl, (b) 0.16 M NaCl, (c) 0.62 M aCl, and (d) 1.00 M NaCl. The sweep rates are 20,50,80,100,150,200 and 500 V/sec.

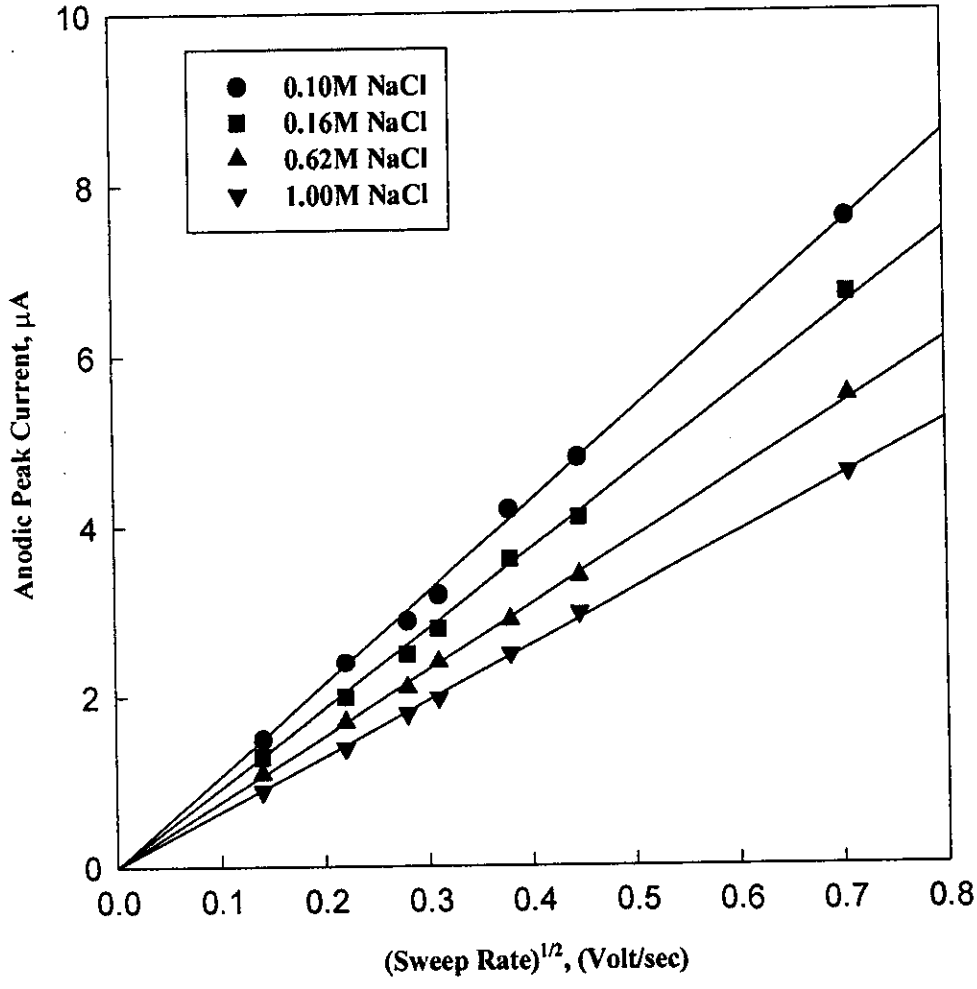

Figure 40: The plots of anodic peak currents versus ($\upsilon^{1/2}$) for C_{18}DMB micellar solutions at different concentrations of salt at 1.2% C_{18}DMB and 0.5mM ferrocene.

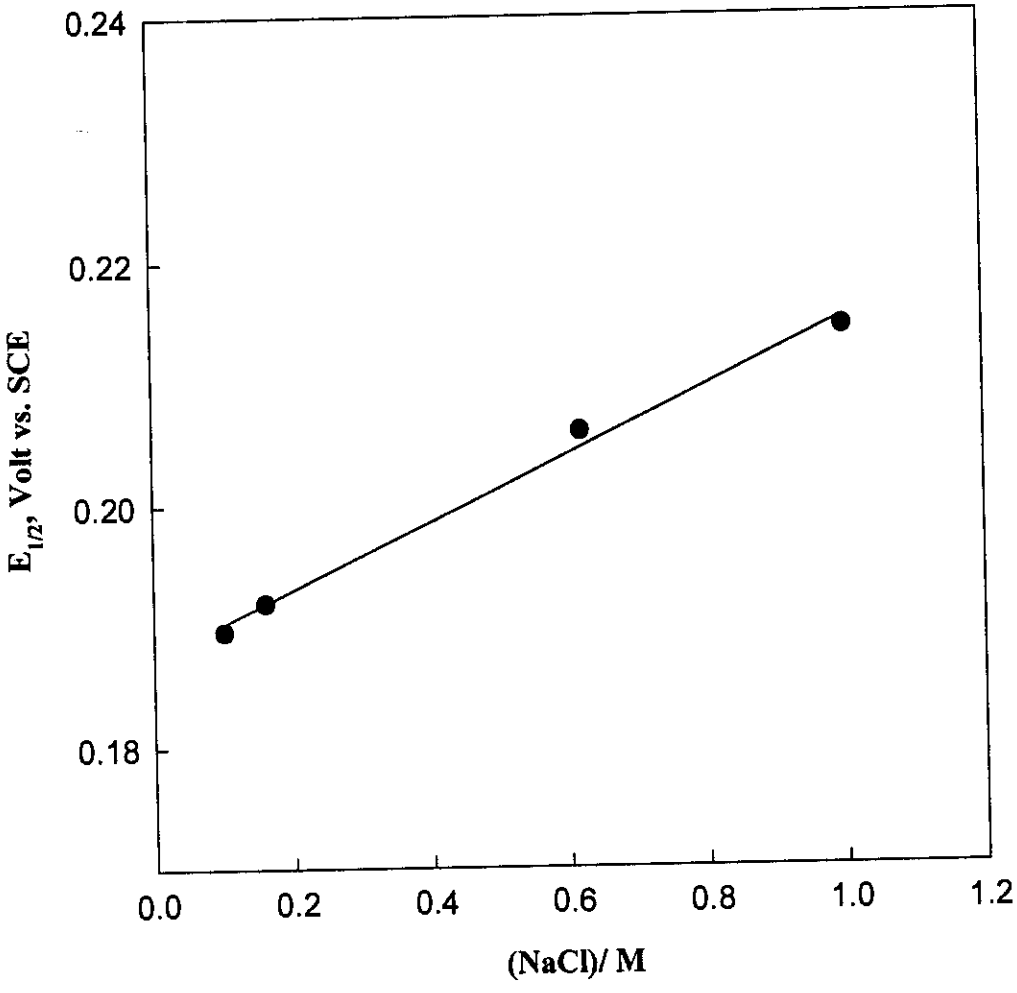

Figure 41: The effect of NaCl concentrations on $E_{1/2}$ of 0.5 mM ferrocene in 1.2% C_{18}DMB micellar solutions.

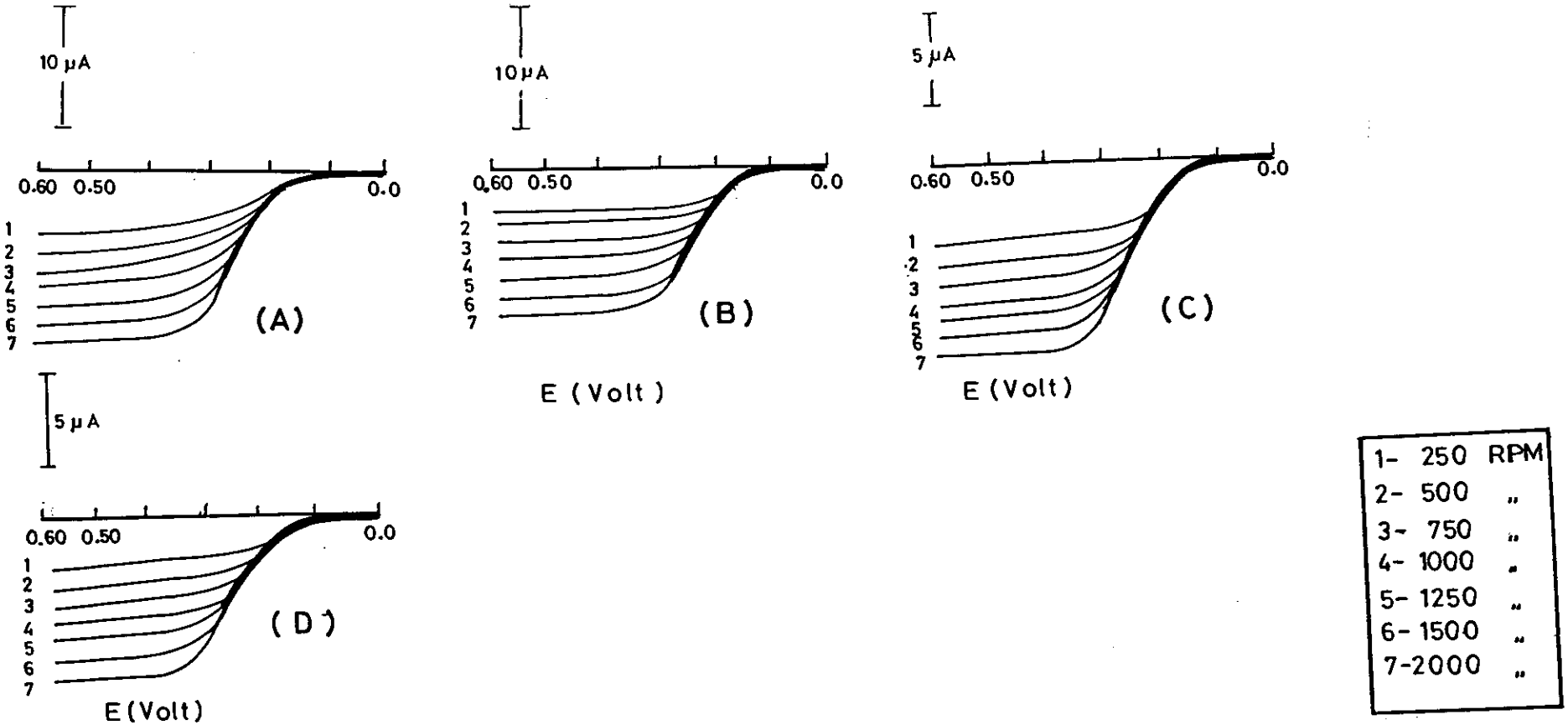

Figure 42: The effect of rotation speed of glassy carbon electrode on the linear sweep voltammograms obtained for 0.5 mM ferrocene in 1.2% C_{18}DMB micellar solutions containing, (a) 0.10 M NaCl, (b) 0.16 M NaCl, (c) 0.62 M NaCl, and (d) 1.0 M NaCl. The rotation speed are 250,500,750,1000,1250,1500 and 2000 RPM.

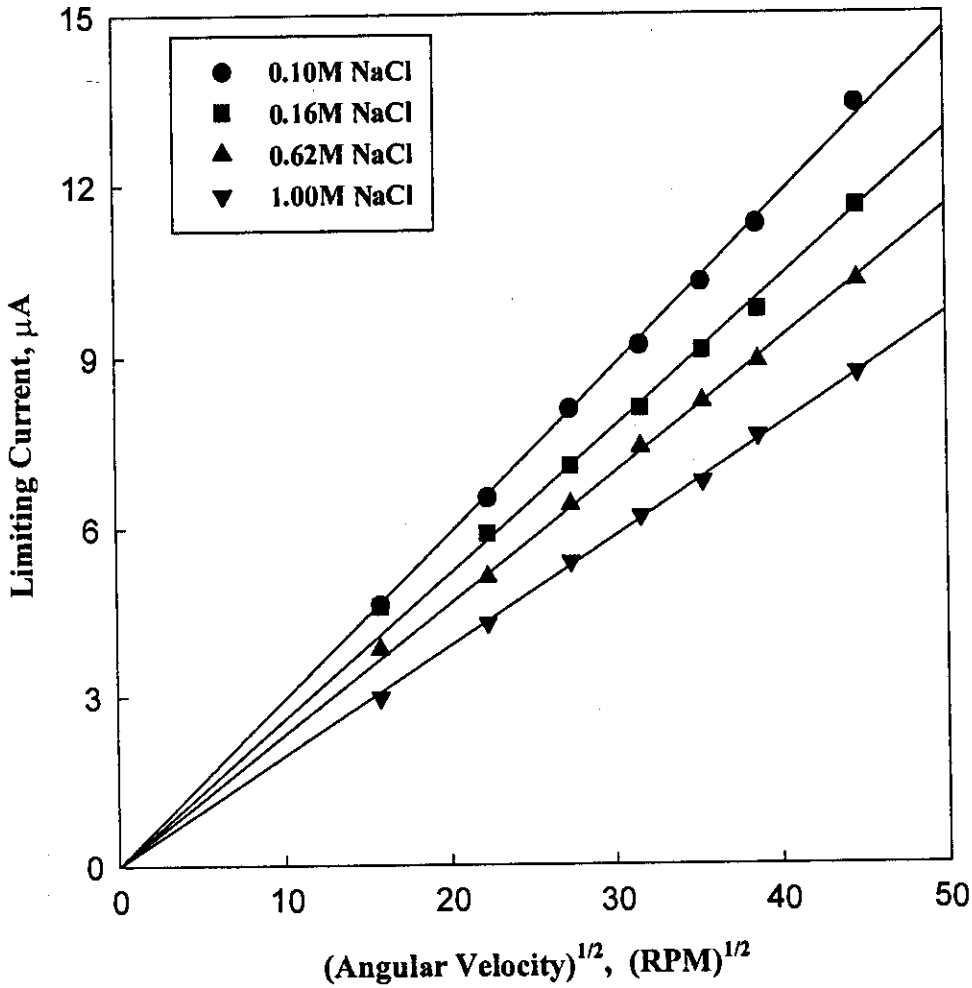

Figure 43: The plots of the limiting currents (i_l) versus the square root of angular velocity ($\omega^{1/2}$) of 0.5 mM ferrocene in 1.2% C_{18}DMB micellar solutions containing different concentrations of NaCl.

Table 16: Cyclic voltammetric data obtained for $7x10^{-5}$ M ferrocene in different amounts of C_{18}DMB micellar solutions at 40 °C.

Sweep Rate mV/sec	$E_{p,a}$ mV	$E_{p,c}$ mV	$I_{p,a}$ µA	$I_{p,c}$ µA	$I_{p,a}/I_{p,}$ -	ΔE_p mV	$E_{1/2}$ mV	$E_{1/2}$(average) mV
(A) 0.05% C_{18}DMB								
20	174	118	0.78	0.75	1.032	56	146	
50	174	118	1.13	1.16	0.970	56	146	
80	174	118	1.60	1.77	0.903	56	146	
100	176	120	1.80	1.87	0.960	57	148	148
150	178	120	2.20	2.34	0.939	58	149	
200	179	121	2.51	2.42	1.035	58	150	
500	179	121	4.20	4.13	1.016	58	150	
(B) 0.10% C_{18}DMB								
20	176	120	1.30	1.27	1.020	56	148	
50	176	120	1.98	2.04	0.967	56	148	
80	177	121	2.50	2.63	0.949	56	149	
100	178	121	2.90	3.03	0.956	58	149	149
150	179	122	3.30	3.49	0.943	58	150	
200	179	123	3.81	3.87	0.983	56	151	
500	179	123	6.20	5.96	1.040	56	151	
(C) 0.20% C_{18}DMB								
20	179	121	0.50	0.51	0.962	58	150	
50	179	121	0.80	0.82	0.967	58	150	
80	180	122	0.98	0.97	1.008	58	151	
100	180	123	1.10	1.08	1.015	57	151	151
150	181	124	1.30	1.27	1.019	57	152	
200	181	125	1.52	1.50	1.010	56	153	
500	182	125	2.54	2.56	0.992	57	153	

Follow:

Sweep Rate mV/sec	$E_{p,a}$ mV	$E_{p,c}$ mV	$I_{p,a}$ μA	$I_{p,c}$ μA	$I_{p,a}/I_{p,c}$ -	ΔE_p mV	$E_{1/2}$ mV	$E_{1/2}$(average) mV
(D) 0.50% C_{18}DMB								
20	181	125	0.91	0.92	0.987	56	153	
50	181	125	1.52	1.53	0.993	56	153	
80	182	126	1.93	1.95	0.985	56	154	
100	183	127	2.28	2.29	0.995	56	155	155
150	184	127	2.70	2.72	0.992	57	155.	
200	186	128	3.10	3.11	0.996	58	157	
500	187	129	4.80	4.81	0.996	58	158	
(E) 0.70% C_{18}DMB								
20	186	126	1.21	1.23	0.979	60	156	
50	186	126	1.81	1.82	0.990	60	156	
80	186	127	2.20	2.25	0.977	59	156	
100	188	128	2.64	2.66	0.990	60	158	158
150	189	129	2.99	3.02	0.989	60	159	
200	189	131	3.51	3.55	0.986	58	160	
500	189	131	5.31	5.36	0.990	58	160	
(F) 1.20% C_{18}DMB								
20	186	127	1.30	1.33	0.977	59	156	
50	186	26	2.14	2.17	0.985	60	156	
80	186	127	2.43	2.47	0.983	59	156	
100	188	128	2.80	2.83	0.989	60	158	157
150	189	129	3.30	3.32	0.992	60	159	
200	189	129	3.81	3.85	0.989	60	159	
500	189	131	6.13	6.17	0.993	58	160	

Table 17 : Diffusion coefficients of solubilized ferrocene in C_{18}DMB micellar solutions obtained from RDV measurements.

% Surfactant wt./wt.	Ferrocene (M)	Diffusion coefficient (10^{-6} cm^2 s^{-1})		
		Electrochemical		
		D_a	D_d	
			Slow[a]	Fast[b]
0.2	$2.50x10^{-4}$	4.070	3.480	3.412
0.7	$3.16x10^{-4}$	2.300	1.659	1.47 0
0.9	$3.47x10^{-4}$	1.540	0.940	0.670
1.2	$3.88x10^{-4}$	0.958	0.452	0.108
1.5	$4.26x10^{-4}$	0.812	0.367	0.082
2.0	$4.90x10^{-4}$	0.771	0.360	0.062

a : calculated in zero-kinetics approximation using Eq. (III.9)

b : calculated in fast-kinetic limit using the linear mole fraction weighting Eq. (III.10)

Table 18 : Cyclic voltammetric data obtained for 0.5mM ferrocene in C_{18}DMB micellar solutions contaning different concentrations of NaCl at 40°C.

Sweep Rate	$E_{p,a}$	$E_{p,c}$	$I_{p,a}$	$I_{p,c}$	$I_{p,a}/I_{p,c}$	ΔE_p	$E_{1/2}$	$E_{1/2}$(average)
mV/sec	mV	mV	µA	µA	-	mV	mV	mV
(A) 0.10M NaCl								
20	212	154	1.50	1.62	0.925	58	183	
50	212	155	2.40	2.43	0.987	57	183	
80	212	155	2.90	2.81	1.032	57	183	
100	213	156	3.20	3.30	0.969	57	184	184
150	213	157	4.28	4.13	1.016	56	185	
200	216	157	4.80	4.90	0.969	59	186	
500	217	157	7.60	7.70	0.987	60	187	
(B) 0.16M NaCl								
20	220	159	1.30	1.40	0.928	61	189	
50	221	159	1.99	2.00	0.995	62	190	
80	223	160	2.50	2.60	0.916	61	191	
100	223	162	2.80	2.89	0.968	61	192	192
150	225	162	3.60	3.67	0.980	63	193	
200	226	164	4.10	4.26	0.962	62	195	
500	227	164	6.70	6.81	0.983	63	195	

Follow:

Sweep Rate	$E_{p,a}$	$E_{p,c}$	$I_{p,a}$	$I_{p,c}$	$I_{p,a}/I_{p,c}$	ΔE_p	$E_{1/2}$	$E_{1/2}$(average)
mV/sec	mV	mV	μA	μA	-	mV	mV	mV
(C) 0.62M NaCl								
20	236	174	1.10	1.20	0.916	62	205	
50	236	175	1.70	1.75	0.971	61	205	
80	237	176	2.10	2.20	0.954	61	206	
100	237	176	2.40	2.46	0.975	61	206	206
150	238	177	2.90	2.93	0.989	61	207	
200	238	178	3.40	3.43	0.991	60	208	
500	239	179	5.50	5.60	0.982	60	209	
(D) 1.00M NaCl								
20	245	179	0.90	0.88	1.011	66	212	
50	247	180	1.40	1.44	0.972	67	213	
80	247	180	1.80	1.92	0.937	67	213	
100	249	182	1.98	1.93	1.025	67	215	214
150	250	183	2.50	2.55	0.980	67	216	
200	250	180	2.90	2.97	0.976	70	215	
500	251	184	4.60	4.73	0.972	67	217	

Table 19 : Effect of salt concentrations on the diffusion coefficients of 0.5 mM ferrocene of 1.2% C_{18}DMB micellar solution from both cyclic voltammetry (CV) and rotating disk voltammetry experiments.

Concentration of NaCl M	**$D_a x10^{-6}$** cm^2/sec (CV)	**$D_a x10^{-6}$** cm^2/sec (RDV)
0.10	1.01	0.97
0.16	0.84	0.82
0.62	0.87	0.81
1.00	0.64	0.58

3.5 Electrochemical Characterization of C_{18}DMB Microemulsion

The cyclic voltammograms of either 1 mM ferrocene or 1 mM potassium ferrocyanide were recorded in zwitterionic C_{18}DMB microemulsion systems of composition 1.6% C_{18}DMB as the surfactant, 2.5% n-dodecane as the oil, 1.88 % n-butanol as the cosurfactant and 0.1 M NaCl as the supporting electrolyte at 40°C. Ferrocene and potassium ferrocyanide were used as the hydrophobic and water-soluble electroactive probes, respectively. The probe concentrations were used in the range of $2x10^{-4}$ to $3x10^{-3}$ M. The cyclic voltammograms of probe were recorded at potential sweep rates varying from 20 to 500 mV/sec. Well defined voltammograms of ferrocene and potassium ferrocyanide in C_{18}DMB microemulsions were obtained as represented in Figs.(44,45). All the voltammograms of ferrocene and potassium ferrocyanide show one anodic and one cathodic peak on the anodic and cathodic sweeps. The anodic peak current, $I_{p,a}$ and cathodic peak current $I_{p,c}$ are of almost equal heights, Tables (20,21). The reversibility of the electrode process can be indicated from the anodic to cathodic peak current ratios ($I_{p,a}/I_{p,c}$) which does not exceed 1.060. The constancy of $I_{p,a}/I_{p,c}$ ratios at unity confirmed that, there is no adsorption at the electrode surface. The peak potential separation ($\Delta E_p = (E_{p,a} - E_{p,c})$) values of ferrocene were found almost around the theoretical value for one-electron transfer (57-63) mV. Whereas, potassium ferrocyanide is chemically reversible one-electrone transfer process and ΔE_p is around 156-164 mV.

The cyclic voltammograms recorded at different sweep rates varying from 20 to 500 mV/sec are similar and show one anodic and one cathodic peak. The reversibility of the electrode reaction of ferrocene oxidations can be confirmed from the constancy of the cathodic and anodic peak potentials, $E_{p,a}$ and $E_{p,c}$, respectively.

The peak potential separation ΔE_p values fall within the range from 57 to 63 mV as given in Table (20). Table (21) showed the results obtained from CV experiment using potassium ferrocyanide.

As expected from the Randles-Sevcik [140] equation the peak currents ($I_{p,a}$ and $I_{p,c}$) were increased as the scan rate is increased. The plots of anodic peak current ($I_{p,a}$) versus root of sweep rate ($\upsilon^{1/2}$) gives straight lines intersecting the origin for both ferrocene and potassium ferrocyanide as shown in Figs. (46,47). These results indicate that the electrode process is diffusion controlled [117]. The slopes of $I_{p,a}$ vs. ($\upsilon^{1/2}$) provides the value of the apparent diffusion coefficient (D_a), Tables (22,23). On using Stokes-Einstein equation [151] the radius of microemulsion droplets can be determined at different probe concentrations using the apparent diffusion coefficients (D_a) and listed in Tables (22,23).

3.5.1 Effect of oil content

The effect of n-dodecane on the phase behaviour, diffusion coefficient and the radius of microemulsion system of C_{18}DMB containing 1.6% C_{18}DMB, 1.88 % n-butanol and 0.1 M NaCl was studied in the range from 0.50% to 2.5% (wt./wt.) of n-dodecane at 40°C using 1mM ferrocene as electroactive probe. The cyclic voltammograms which obtained at different percentages of n-dodecane indicate the slight decrease in the peak current on increasing n-dodecane percentages in C_{18}DMB microemulsion system, as shown from Fig.(48). As the oil content is increased the heterogeneity of the microemulsion increased as shown in Table (24). The increased heterogeneity of microemulsion system reflects the increase of droplet size. Fig (49), illustrates the effect of n-dodecane percentages on the half-wave potential ($E_{1/2}$) of ferrocene solubilized microemulsion. It showed a positive

shift of ($E_{1/2}$) as the oil content is increased. The half-wave potential of the electroactive probe is dependent on the composition of microemulsion system, Table (24).

3.5.2 Effect of salt concentration

The effect of NaCl concentration on diffusion coefficient for C_{18}DMB microemulsion containing 1.6% C_{18}DMB, 1.88% butanol, and 2.5% n-dodecane was studied at 0.08, 0.10 and 0.12 M NaCl at 40°C where after 0.12 M NaCl two layers were seperated forming upper phase oil. The anodic peak currents were decreased as the salinity is increased as represented from Fig. (50). Table (25) showed the results obtained from cyclic voltammetry at different salinity. The plots of anodic peak currents ($I_{p,a}$) against ($\upsilon^{1/2}$) is shown in Fig.(51). The slopes of the plots were used to determine the apparent diffusion coefficient values. The diffusion coefficient values were found to decreas on increasing NaCl concentration, Table (26).

3.5.3 Effect of surfactant concentration

The effect of C_{18}DMB concentration on the diffusion coefficient was studied for microemulsions containing 1.88% n-butanol, 2.5 % n-dodecane and 0.1M NaCl. The concentration of C_{18}DMB was varied in the range from 1.6 % to 3.0 % (wt./wt.). The cyclic voltammograms were recorded at different sweep rates and represented in Fig.(52). The plots of anodic peak current $I_{p,a}$ vs ($\upsilon^{1/2}$) is linear and shown in Fig.(53). The slopes provide the value of the diffusion coefficients. Table (27) showed an increase in the diffusion coefficient as the surfactant concentration is increased. This behaviour may attributed to the increase in interfacial tention on increasing the surfactant concentration and therefore microemulsion droplets splitted

into ones of smaller sizes to comple4nsate this behaviour.

3.5.4 Rotating disk voltammetry (RDV)

Rotating disk voltammetry experiments were carried out on C_{18}DMB microemulsions containing 1.6% C_{18}DMB as the surfactant, 2.5% n-dodecane as the oil, 1.88 % n-butanol as the cosurfactant and 0.1 M NaCl as the supporting electrolyte at 40°C. The voltammograms for C_{18}DMB microemulsions containing different amounts of ferrocene as probe from $2x10^{-4}$ to $3x10^{-3}$ M were recorded, Fig. (54). The effect of rotation speed of the glassy carbon electrode was recorded at small sweep rate, 5 mV/sec, to avoid peaked shape and to obtain a steady state plateau. All the voltammograms showed the one-step oxidation-plateau. The effect of rotation speed on the voltammograms of ferrocene solubilized C_{18}DMB microemulsion systems was recorded at angular velocities 250, 750, 1000, 1250, 1500 and 2000 RPM. The values of current between 400 to 500 mV were constant and considered as the limiting current values. In accordance with Levich equation (III.2), values of the limiting current, i_l increase linearly with the square root of rotation speed as shown in Fig.(55). The linear dependence of the limiting current on the square root of rotation speed ($\omega^{1/2}$) indicate that electrochemical reactions are under mass transfer control. The slopes of these linear plots were used to determine the apparent diffusion coefficients of C_{18}DMB microemulsion as a function of ferrocene concentration. There is a good agreement between the diffusion coefficient values obtained from both rotating disk voltammetry and cyclic voltammetry, Table (22). The limiting currents increased as the probe concentration increased as expected from Eq. (III.2) and shown in Fig.(55).

The half-wave potential and the number of electrons transferred can be calculated from the following equation [117] .

$$E = E_{1/2} - 2.303\ RT/\ nF.\log\ [i/(i_l - i)]$$

where i is the current at potential E. Plots of E versus log $[i/(i_l - i)]$for 1mM ferrocene in C_{18}DMB microemulsion at 1000 RPM were linear with a reciprocal slope 60 mV, which is consistent with a single electron transfer process, Fig (56). The half-wave potential of the system ($E_{1/2}$) was determined from the potential axis at $\log[i/(i_l - i)]$ value equal to zero, where $i = i_l/2$ at the $E_{1/2}$ value. The half-wave potentials was determined and found to be 161 mV.

3.5.4.1 Effect of hydrocarbon and salt concentration

The effect of n-dodecane percentages on the diffusion coefficient of C_{18}DMB microemulsion was studied using rotating disk voltammetry. The percentages of n-dodecane were varied in the range from 1.6% to 3.0% (wt./wt.). RDV voltammograms showed a slight decrease in limiting current on increasing the oil content in microemulsion system as represented in Fig. (57).

Also, the effect of salt concentration on the diffusion coefficient of C_{18}DMB microemulsion using 1mM ferrocene electroactive probe was studied using RDV technique. The composition of solutions studied was the same as that studied using CV technique. Fig. (58) showed RDV voltammograms and Fig. (59) showed the plot of limiting current versus square root of rotation speed at 0.05, 0.08, 0.10 and 0.12 M NaCl. This results which obtained from RDV were similare to that obtained from CV

experiment.

3.5.5 Chronocoulometry (CC)

The chronocoulometric respones of ferrocene in C_{18}DMB micelle and microemulsion systems were recorded by plotting the total amount of diffusional charge (Q_{tot}) versus time (t). The stepping potential was from 0.0 to 500 mV. Typical chronocoulograms of these systems are shown in Figs. (60a, 60b). The typical values of Γ_o of ferrocene in C_{18}DMB micelle and moles microemulsion was found in the range 10^{-12} to 10^{-13} moles which indicating a negligible adsorption on the electrode surface.

3.3 Partitioning of Ferrocene in C_{18}DMB

The partioning effect of ferrocene between the hydrophobic core and the hydrophilic medium is discussed for C_{18}DMB micelles and C_{18}DMB microemulsion systems. By considering that both the reductant Fc and oxidant Fc^+ exist in the aqueous and micellar phases, respectively.

By considering the solubility of Fc^+ in microemulsion or micelles to be higher than Fc only in pure aqueous. The value of K_{Fc} which is equal to $[Fc]_w/[Fc]_m$ is almost ~ $5x10^{-3}$ as determined from solubilities of oxidant and reductant species in solution.

On using equation (III.15) and (III.16) the ratio of D_{Fc+}/D_{Fc} for C_{18}DMB micelles and microemulsion is determined by both CV and RDV techniques. The typical ratio (D_{Fc+}/D_{Fc}) in micelles were found to be $1.78x10^2$ and $0.72x10^2$ using CV and RDV, respectively. Also, the ratio (D_{Fc+}/D_{Fc}) in microemulsion containing C_{18}DMB was found to be $6.48x10^2$ and $2.34x10^2$ using CV and RDV, respectively.

When Fc and Fc^+ both predominately exist in the microemulsion droplets, the half-wave potential ($E_{1/2}$) obtained from cyclic voltammetry measurements could be used in determining the ratio of compartmentalization constants (K_{Fc+}/K_{Fc}) using using equation (III.18).

Since the value of E^o_w was 0.160 $\pm$ 0.005 V versus SCE and $E_{1/2}$ (CV) = 191 mV, the ratio (K_{Fc+}/K_{Fc}) is equal to 42.34 in C_{18}DMB microemulsion.

It is also, concluded that ferrocene was predominately solubilized in the droplet and $D_{Fc} \simeq D_m$ and therefore, the partitioning effect of ferrocene could be waved.

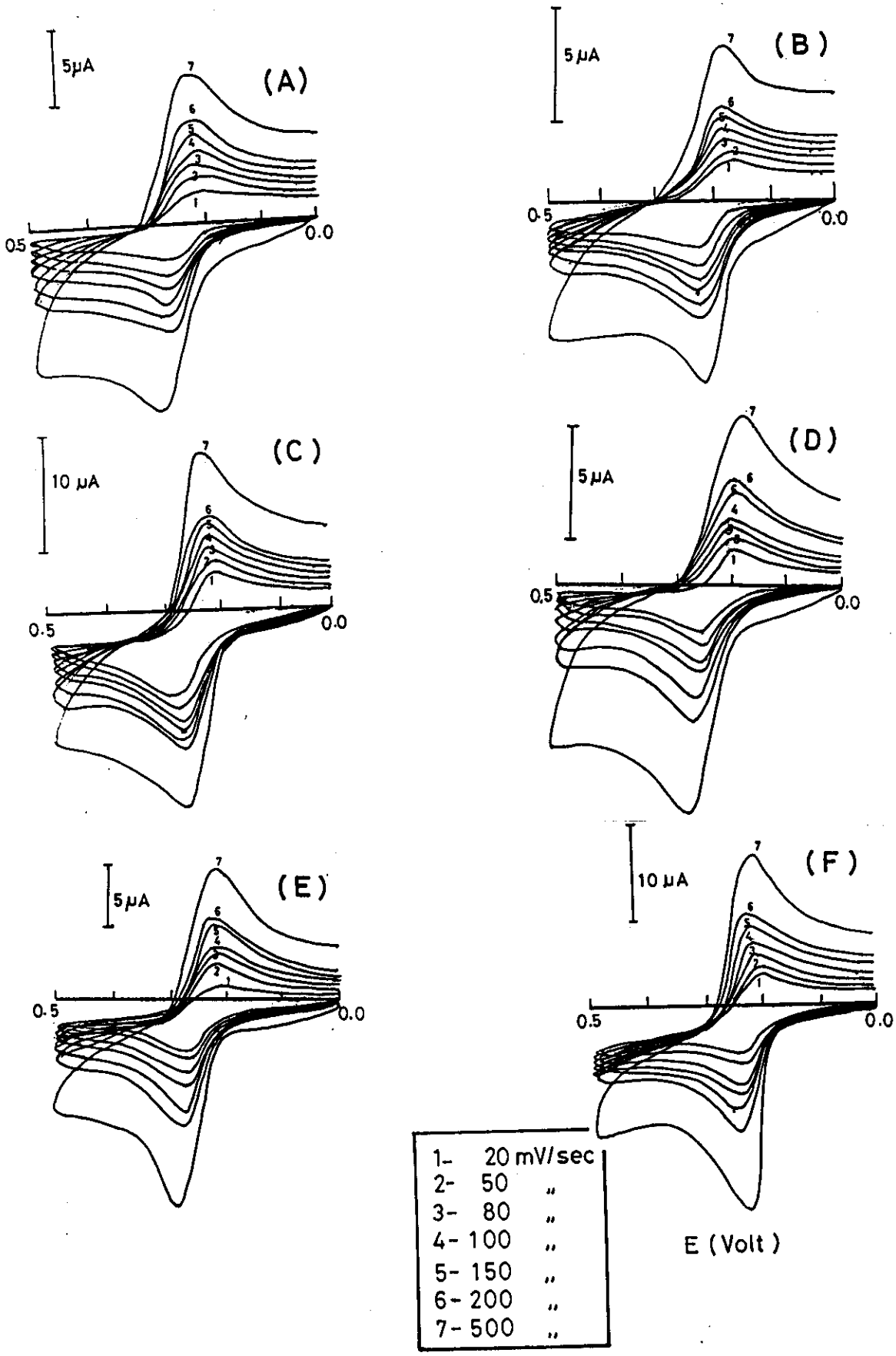

gure 44: Cyclic voltammograms of ferrocene recorded in C_{18}DMB microemulsion stems containing (a) $2x10^{-4}$ M ferrocene (b) $4x10^{-4}$ M ferrocene, (c) $8x10^{-4}$ M ferrocene, $1x10^{-3}$ M ferrocene (e) $2x10^{-3}$ M ferrocene and (f) $3x10^{-3}$ M ferrocene. The sweep rates 20,50,80,100,150,200 and 500 mV/sec.

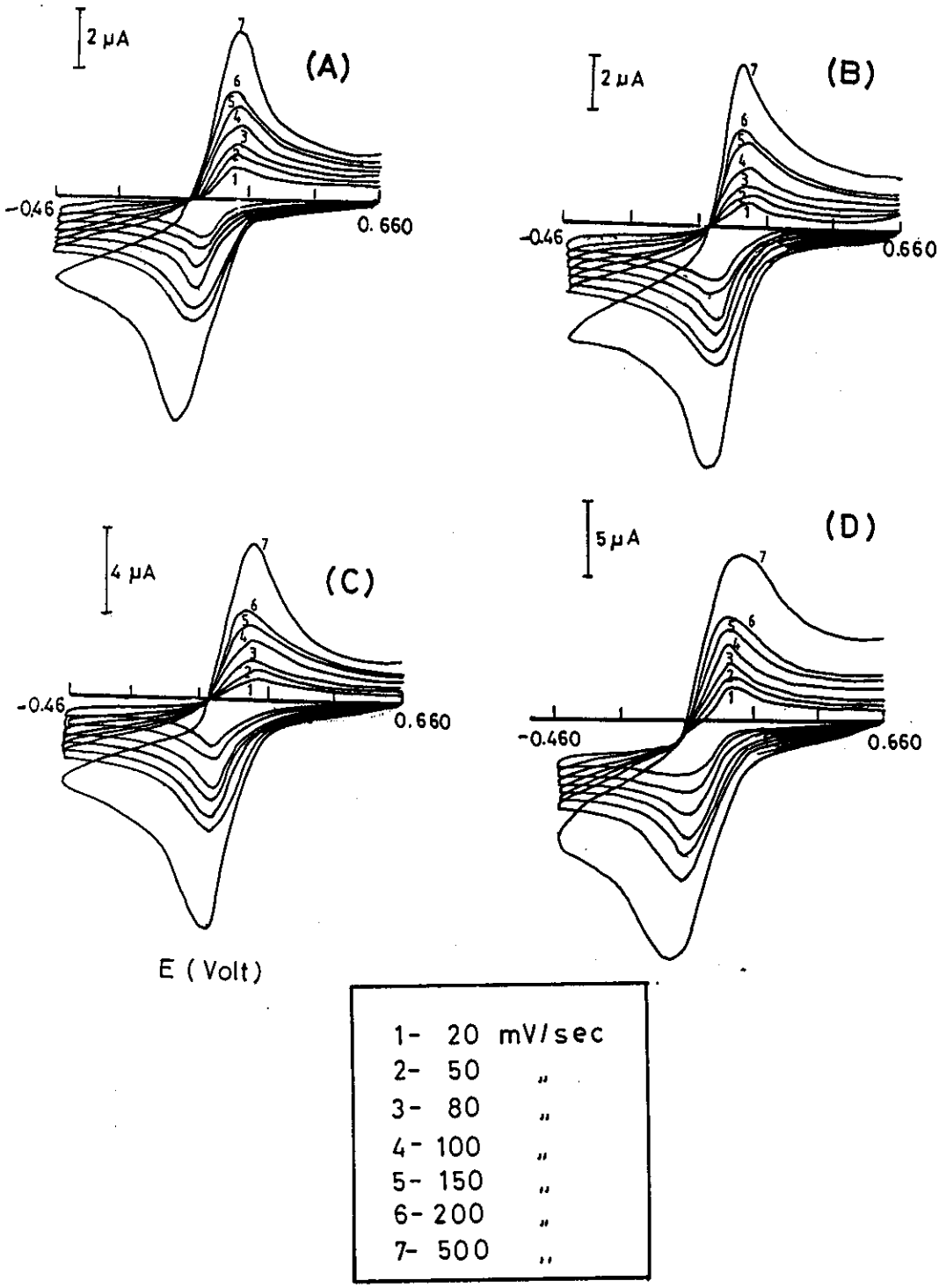

Figure 45: Cyclic voltammograms of potassium ferrocyainde recorded in C_{18}DMB microemulsion systems containing (a) $2x10^{-4}$ M $K_4[Fe(CN)_6]$, (b) $8x10^{-4}$ M $K_4[Fe(CN)_6]$, (c) $1x10^{-3}$ M $K_4[Fe(CN)_6]$, (d) $2x10^{-3}$ M $K_4[Fe(CN)_6]$ and (e) $3x10^{-3}$ M $K_4[Fe(CN)_6]$. The sweep rates are 20,50,80,100,150,200 and 500 mV/sec.

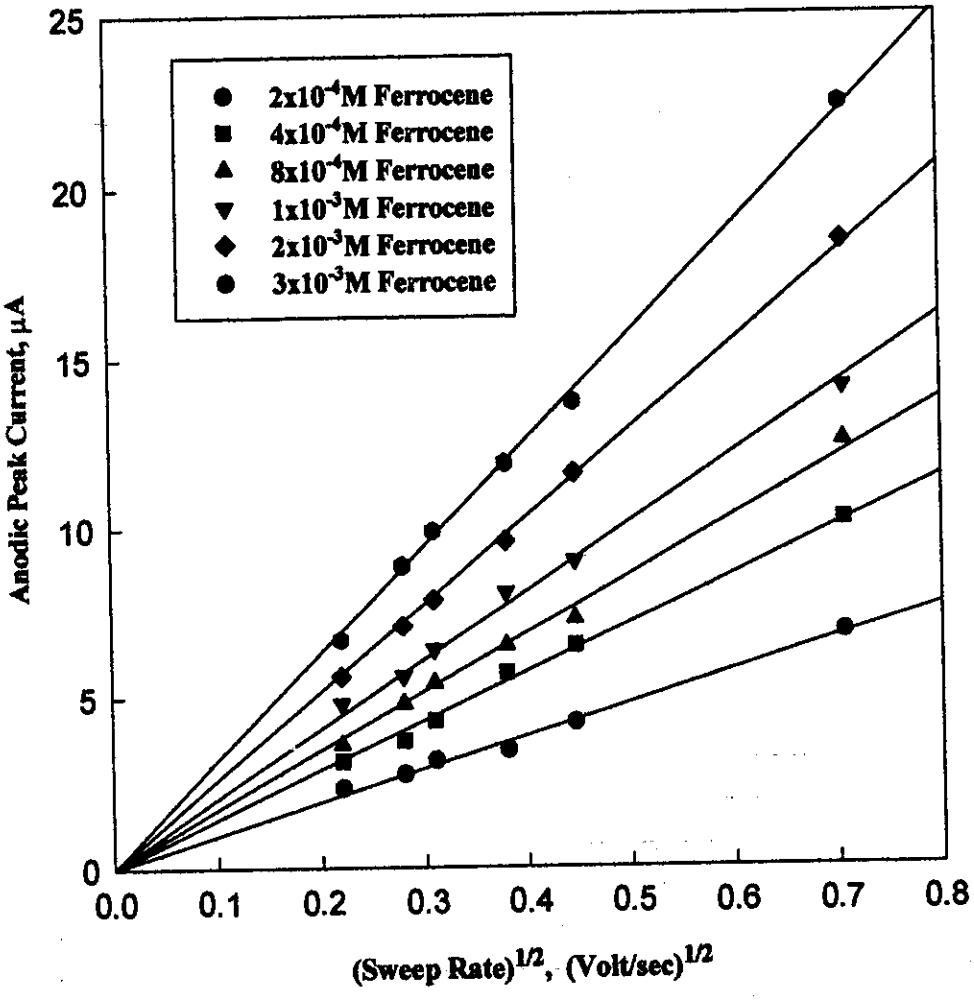

Figure 46: The plots of anodic peak currents versus ($\upsilon^{1/2}$) for ferrocene in C_{18}DMB microemulsion systems at 40°C.

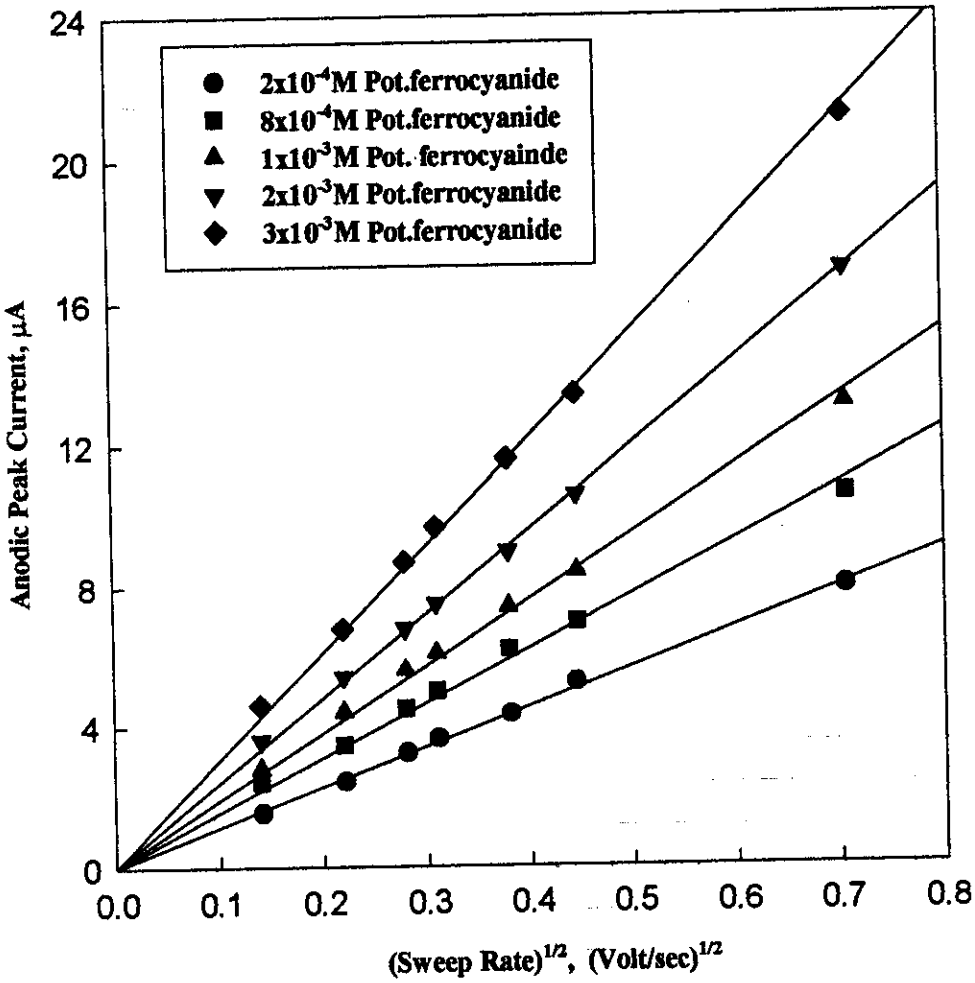

Figure 47: The plots of anodic peak currents versus ($\upsilon^{1/2}$) of Potassium ferrocyanide in C_{18}DMB microemulsion systems at 40°C.

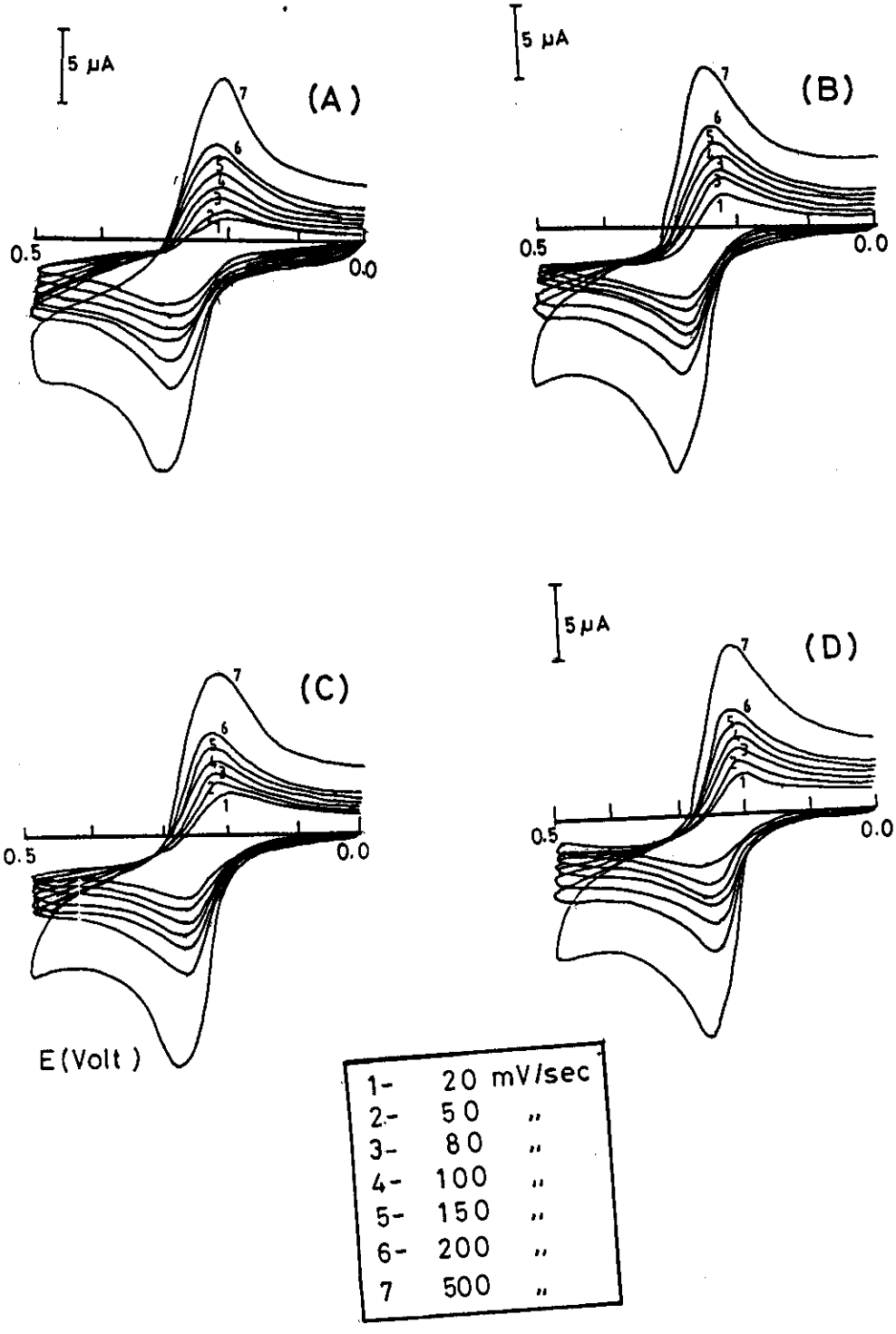

Figure 48: Cyclic voltammograms of 1mM ferrocene recorded in C_{18}DMB microemulsion systems containing (a) 0.5% n-dodecane, (b) 1.5% n-dodecane, (c) 2.0% n-dodecane and (d) 2.5% n-dodecane. The sweep rates are 20,50,80,100,150,200 and 500 mV/sec.

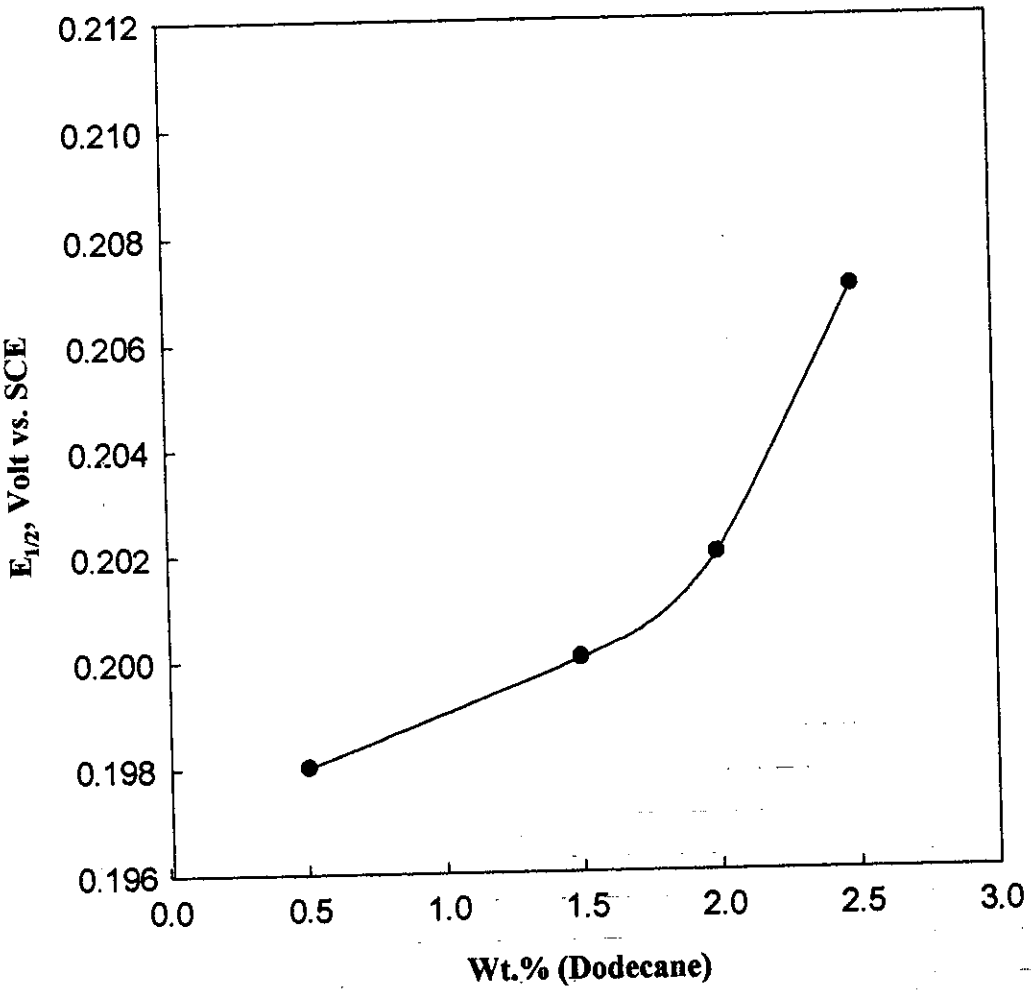

Figure 49: The dependence of half-wave potential ($E_{1/2}$) of 1 mM ferrocene in C_{18}DMB microemulsion on the hydrocarbon contents.

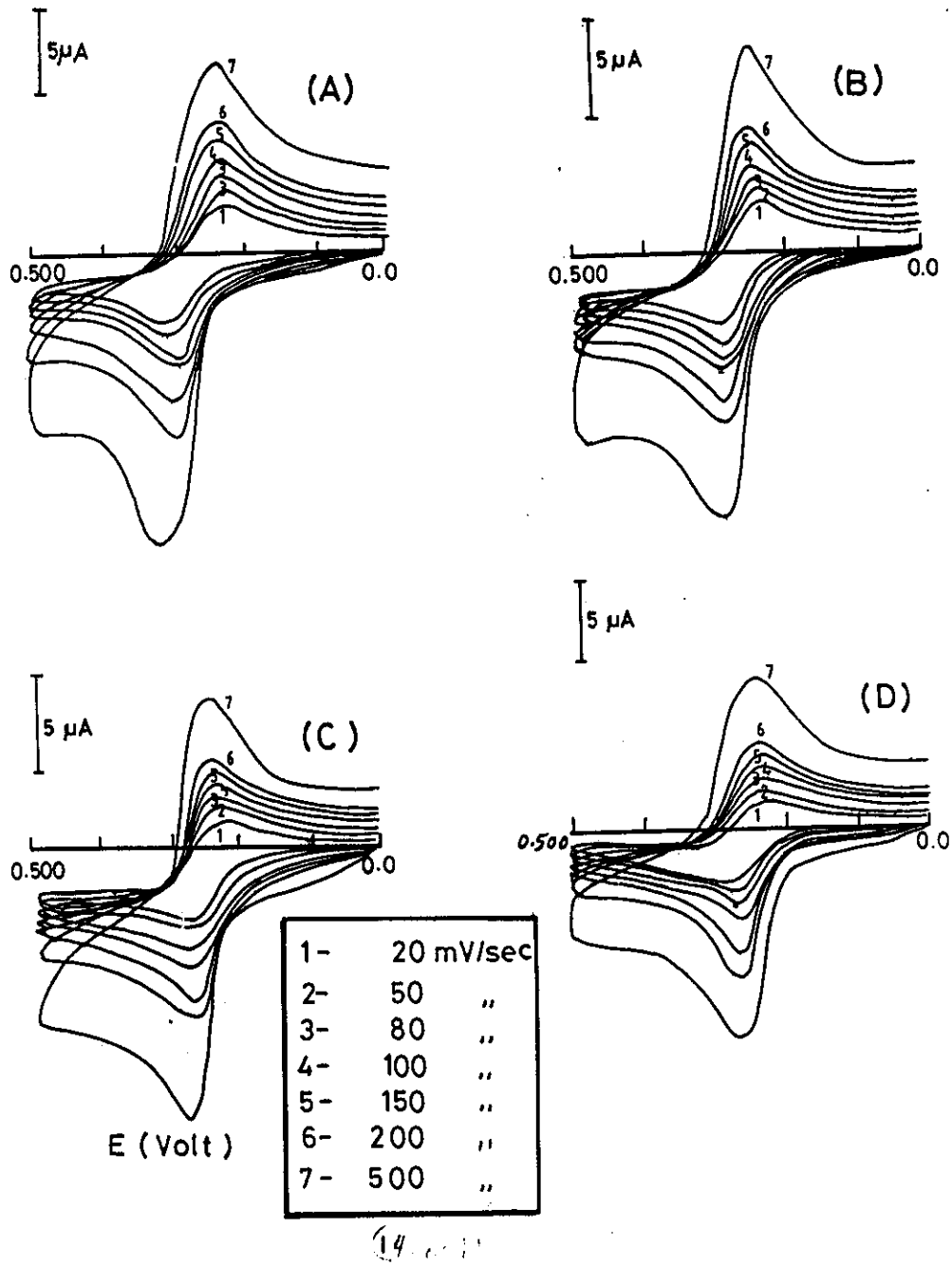

Figure 50: Cyclic voltammograms of 1mM ferrocene recorded in C_{18}DMB microemulsion systems containing (a) 0.05 M NaCl, (b) 0.08 M NaCl, (c) 0.10 M NaCl and (d) 0.12 M NaCl. The sweep rates are 20,50,80,100,150,200 and 500 mV/sec.

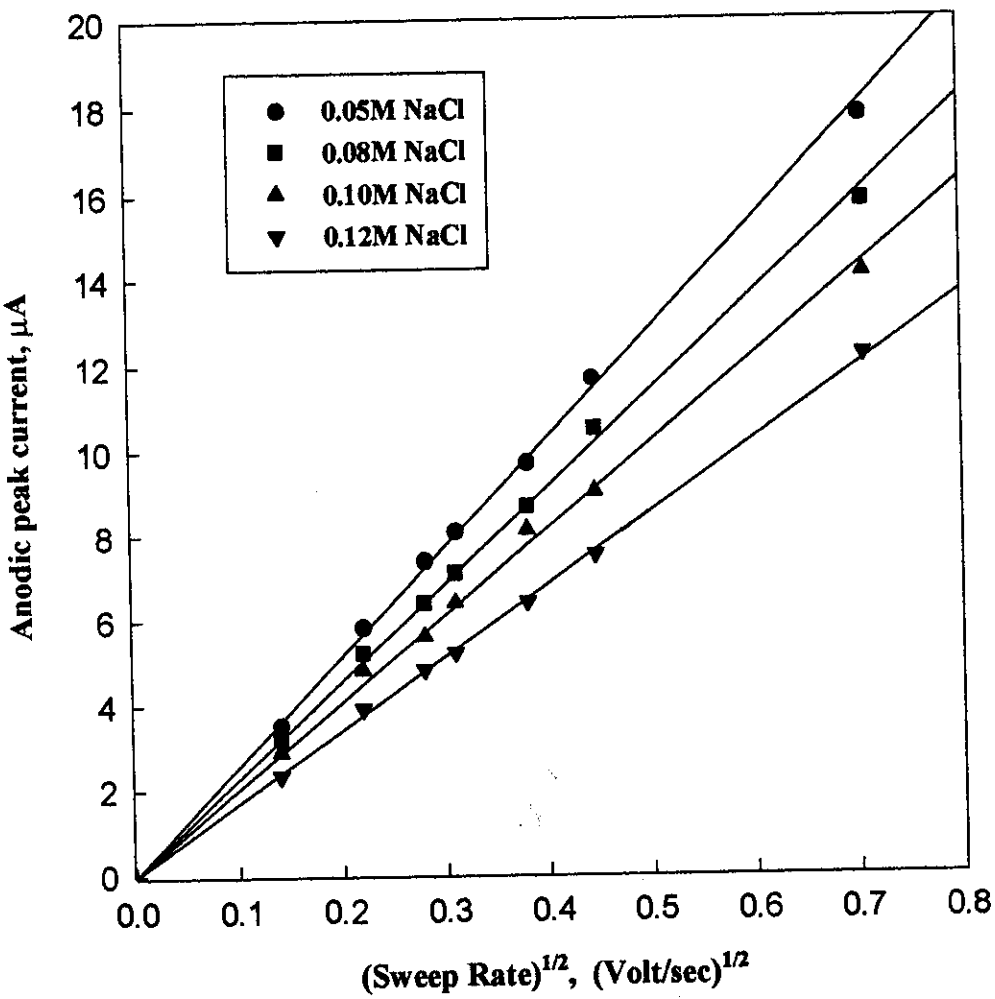

Figure 51: The plots of anodic peak currents versus ($\upsilon^{1/2}$) for 1mM ferrocene in C_{18}DMB microemulsion as a function of NaCl concentration.

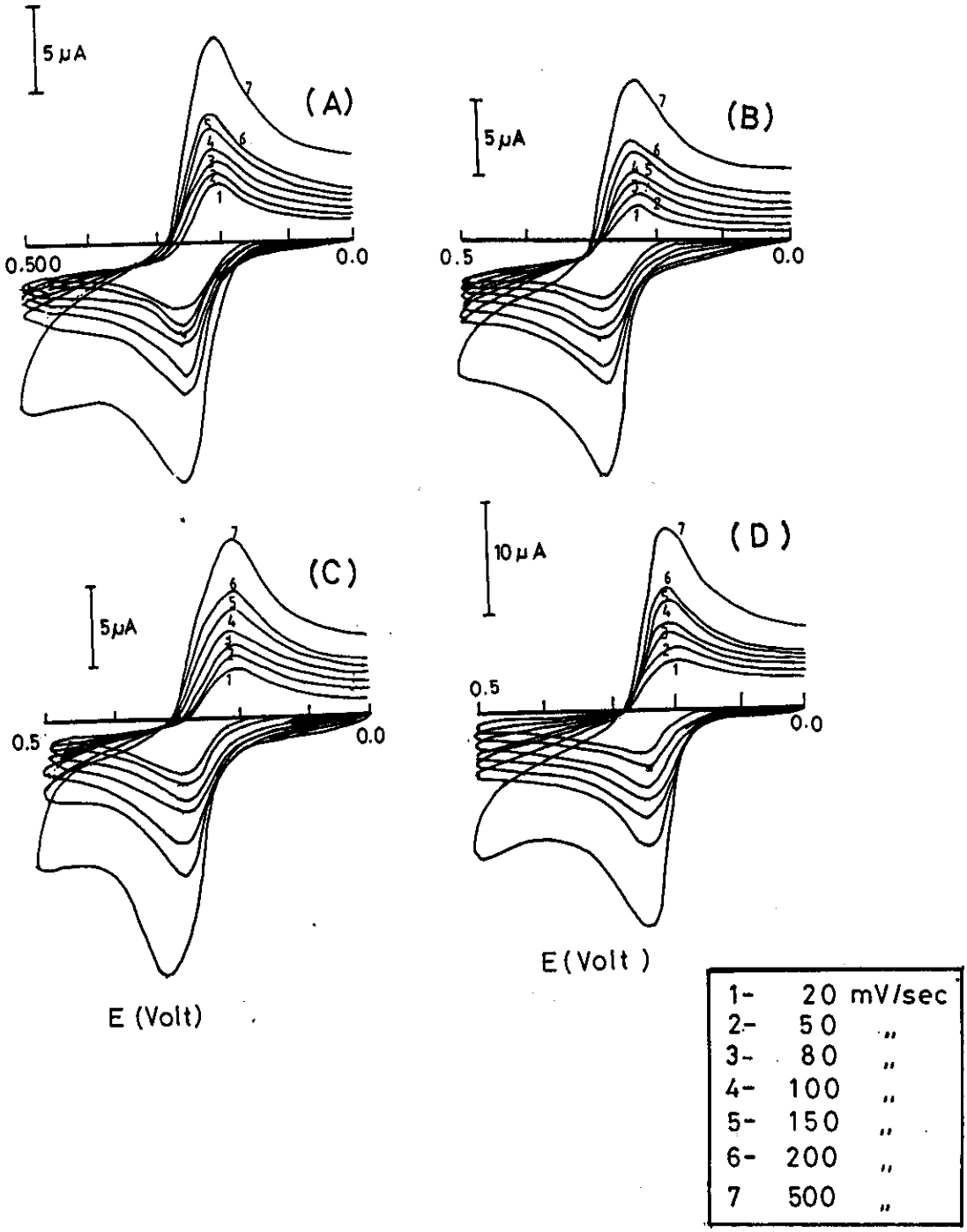

Figure 52: Cyclic voltammograms of 1mM ferrocene recorded in C_{18}DMB microemulsion systems containing (a) 1.6% C_{18}DMB, (b) 2.0% C_{18}DMB, (c) 2.5% C_{18}DMB and (d) 3.0% C_{18}DMB. The sweep rates are 20, 50, 80, 100, 150, 200 and 500 mV/sec.

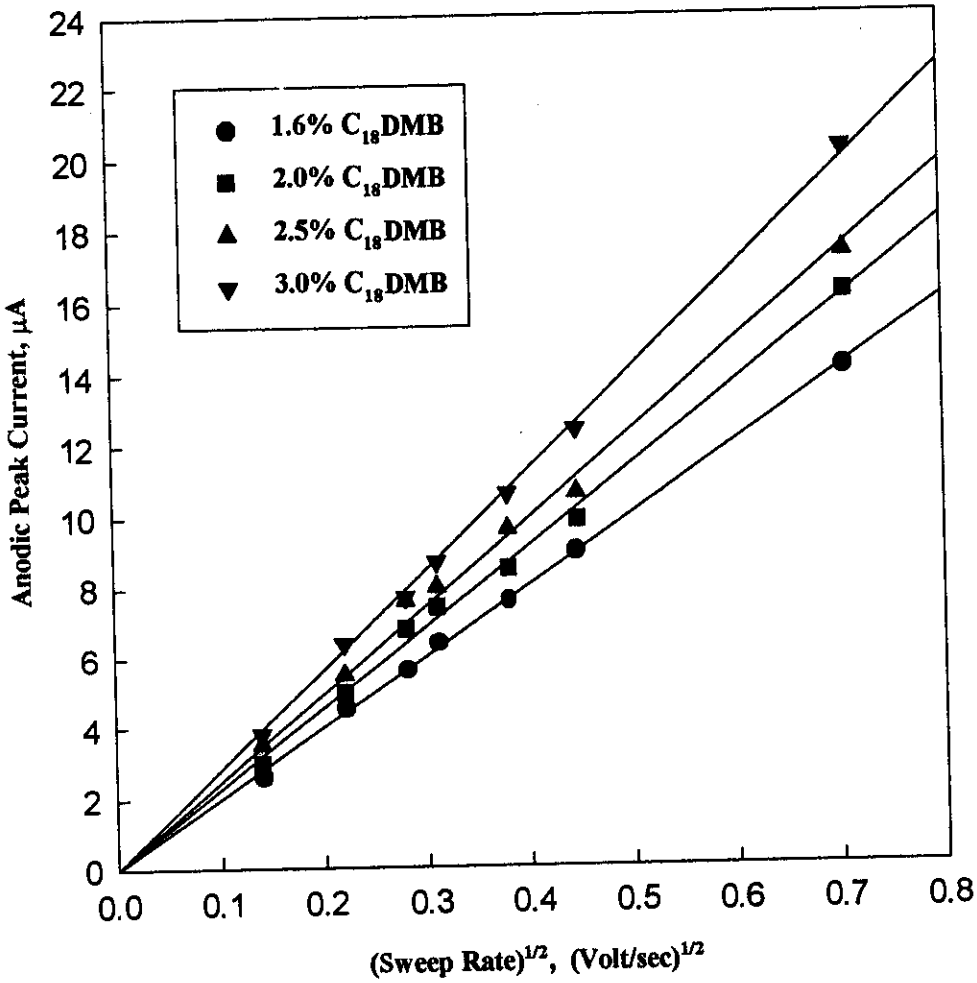

Figure 53: The plots of anodic peak currents versus ($\upsilon^{1/2}$) of 1mM ferrocene in C_{18}DMB microemulsion containing different amounts of surfactant at a constant oil content.

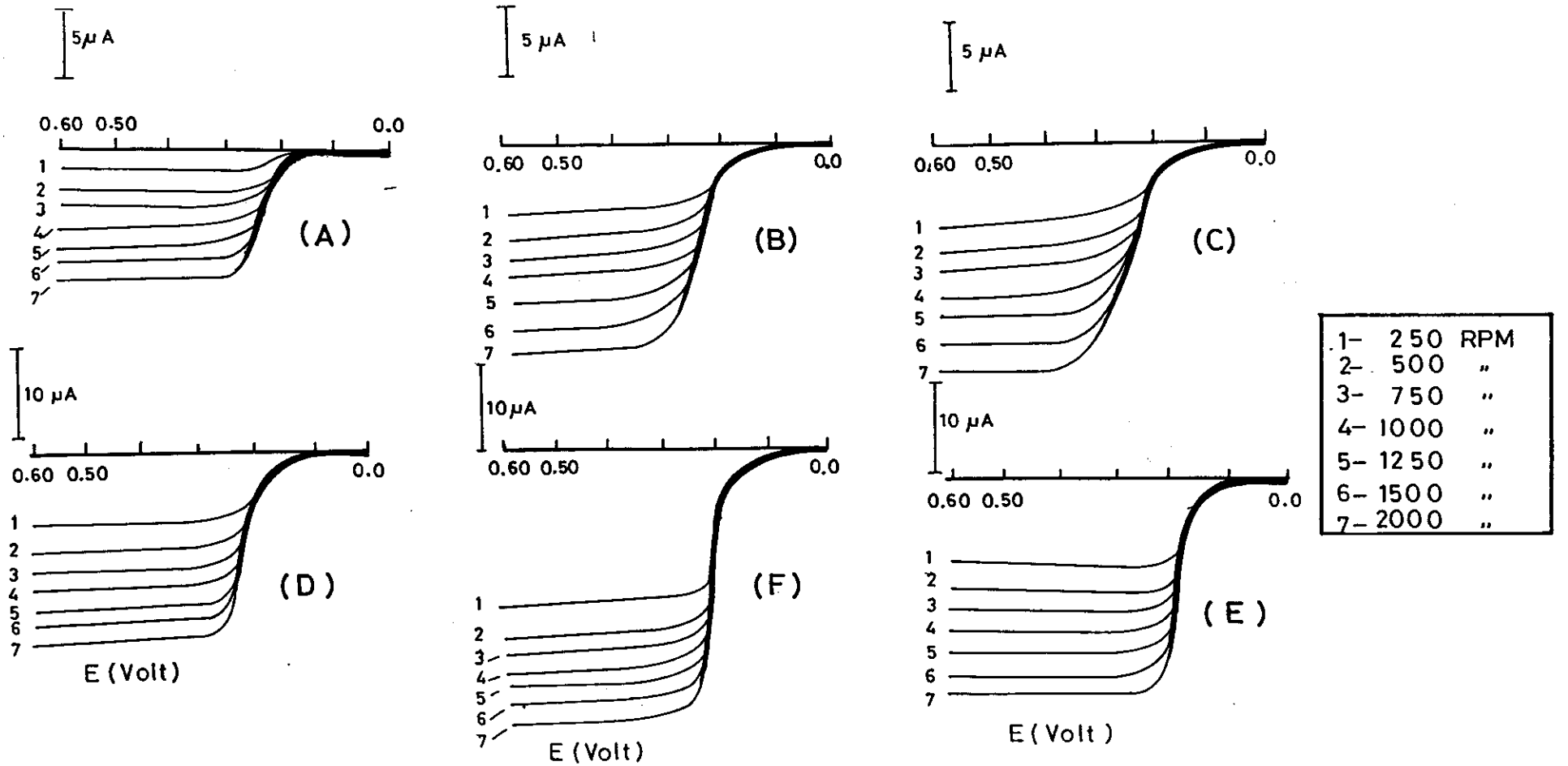

Figure 54: The effect of rotation speed of glassy carbon electrode on the linear sweep voltammograms obtained for C_{18}DMB microemulsion systems containing (a) $2x10^{-4}$ M ferrocene, (b) $4x10^{-4}$ M ferrocene, (c) $8x10^{-4}$ M ferrocene, (d) $1x10^{-3}$ M ferrocene, (e) $2x10^{-3}$ M ferrocene and (f) $3x10^{-3}$ M ferrocene. The rotation speeds are 250, 500, 750, 1000, 1250, 1500 and 2000 RPM.

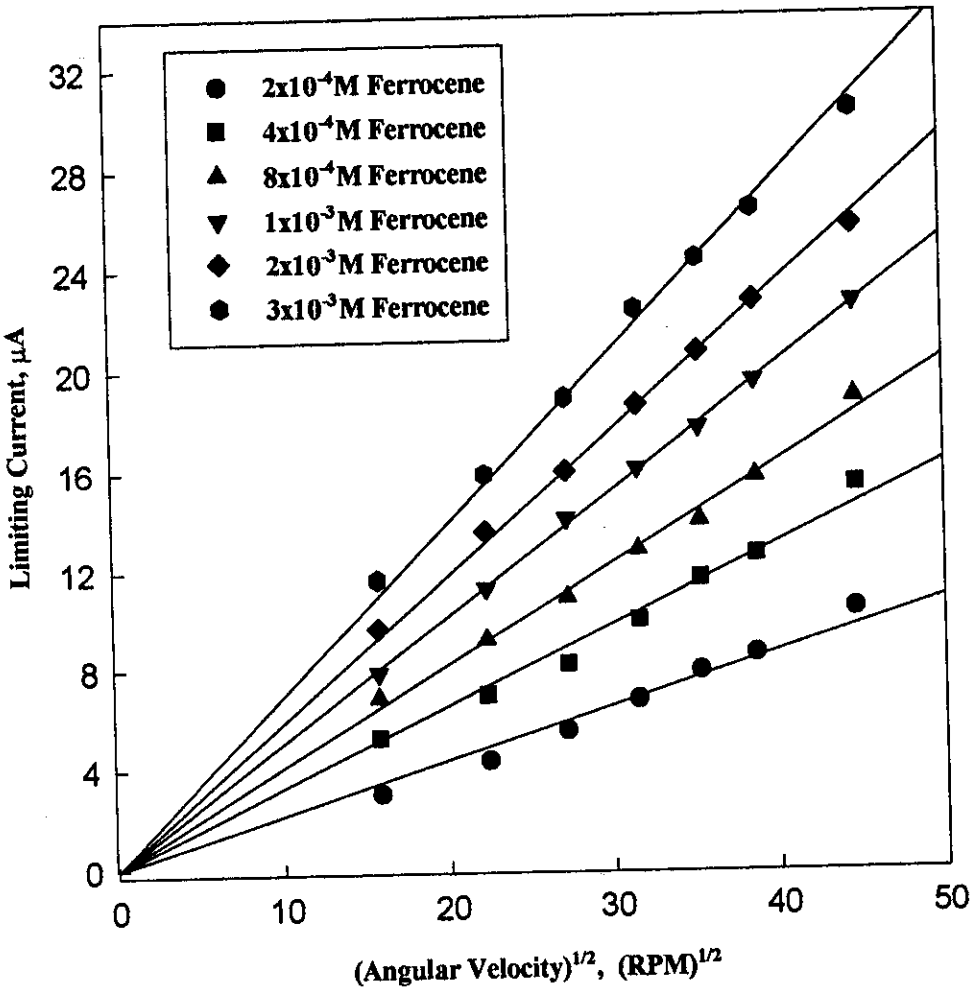

Figure 55 : The plots of the limiting current (i_l) versus the square root of angular velocity ($\omega^{1/2}$) for ferrocene in C_{18}DMB microemulsion systems.

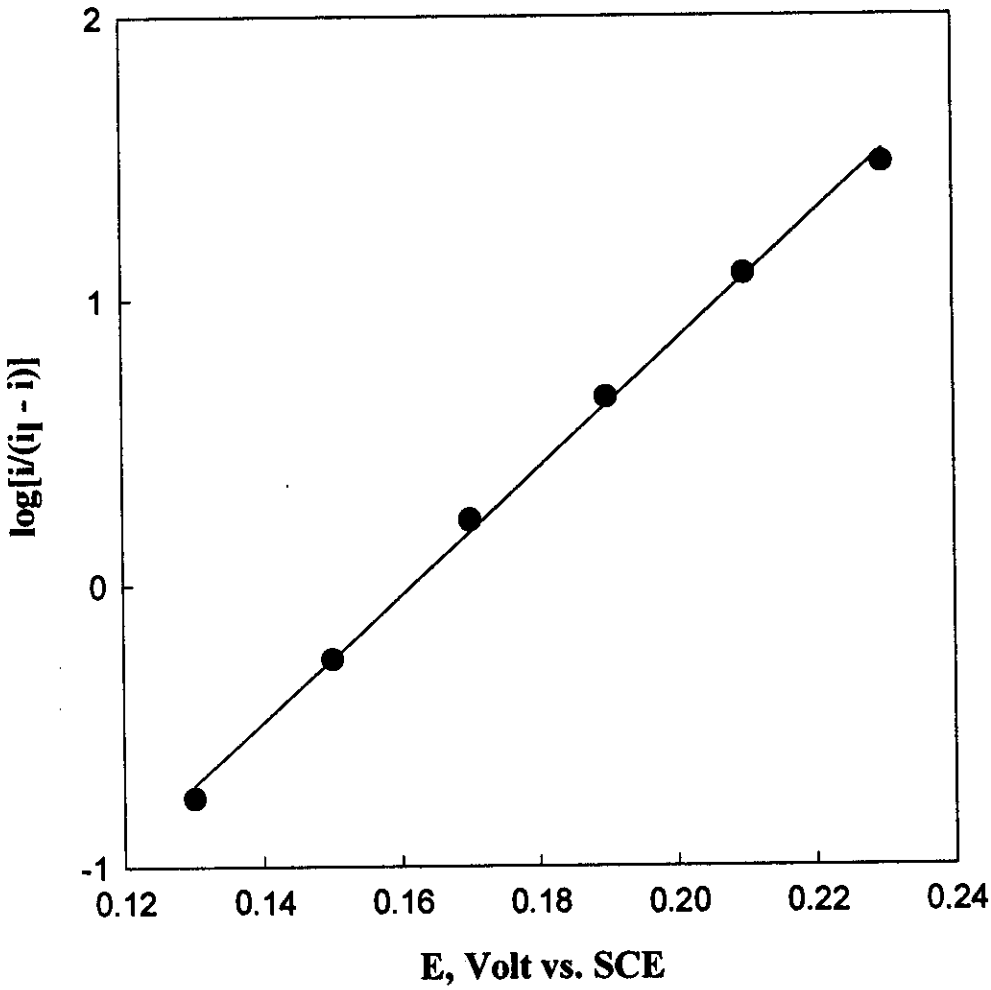

Figure 56: RDV-Logarithmic analaysis of 1mM ferrocene in C_{18}DMB microemulsion system.

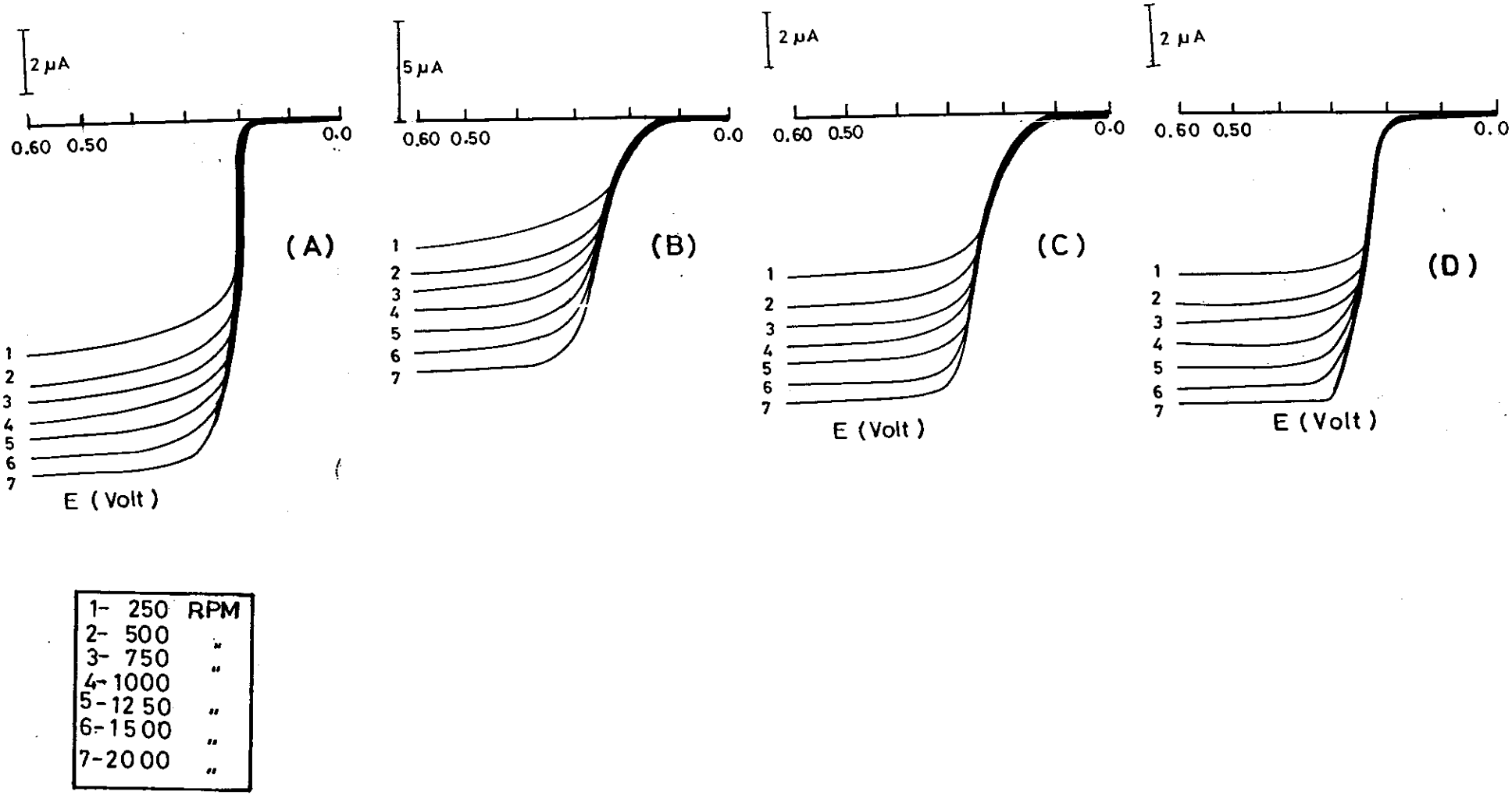

Figure 57: The effect of rotation speed of glassy carbon electrode on the linear sweep voltammograms obtained for 1 mM ferrocene in C_{18}DMB microemulsion systems containing, (a) 0.5% n-dodecane, (b) 1.5% n-dodecane, (c) 2.0% n-dodecane and (d) 2.5% n-dodecane. The rotation speed are 250, 500, 750, 1000, 1250, 1500 and 2000 RPM.

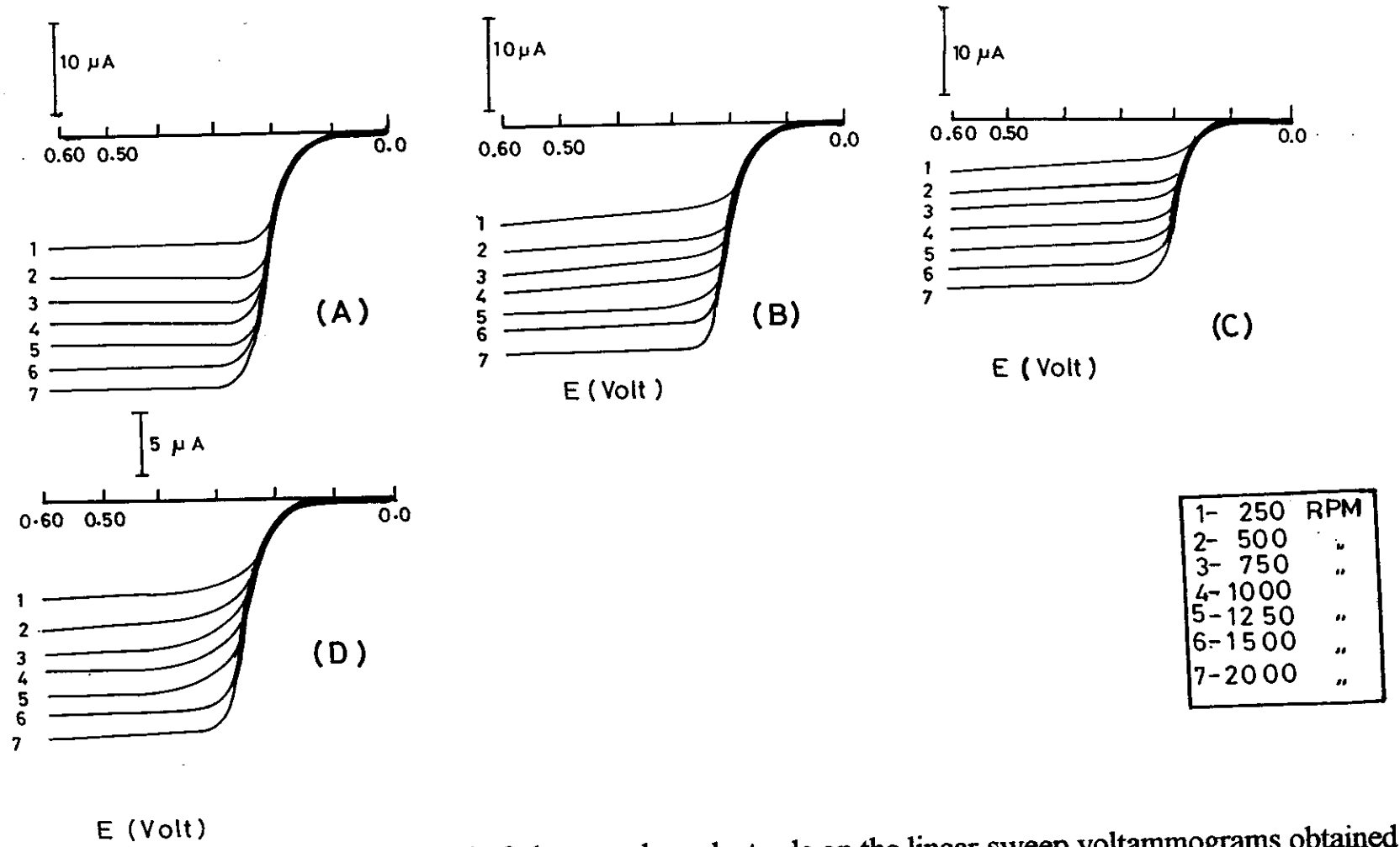

Figure 58: The effect of rotation speed of glassy carbon electrode on the linear sweep voltammograms obtained for 1 mM ferrocene in C_{18}DMB microemulsion systems containing, (a) 0.05 M NaCl, (b) 0.08 M NaCl, (c) 0.10 M NaCl, and (d) 0.12 M NaCl. The rotation speed are 250, 500, 750, 1000, 1250, 1500 and 2000 RPM.

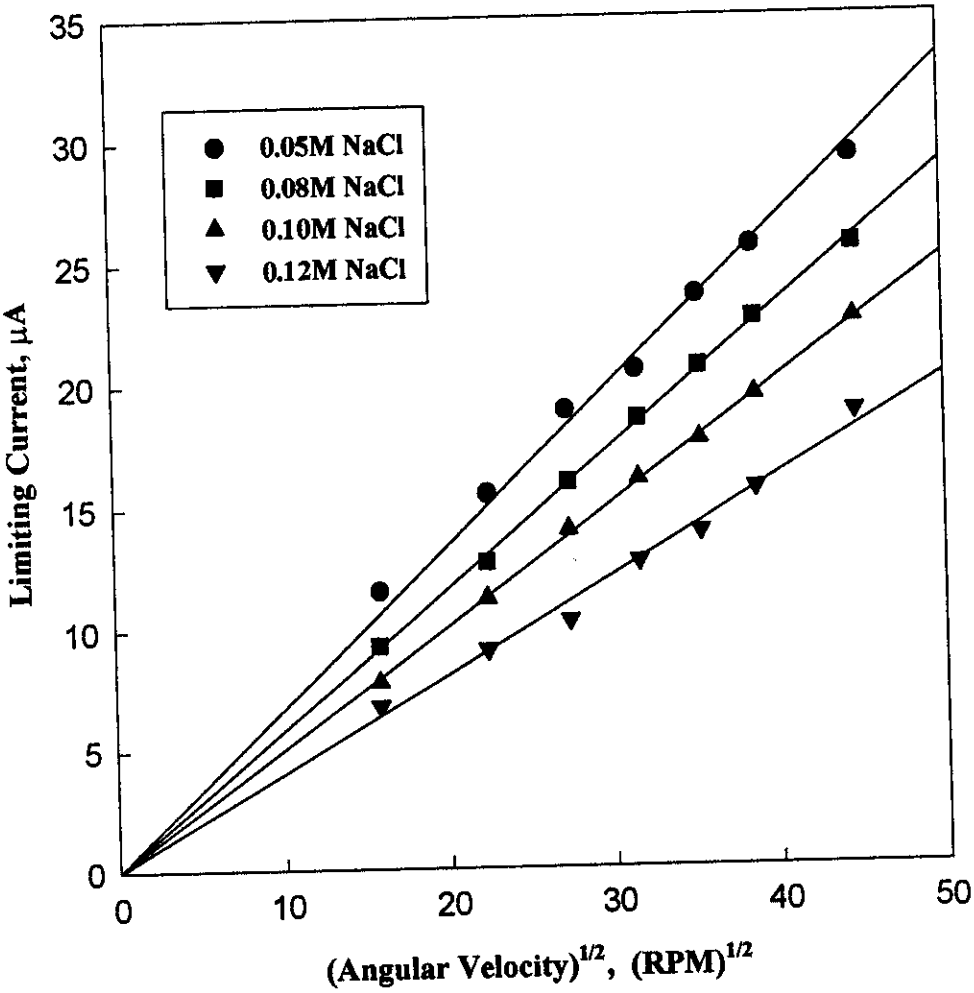

Figure 59: The plots of the limiting current (i_l) versus the square root of angular velocity ($\omega^{1/2}$) for 1mM ferrocene in C_{18}DMB microemulsion as a function of NaCl concentration.

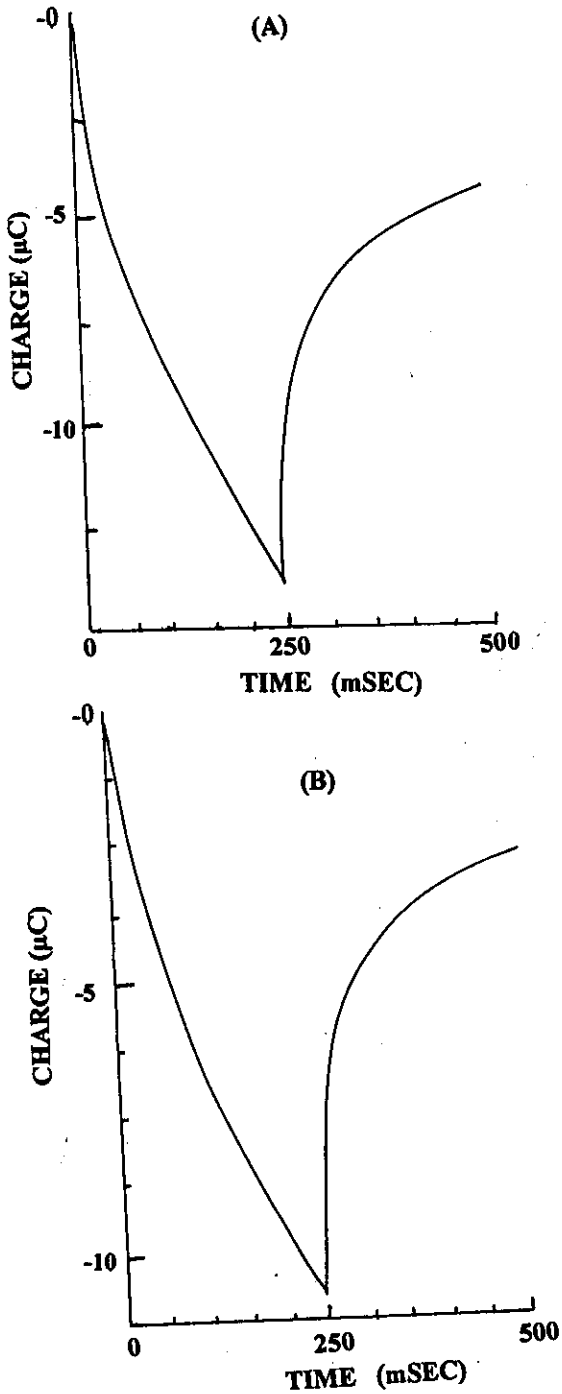

Figure 60 : Chronocoulometric responses of 1.0 mM ferrocene in (a) C_{18}DMB micelle and (b) C_{18}DMB microemulsion. Charge versus time.

Table 20: Cyclic voltammetric data obtained for different concentrations of ferrocene in C_{18}DMB microemulsion system.

Sweep Rate	$E_{p,a}$	$E_{p,c}$	$I_{p,a}$	$I_{p,c}$	$I_{p,a}/I_{p,}$	ΔE_p	$E_{1/2}$	$E_{1/2}$(average)
mV/sec	mV	mV	µA	µA	-	mV	mV	mV
(A) $2x10^{-4}$ M Ferrocene								
20	221	162	1.10	1.20	0.916	59	191	
50	221	162	2.10	2.20	0.954	59	191	
80	222	163	2.70	2.80	0.960	59	192	
100	222	163	3.10	3.30	0.940	59	192	191
150	222	163	3.40	3.70	0.940	59	192	
200	222	163	4.10	4.20	0.976	59	192	
500	217	160	6.90	6.90	1.000	57	188	
(B) $4x10^{-4}$ M Ferrocene								
20	221	164	2.10	2.30	0.913	57	192	
50	221	164	3.10	2.90	1.060	57	192	
80	221	164	3.70	3.60	1.020	57	192	
100	219	162	4.30	4.20	1.020	57	190	191
150	219	162	5.70	5.60	1.010	57	190	
200	221	164	6.50	6.40	1.010	57	192	
500	221	164	10.20	10.40	0.980	57	192	
(C) $8x10^{-4}$ M Ferrocene								
20	223	166	2.60	2.80	0.928	57	194	
50	223	166	3.60	3.50	1.028	57	194	
80	224	166	4.80	5.10	0.960	58	195	
100	225	166	5.40	5.40	1.000	59	195	195
150	225	165	6.50	6.50	1.000	60	195	
200	225	165	7.30	7.60	0.960	60	195	
500	225	165	12.50	12.80	0.976	60	195	

Follow:

Sweep Rate mV/sec	$E_{p,a}$ mV	$E_{p,c}$ mV	$I_{p,a}$ µA	$I_{p,c}$ µA	$I_{p,a}/I_{p,}$ -	ΔE_p mV	$E_{1/2}$ mV	$E_{1/2}$(average) mV
(D) $1x10^{-3}$ M Ferrocene								
20	221	164	3.80	4.10	0.926	57	192	
50	221	164	4.80	4.70	1.020	57	192	
80	221	164	5.60	5.80	0.960	57	192	
100	219	162	6.40	6.10	1.049	57	190	191
150	219	162	8.10	7.90	1.020	57	190	
200	221	164	9.01	9.50	0.950	57	192	
500	221	164	14.10	14.30	0.986	57	192	
(E) $2x10^{-3}$ M Ferrocene								
20	223	164	4.60	4.80	0.958	59	193	
50	223	164	5.60	5.50	1.018	59	193	
80	223	164	7.10	6.90	1.028	59	193	
100	222	162	7.90	7.80	1.012	60	192	193
150	225	163	9.60	9.50	1.010	62	194	
200	225	164	11.60	11.80	0.980	61	194	
500	222	164	18.40	18.10	1.016	58	193	
(F) $3x10^{-3}$ M Ferrocene								
20	222	164	5.70	5.90	0.966	58	193	
50	223	164	6.70	6.60	1.010	59	193	
80	223	164	8.90	9.10	0.978	59	193	
100	222	162.	9.90	10.10	0.980	60	192	193
150	225	162	11.90	12.10	0.983	63	193	
200	226	164	13.70	13.90	0.985	62	195	
500	223	165	22.40	22.40	1.000	58	194	

Table 21 : Cyclic voltammetric data obtained for different concentrations of potassium ferrocyanide in C_{18}DMB micremulsion system.

Sweep Rate	$E_{p,a}$	$E_{p,c}$	$I_{p,a}$	$I_{p,c}$	$I_{p,a}/I_{p,c}$	ΔE_p	$E_{1/2}$	$E_{1/2}$(average)
mV/sec	mV	mV	µA	µA	-	mV	mV	mV
(A) $2x10^{-4}$ M Potassium ferrocyanide								
20	177	18	1.50	1.52	0.981	159	97	
50	174	16	2.40	2.49	0.961	158	95	
80	177	16	3.20	3.25	0.984	161	96	
100	174	17	3.60	3.64	0.987	157	95	96
150	176	16	4.30	4.402	0.977	160	96	
200	177	17	5.20	5.23	0.994	160	97	
500	175	19	7.98	8.10	0.984	156	97	
(B) $8x10^{-4}$ M Potassium ferrocyanide								
20	177	16	2.40	2.45	0.978	161	96	
50	177	16	3.46	3.60	0.961	161	96	
80	177	16	4.50	4.57	0.984	161	96	
100	176	17	4.99	5.14	0.970	159	96	96
150	176	17	6.20	6.34	0.977	159	96	
200	177	17	6.98	6.99	0.998	160	97	
500	178	18	10.61	10.72	0.989	160	98	
(C) $1x10^{-3}$ M Potassium ferrocyanide								
20	175	15	2.80	2.83	0.989	160	95	
50	175	15	4.40	4.41	0.997	160	95	
80	176	15	5.60	5.64	0.992	161	95	
100	176	16	6.10	6.25	0.976	160	96	95
150	176	16	7.40	7.43	0.995	160	96	
200	177	16	8.40	8.56	0.981	161	96	
500	178	17	13.10	13.32	0.983	161	97	

Follow:

Sweep Rate	$E_{p,a}$	$E_{p,c}$	$I_{p,a}$	$I_{p,c}$	$I_{p,a}/I_{p,c}$	ΔE_p	$E_{1/2}$	$E_{1/2}$(average)
mV/sec	mV	mV	µA	µA	-	mV	mV	mV
(D) $2x10^{-3}$ M Potassium ferrocyanide								
20	178	17	3.60	3.52	1.022	161	97	
50	178	17	5.40	5.61	0.962	161	97	
80	178	17	6.80	6.83	0.995	162	98	
100	179	18	7.50	7.62	0.984	161	98	98
150	179	19	8.98	8.91	1.007	160	99	
200	180	19	10.60	10.70	0.990	161	99	
500	180	21	16.90	17.20	0.982	159	100	
(E) $3x10^{-3}$ M Potassium ferrocyanide								
20	183	19	4.60	4.73	0.972	164	101	
50	183	20	6.80	6.92	0.982	163	101	
80	183	22	8.70	8.90	0.977	161	102	
100	184	22	9.70	10.10	0.960	162	103	103
150	185	23	11.60	11.70	0.991	162	104	
200	186	23	13.40	13.63	0.983	163	104	
500	188	24	21.20	21.00	1.009	164	106	

Table 22 : Diffusion coefficients and the radius of microemulsion droplets of ferrocene in C_{18}DMB microemulsion at 40°C.

ferrocene	(CV)		(RDV)	
Concentration	$D_a x10^{-6}$	R_h	$D_a x10^{-6}$	R_h
mM	cm^2/sec	A°	cm^2/sec	A°
0.2	8.83	27	8.53	28
0.4	4.93	49	4.85	50
0.8	1.77	138	1.48	165
1.0	1.53	160	1.51	162
2.0	0.64	385	0.61	402
3.0	0.42	584	0.36	681

Table 23 : Diffusion coefficients and the radius of microemulsion droplets of potassium ferrocyanide in C_{18}DMB microemulsion at 40°C.

$K_4[Fe(CN)_6]$	$D_a x10^{-6}$	R_h
Concentration	cm^2/sec	A°
mM		
0.2	12.30	19.9
0.8	5.75	42.6
1.0	2.18	112.4
2.0	2.15	114.0
3.0	0.87	279.0

Table 24: Cyclic voltammetric data obtained for 1mM ferrocene in C_{18}DMB microemulsion systems contaning different amounts of dodecane at 40°C.

Sweep Rate mV/sec	$E_{p,a}$ mV	$E_{p,c}$ mV	$I_{p,a}$ µA	$I_{p,c}$ µA	$I_{p,a}/I_{p,}$ -	ΔE_p mV	$E_{1/2}$ mV	$E_{1/2}$(average) mV
(A) 0.50% Dodecane								
20	228	164	3.10	3.20	0.968	64	196	
50	228	164	4.21	4.20	0.100	64	196	
80	227	164	5.64	5.46	1.032	63	195	
100	229	168	7.17	7.15	1.002	61	198	197
150	231	166	8.20	8.18	1.002	65	198	
200	233	167	9.23	9.19	1.004	66	200	
500	234	170	14.60	14.52	1.005	64	202	
(B) 1.5% Dodecane								
20	235	175	3.07	3.00	1.023	60	205	
50	235	175	4.13	4.21	0.980	60	205	
80	236	175	5.81	5.70	1.019	61	205	
100	236	177	6.98	6.81	1.024	59	206	206
150	283	178	8.01	8.07	0.992	60	208	
200	240	178	8.92	8.98	0.993	62	209	
500	240	179	14.52	14.61	0.993	61	209	

Follow:

Sweep Rate mV/sec	$E_{p,a}$ mV	$E_{p,c}$ mV	$I_{p,a}$ µA	$I_{p,c}$ µA	$I_{p,a}/I_{p,}$ -	ΔE_p mV	$E_{1/2}$ mV	$E_{1/2}$(average) mV
(C) 2.0% Dodecane								
20	231	169	2.90	2.80	1.053	62	200	
50	231	169	4.00	4.10	0.975	62	200	
80	231	170	5.78	5.80	0.996	61	200	
100	232	171	6.80	6.87	0.989	61	201	201
150	233	172	8.00	8.10	0.981	61	202	
200	234	172	8.70	8.90	0.977	62	202	
500	235	170	14.41	14.50	0.993	65	203	
(D) 2.5% Dodecane								
20	238	177	2.80	2.89	0.968	61	207	
50	238	177	3.89	3.90	0.997	61	207	
80	239	178	5.50	5.60	0.982	61	208	
100	240	179	6.30	6.40	0.984	61	209	209
150	242	180	7.20	7.30	0.986	62	211	
200	244	181	7.89	7.92	0.996	63	212	
500	246	182	14.20	14.30	0.993	64	214	

Table 25: Cyclic voltammetric data obtained for 1mM ferrocene in C_{18}DMB microemulsion system containg different concentrations of NaCl.

Sweep Rate	$E_{p,a}$	$E_{p,c}$	$I_{p,a}$	$I_{p,c}$	$I_{p,a}/I_{p,c}$	ΔE_p	$E_{1/2}$	$E_{1/2}$(average)
mV/sec	mV	mV	µA	µA	-	mV	mV	mV
(A) 0.05M NaCl								
20	203	149	3.50	3.57	0.980	54	176	
50	204	149	5.80	5.90	0.983	55	176	
80	204	149	7.40	7.50	0.986	55	176	
100	204	149	8.10	8.00	1.012	55	176	176
150	198	150	9.70	9.80	0.989	48	174	
200	198	150	11.68	11.60	1.006	48	174	
500	207	156	17.80	17.90	0.994	51	181	
(B) 0.08M NaCl								
20	220	163	3.20	3.10	1.032	58	191	
50	221	163	5.20	5.30	0.981	58	192	
80	220	162	6.40	6.39	1.001	58	191	
100	220	162	7.10	7.20	0.986	58	191	192
150	220	162	8.67	8.70	0.996	58	191	
200	220	171	10.49	10.40	1.008	49	195	
500	225	171	15.80	15.90	0.993	54	198	

Follow:

Sweep Rate mV/sec	$E_{p,a}$ mV	$E_{p,c}$ mV	$I_{p,a}$ µA	$I_{p,c}$ µA	$I_{p,a}/I_{p,c}$ -	ΔE_p mV	$E_{1/2}$ mV	$E_{1/2}$(average) mV
(A) 0.010M NaCl								
20	221	164	2.90	3.10	0.935	57	192	
50	221	164	4.80	4.90	0.979	57	192	
80	221	164	5.60	5.76	0.987	57	192	
100	219	162	6.40	6.50	0.984	57	190	191
150	219	162	8.10	8.20	0.987	57	190	
200	221	164	9.01	9.00	1.001	57	192	
500	221	164	14.10	14.00	1.007	57	192	
(B) 0.12M NaCl								
20	277	218	2.30	2.40	0.958	59	247	
50	277	219	3.40	3.48	0.977	58	248	
80	280	220	4.30	4.40	0.977	60	250	
100	280	220	4.90	5.10	0.960	60	250	250
150	282	227	5.90	5.97	0.988	55	245	
200	283	227	6.90	6.98	0.988	56	255	
500	283	230	11.10	11.20	0.991	53	256	

Table 26 : Diffusion coefficient and the radius of microemulsion droplets values of 1 mM ferrocene in C_{18}DMB microemulsion system containing 1.6% C_{18}DMB, 2.5% n- dodecane and 1.88 n-butanol at different concentrations of NaCl using CV.

NaCl Concentration mM	$D_a x10^{-6}$ cm^2/sec	R_h A°
0.05	2.50	98
0.08	1.97	123
0.10	1.53	160
0.12	1.11	220

Table 27 : Diffusion coefficient and the radius of microemulsion droplets values of 1 mM ferrocene in C_{18}DMB microemulsion system containing, 2.5% n- dodecane 1.88% n-butanol and 0.1 M NaCl at different amount of surfactant using CV' .

% C_{18}DMB	$D_a x10^{-6}$ cm^2/sec	R_h A°
1.6	1.53	160
2.0	1.98	123
2.5	2.34	104
3.0	3.03	80

3.6 Electrachemical Investigations in Micelles and Microemulsion Media.

Compounds possessing quinoid structure play an important role in electron and proton transfer reactions in biological systems [155-157]. For instance, the biological activity of vitamin K, which is 1,4-naphtho-quinone, is due to its role as an oxidising agent [158]. K vitamins are present in vegetables where they seem to play an active role in photosynthetic mechanisms [159]. They also play a role in cellular respiration as electron transporters [160] and in oxidation phosphorylation [161]. These properties result from the reversible character of the quinone / hydroquinone redox system.

In the human body, they are synthesized by microorganisms in the intestine to provide the required physiological quantities and implication in synthesis of four blood coagulation factors in the liver [162,163]. The diffeciency of vitamin K in the body are in frequent, but may occur if obstruction of the bile or intestine occurs and in cases of liver disease such as cirrhosis [162,163]. Diffeciencies are generally accompanied by a decrease in the prothrombin level with an increase in blood coagulation time. At advanced stages, the capillaties may become fragile and hemorrage. Symptoms are reversed by incorporation of K vitamin in diet, except in cases of liver diseases.

In general, the electrochemistry of quinone / hydroquinone couple has been the subject of many investigators. However, the mechanisms and kinetics of the exchange of two electrons and two protons are not yet fully understood even for the simplest system p-benzoquinone / hydroquinone .

The effect of surfactants on the photochemical changes of menadione were followed polarographically in phosphate buffer pH = 5.9 by Thoma et. al. [164].

The electrochemical activity of these group (vitamin K) were recorded polarographicaly [165-167].

Vitamin K_3 (2-methyl-1,4-naphthoquinone, menadione) has received the most attention by Burger [168]. He determined vitamin K_3 electrochemically in mixtures of multivitamins and in tablets using either 0.5 M KCl or, preferably, in a solvent consisting of 53% 2-propanol, 40% diethylether, and 7% H_2O containing 0.05 M NH_3 and 0.05 M NH_4Cl.

Lindquist et. al. [169] determined 2-methyl-1,4-naphthoquinone (menadione) from acetate buffer of pH = 5.0, containing 25% methanol using differential pulse polarography. He obtained a detection limit of 0.02 ppm.

3.6.1 1,4-Naphthoquinone (I)

A- Cyclic voltammetry

The cyclic voltammograms of 1 mM of 1,4-naphthoquinone were recorded in micelles and microemulsion media of three different surfactants as well as in pure aqueous solution, it is poorly soluble in water (solubility $6x10^{-4}$ M). Its solubility is greatly enhanced by micelles and micro-emulsion. Cationic (cetyltrimethylammonium bromide, CTAB), anionic [bis(2-ethylhexyl) sulfosuccinate, AOT] and zwitterionic (octadecyl-dimethyl betaine, C_{18}DMB) model surfactants were used in this investi-gation of composition listed in Table (1).

The voltammograms displayed one cathodic peak on the cathodic scan and one anodic peak on the reverse scan in all micelles and microemulsion media, except in C_{18}DMB micelles it displayed two oxidation peaks of almost equal heights, Fig. (61).

The voltammograms of 1,4-naphthoquinone in the corresponding pure aqueous solution containing only 0.10 M NaCl supporting electrolyte showed a similar voltammetric response, a single redox peak, Fig.(62). The voltammograms recorded at different sweep rates varying from 20 to 500 mV/sec are essentially similar displaying a single redox peak.

The peak potential separation ΔE_P is slightly increased on increasing sweep rate. The voltammetric data of 1,4-naphthoquinone in pure aqueous and various surfactant systems are summarized in Tables (28 - 30). Since the peak potential separation ΔE_P is equal 0.059/n and equal to $(E_{p,a} - E_{p,c})$ it was found very close to 30 mV at very small sweep rates in CTAB microemulsion system and around the theoritical value for 2-electron transfer process, Table (30). In other media, the peak potential separation (ΔE_P) is increased on increasing the sweep rate which leads generally to the fact that the electrochemical-chemical-electrochemical (ECE) reaction

nature takes place, Tables (28,29). Protonation of the anion free radical generally leads to a disproportionation reaction [170, 171].

The peak currents on the cathodic and anodic branches of sweep are slightly different and the ratio $I_{p,a}/I_{p,c}$ is slightly less than unity in micelles and microemulsion systems, Tables (28-30). These results indicated the very weak adsorption contribution.

On employing the Randles-Sevcik equation [140], the plots of the cathodic peak currents ($I_{p,c}$) as well as the anodic one ($I_{p,a}$) versus $\upsilon^{1/2}$ for 1,4-naphthoquinone in micelles and microemulsion of different surfactant systems showed linear correlations almost passing through the origin, Figs. (63,64). This behaviour confirming that the electrode reaction is mainly controlled by diffusion with slight adsorption contribution at the electrode surface. On the other hand, the plots of the cathodic peak currents ($I_{p,c}$) as well as the anodic one ($I_{p,a}$) versus $\upsilon^{1/2}$ for 1,4-naphthoquinone in pure aqueous solution is slightly deviated from the origin, as shown from Fig.(62b). This behaviour may be attributed to the presence of some adsorption contribution to the electrode process. The slopes of I_p-$\upsilon^{1/2}$ plots were used to estimate the apparent diffusion coefficients of the reduced and oxidized forms of species D_R and D_O, Table (31). The values of the apparent diffusion coefficients indicate the partitioning of 1,4-naphthoquinone between oil droplet, surfactant film and aqueous domain.

An important aspect to be considered in electrochemical investigations in surfactant solutions is adsorption of the surfactant on the electrode surface and its effect on the electrochemical reactions. Our previous electrochemical investigation of ferrocene in AOT and C_{18}DMB micelles and microemulsions did not show any significant effect that could be ascribed to surfactant adsorption on the electrode surface. All the results observed in these studies could be explained based on electrostatic and

hydrophobic interactions of the surfactant with the various species (reactant, intermediates and products) of the electrochemical reaction. In the absence of such interactions the electrochemical behaviour is not significantly affected [32]. In the present investigation, the ratio $I_{p,a}/I_{p,c}$ is slightly less than unity in micelles and microemulsion systems, Tables (29,30). These results indicated the very weak adsorption contribution.

Cationic surfactants are known to be stabilize anion radicals [172]. The slightly smaller ΔE_P (40 mV) in CTAB microemulsions and about 74 mV in micellar solutions compared to that of both AOT and C_{18}DMB micellar and microemulsions shows that the stabilization for cationic surfactants is higher than for anionic and zwitterionic surfactants . This is because the electrostatic effects are generally less in anionic and zwitterionic surfactants than in cationic surfactants. Also, ΔE_P values are close to 30 mV at very slow sweep rates and increase with increasing sweep rates. These characteristics are typical of a reversible charge transfer reaction followed by a slow chemical reaction [124].

Differences are observed in the values of E_p, ΔE_P between micellar solutions or microemulsions Table (28-30). Also changes in half-wave potential ($E_{1/2}$) are expected due to the different effects of the surfactant as local microenvironment on the relative stabilities of the reactants and product of the electron transfer reaction. $E_{1/2}$ shifted to less negative value in the CTAB micellar solution and microemulsion as shown in Table (32).

B- Rotating disk voltammetry (RDV)

The rotating disk voltammograms of 1mM of 1,4-naphthoquinone were recorded in pure aqueous solution as well as in micelles and microemulsion systems of three different surfactant types. Cationic (CTAB), anionic AOT and zwitterionic C_{18}DMB surfactants were used in this investigation. The rotating disk voltammograms were recorded at small sweep rate (5 mV/sec) in the potential window 800 to -1000 mV. The recorded voltammograms of 1,4-naphthoquinone displayed single reduction wave in pure aqueous and in micelles and microemulsion media as represented in Figs. (65a,66). Except, in C_{18}DMB micelles it displayed two waves as observed from cyclic voltammetry, Fig. (66e). The effect of rotation speed (ω) on the voltammogram was recorded from 250 to 2000 RPM. It was found that on increasing the rotation speed there is a negative shift (~20 mV) in the half-wave potential ($E_{1/2}$) indicating the chemical reversibility which coincides with the greater ΔE_P values obtained from CV measurements.

Logarithmic analysis of the rotating disk voltammograms were performed for testing the thermodynamic reversibility using equation (III.2). The plots of log (i/i_l-i) versus E for 1,4-naphthoquinon in pure aqueous as well as micelles and microemulsion media displayed linear correlations, Figs. (67-69). The slopes of these plots were listed in Table (33). Inspection of the data obtained indicating the quasi-reversible electron transfer process.

On using Levich equation [133], the plots of i_l versus $\omega^{1/2}$ in all media showed linear correlations passing through the origin, Figs.(65b,70&71). This behaviour indicates that the reduction process takes place under mass transfer control. The slopes of these plots were used to determine the apparent diffusion coefficients in various media, Table (31).

C- Chronocoulometry of 1,4-naphthoquinone

The chronocoulometric responses of 1,4-naphthoquinone were recorded in micellar solutions and microemulsion systems of three different types of surfactants as well as in pure aqueous solution. CTAB, AOT and C_{18}DMB model surfactants were used in this investigation. The chronocoulograms of 1,4-naphthoquinone in micellar solutions were recorded by plotting the charge (Q_{tot}) versus time (t) after taking the cyclic voltammograms in the same potential window. The stepping time was 250 millisecond and the potential window was from 300 to –800 mV, Figs. (72a, 72c, 72e). A similar chronocoulograms were observed in microemulsion systems, Figs. (72b, 72d, 72f) and in pure aqueous solution, Fig. (73). The values of the amount of adsorbed reactant species Γ_o were listed in Table (34). This is by considering that there is no alteration or negligible contribution by adsorption on Helmoholtz diffusion layer structure. Therefore, the capacitive term of charge (Q_c) for both forward and reverse reactions should be the same.

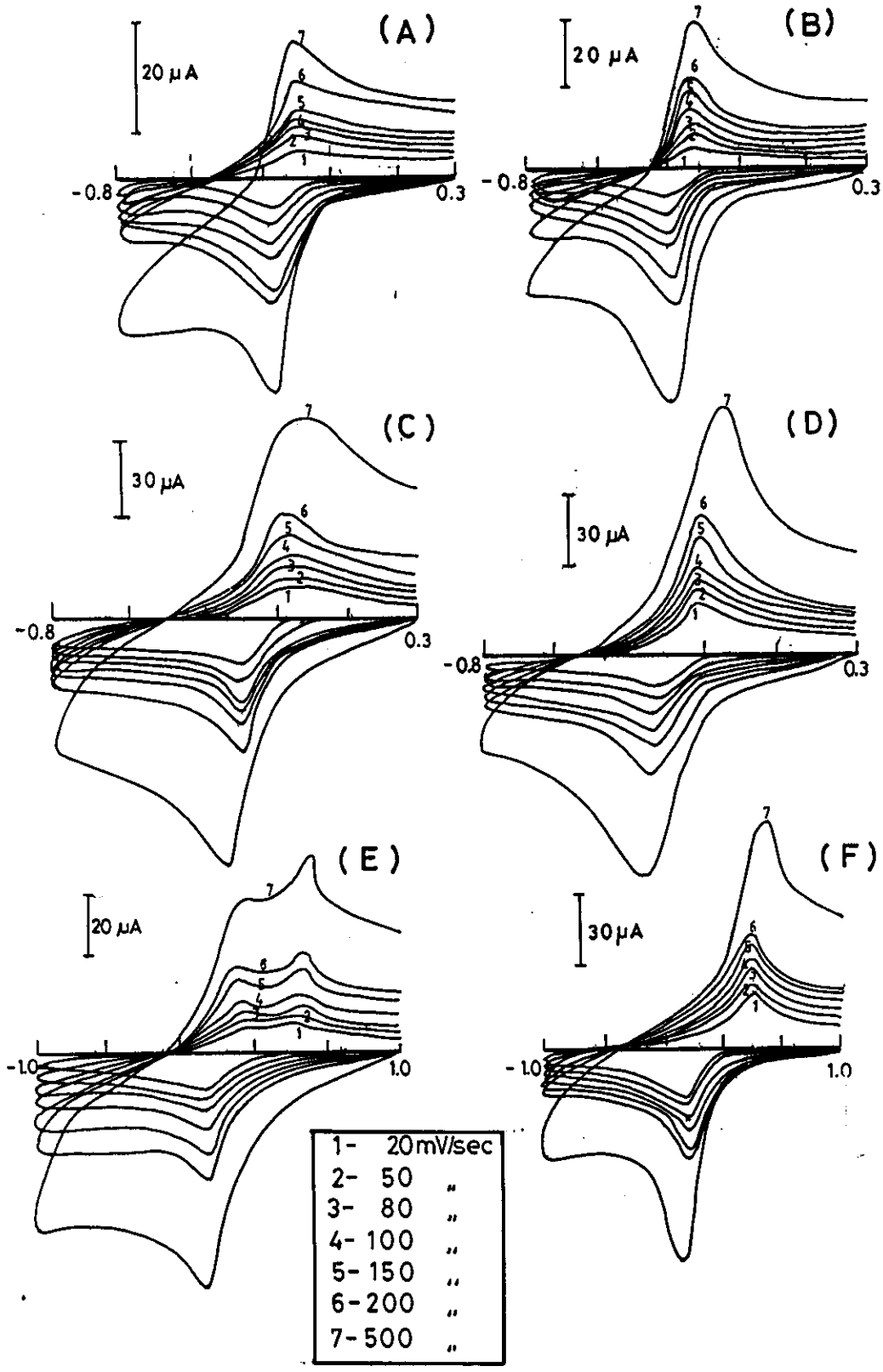

Figure 61 : Cyclic voltammograms of 1,4-naphthoquinone in different systems, (a) CTAB micellar solution, (b) CTAB microemulsion, (c) AOT micellar solution, (d) AOT microemulsion, (e) C_{18}DMB micellar solution, and (f) C_{18}DMB microemulsion. The sweep rates are 20, 50, 80, 100, 150, 200 and 500 mV/sec.

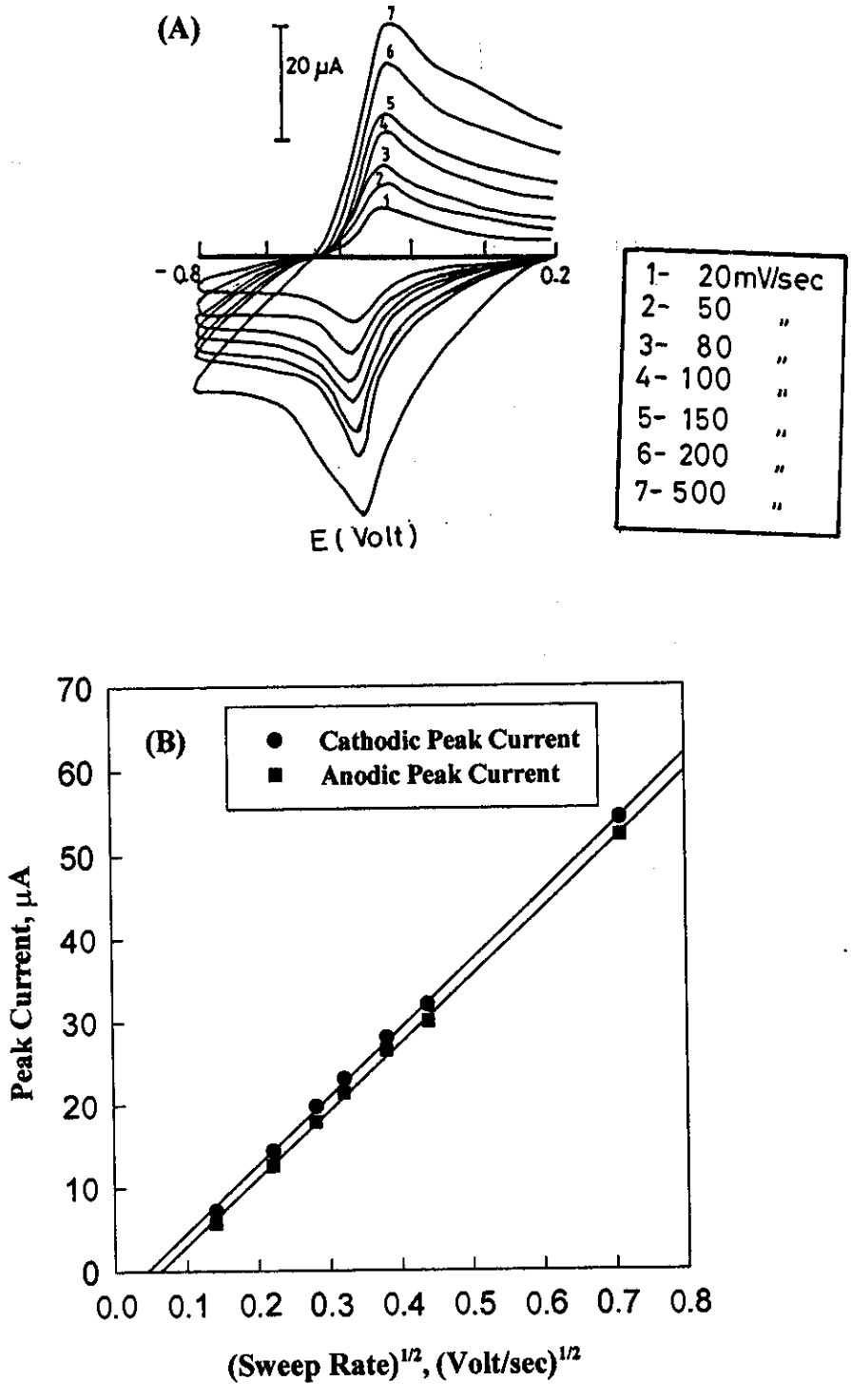

Figure 62 : (a) cyclic voltammogram of 1,4-naphthoquinone in aqueous media and (b) its I_p-$\upsilon^{1/2}$ plot. The sweep rates are 20, 50, 80, 100, 150, 200 and 500 mV/sec.

Peak Current of 1,4-naphthoquinone in different Micellar Solutions.

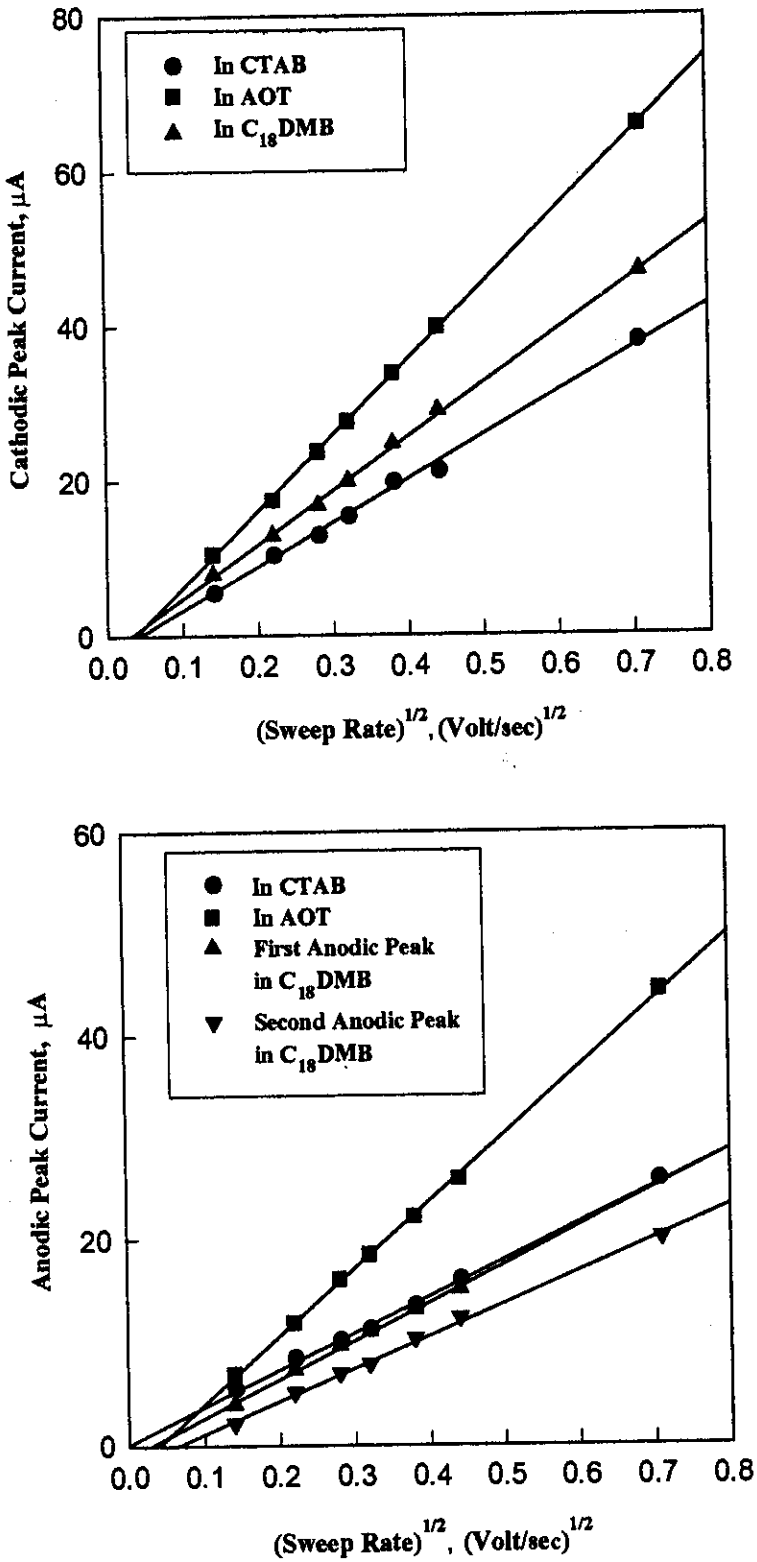

Figure 63

Peak Current of 1,4-naphthoquinone in different Microemulsion Systems

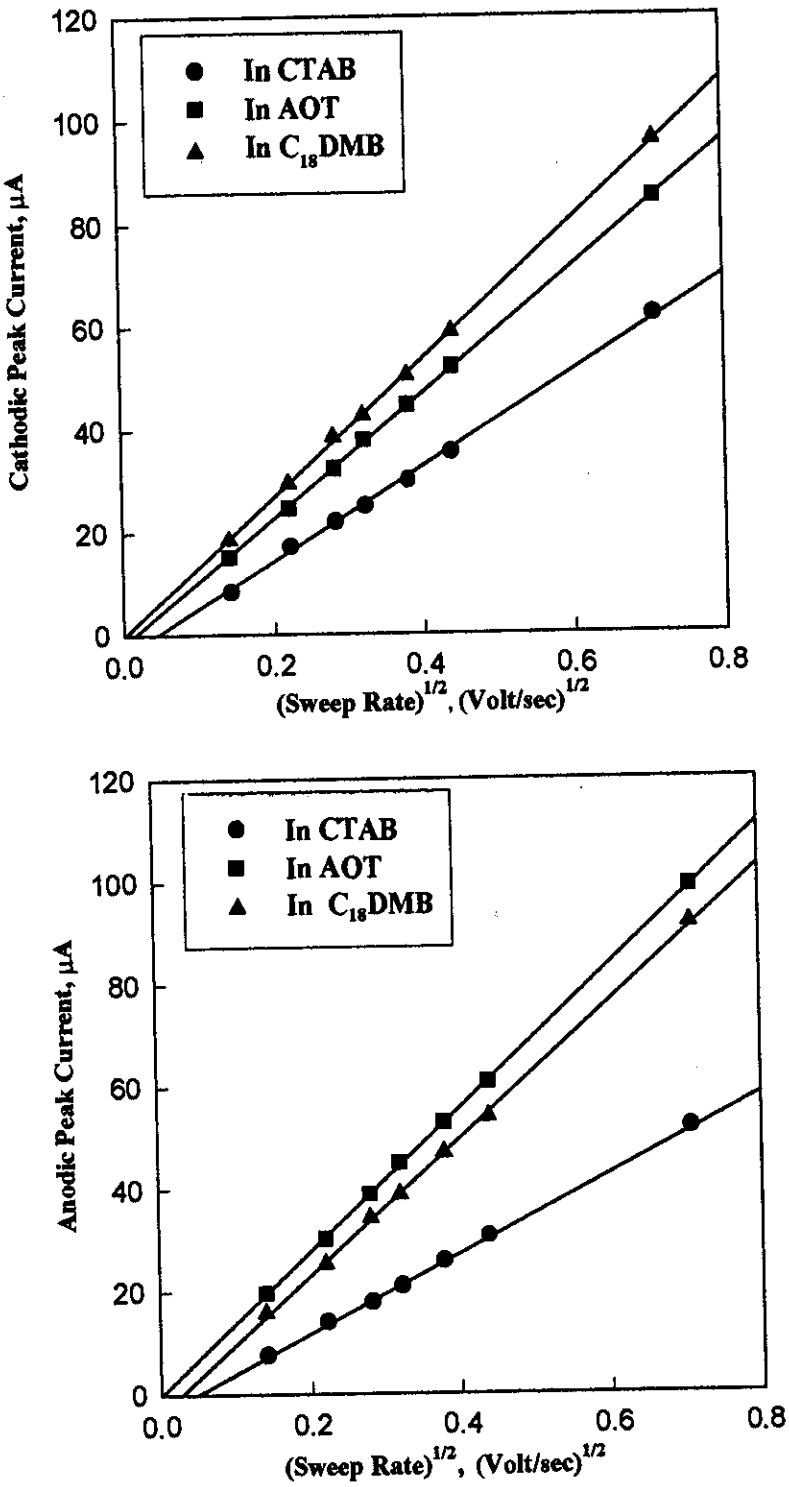

Figure 64:

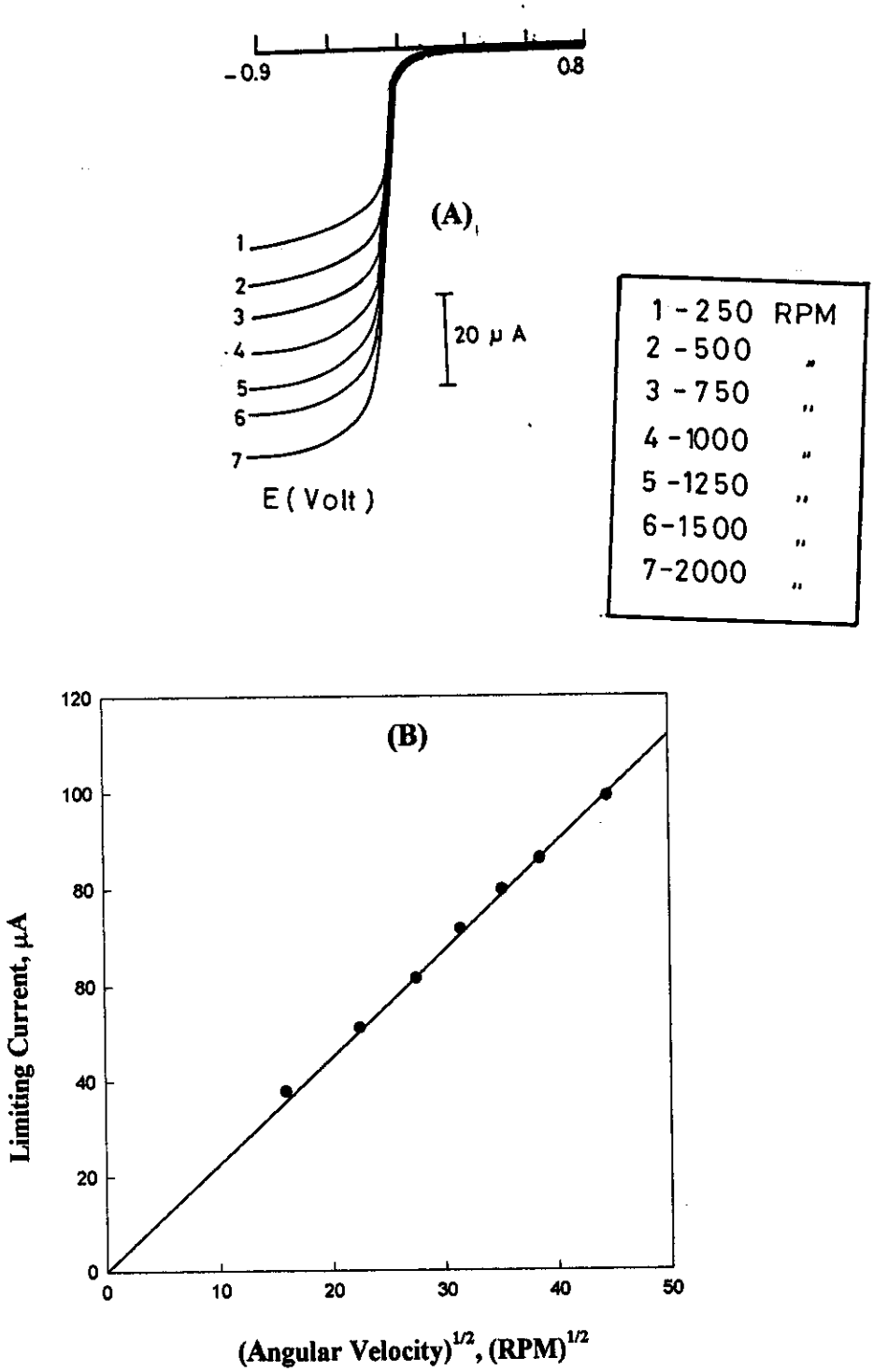

Figure 65: The effect of rotation speed of glassy carbon electrode on the linear sweep voltammogram obtained for 1,4-naphthoquinone in aqueous solution, (a) and the plots of limiting current (i_l) versus square root of angular velocity ($\omega^{1/2}$), (b).

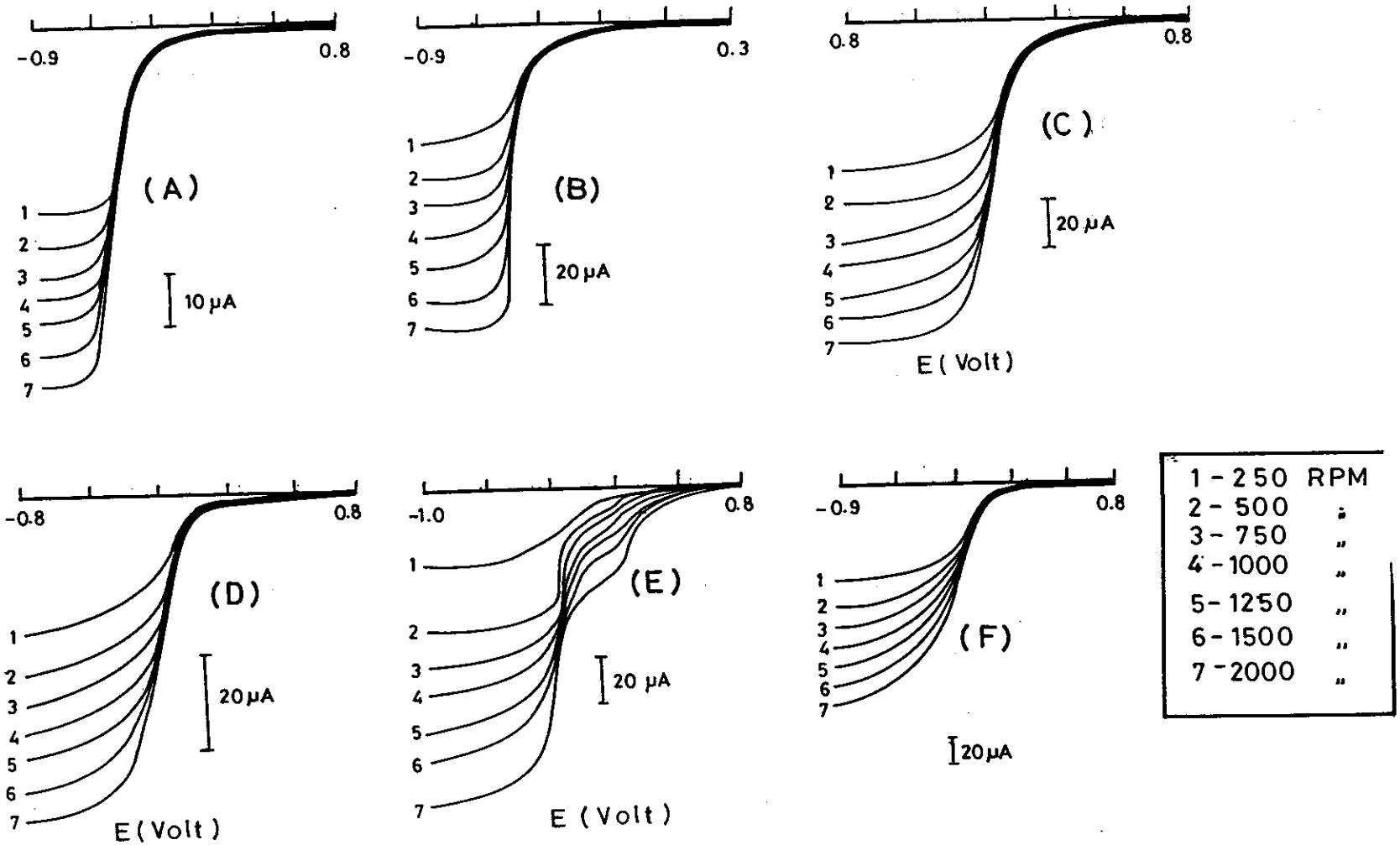

Figure 66: The effect of rotation speed of glassy carbon electrode on the linear sweep voltammograms of 1,4 naphthoquinone in different systems, (a) CTAB micellar solution, (b) CTAB microemulsion, (c) AOT micellar solution, (d) AOT microemulsion, (e) C_{18}DMB micellar solution, and (f) C_{18}DMB microemulsion. The speeds are 250, 500, 750, 1000, 1250, 1500 and 2000 RPM.

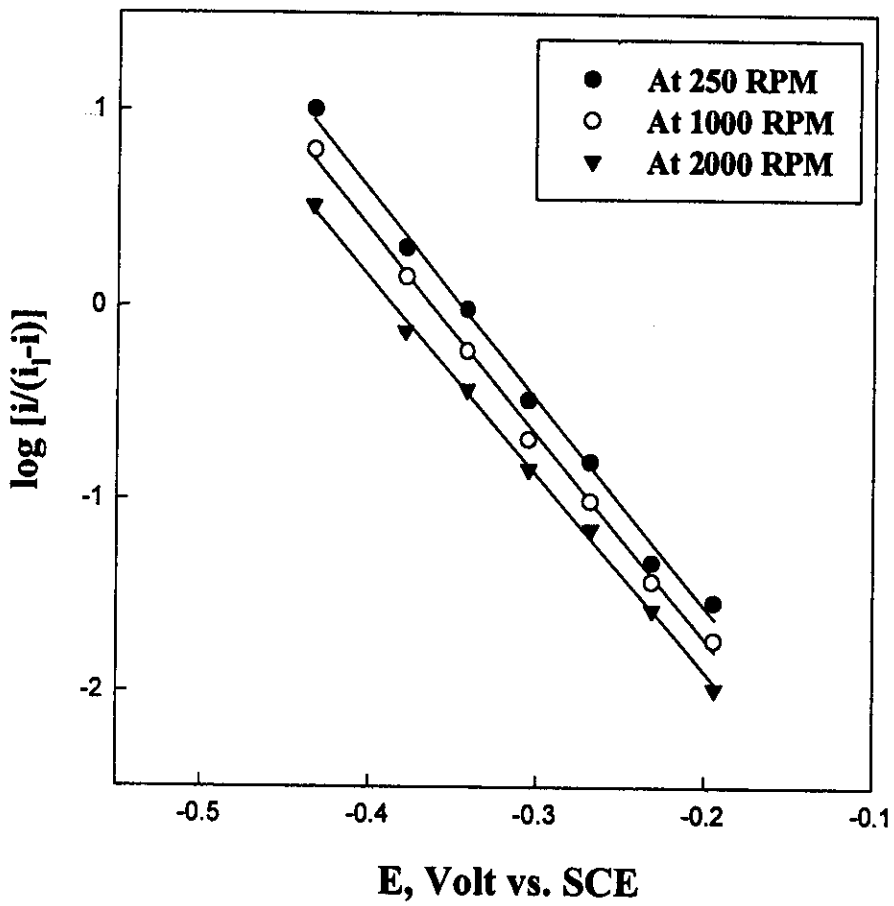

Figure 67: RDV-Logarithmic analysis of 1,4-naphthoquinone in aqueous media.

A- in CTAB
B- in AOT
C- in C_{18}DMB

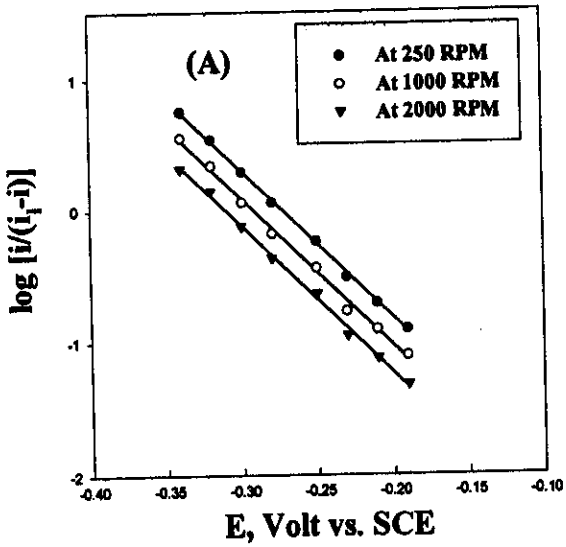

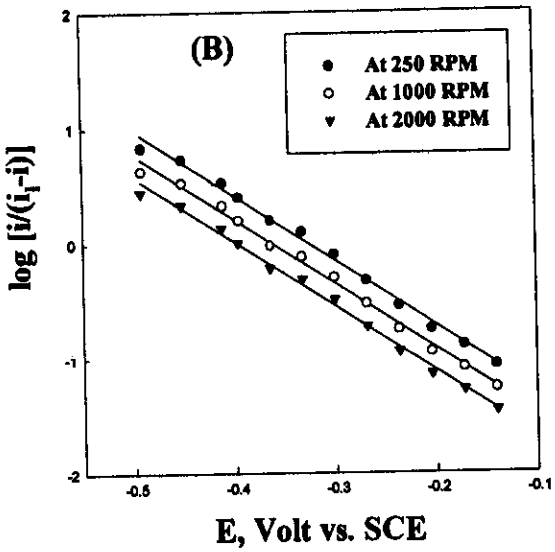

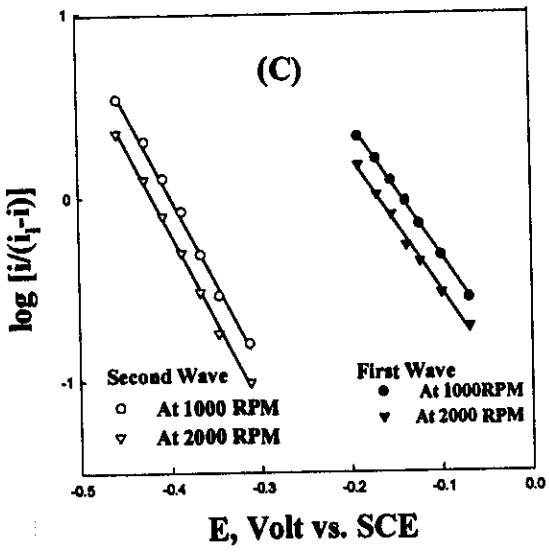

Figure 68: RDV-Logarithmic analysis of 1,4-naphthoquinone in micellar solutions.

A- in CTAB
B- in AOT
C- in C_{10}DMB

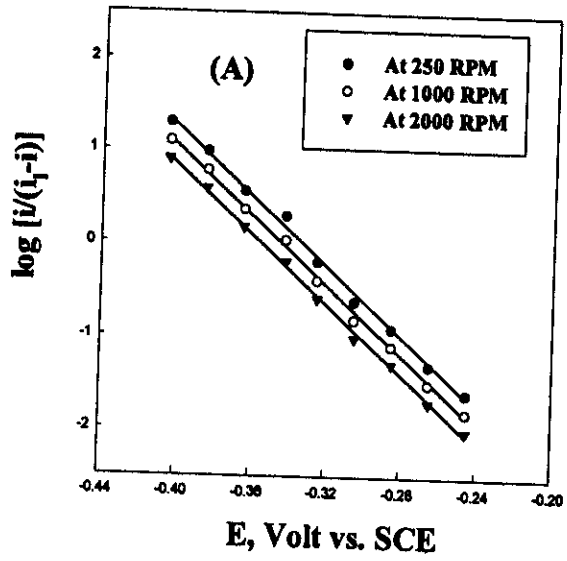

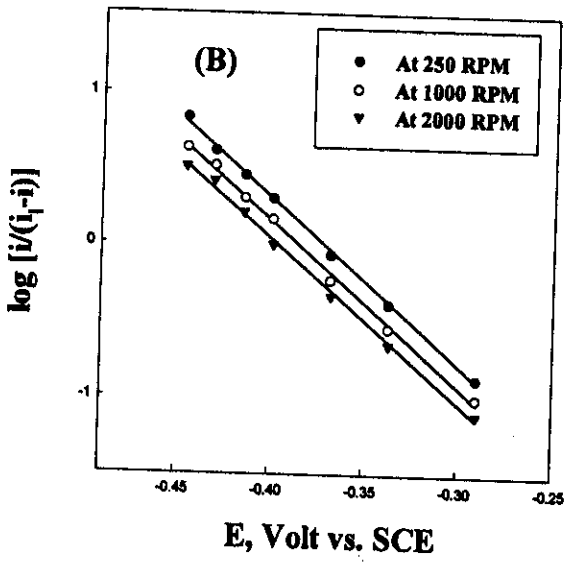

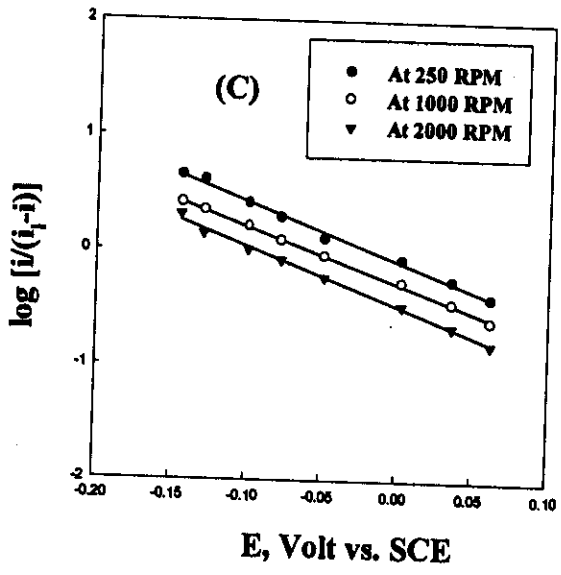

gure 69: RDV-Logarithmic analysis of 1,4-naphthoquinone in microemulsion systems.

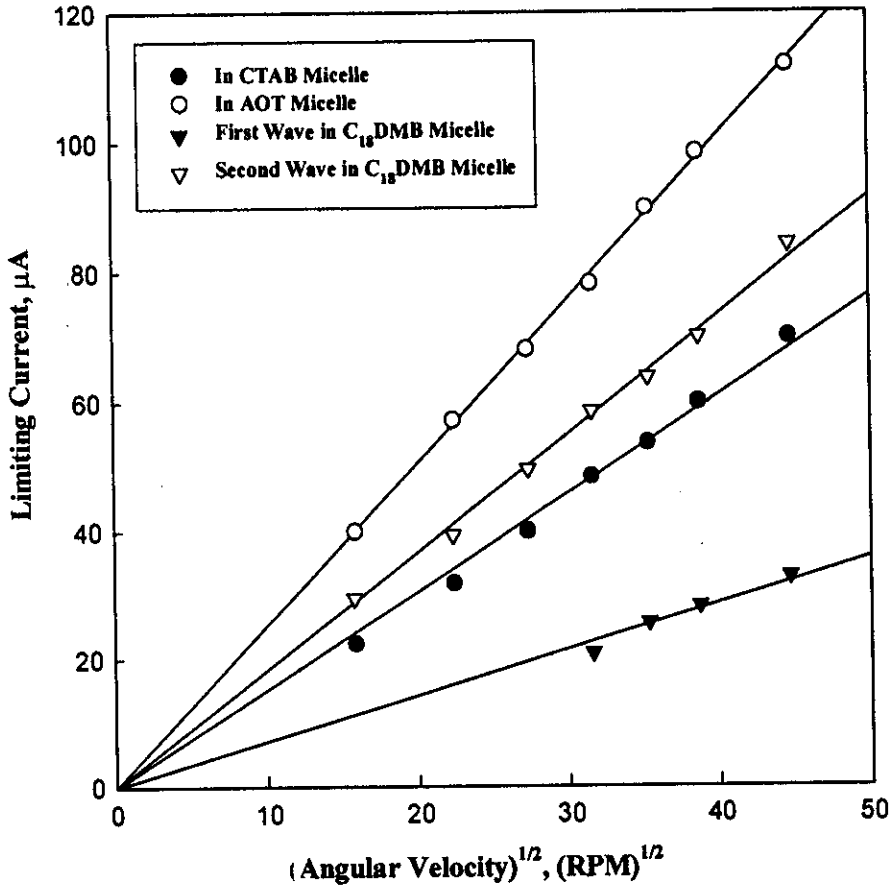

Figure 70: The plots of the limiting (i_l) versus square root of angular velocity ($\omega^{1/2}$) for 1,4-naphthoquinone in different micellar solutions.

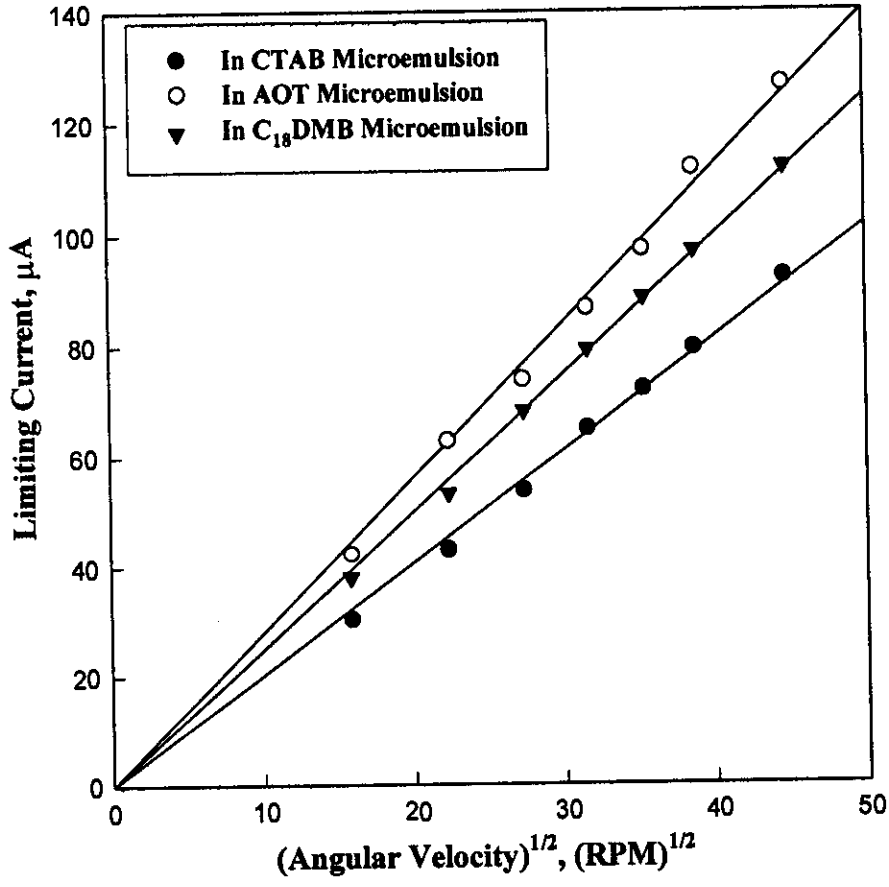

Figure71: The plots of the limiting (i_l) versus square root of angular velocity ($\omega^{1/2}$) for 1,4-naphthoquinone in different microemulsion systems.

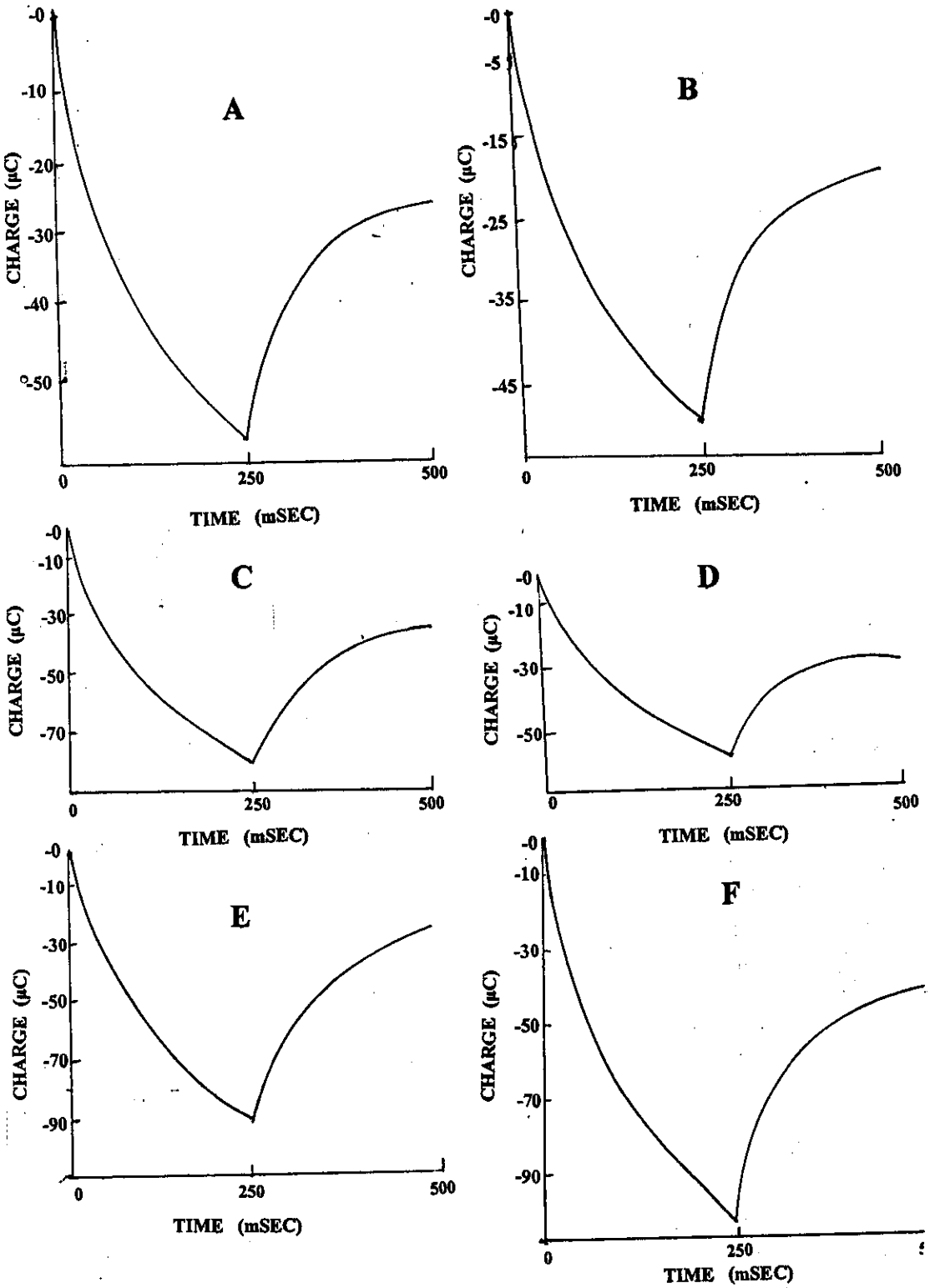

Figure72: Chronocoulometric responses of 1,4-naphthoquinone in different systems, (a) CTAB micellar solution, (b) CTAB microemulsion, (c) AOT micellar solution, (d) AOT microemulsion, (e) C_{18}DMB micellar solution, and (f) C_{18}DMB microemulsion.

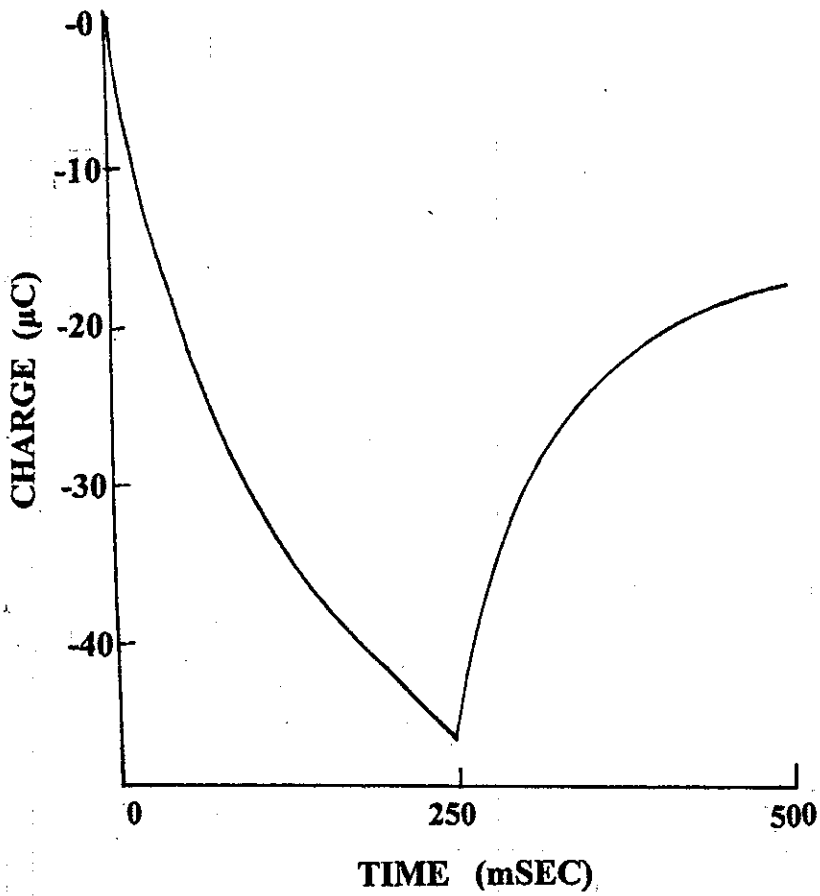

Figure 73 : Chronocoulometric responses of 1,4-naphthoquinone in pure aqueous solution. Charge versus time.

Table 28: Cyclic voltammetric data obtained for 1mM of 1,4-naphthoquinone in pure aqueous media at 25°C.

Sweep Rate	$-E_{p,a}$	$-E_{p,c}$	$I_{p,a}$	$I_{p,c}$	$I_{p,a}/I_{p,c}$	ΔE_p
mV/sec	mV	mV	μA	μA	-	mV
20	381	341	5.69	7.12	0.799	40
50	382	341	12.60	14.30	0.881	41
80	382	342	17.86	19.68	0.907	40
100	383	343	21.34	23.01	0.927	40
150	384	342	26.50	28.01	0.946	42
200	384	344	30.04	31.99	0.939	40
500	386	345	52.30	54.30	0.963	41

Table 29: Cyclic voltammetric data obtained for 1mM of 1,4-naphthoquinone in micellar solutions.

System	Sweep Rate	$-E_{p,c}$	$-E_{p,a1}$	$-E_{p,a1}$	$I_{p,c}$	$I_{p,a1}$	$I_{p,a2}$	$I_{p,a}/I_{p,c}$	ΔE_p
	mV/sec	mV	mV	mV	µA	µA	µA	-	mV
(A) CTAB Micellar Solution									
	20	328	257	-	5.63	5.34	-	0.948	71
	50	331	256	-	10.56	8.33	-	0.788	75
	80	331	253	-	13.08	10.05	-	0.768	78
	100	330	253	-	15.44	12.10	-	0.777	77
	150	331	253	-	19.91	15.40	-	0.773	78
	200	331	257	-	21.43	18.00	-	0.843	74
	500	335	262	-	38.12	28.70	-	0.752	73
(B) AOT Micellar Solution									
	20	408	300	-	10.50	6.87	-	0.654	108
	50	408	301	-	17.50	11.87	-	0.678	107
	80	409	302	-	23.70	16.10	-	0.679	107
	100	410	302	-	27.60	18.50	-	0.670	108
	150	410	304	-	33.20	22.20	-	0.655	106
	200	410	304	-	39.89	25.90	-	0.649	106
	500	412	306	-	65.98	44.40	-	0.672	106
(C) C_{18}DMB Micellar Solution									
	20	426	261	113	7.90	3.89	2.10	-	-
	50	426	261	113	12.89	7.30	5.10	-	-
	80	427	262	116	16.80	9.60	6.90	-	-
	100	427	264	117	19.90	11.76	7.80	-	-
	150	427	264	118	24.70	13.10	10.29	-	-
	200	427	265	120	29.00	15.17	12.30	-	-
	500	429	267	122	46.98	24.90	20.10	-	-

Table 30: Cyclic voltammetric data obtained for 1mM of 1,4-naphthoquinone in microemulsion systems.

System	Sweep Rate	$-E_{p,c}$	$-E_{p,a}$	$I_{p,c}$	$I_{p,a}$	$I_{p,a}/I_{p,c}$	ΔE_p
	mV/sec	mV	mV	μA	μA	-	mV
(A) CTAB Microemulsion							
	20	358	324	8.60	7.20	0.837	34
	50	355	321	17.60	13.80	0.784	34
	80	354	319	22.30	17.63	0.790	35
	100	358	318	25.30	20.76	0.820	40
	150	358	317	30.40	25.63	0.843	41
	200	362	317	35.80	30.46	0.850	45
	500	362	313	62.30	51.47	0.826	49
(B) AOT Microemulsion							
	20	452	362	19.60	15.30	0.921	90
	50	452	362	30.20	24.70	0.817	90
	80	453	363	38.90	32.50	0.835	90
	100	455	364	45.00	38.00	0.844	91
	150	456	363	52.86	44.80	0.847	93
	200	457	363	60.85	52.30	0.859	94
	500	458	364	98.90	84.90	0.858	94
(B) C_{18}DMB Microemulsion							
	20	113	-138	18.60	15.80	0.849	251
	50	114	-138	29.60	25.30	0.854	252
	80	113	-139	38.60	34.20	0.886	250
	100	115	-141	42.85	38.77	0.904	256
	150	117	-143	50.60	46.90	0.926	260
	200	117	-143	58.90	53.90	0.915	260
	500	118	-145	95.90	91.60	0.955	263

Table 31: Diffusion coefficient values of reductant and oxidant species for 1,4-naphthoquinone in different systems.

System	(CV)			(RDV)
	$D_R x10^{-6}$ cm^2/sec	$D_{O1} x10^{-6}$ cm^2/sec	$D_{O2} x10^{-6}$ cm^2/sec	$Dx10^{-6}$ cm^2/sec
A- In Aqueous Solution				
	7.19	7.04	-	7.17
B- In CTAB Micellar Solution				
	1.66	0.62	-	1.28
C- In CTAB Microemulsion				
	3.29	2.31	-	2.77
D- In AOT Micellar Solution				
	3.36	1.70	-	2.76
E- In AOT Microemulsion				
	7.46	5.76	-	6.05
F- In C_{18}DMB Micellar Solution				
	3.90	1.12	0.80	(0.69^a, 1.13^b)
G- In C_{18}DMB Microemulsion				
	7.01	6.82	-	6.32

a,b- for first and second wave respectively.

Table 32 : Half-wave potential for 1,4-naphthoquinone in differrent systems at 25°C.

System	$-E_{1/2}$(mV vs. SCE)	
	(CV)	(RDV)
A- In Aqueous Solution	362	359
B- In CTAB Micellar Solution	293	285
C- In CTAB Microemulsion	338	336
D- In AOT Micellar Solution	356	330
E- In AOT Microemulsion	408	383
F- In C_{18}DMB Micellar Solution	269[a]	(116[b],391[c])[a]
G-In C_{18}DMB Microemulsion	-12[a]	47[a]

a- Measured at 40°C.
b,c- for first and second wave respectively.

Table33: The slopes of the plots of log $(i/(i_l-i))$ versus E for 1,4-naphthoquinone in differrent systems at 25°C.

System	Slope (V^{-1})
A- In Aqueous Solution	10.75
B- In CTAB Micellar Solution	11.18
C- In CTAB Microemulsion	18.56
D- In AOT Micellar Solution	5.85
E- In AOT Microemulsion	10.75
F- In C_{18}DMB Micellar Solution	$(7.37^{b}, 9.68^{c})^{a}$
G-In C_{18}DMB Microemulsion	4.82^{a}

b,c- for first and second wave respectively.

a- Measured at 40°C.

Table 34: Γ_o values obtained from chronocoulometric data of 1,4-naphthoquinone in pure aqueous, micelles and microemulsion systems.

Systems	Γ_o moles/cm^2
(A) Pure Aqueous	2.13×10^{-9}
(B) CTAB Micelles	3.29×10^{-9}
(C) CTAB Microemulsion	2.72×10^{-9}
(D) AOT Micelles	5.15×10^{-9}
(E) AOT Microemulsion	4.29×10^{-9}
(F) C_{18}DMB Micelles	6.91×10^{-9}
(G) C_{18}DMB Microemulsion	6.95×10^{-9}

3.6.2 2-methyl-1,4- naphthoquinone (II)

A- Cyclic voltammetry

The voltammograms of 1mM of 2-methyl-1,4-naphthoquinone were recorded in different micelles and microemulsion systems containing CTAB, AOT and C_{18}DMB as model surfactants at the glassy carbon electrode and in pure aqueous solution. 2-methyl-1,4-naphthoquinone is poorly souble in water and its solubility is $8.6x10^{-4}$ M [173]. The solubility is greatly enhanced by micelles and microemulsion.

The cyclic voltammograms displayed one cathodic peak on the cathodic scan and one anodic peak on the reverse scan in all micelles and microemulsion media, except in CTAB microemulsion it displayed two reduction peaks at small scan rate of almost equal heights. In C_{18}DMB micelle it displayed two oxidation peaks of almost equal heights, as represent in Fig. (74).

The voltammograms of 0.86 mM 2-methyl-1,4-naphthoquinone in the corresponding pure aqueous solution containing only 0.10 M NaCl supporting electrolyte showed a similar voltammetric response, a single redox peak, Fig. (75a). The voltammograms recorded at different sweep rates varying from 20 to 500 mV/sec are essentially similar displaying a single redox peak. The peak potential separation ΔE_P is slightly increased on increasing sweep rate.

The voltammetric data of 2-methyl-1,4-naphthoquinone in pure aqueous and various surfactant systems are summarized in Tables (35-37). The peak potential separation ΔE_P ($\Delta E_P = E_{p,c} - E_{p,a}$) is very close to 30 mV at very small sweep rates in aqueous and in CTAB micellar solution. Since ΔE_P equal to 0.059/n V, the obtained data suggested that reduction of 2-methyl-1,4-naphthoquinone is chemically reversible with a net transfer of two electrons. In other media, the peak potential separation ΔE_P is increased

from 113 to 258 mV, Table (36). These facts lead generally to the fact that the electrochemical-chemical-electrochemical (ECE) reaction nature. Protonation of the anion radical generally leads to a disproportionation reaction [170, 171].

The ratio $I_{p,a}/I_{p,c}$ is slightly less than unity in micelles and microemulsion systems, Tables (35,36,37). These results indicated the very weak adsorption contribution. On employing the Randles-Sevcik equation [140], The plots of the cathodic peak currents ($I_{p,c}$) as well as the anodic one ($I_{p,a}$) versus $\upsilon^{1/2}$ for 2-methyl-1,4-naphthoquinone in micelles and microemulsion of different surfactant systems as well as in pure aqueous showed linear correlations almost passing through the origin Fig. (75a,76&77). This behaviour confirming that the electrode reaction is mainly controlled by diffusion with slight adsorption contribution [140]. The slopes of I_p-$\upsilon^{1/2}$ plots were used to estimate the apparent diffusion coefficients of the reduced and oxidized forms of the species D_R and D_O, Table (38). The values of the apparent diffusion coefficients indicate the partitioning of 2-methyl-1,4-naphthoquinone between oil droplet, surfactant film and aqueous domain.

The slightly smaller ΔE_P (30 mV) in CTAB micellar solutions compared to about 62 mV in microemulsions shows that the stabilization in microemulsion is less than in micellar solutions. This is because the electrostatic effects are generally less in microemulsions than in micellar solutions due to the decreased charge density on the surface of the microemulsion droplets compared to micelles. Also, ΔE_P values are close to 30 mV at very slow sweep rates and increase with increasing sweep rates. These characteristics are typical of a reversible charge transfer reaction followed by slow chemical reaction [124].

The changes in half-wave potential ($E_{1/2}$) are expected due to the different effects of the surfactant as local environment on the relative stabilities of the reactant and products of the electron transfer reaction. $E_{1/2}$ shifted to less negative value in the CTAB micellar solution as shown in Table (39).

B- Rotating disk voltammetry (RDV)

The voltammograms of 1 mM of 2-methyl-1,4- naphthoquinone were recorded in micellar solutions and microemulsion media of three different surfactants. Cationic (CTAB), anionic AOT and zwitterionic C_{18}DMB surfactants were used in this investigation. The rotating disk voltammograms were recorded at small sweep rate (5 mV/sec) in the potential window 500 to -1000 mV. A well defined single reduction wave was observed in all micelles and microemulsion media as represented in Figs. (78,79). The effect of rotation speed (ω) on the voltammogram was recorded from 250 to 2000 RPM. There is a negative shift (~20 mV) in the half- wave potential ($E_{1/2}$) was observed on increasing the rotation speed indicating the chemical reversibility.

Logarithmic analysis of the rotating disk voltammograms were performed for testing the thermodynamic reversibility using equation (III.2). The plots of log ($\frac{i}{i_l - i}$) versus E straight lines in all micelles and microemulsion media are obtained as showen in Figs. (80-82). The slopes of these plots were listed in Table (40). Inspection of the data obtained indicating the quasi-reversible electron transfer process.

On employing the Levich equation [133], the plots of the limiting current (i_l) versus square root of the angular velocity ($\omega^{1/2}$) in all media showed linear correlations intersecting the origin, Figs.(78b,83&84). This behaviour indicates that the reduction process takes place under mass

transfer control. The slopes of these plots were used to determine the apparent diffusion coefficients in various media, Table (38).

C- Chronocoulometry of 2- methyl-1,4-naphthoquinone

The chronocoulometric responses of 2-methyl-1,4-naphthoquinone were recorded in CTAB, AOT and C_{18}DMB micelles and microemulsion systems different as well as in pure aqueous solution. The chronocoulograms of 2-methyl-1,4-naphthoquinone in micellar solutions and microemulsion systems were recorded by plotting the total amount of diffusional charge (Q_{tot}) versus time (t). The stepping time was 250 millisecond and the potential window was from 300 to - 800 mV which pre-selected from cyclic behaviour of 2-methyl-1,4-naphthoquinone recorded in CTAB, AOT and C_{18}DMB micelles and microemulsion system, as represented in Figs. (85a, 85c, 85e) for micelles and in Figs. (85b, 85d, 85f) for microemulsion systems. Also, the chronocoulogram of 2-methyl-1,4-naphthoquinone in pure aqueous solution was represented in Fig. (86). Table (41), showed the values of the amount of adsorbed reactant species Γ_o (moles/cm^2), which were found to be in the order of 10^{-9} (moles/cm^2) which are negligible.

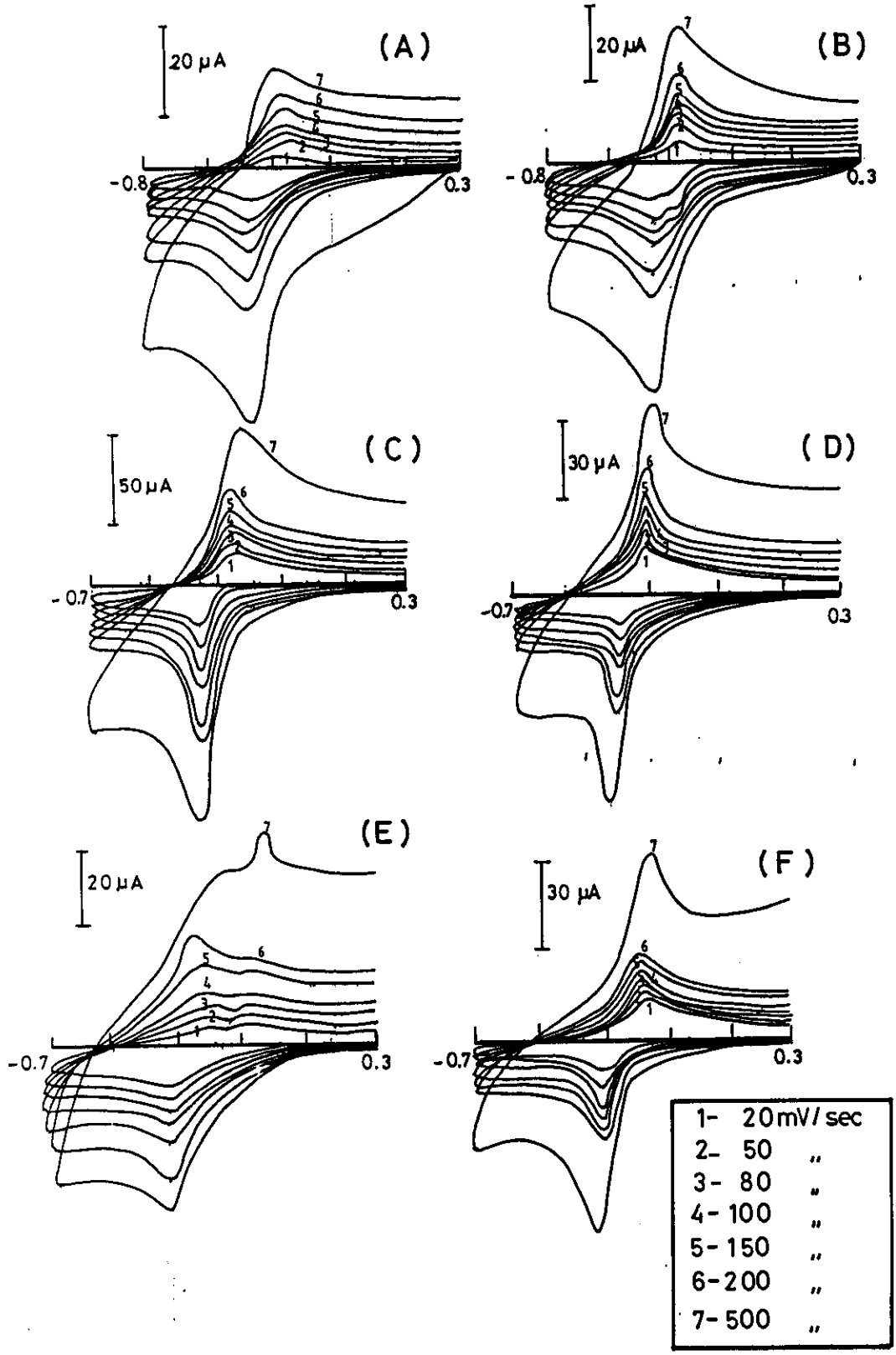

Figure 74: Cyclic voltammograms of 2-methyl-1,4-naphthoquinone in different systems, (a) CTAB micellar solution, (b) CTAB microemulsion, (c) AOT micellar solution, (d) AOT microemulsion, (e) C_{18}DMB micellar solution, and (f) C_{18}DMB microemulsion. The sweep rates are 20, 50, 80, 100, 150, 200 and 500 mV/sec.

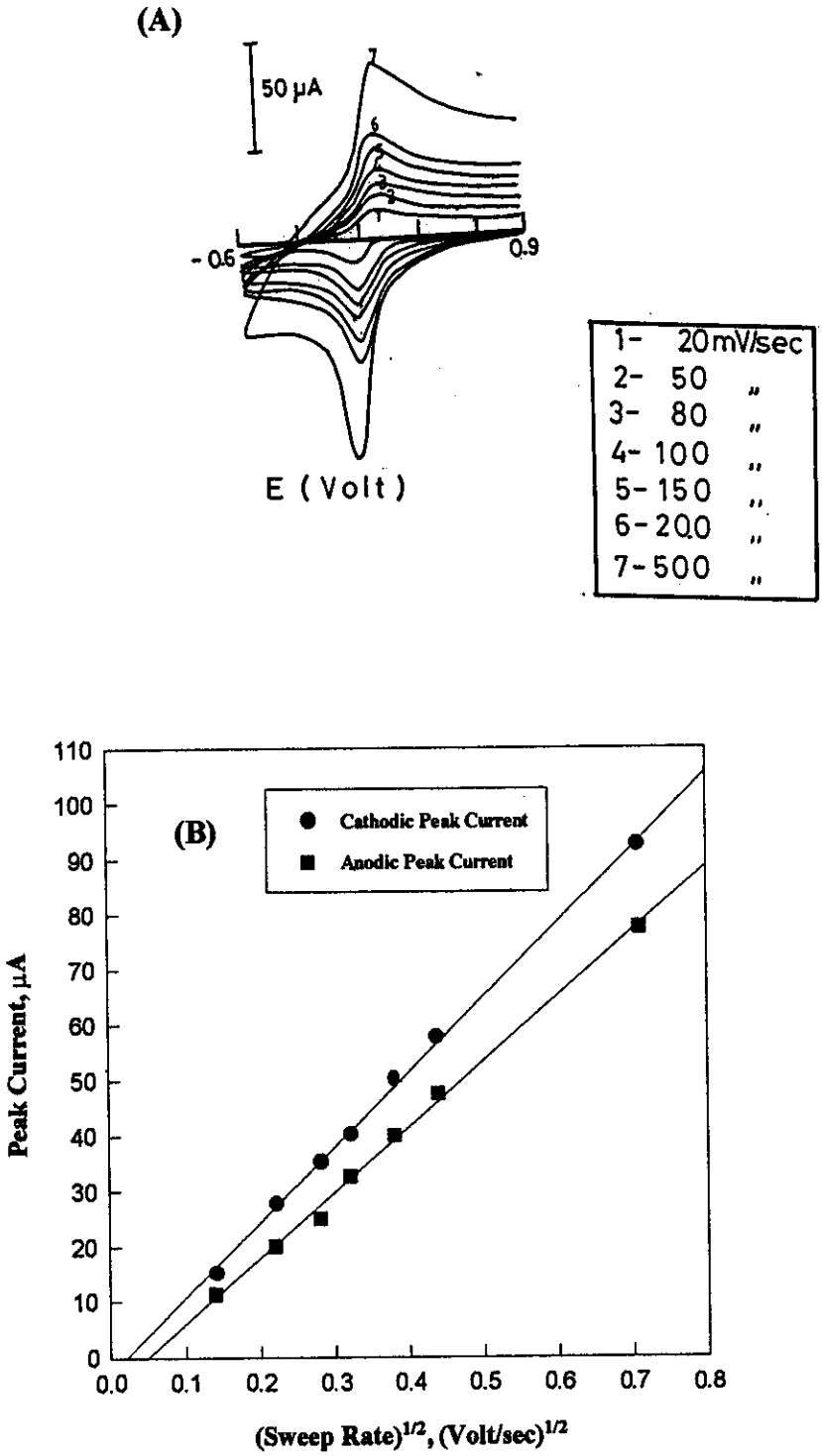

Figure 75: Cyclic voltammogram of 2-methyl-1,4-naphthoquione in aqueous media, (a) and the plots of peak currents versus $\upsilon^{1/2}$, (b).

2-methyl-1,4-naphthoquinone in different Micellar Solutions.

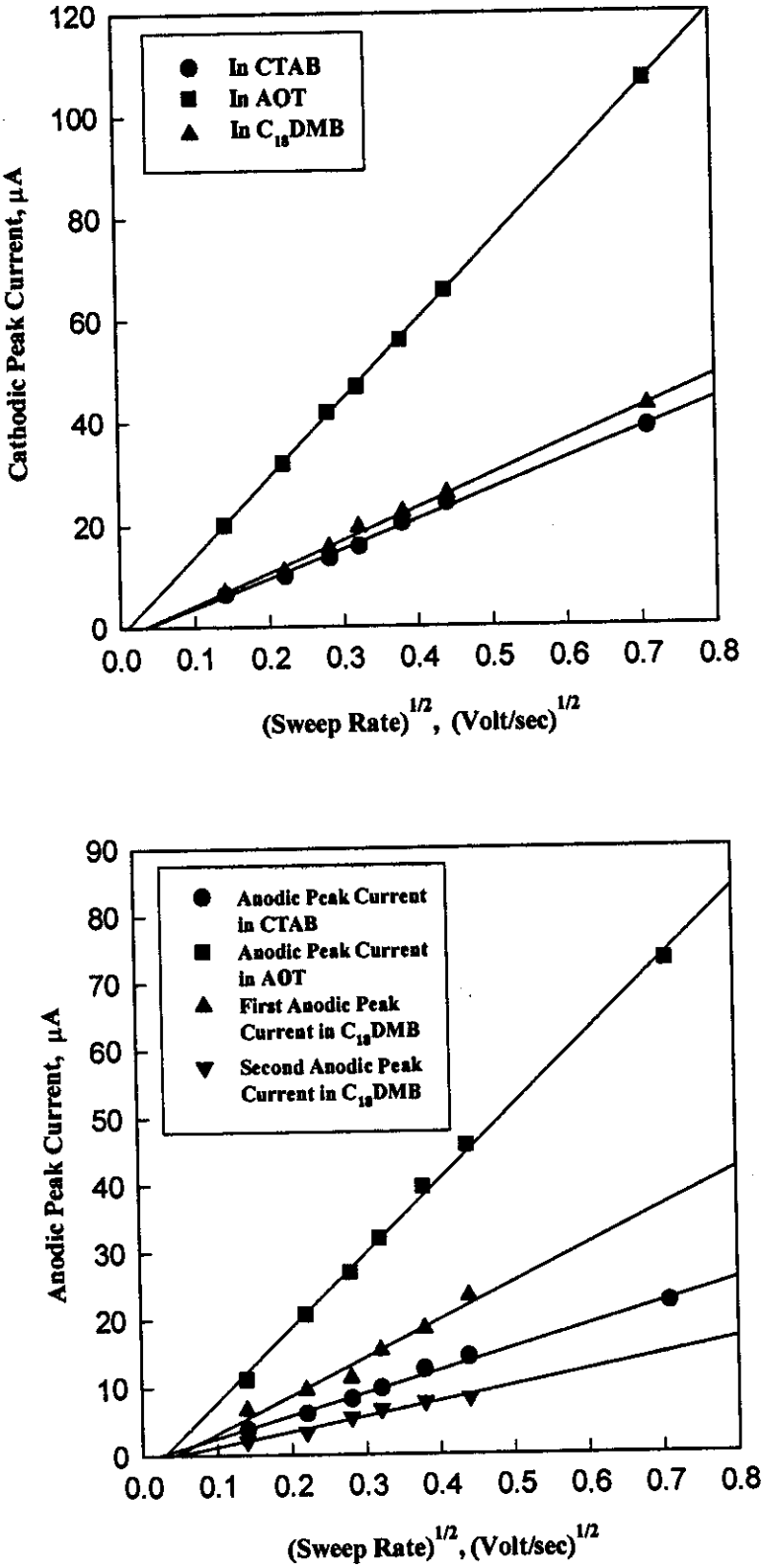

Figure 76:

2-methyl-1,4-naphthoquinone in Microemulsion Systems

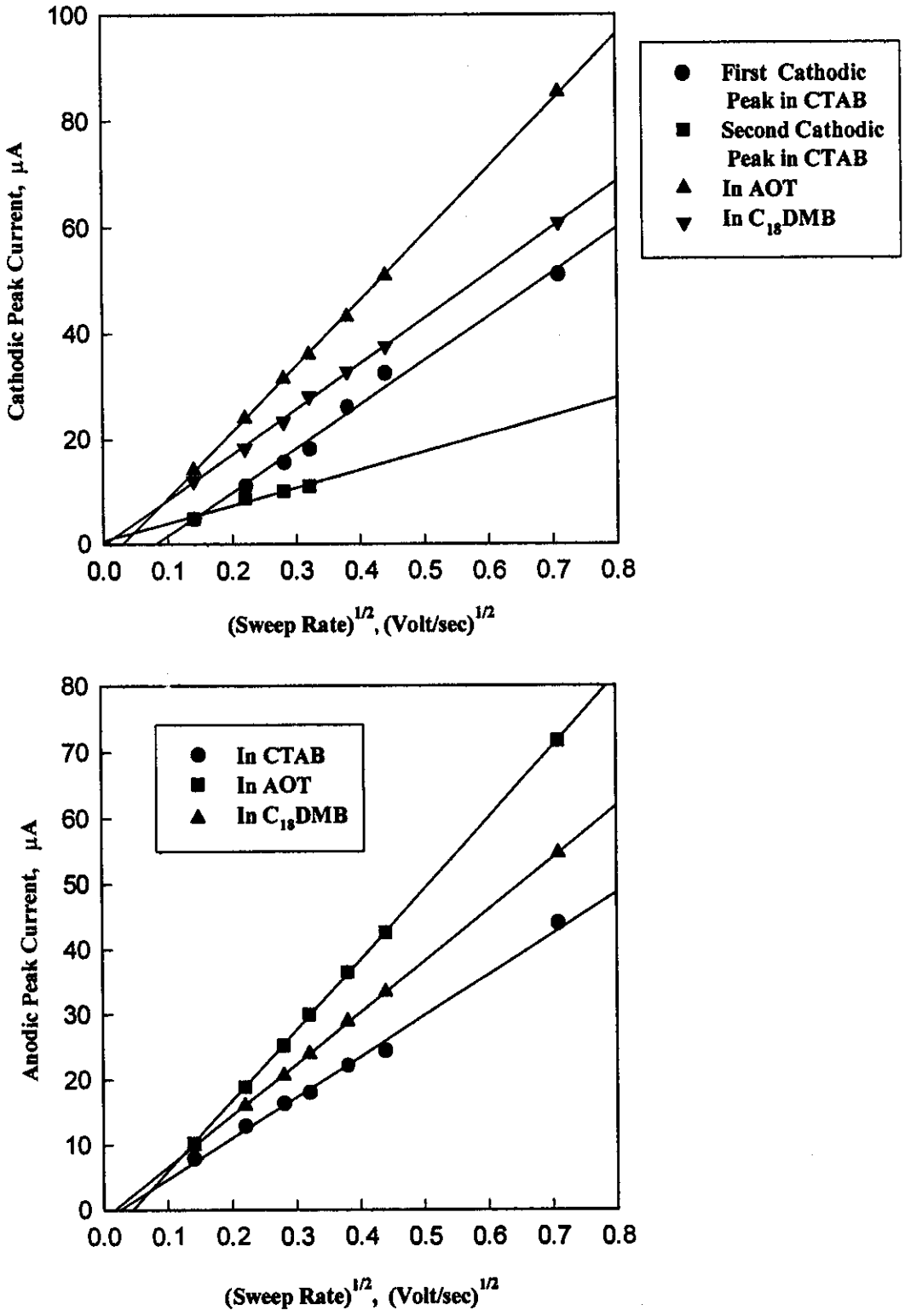

Figure 77:

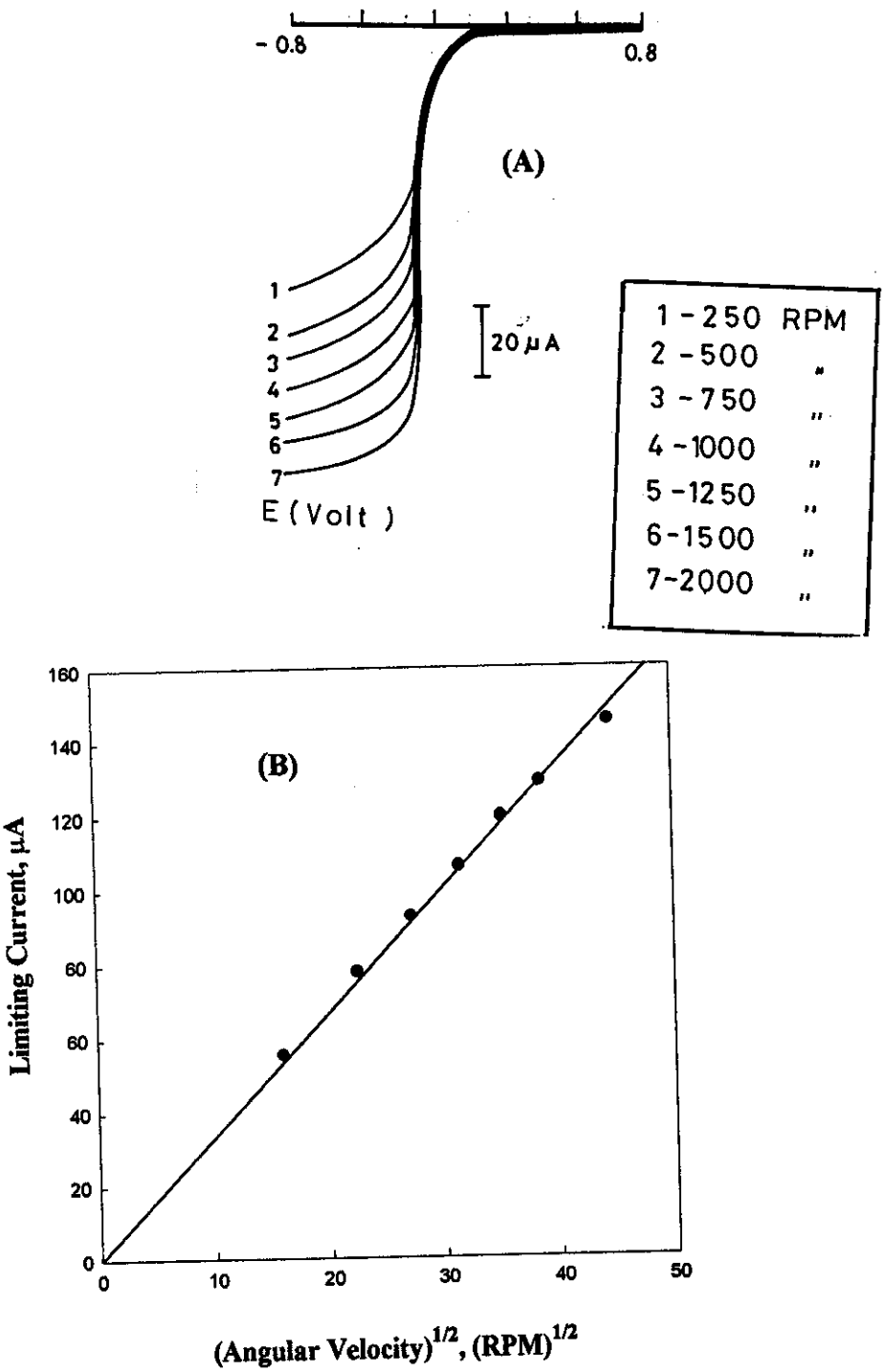

Figure 78: : (a) The effect of rotation speed of glassy carbon electrode on the linear sweep voltammogram obtained for 2-methyl-1,4-naphthoquinone in aqueous solution, and (b) the plots of (i_l) versus ($\omega^{1/2}$).

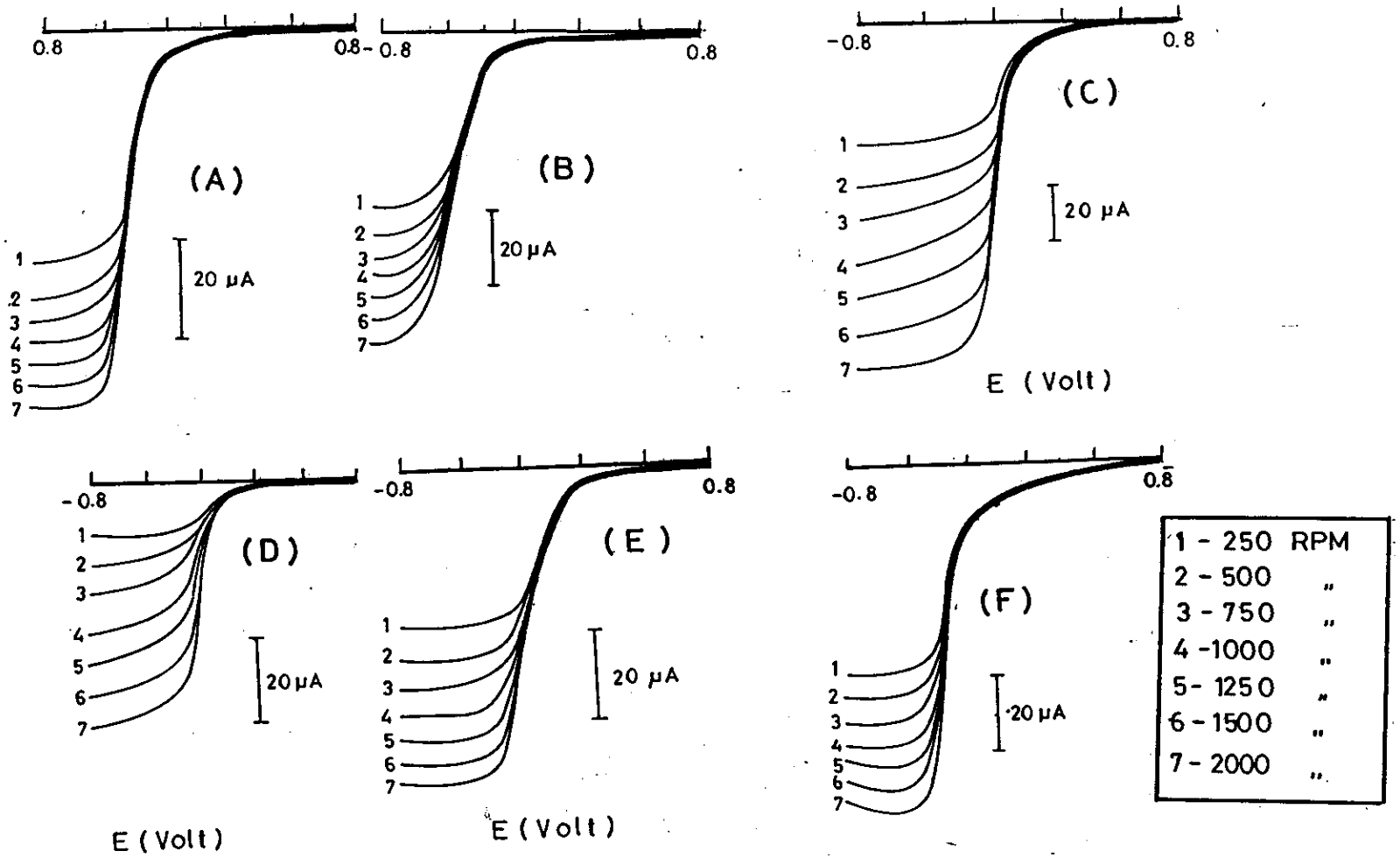

Figure 79: The effect of rotation speed of glassy carbon electrode on the linear sweep voltammograms of 2-methyl-1,4 naphthoquinone in different systems, (a) CTAB micellar solution, (b) CTAB microemulsion, (c) AOT micellar solution, (d) AOT microemulsion, (e) C_{18}DMB micellar solution, and (f) C_{18}DMB microemulsion. The speeds are 250, 500, 750, 1000, 1250, 1500 and 2000 RPM.

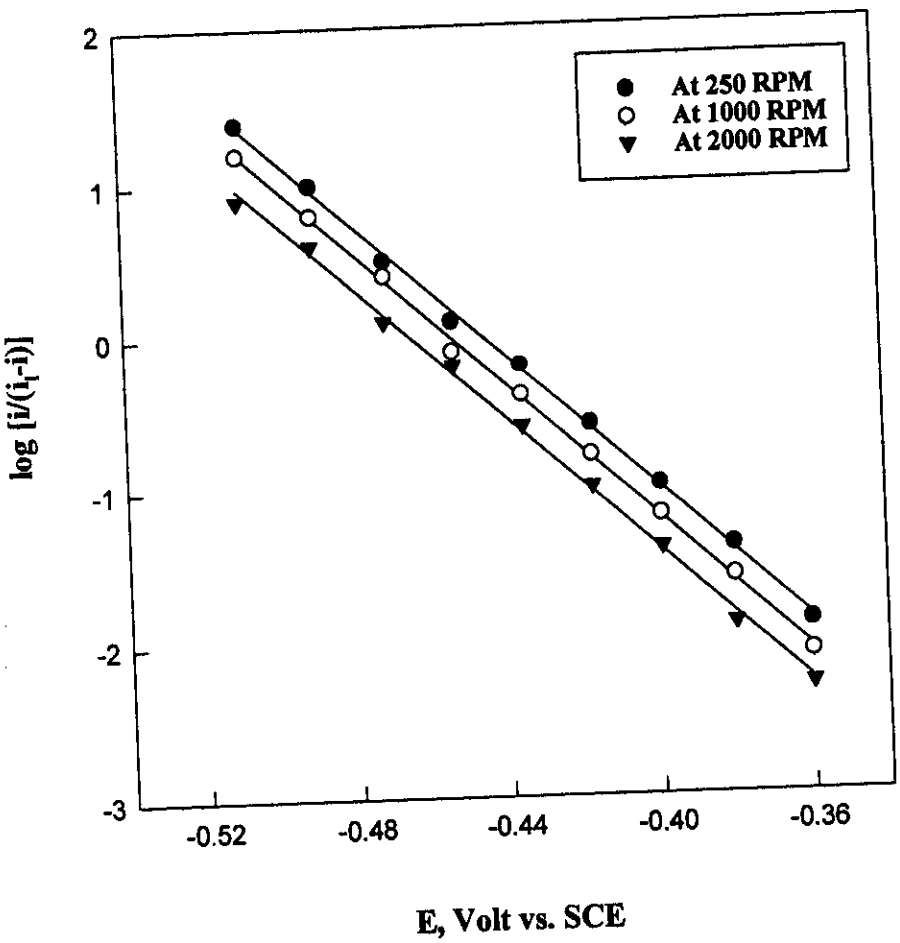

Figure 80 : Logarithmic analysis of 2-methyl-1,4-naphthoquinone in aqueous solution.

A- CTAB

B- AOT

C- C_{18}DMB

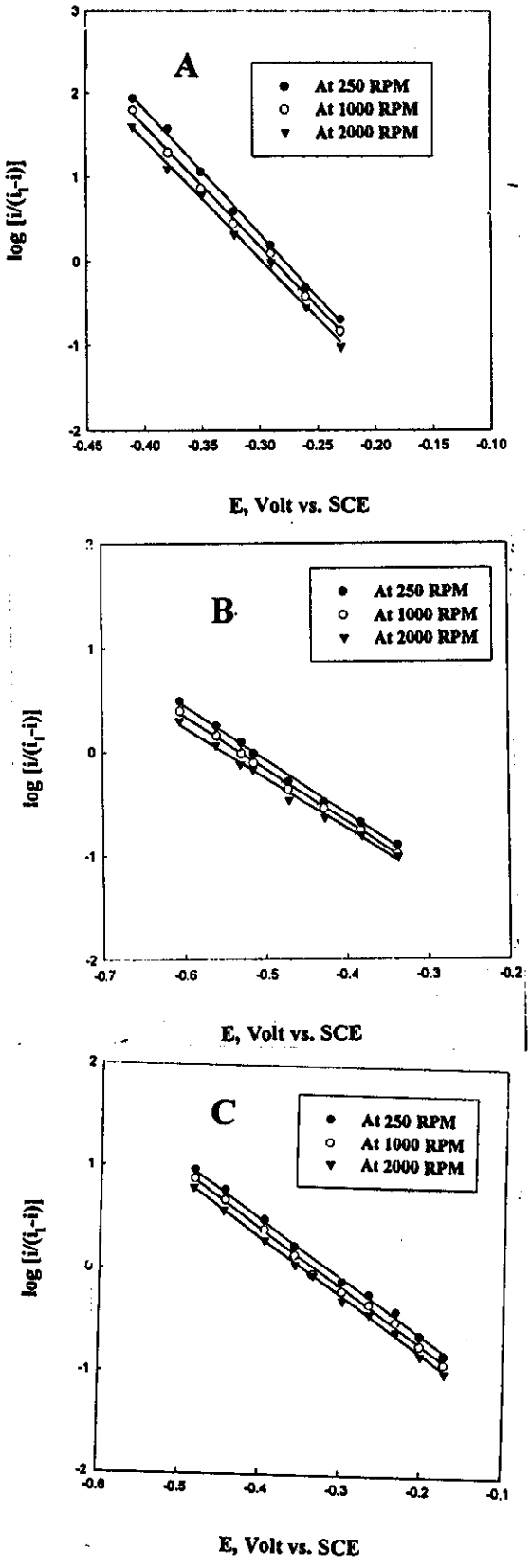

Figure 81: Logarithmic analysis of 2-methyl-1,4-naphothoquinone in different micellar solutions, a- CTAB, b- AOT and c- C_{18}DMB.

A- CTAB

B- AOT

C- C_{18}DMB

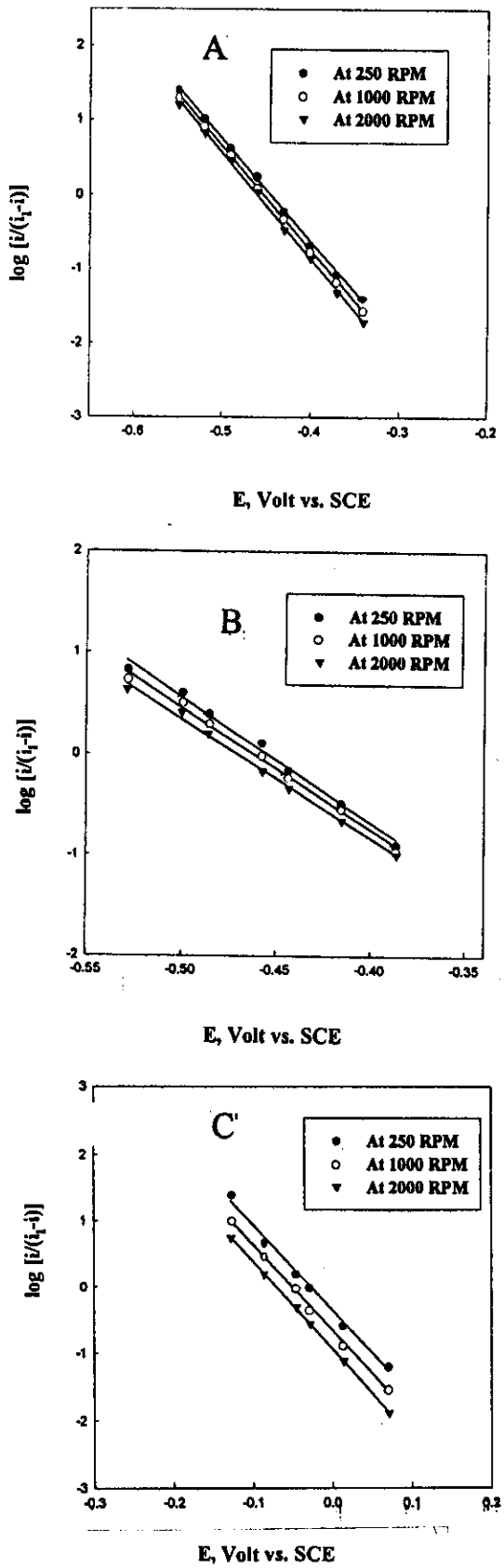

Figure 82: Logarithmic analysis of 2-methyl-1,4-naphothoquinone in different microemulsion systems, a- CTAB, b- AOT and c- C_{18}DMB.

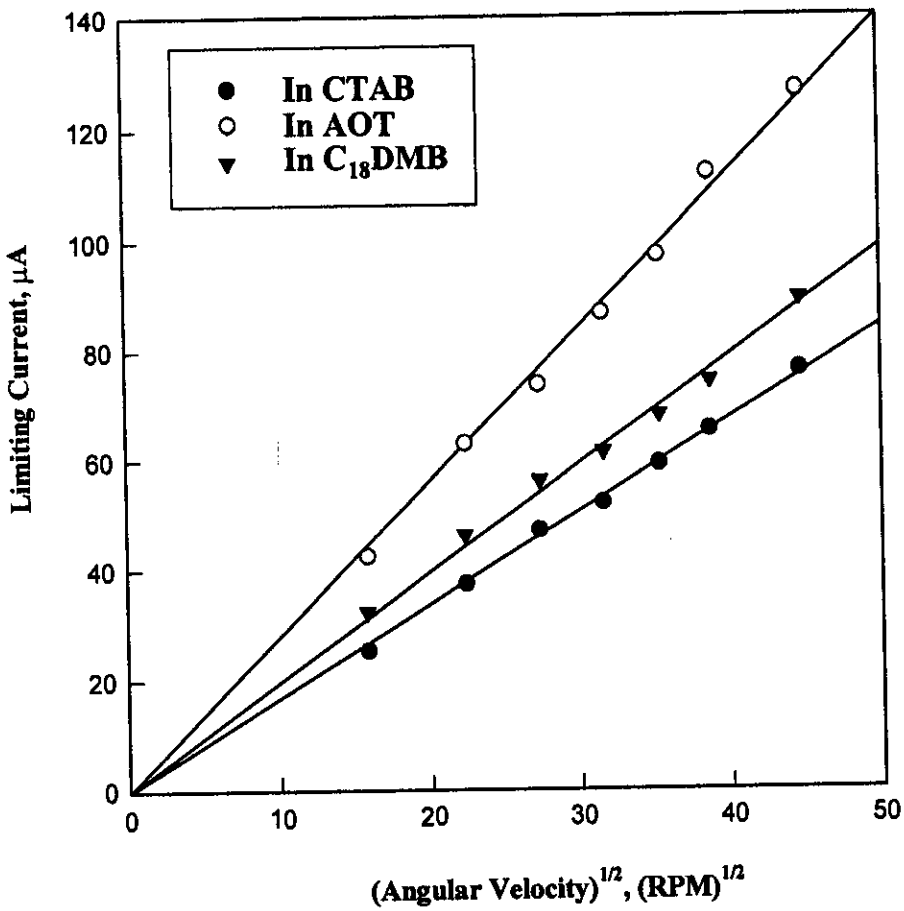

Figure 83: The plots of the limiting (i_l) versus square root of angular velocity ($\omega^{1/2}$) for 2-methyl-1,4-naphthoquinone in different micellar solution.

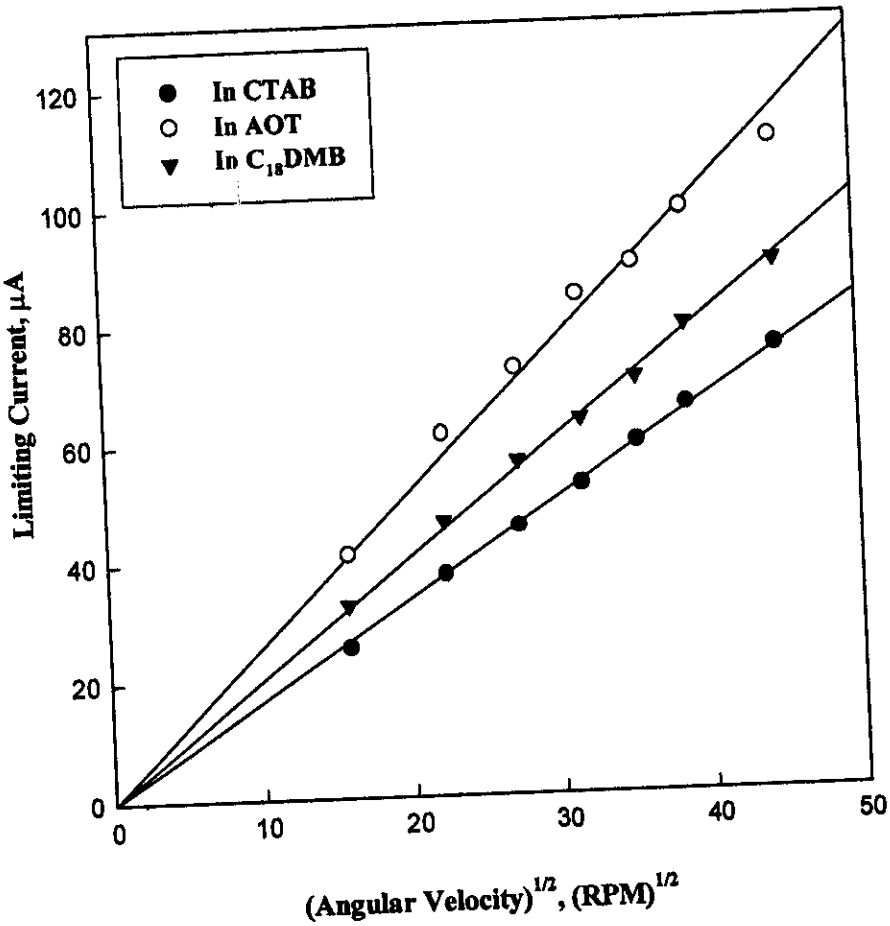

Figure 84: The plots of the limiting (i_l) versus square root of angular velocity ($\omega^{1/2}$) for 2-methyl-1,4-naphthoquinone in microemulsion systems.

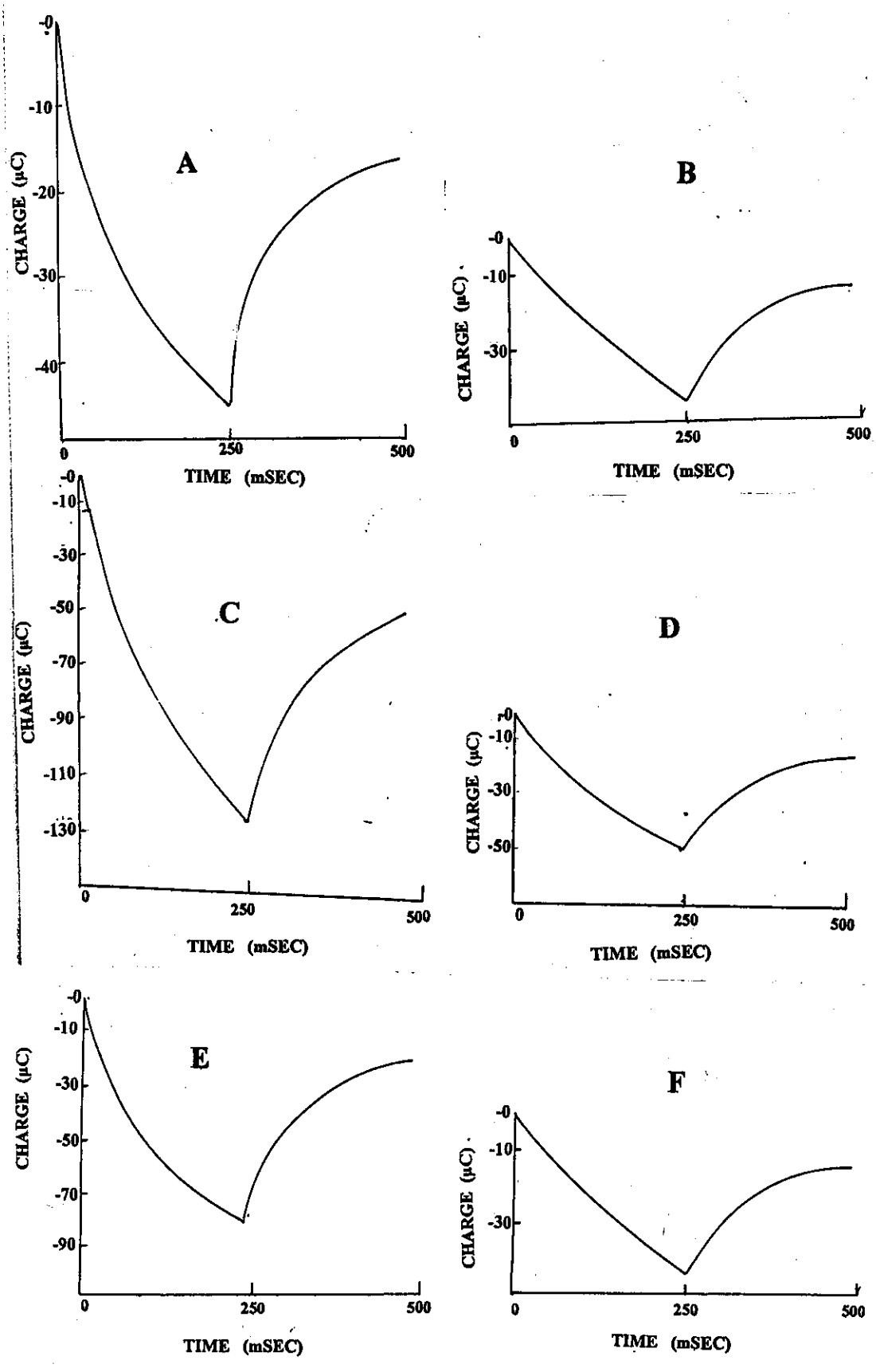

Figure 85: Chronocoulometric responses of 2-methyl-1,4-naphthoquinone in different systems, (a) CTAB micellar solution, (b) CTAB microemulsion , (c)AOT micellar solution, (d) AOT microemulsion, (e) C_{18}DMB micellar solution, and (f) C_{18}DMB microemulsion.

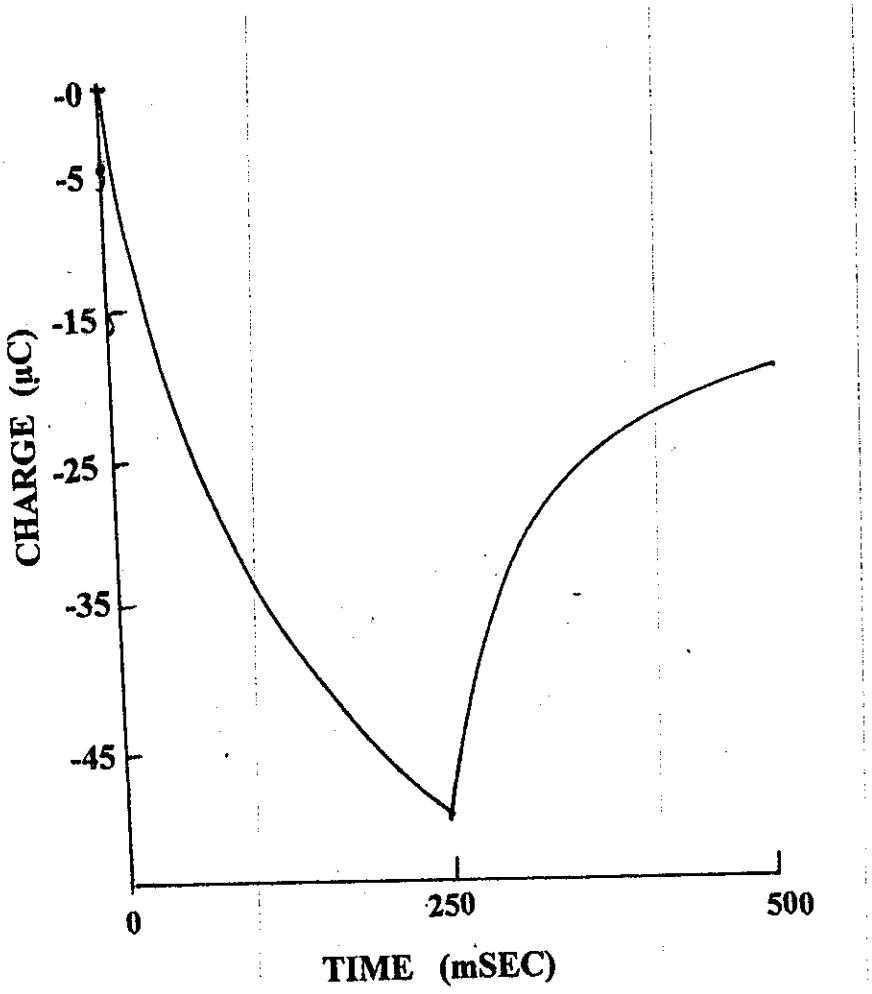

Figure 86: Chronocoulometric responses of 2-methyl-1,4-naphthoquinone in pure aqueous solution. Charge versus time.

Table 35: Cyclic voltammetric data obtained for 1mM of 2-methyl-1,4-naphthoquinone in pure aqueous media at 25°C.

Sweep Rate mV/sec	$-E_{p,a}$ mV	$-E_{p,c}$ mV	$I_{p,a}$ µA	$I_{p,c}$ µA	$I_{p,a}/I_{p,c}$ -	ΔE_p mV
20	485	444	15.00	11.30	0.753	41
50	486	444	27.50	20.00	0.727	42
80	486	445	20.08	25.00	0.714	41
100	487	446	35.00	32.50	0.812	41
150	488	445	40.00	40.00	0.800	43
200	488	445	57.50	47.50	0.826	43
500	489	447	92.500	77.50	0.837	42

Table 36: Cyclic voltammetric data obtained for 1mM of 2-methyl-1,4-naphthoquinone in micellar solutions.

System	Sweep Rate	$-E_{p,c}$	$-E_{p,a1}$	$E_{p,a2}$	$I_{p,c}$	$I_{p,a1}$	$I_{p,a2}$	$I_{p,a}/I_{p,c}$	ΔE_p
	mV/sec	mV	mV	mV	µA	µA	µA	-	mV
A) CTAB Micellar Solution									
	20	418	388	-	6.60	3.82	-	0.579	30
	50	423	386	-	10.26	6.10	-	0.594	37
	80	423	386	-	13.66	8.15	-	0.596	37
	100	427	386	-	15.93	9.74	-	0.611	41
	150	430	382	-	20.50	12.47	-	0.608	48
	200	431	382	-	24.33	14.29	-	0.587	49
	500	432	378	-	38.77	22.23	-	0.573	54
(B) AOT Micellar Solution									
	20	512	356	-	20.10	11.20	-	0.557	156
	50	512	356	-	30.60	19.60	-	0.640	156
	80	513	357	-	40.20	25.42	-	0.632	156
	100	514	358	-	45.60	28.77	-	0.630	156
	150	514	357	-	55.30	37.47	-	0.677	157
	200	514	356	-	67.30	45.80	-	0.680	159
	500	516	357	-	107.00	78.95	-	0.737	159
(C) C_{18}DMB Micellar Solution									
	20	513	270	52	6.90	6.70	2.10	-	-
	50	513	270	52	10.90	9.60	3.40	-	-
	80	514	270	52	15.60	11.30	5.55	-	-
	100	514	331	52	19.48	15.30	6.66	-	-
	150	514	335	54	22.40	18.50	7.77	-	-
	200	514	332	56	25.90	23.30	8.33	-	-
	500	516	-	-	42.80	-	-	-	-

Table 37: Cyclic voltammetric data obtained for 1mM of 2-methyl-1,4-naphthoquinone in microemulsion systems.

ystem	Sweep Rate mV/sec	$-E_{p,c1}$ mV	$-E_{p,c2}$ mV	$-E_{p,a1}$ mV	$I_{p,c1}$ µA	$I_{p,c2}$ µA	$I_{p,a1}$ µA	$I_{p,a}/I_{p,c}$ -	ΔE_p mV
A) CTAB Microemulsion									
	20	483	373	430	5.00	5.00	7.80	-	53
	50	476	377	427	11.25	8.90	12.80	-	49
	80	476	389	415	15 .75	10.20	16.3	-	61
	100	475	392	415	18.30	11.20	18.00	-	60
	150	472	-	408	28.25	-	22.16	-	64
	200	475	-	408	32.50	-	24.40	-	67
	500	482	-	400	51.50	-	43.94	-	83
B) AOT Microemulsion									
	20	530	-	417	14.20	-	9.80	0.690	113
	50	531	-	417	23.10	-	17.50	0.757	114
	80	532	-	418	28.98	-	24.30	0.839	114
	100	532	-	419	33.56	-	26.30	0.783	113
	150	533	-	417	43.22	-	35.60	0.823	116
	200	534	-	418	49.22	-	42.60	0.865	116
	500	535	-	416	85.43	-	61.70	0.839	119
(C) C_{18}DMB Microemulsion									
	20	191	-	-60	12.20	-	9.80	0.803	251
	50	191	-	-60	18.30	-	15.62	0.853	251
	80	192	-	-61	23.14	-	19.53	0.833	253
	100	193	-	-61	28.12	-	23.43	0.833	254
	150	194	-	-62	32.80	-	28.90	0.881	256
	200	194	-	-63	37.60	-	32.80	0.872	257
	500	195	-	-63	60.90	-	56.25	0.923	258

Table 38: Diffusion coefficient values of reductant and oxidant species for 2-methyl-1,4-naphthoquinone in different systems.

System	(CV)			(RDV)
	$D_{R1}x10^{-6}$ cm^2/sec	$D_{O1}x10^{-6}$ cm^2/sec	$D_{O2}x10^{-6}$ cm^2/sec	$Dx10^{-6}$ cm^2/sec
A- In Aqueous Solution				
	9.79	7.44	-	8.69
B- In CTAB Micellar Solution				
	1.21	0.39	-	0.98
C- In CTAB Microemulsion				
	2.46	1.40	-	2.51
D- In AOT Micellar Solution				
	8.66	4.46	-	6.32
E- In AOT Microemulsion				
	5.62	4.80	-	5.34
F- In C_{18}DMB Micellar Solution				
	2.85[c]	2.46[c]	0.35[c]	3.12[c]
G- In C_{18}DMB Microemulsion				
	3.23[c]	2.54[c]	-	2.65[c]

c- Measured at 40°C.

Table 39: Half-wave potential for 2-methyl-1,4-naphthoquinone.

System	$-E_{1/2}$(mV vs. SCE)	
	(CV)	(RDV)
A- In Aqueous Solution	465	454
B- In CTAB Micellar Solution	404	281
C- In CTAB Microemulsion	442	450
D- In AOT Micellar Solution	435	525
E- In AOT Microemulsion	474	456
F- In C_{18}DMB Micellar Solution	407[a]	331[a]
G-In C_{18}DMB Microemulsion	65[a]	50[a]

a- Measured at 40°C.

Table 40: The slopes of the plots of log $(i/(i_l-i))$ versus E for 2-methyl-1,4-naphthoquinone in different systems at 25°C.

System	Slope (V^{-1})
A- In Aqueous Solution	23.25
B- In CTAB Micellar Solution	26.39
C- In CTAB Microemulsion	13.66
D- In AOT Micellar Solution	6.68
E- In AOT Microemulsion	7.57
F- In C_{18}DMB Micellar Solution	5.57[a]
G-In C_{18}DMB Microemulsion	4.32[a]

a- Measured at 40°C.

Table 41: Γ_o values obtained from chronocoulometric data of 2-methyl-1,4-naphthoquinone in pure aqueous, micelles and microemulsion systems.

Systems	Γ_o moles/cm^2
(A) Pure Aqueous	2.61×10^{-9}
(B) CTAB Micelles	2.37×10^{-9}
(C) CTAB Microemulsion	2.88×10^{-9}
(D) AOT Micelles	1.02×10^{-8}
(E) AOT Microemulsion	4.00×10^{-9}
(F) C_{18}DMB Micelles	6.85×10^{-9}
(G) C_{18}DMB Microemulsion	3.84×10^{-9}

3.6.3 2-hydroxy-1,4-naphthoquinone

A- Cyclic voltammetry

The cyclic voltammograms of 1mM of 2-hydroxy-1,4-naphthoquinone were recorded in micelles and microemulsion systems of three different surfactants as well as in pure aqueous solution. Cationic (CTAB), anionic (AOT) and zwitterionic (C_{18}DMB) model surfactants were used in this investigation.

The recorded voltammograms in micelles and microemulsion systems showed two cathodic peaks on the cathodic scan and two anodic peaks on the reverse scan, Fig. (87). Whereas, in C_{18}DMB micelles it displayed one redox peak, and in C_{18}DMB microemulsion it showed one oxidation and two reduction peaks, Fig. (87). The voltammograms of 2-hydroxy-1,4-naphthoquinone in the corresponding pure aqueous solution containing only 0.10 M NaCl supporting electrolyte showed a similar voltammetric response, two redox peaks, Fig.(88a). The voltammograms recorded at different sweep rates varying from 20 to 500 mV/sec are essentially similar displaying two redox peaks.

The peak potential separation ΔE_P is slightly increased on increasing sweep rate. The voltammetric data of 2-hydroxy-1,4-naphthoquinone in all systems are summarized in Tables (42-44). The peak potential separation ΔE_P is very close to 30 mV at very small sweep rates in CTAB micelle for the first redox peak, but for second redox peak it is around 280 mV, Table (43). In other media, the peak potential value listed in Tables (42,44) leads generally to the fact that the electrochemical-chemical-electrochemical (ECE) reaction nature. Protonation of the anion radical generally leads to a disproportionation reaction [170, 171].

The peak current ratios $I_{p,a}/I_{p,c}$ is slightly less than unity in micelles and microemulsion systems as shown from Tables (42-44).

By using the Randles-Sevcik equation [140], the plots of the cathodic peak currents ($I_{p,c}$) as well as the anodic one ($I_{p,a}$) versus $\upsilon^{1/2}$ for 2-hydroxy-1,4-naphthoquinone in micelles and microemulsion systems showed linear correlations almost passing through the origin, Figs. (89,90). From this behoviour the electrode reaction is mainly controlled by diffusion with slight adsorption contribution. The plots of the cathodic peak currents ($I_{p,c}$) as well as the anodic one ($I_{p,a}$) versus $\upsilon^{1/2}$ for 1,4-naphthoquinone in pure aqueous solution is slightly deviated from the origin, Fig.(88b). This behaviour may be attributed to weak adsorption contribution to the electrode surface. The slopes of I_p-$\upsilon^{1/2}$ plots were used to estimate the apparent diffusion coefficients of the reduced and oxidized forms of the species D_R and D_O, Table (45).The values of the apparent diffusion coefficients indicate the partitioning of 2-hydroxy-1,4-naphthoquinone between oil droplet, surfactant film and aqueous domain.

Since cationic surfactants are known to be stabilize anion radicals [172]. The slightly smaller ΔE_P (20 mV) in CTAB micelle and about 139 mV in microemulsion for first redox peak compared to that of both AOT and C_{18}DMB micellar and microemulsions showed that the stabilization by cationic surfactants is higher than for anionic and zwitterionic surfactants. This is because the electrostatic effects are generally less in anionic and zwitterionic surfactants than in cationic surfactants. Also, ΔE_P values are close to 30 mV at very slow sweep rates and increase with increasing sweep rates. These characteristics are typical of a reversible charge transfer reaction followed by a slow chemical reaction [124].

There are differences observed in the values of E_p, ΔE_P between micellar solutions or microemulsions (Table (42-44)). Changes in half-wave potential ($E_{1/2}$) are expected due to the different effects of the surfactant as local environment on the relative stabilities of the reactant and products of the electron transfer reaction. $E_{1/2}$ shifted to less negative

value in the CTAB and AOT micellar solution and microemulsion as shown from Table (46).

B- Rotating disk voltammetry (RDV)

The rotating disk voltammograms of 1mM of 2-hydroxy-1,4-naphthoquinone were recorded in micelles and microemulsion systems of cationic (CTAB), anionic AOT and zwitherionic C_{18}DMB surfactants as well as in pure aqueous solution. The rotating disk voltammograms were recorded at small sweep rate (5 mV/sec) in the potential window 1000 to -1000 mV. The recorded voltammograms displayed two reduction waves in pure aqueous and in micelles and microemulsion systems as showed in Figs. (91,92). Except, in C_{18}DMB micelles and microemulsion systems it displayed single waves, Fig. (92e). The effect of rotation speed (ω) on the voltammogram was recorded from 250 to 2000 RPM. And it was found that on increasing the rotation speed there is a negative shift (~20 mV) in the half-wave potential ($E_{1/2}$) indicating the chemical reversibility.

The plots of log $(\frac{i}{i_l - i})$ versus E for 2-hydroxy-1,4-naphthoquinone in pure aqueous as well as in micelles and microemulsion media at 250, 1000, and 200 RPM showed linear correlations, Figs. (93-95). The slopes of these plots were listed in Table (47). The data obtained indicating the quasi-reversible electron transfer process.

On using Levich equation [133], the plots of i_l versus $\omega^{1/2}$ in all systems showed linear correlations passing through the origin, Figs.(91b,96&97). This behaviour indicates that the reduction process takes place under mass transfer control. Table (45) showed the apparent diffusion coefficients of 2-hydroxy-1,4-naphthoquinone in various media.

C- Chronocoulometry of 2-hydroxy-1,4-naphthoquinone

The chronocoulometric responses of 2-hydroxy-1,4-naphthoquinone were recorded in different micells and microemulsion systems containing CTAB, AOT and C_{18}DMB model surfactants and in pure aqueous solution. The chronocoulograms of 2-hydroxy-1,4-naphthoquinone in different media were recorded by plotting the charge (Q_{tot}) versus time (t) and by stepping the potential from 900 to -1100 mV and switched back to the original value by applying pulse width of 250 millisecond, as represented in Fig. (98). Fig. (99) showed the chronocoulogram 2-hydroxy-1,4-naphthoquinone in pure aqueous solution. Typical values of the amount of adsorbed reactant species Γ_o were listed in Table (48).

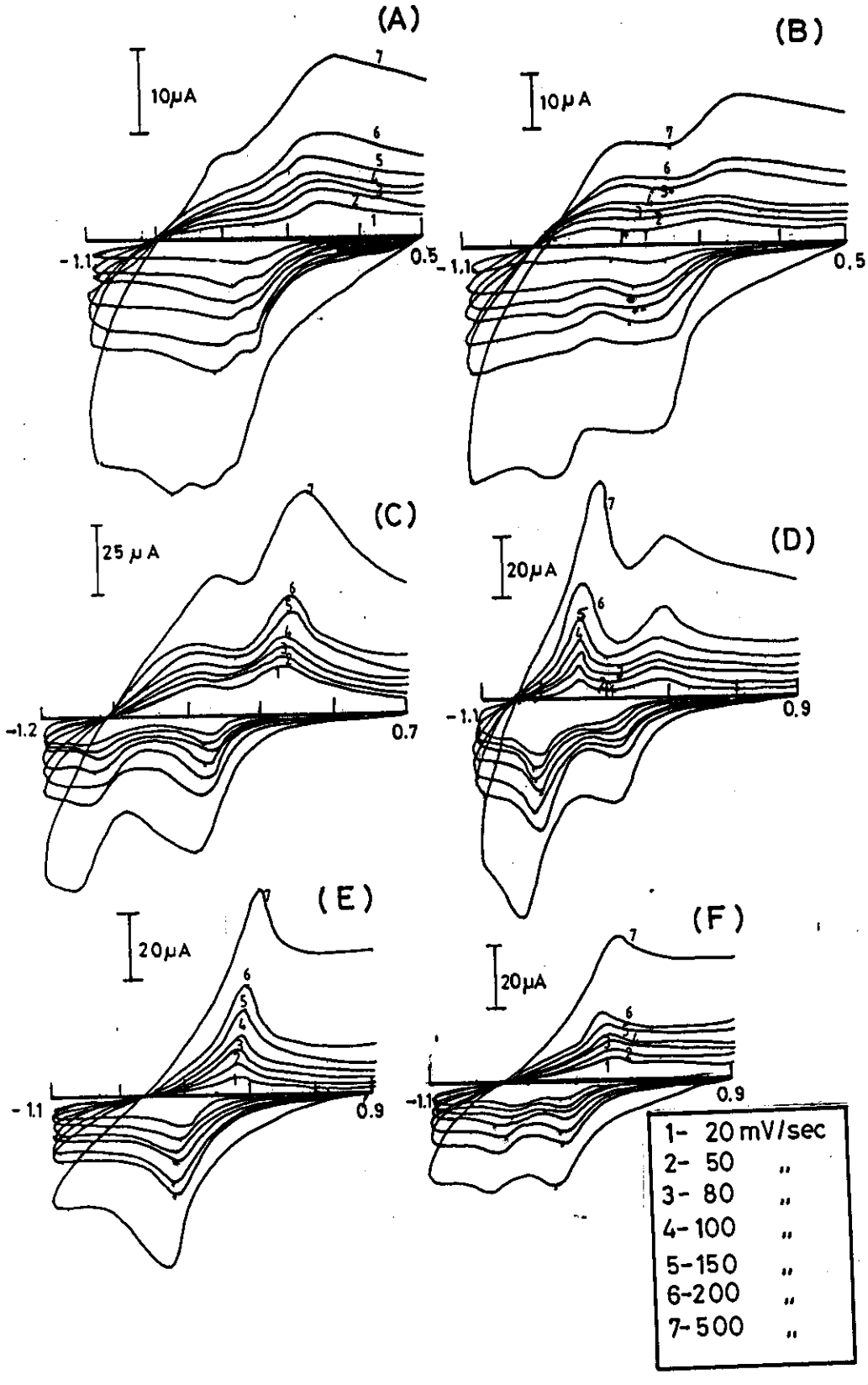

Figure 87: Cyclic voltammograms of 2-hydroxy-1,4-naphthoquinone in different systems, (a) CTAB micellar solution, (b) CTAB microemulsion, (c) AOT micellar solution, (d) AOT microemulsion, (e) C_{18}DMB micellar solution, and (f) C_{18}DMB microemulsion. The sweep rates are 20, 50, 80, 100, 150, 200 and 500 mV/sec.

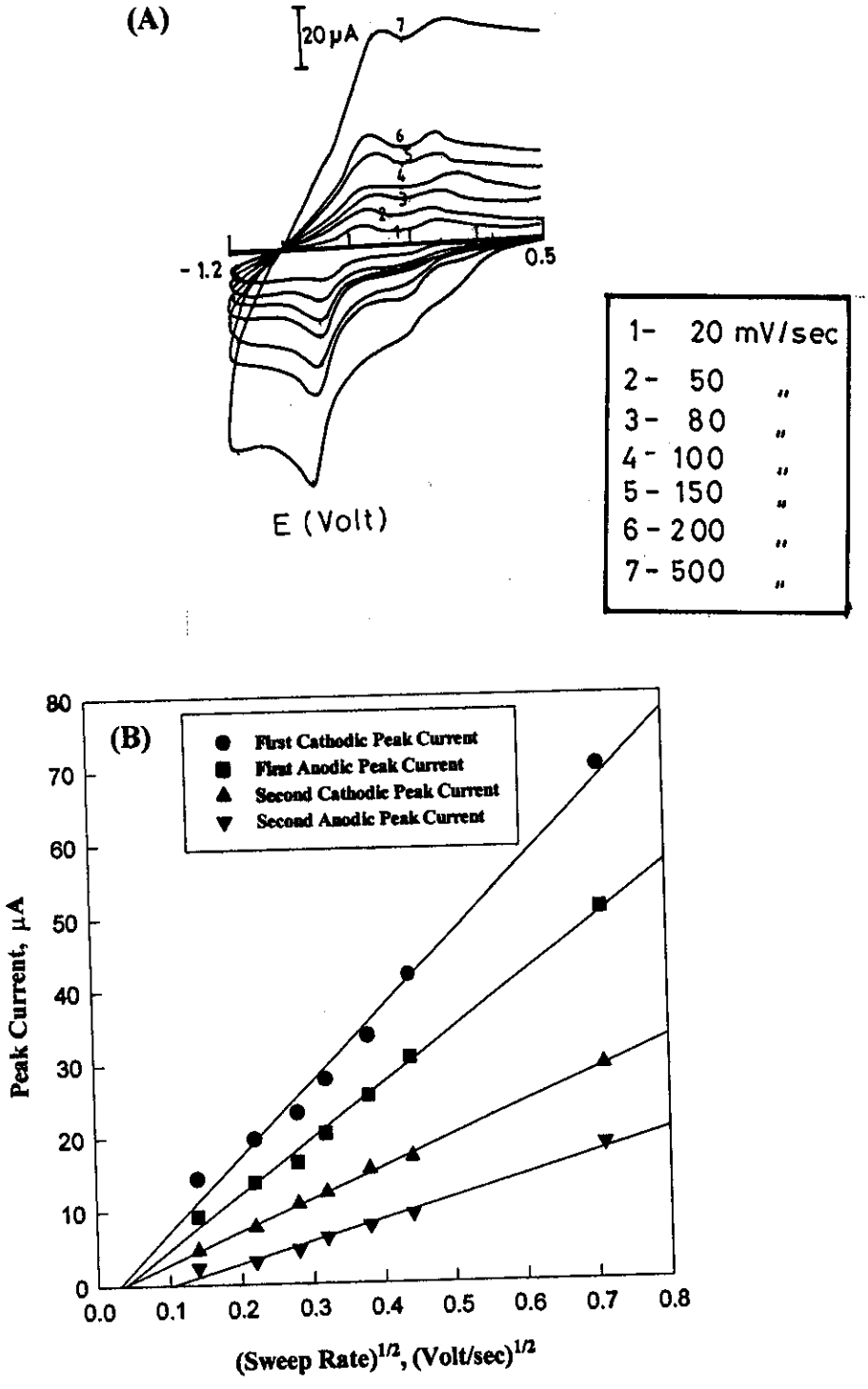

Figure 88: Peak currents of 2-hydroxy-1,4-naphthoquinone (Lawsone) in aqueous media obtained from cyclic voltammetry, (a) and its plot versus $\upsilon^{1/2}$, (b).

Peak Current of 2-hydroxy-1,4-naphthquione in Micellar Solutions.

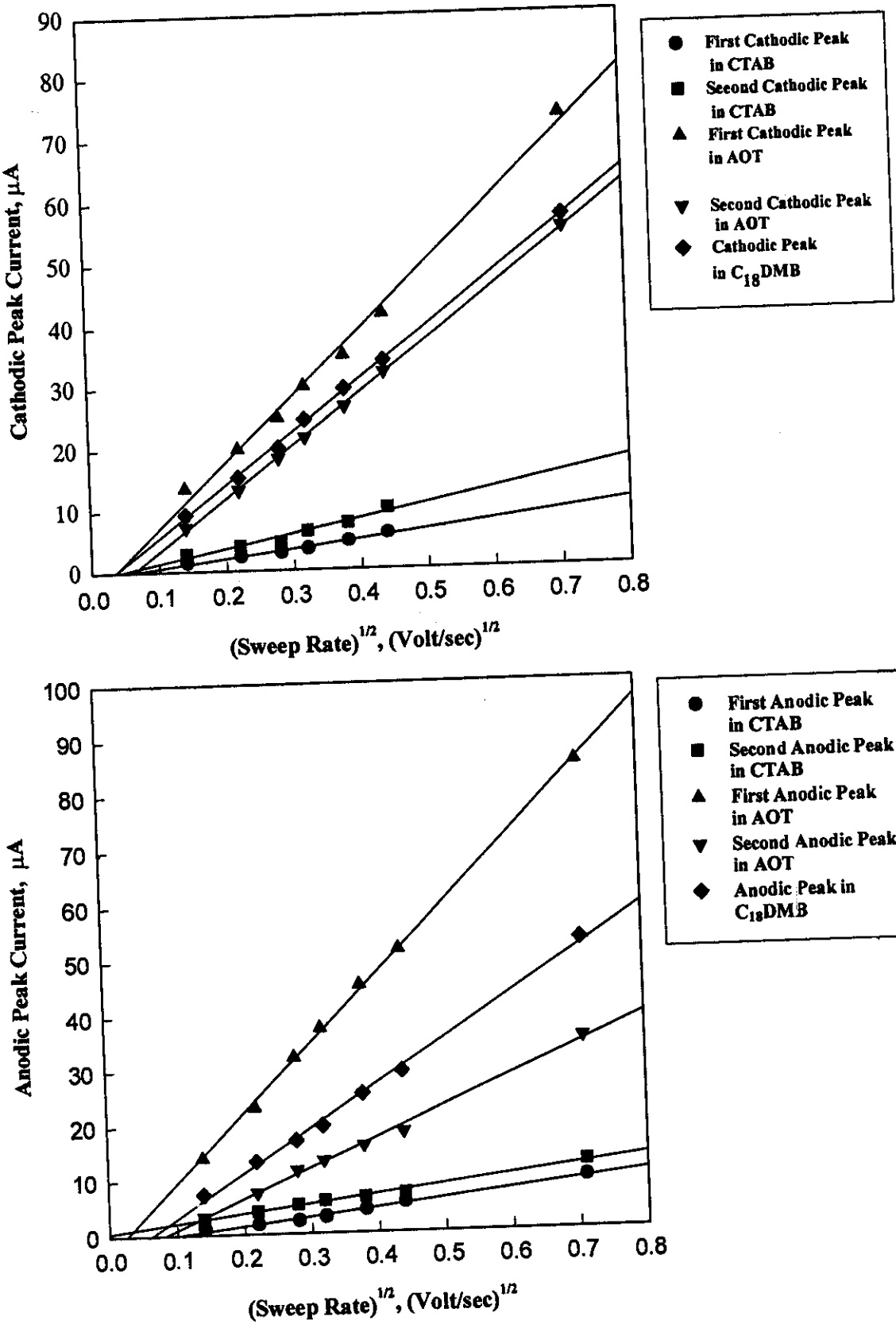

Figure 89:

Peak Current of 2-hydroxy-1,4-naphthoquione in different Microemulsion Systems

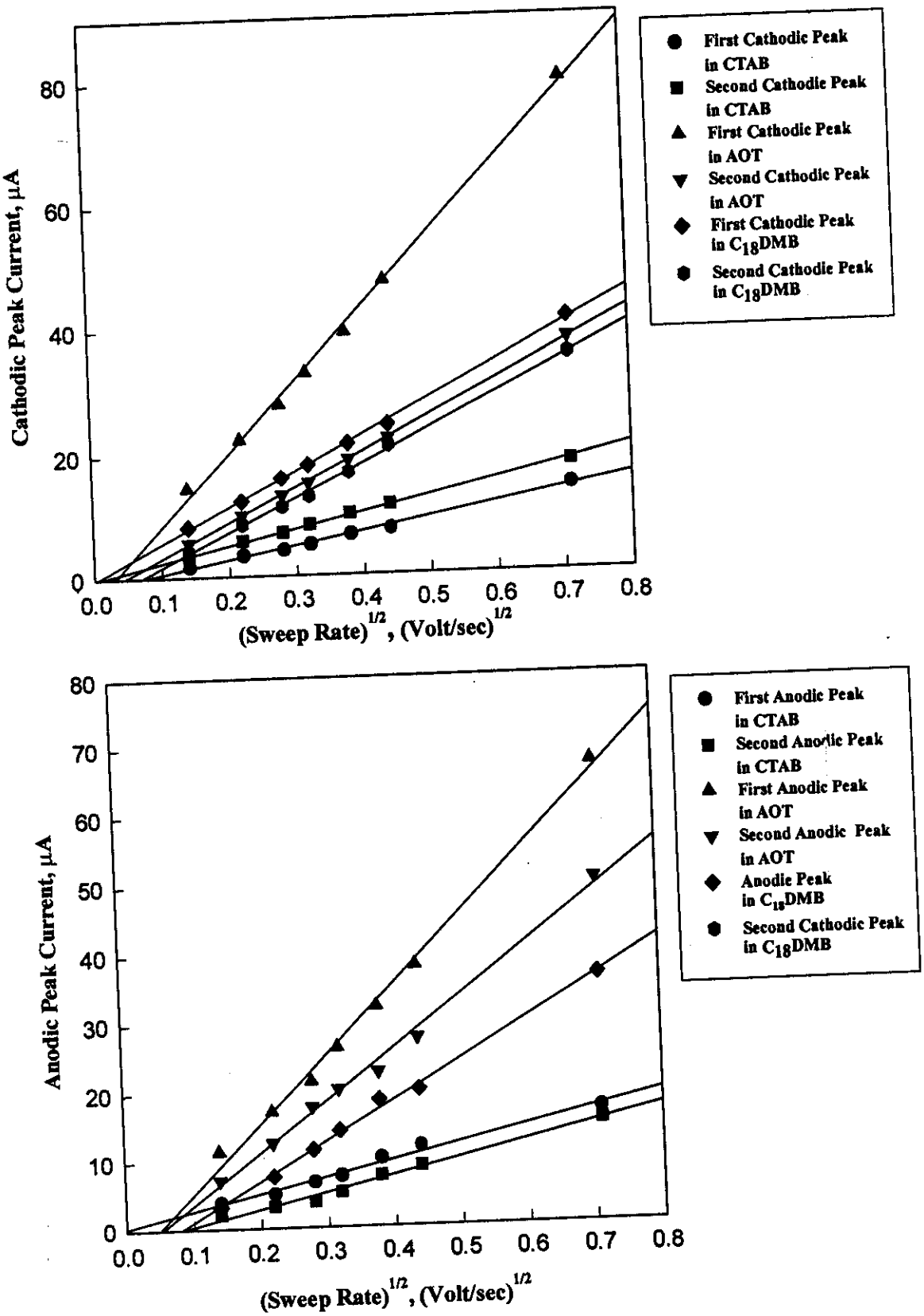

Figure 90:

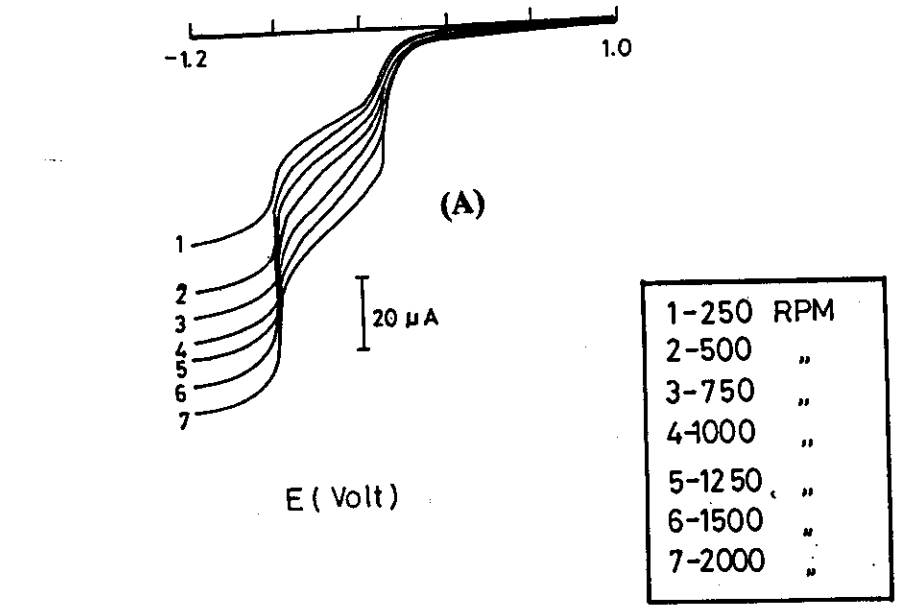

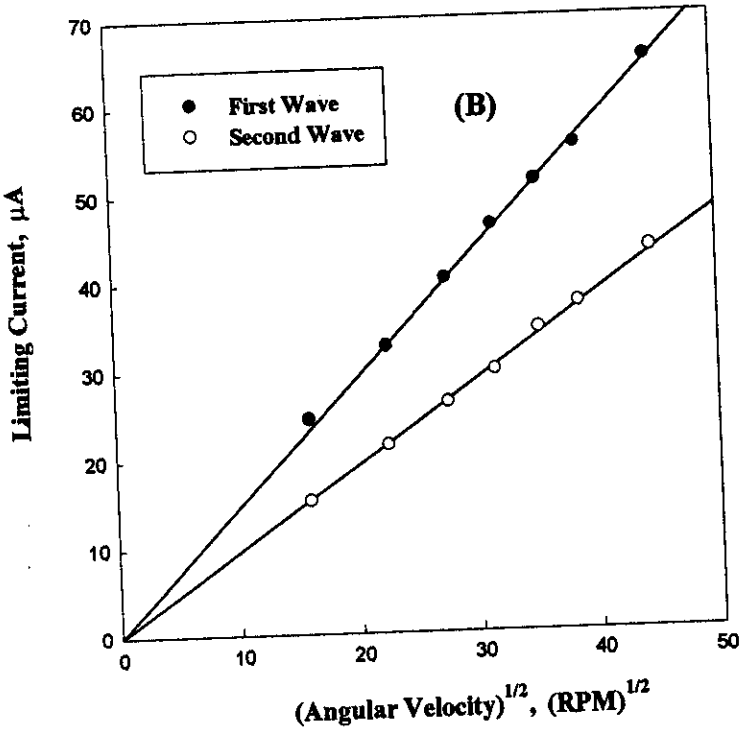

Figure 91: The effect of rotation speed of glassy carbon electrode on the linear sweep voltammogram obtained for 2-hydroxy-1,4-naphthoquinone in aqueous solution, (a) and the plots of (i_l) versus ($\omega^{1/2}$), (b).

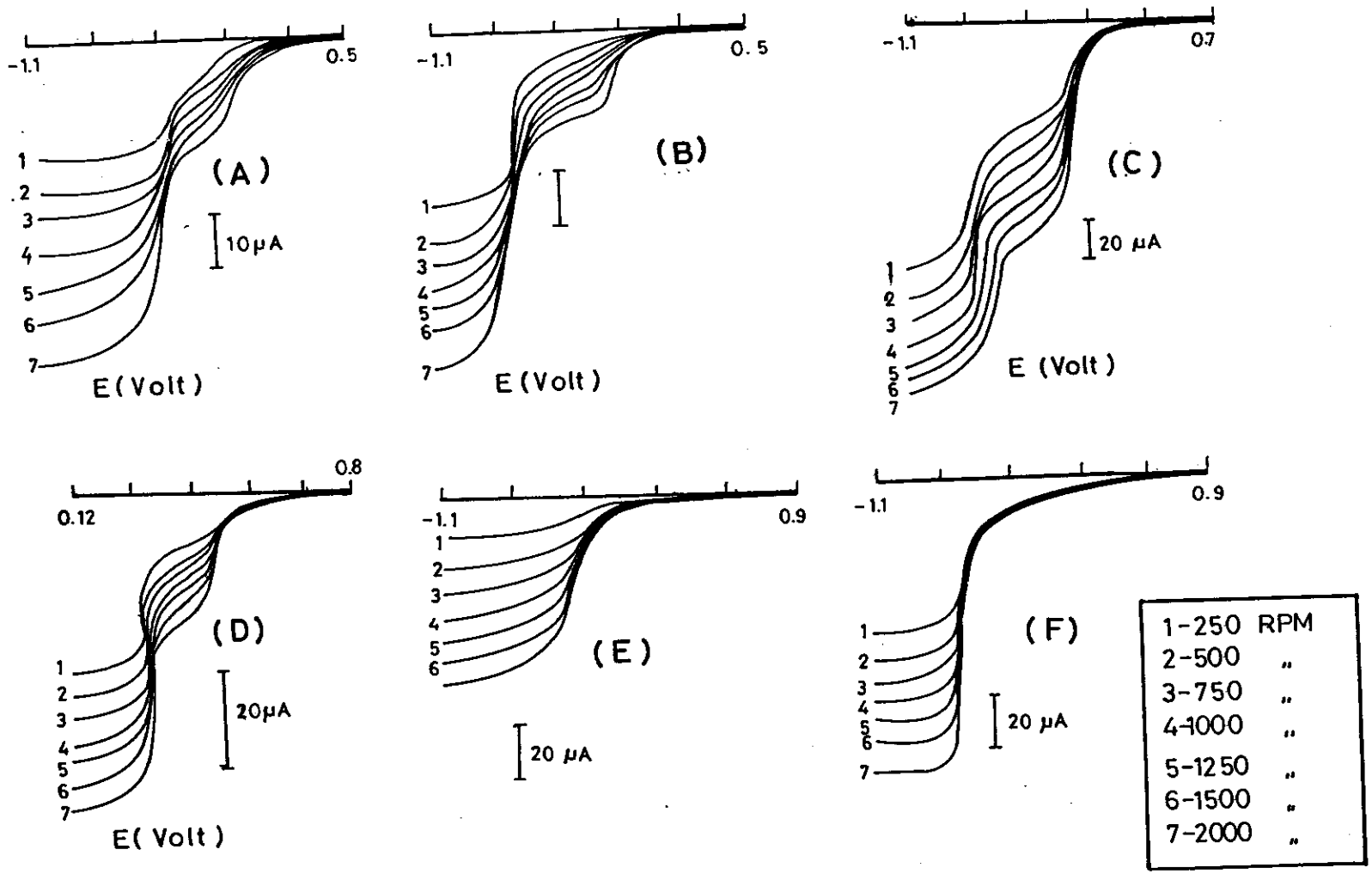

Figure 92: The effect of rotation speed of glassy carbon electrode on the linear sweep voltammograms of 2-hydroxy-1,4 naphthoquinone in different systems, (a) CTAB micellar solution, (b) CTAB microemulsion, (c) AOT micellar solution, (d) AOT microemulsion, (e) C_{18}DMB micellar solution, and (f) C_{18}DMB microemulsion. The speeds are 250, 500, 750, 1000, 1250, 1500 and 2000 RPM.

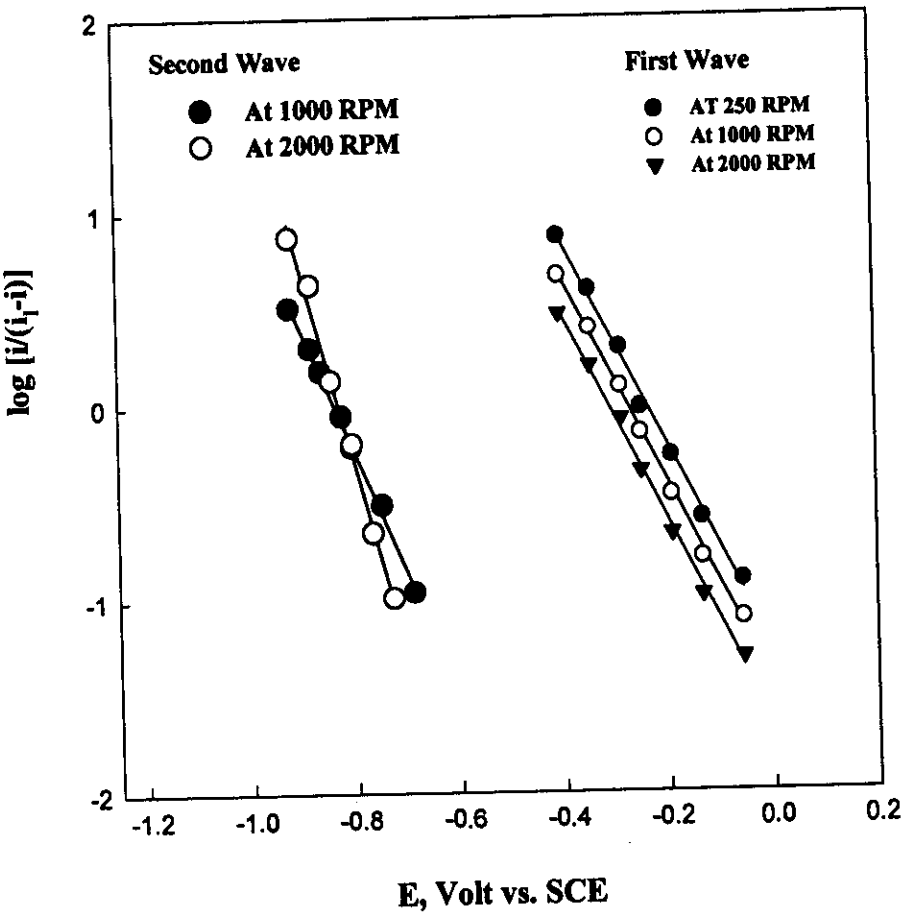

Figure 93: RDV-Logarithmic analysis of 2-hydroxy-1,4-naphthoquinone in aqueous media.

A- in CTAB
B- in AOT
C- in C_{18}DMB

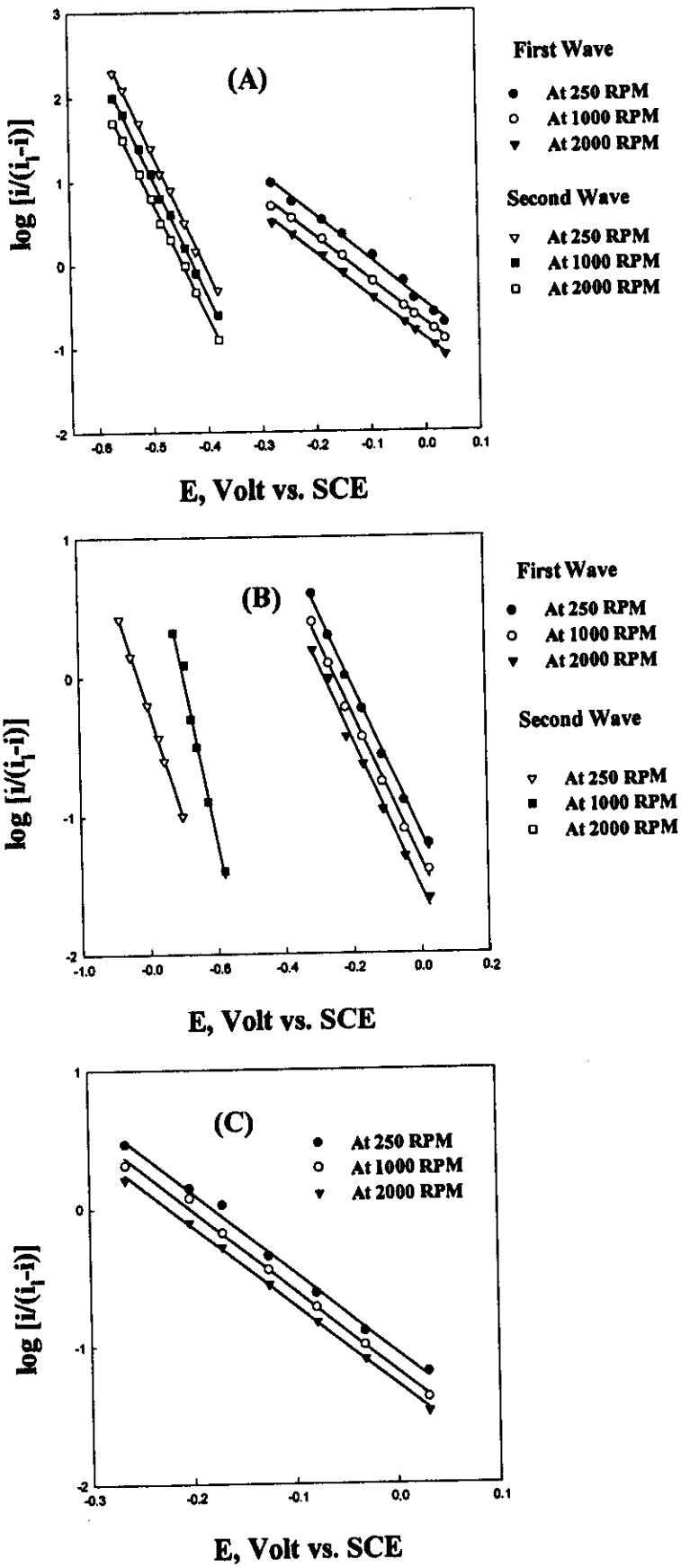

Figure 94: RDV-Logarithmic analysis of 2-hydroxy-1,4-naphthoquinone in micellar solutions.

A- in CTAB
B- in AOT
C- in C_{18}DMB

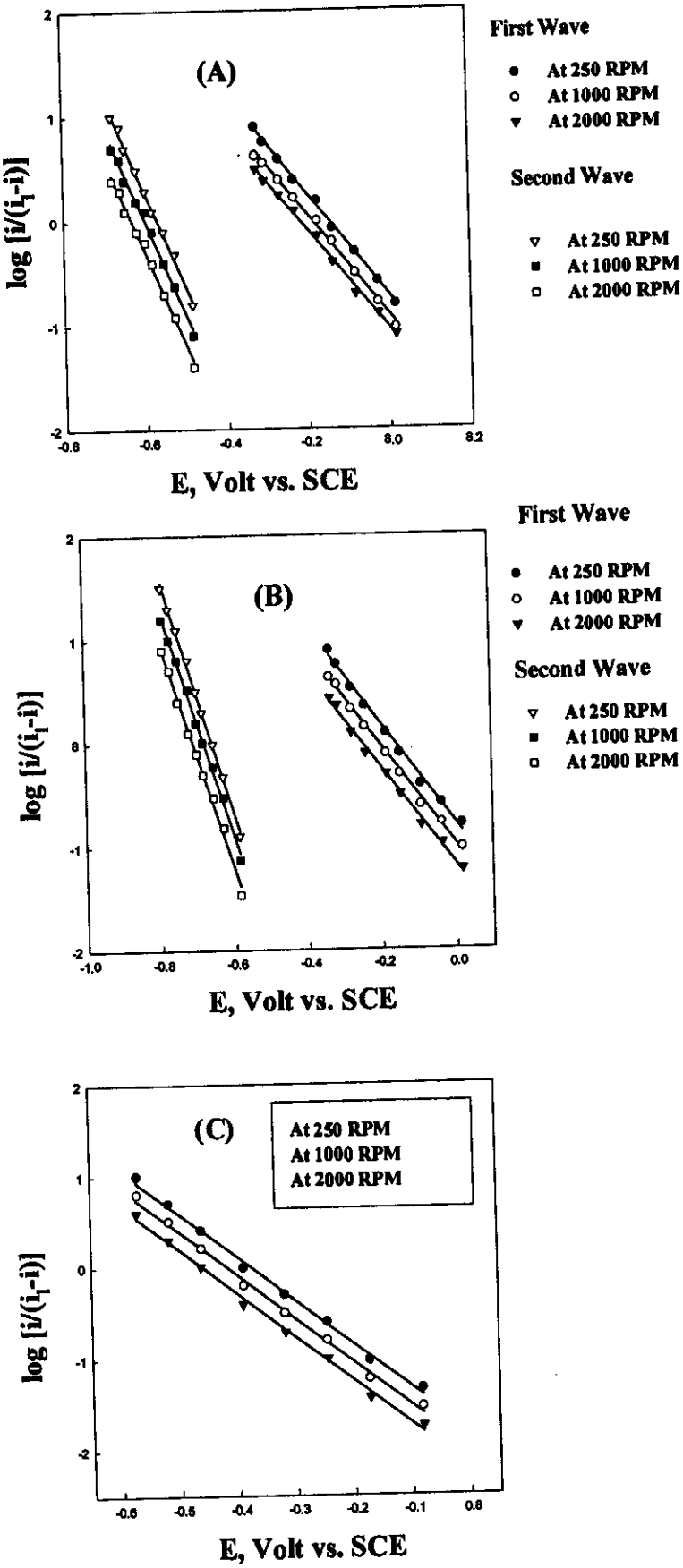

Figure 95: RDV-Logarithmic analysis of 2-hydroxy-1,4-naphthoquinone in microemulsion systems.

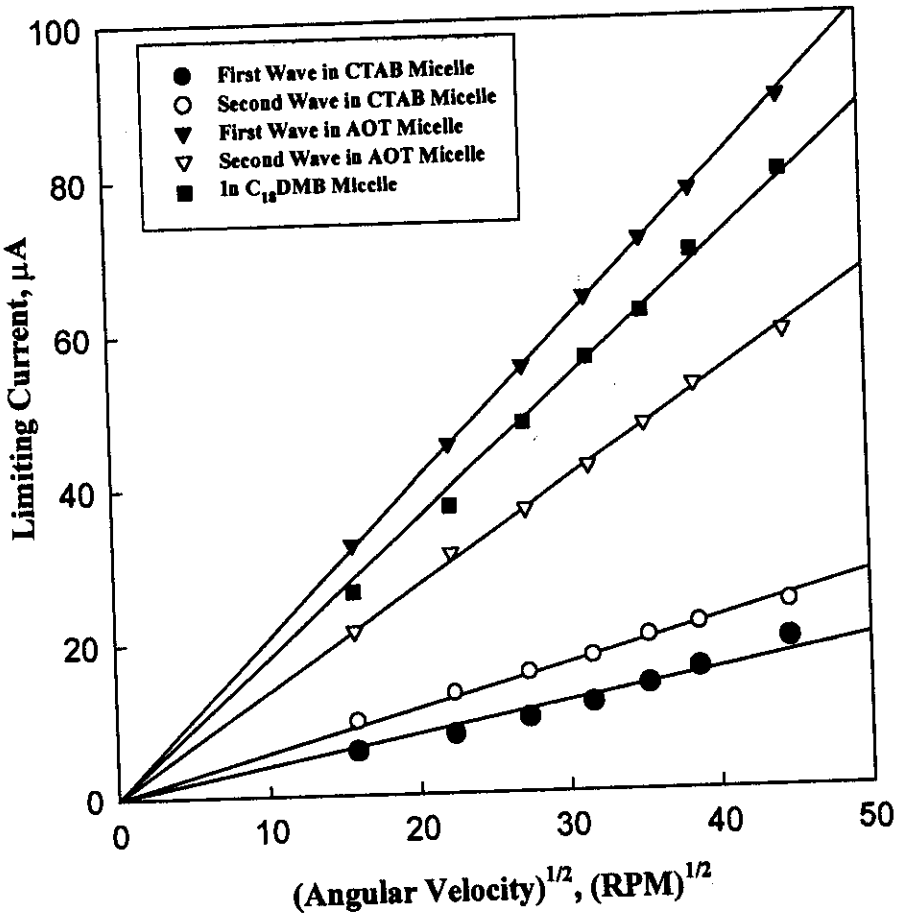

Figure 96: The plots of the limiting (i_l) versus square root of angular velocity ($\omega^{1/2}$) for 2-hydroxy-1,4-naphthoquinone in different micellar solutions.

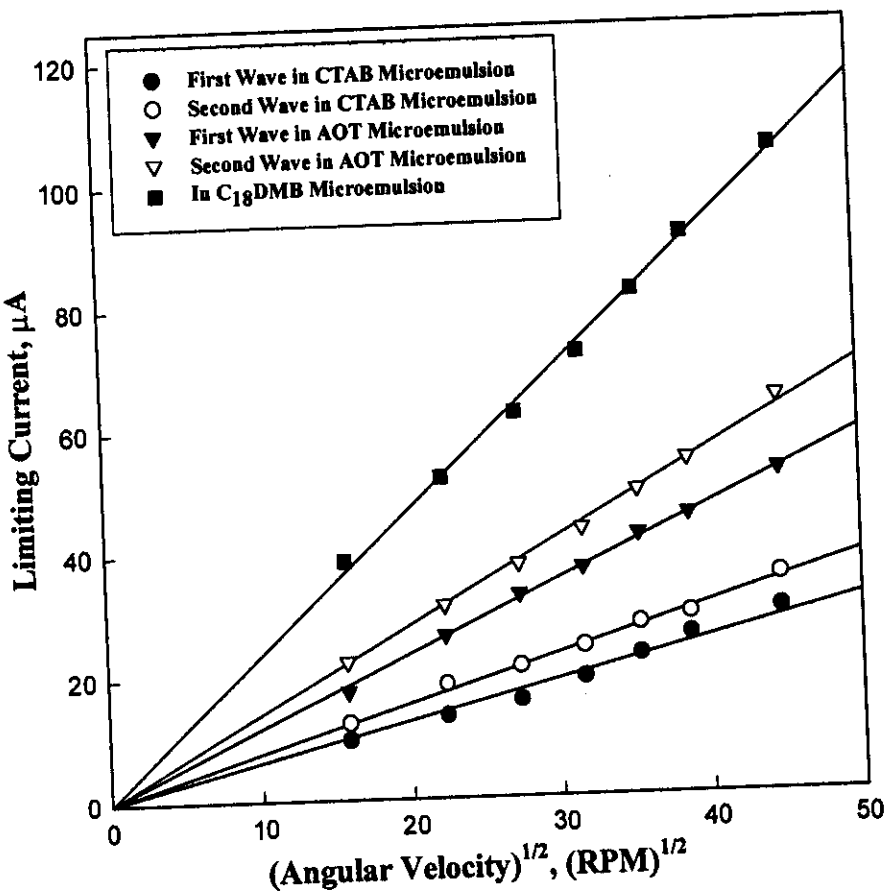

Figure 97: The plots of the limiting (i_l) versus square root of angular velocity ($\omega^{1/2}$) for 2-hydroxy-1,4-naphthoquinone in different microemulsion systems.

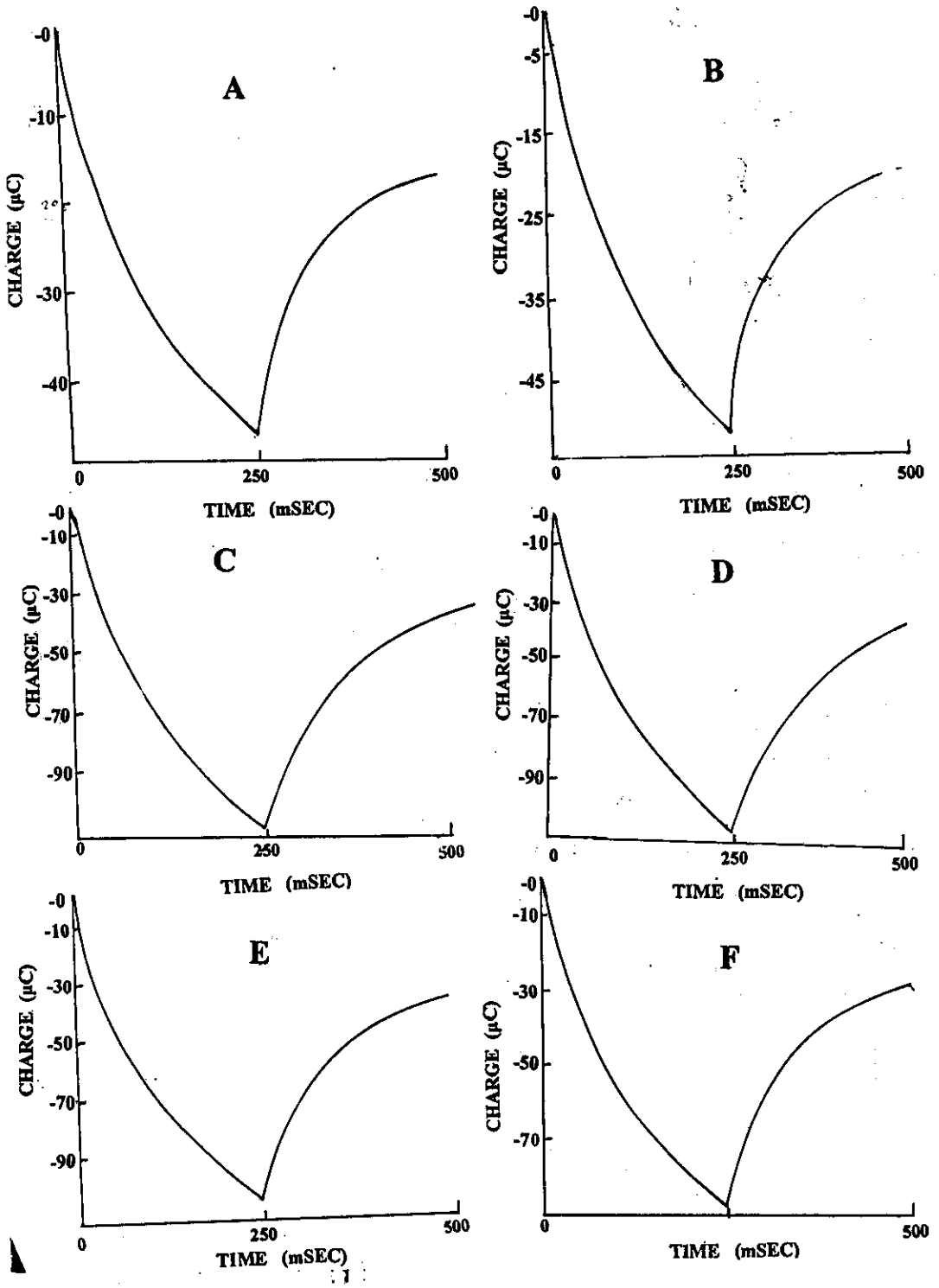

Figure 98: Chronocoulometric responses of 2-hydroxy-1,4-naphthoquinone in different systems, (a) CTAB micellar solution, (b) CTAB microemulsion, (c) AOT micellar solution, (d) AOT microemulsion, (e) C_{18}DMB micellar solution, and (f) C_{18}DMB microemulsion.

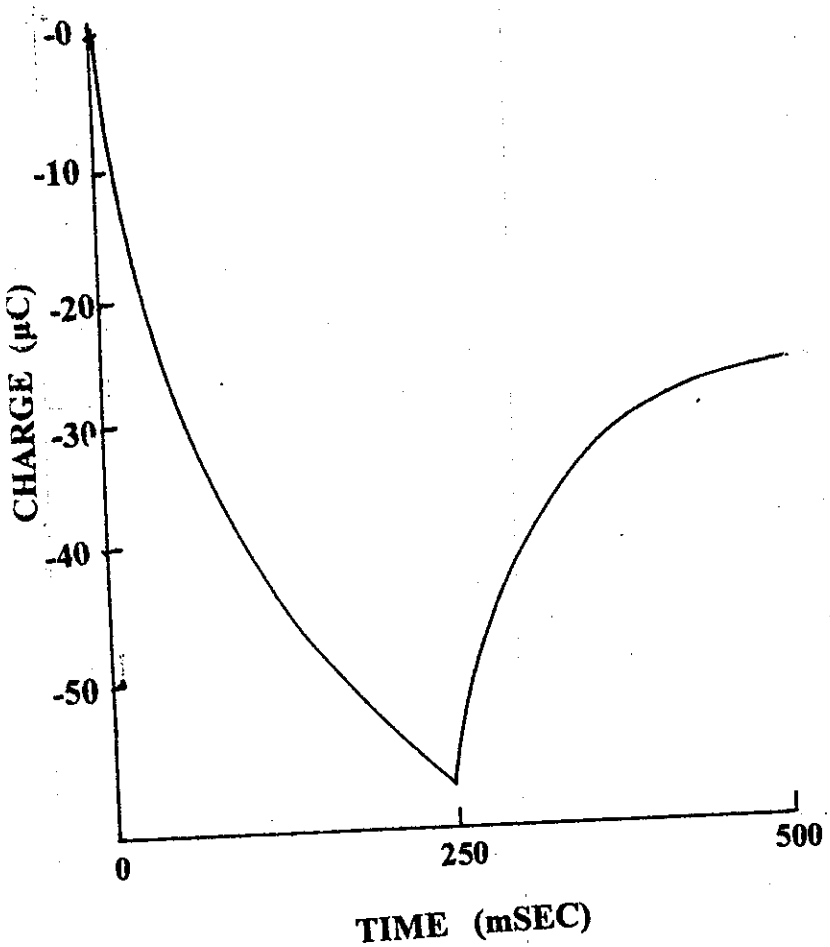

Figure 99: Chronocoulometric responses of 2-hydroxy-1,4-naphthoquinone in pure aqueous solution. Charge versus time.

Table 42: Cyclic voltammetric data obtained for 1mM of 2-hydroxy-1,4-naphthoquinone in pure aqueous media at 25°C.

Sweep Rate	$-E_{p,c1}$	$-E_{p,c2}$	$-E_{p,a1}$	$E_{p,a2}$	$I_{p,c1}$	$I_{p,c2}$	$I_{p,a1}$	$I_{p,a2}$	$I_{p,a1}/I_{p,c1}$	$I_{p,a2}/I_{p,c2}$	ΔE_{p1}	ΔE_{p2}
mV/sec	mV	mV	mV	mV	µA	µA	µA	µA	-	-	mV	mV
20	808	479	530	134	14.30	4.61	9.23	2.31	0.645	0.501	278	345
50	808	478	529	134	19.60	7.69	13.80	3.07	0.704	0.399	279	344
80	808	475	528	136	23.07	10.76	16.50	4.61	0.715	0.428	280	339
100	806	475	529	136	27.07	12.30	20.30	6.15	0.733	0.500	277	339
150	806	475	528	137	33.60	15.38	25.38	7.69	0.755	0.500	278	338
200	806	473	527	138	41.80	16.92	30.60	9.23	0.732	0.545	279	335
500	805	472	527	138	70.10	29.23	50.70	18.40	0.723	0.629	278	334

Table 43: Cyclic voltammetric data obtained for 1mM of 2-hydroxy-1,4-naphthoquinone in micellar solutions.

tem	Sweep Rate	$-E_{p,c1}$	$-E_{p,c2}$	$-E_{p,a1}$	$-E_{p,a2}$	$I_{p,c1}$	$I_{p,c2}$	$I_{p,a1}$	$I_{p,a2}$	$I_{p,a1}/I_{p,c1}$	$I_{p,a2}/I_{p,c2}$	ΔE_{p1}	ΔE_{p2}
	mV/sec	mV	mV	mV	mV	µA	µA	µA	µA	-	-	mV	mV
CTAB Micellar Solution													
	20	461	273	441	-13	1.47	2.94	1.17	2.94	0.795	1.000	20	260
	50	461	280	441	-6	2.35	4.11	1.76	4.11	0.748	0.998	20	274
	80	462	280	441	-6	2.94	4.70	2.35	5.29	0.799	1.124	21	274
	100	467	280	442	0	3.52	6.47	2.94	5.88	0.835	0.908	25	280
	150	472	285	443	6	4.75	7.64	4.11	6.47	0.866	0.846	29	291
	200	473	285	444	6	5.88	10.00	5.29	7.05	0.899	0.705	29	291
	500	475	287	447	13	-	-	9.41	12.35	-	-	28	300
) **AOT Micellar Solution**													
	20	833	268	338	20	13.60	7.30	14.00	3.30	1.029	0.452	495	288
	50	833	268	338	19	19.60	13.30	23.10	7.50	1.160	0.563	495	287
	80	835	269	339	20	25.00	18.33	32.20	11.60	1.288	0.632	496	289
	100	835	269	341	21	30.00	21.66	37.50	13.30	1.250	0.614	494	290
	150	836	270	340	22	35.00	26.60	45.20	16.00	1.290	0.601	496	292
	200	837	272	340	22	41.66	32.10	51.66	18.30	1.240	0.570	497	250
	500	840	275	334	28	73.30	55.00	85.00	35.00	1.159	0.636	506	303
) **C_{18}DMB Micellar Solution**													
	20	286	-	42	-	9.30	-	7.30	2.31	0.784	-	365	-
	50	286	-	42	-	15.30	-	13.30	3.07	0.869	-	332	-
	80	287	-	43	-	20.00	-	17.08	4.61	0.854	-	332	-
	100	288	-	43	-	24.60	-	19.70	6.15	0.800	-	331	-
	150	288	-	44	-	28.00	-	25.30	7.69	0.903	-	330	-
	200	287	-	45	-	34.00	-	29.30	9.23	0.861	-	328	-
	500	313	-	52	-	57.00	-	53.00	18.40	0.614	-	328	-

Table 44: Cyclic voltammetric data obtained for 1mM of 2-hydroxy-1,4-naphthoquinone in microemulsion systems.

stem	Sweep Rate	$-E_{p,c1}$	$-E_{p,c2}$	$-E_{p,a1}$	$-E_{p,a2}$	$I_{p,c1}$	$I_{p,c2}$	$I_{p,a1}$	$I_{p,a2}$	$I_{p,a1}/I_{p,c1}$	$I_{p,a2}/I_{p,c2}$	ΔE_{p1}	ΔE_{p2}
	mV/sec	mV	mV	mV	mV	µA	µA	µA	µA	-	-	mV	mV
)CTAB Microemulsion													
	20	622	246	498	59	1.66	2.80	3.80	2.10	2.100	0.750	124	178
	50	625	247	493	44	3.50	5.83	5.00	3.20	1.400	0.548	132	203
	80	627	249	489	44	4.33	7.08	6.60	3.80	1.520	0.536	138	205
	100	627	250	488	39	5.16	8.33	7.50	5.16	1.450	0.621	139	211
	150	628	249	489	39	6.66	10.00	10.0	7.50	1.550	0.750	139	210
	200	629	252	485	38	7.50	11.40	11.66	8.80	1.551	0.771	144	214
	500	632	256	480	38	14.16	17.98	16.66	15.00	1.176	0.834	594	218
) AOT Microemulsion													
	20	770	270	582	52	14.50	5.60	11.30	7.20	0.779	1.285	189	219
	50	770	272	583	52	22.30	10.0	17.10	12.50	0.766	1.250	188	220
	80	772	270	582	51	27.80	13.20	21.51	17.72	0.773	1.342	188	219
	100	772	273	585	50	32.90	15.18	26.30	20.25	0.779	1.333	187	223
	150	768	270	580	43	39.24	18.90	32.10	22.70	0.818	1.201	190	229
	200	767	275	579	40	47.46	22.15	37.97	27.50	0.800	1.241	187	229
	500	767	286	578	39	79.74	37.60	67.00	50.00	0.840	1.329	88	247
) C_{18}DMB Microemulsion													
	20	694	226	18	-	8.20	4.20	3.20	-	-	-	-	-
	50	696	224	17	-	12.32	8.50	7.60	-	-	-	-	-
	80	698	225	19	-	15.98	11.30	11.42	-	-	-	-	-
	100	697	226	18	-	18.10	12.98	14.14	-	-	-	-	-
	150	697	226	17	-	21.40	16.80	18.57	-	-	-	-	-
	200	692	227	17	-	24.28	21.00	20.00	-	-	-	-	-
	500	706	278	69	-	40.90	35.10	36.12	-	-	-	-	-

Table 45: Diffusion coefficient values of reductant and oxidant species for 2-hydroxy-1,4-naphthoquinone in different systems.

System	(CV)				(RDV)	
	$D_{R1}x10^{-6}$ cm^2/sec	$D_{R2}x10^{-6}$ cm^2/sec	$D_{O1}x10^{-6}$ cm^2/sec	$D_{O2}x10^{-6}$ cm^2/sec	$(Dx10^{-6})^a$ cm^2/sec	$(Dx10^{-6})^b$ cm^2/sec
A- In Aqueous Solution						
	3.84	0.73	2.03	0.24	4.11	0.76
B- In CTAB Micellar Solution						
	0.18	0.28	0.25	0.10	0.11	0.18
C- In CTAB Microemulsion						
	0.16	0.31	0.24	0.21	0.22	0.29
D- In AOT Micellar Solution						
	3.14	2.73	4.31	1.15	1.26	0.68
E- In AOT Microemulsion						
	4.51	1.55	3.84	1.88	0.55	0.79
F- In C_{18}DMB Micellar Solution						
	2.79[c]	-	2.26[c]	-	2.03	-
G- In C_{18}DMB Microemulsion						
	2.66[c]	2.44[c]	2.71[c]	-	2.56	-

a,b- for first and second wave respectively.

c- Measured at 40°C.

Table 46 : The half-wave potential for 2-hydroxy-1,4-naphthoquinone in different systems.

System	$-E_{1/2}$(mV vs. SCE)			
	(CV)		(RDV)	
	a	b	c	d
A- In Aqueous Solution	169	667	228	828
B- In CTAB Micellar Solution	140	454	137	412
C- In CTAB Microemulsion	146	557	150	583
D- In AOT Micellar Solution	146	586	220	780
E- In AOT Microemulsion	159	675	212	654
F- In C_{18}DMB Micellar Solution	167	-	193	-
G-In C_{18}DMB Microemulsion	356	-	398	-

a,b- First Peak and Second Peak, respectively.

c,d- for first and second wave respectively

Table 47: The slopes of the plots of log $(i/(i_l-i))$ versus E for 2-hydroxy-1,4-naphthoquinone in differrent systems at 25°C.

System	Slope (V^{-1})	
	a	b
A- In Aqueous Solution	5.27	(6.28[c],10.01[d])
B- In CTAB Micellar Solution	5.26	14.20
C- In CTAB Microemulsion	4.91	9.24
D- In AOT Micellar Solution	5.59	(7.90[c],12.59[d])
E- In AOT Microemulsion	4.81	11.81
F- In C_{18}DMB Micellar Solution	5.80	-
G-In C_{18}DMB Microemulsion	4.80	-

a,b- for first and second wave respectively.

c,d- at 1000 and 2000 RPM,respectively.

Table 48: Γ_o values obtained from chronocoulometric data of 2-hydroxy-1,4-naphthoquinone in pure aqueous, micelles and microemulsion systems.

Systems	Γ_o moles/cm^2
(A) Pure Aqueous	2.16×10^{-9}
(B) CTAB Micelles	2.54×10^{-9}
(C) CTAB Microemulsion	3.36×10^{-9}
(D) AOT Micelles	8.40×10^{-9}
(E) AOT Microemulsion	8.85×10^{-9}
(F) C_{18}DMB Micelles	6.95×10^{-9}
(G) C_{18}DMB Microemulsion	5.11×10^{-9}

3.6.4 1,2- Naphthoquinone-4-sodium sulfonate

A- Cyclic voltammetry

The cyclic voltammograms of 1mM of 1,2-naphthoquinone-4-sodium sulfonate were recorded in CTAB, AOT and C_{18}DMB micelles and microemulsion media as well as in pure aqueous. The voltammograms were recorded in the potential window from -1200 to +1100 mV (versus SCE) and at potential sweep rates between 20 to 500 mV/sec. Well defined voltammograms were obtained in all micellar solutions and microemulsion media as well as aqueous solution as represented in Figs. (100,101). The voltammograms showed a single redox couple of peaks on the cathodic and anodic branches of sweep in all micelles and microemulsion media as well as in pure aqueous solution, except in AOT micelles it displayed two oxidation peaks of almost equal heights, Fig. (101c). Also, two reduction peaks were observed in C_{18}DMB microemulsion system, Fig. (101f).

The anodic peak current, $I_{p,a}$ and the cathodic peak current, $I_{p,c}$ are slightly different as shown from Tables (49-51). The anodic to cathodic peak current ratios ($I_{p,a}/I_{p,c}$) does not exceed 0.966 in micelles and microemulsion systems. These results indicated the very weak adsorption on the electrode surface.

The peak potential separation in microemulsion systems of different surfactant types ΔE_P is around the theoretical value for two-electron transfer ~ 31 mV in AOT microemulsion and around 40 mV in CTAB microemulsion system. These results indicate that the behaviour of 1,2-naphthoquinone-4-sodium sulfonate is completely reversible in AOT microemulsion system and quasi-reversible in CTAB microemulsion. On the other hand, the peak potential separation in zwitterionic C_{18}DMB microemulsion is very high ~ 925 mV indicating that the redox process takes place irreversibly in this system.

The peak potential separation in micellar solutions was found ~ 40 mV in CTAB micelles indicating the quasi-reversible electron transfer. Whereas, in AOT and C_{18}DMB a larger peak potential separation was observed ~ 334 and 227 mV, respectively. The larger peak potential separation indicating the irreversibility of the process increased in these systems. This is more or less comparable with that obtained in aqueous solution (~ 173 mV).

The results obtained indicate the different effects of micelles and microemulsion systems on the stabilities of the free radical anion formed following the first electron transfer. Such effects are explained on the of electrostatic and or hydrophobic. It is known that micelles are more electrostatic than microemulsion systems due to the additional oil component.

Stabilizations of the free anion radical by cationic CTAB systems micelles and microemulsion was observed from the smaller peak potential separation, ΔE_P, Tables (50,51). And the predominant effect is attributed to electrostatic stabilizations of the product of the electron transfer process as observed from the same peak potential separation in both systems. In AOT micelles and microemulsion systems the mechanism of stabilization takes place via hydrophobic effects. Since AOT is negatively charged the stabilization of the free anion radical at the negatively charged electrode is more hydrophobic in nature. Where anionic surfactants are known to kinetically stabilize anion radicals [28].

In zwitterionic surfactants the behaviour of 1,2-naphthoquinone-4-sodium sulfonate is more less same as pure aqueous solutions and becomes irreversible and quasi-reversible, respectively.

Since 1,2-naphthoquinone-4-sodium sulfonate is soluble in water, the obtained data suggested that it is puried or partitioned into the surfactant film as observed from the diffusion coefficient data, Table (52).

On employing the Randles-Sevcik equation [140]. The plots of both cathodic peak currents ($I_{p,c}$) and the anodic peak currents ($I_{p,a}$) versus square root of sweep rate ($\upsilon^{1/2}$) for 1,2-naphthoquinone-4-sodium sulfonate in micelles and microemulsion of different surfactant systems showed straight lines almost passing through the origin, Figs. (102,103). These results indicate that the electrode process is mainly diffusion controlled [140]. Also, The plots of the cathodic peak currents ($I_{p,c}$) as well as the anodic one ($I_{p,a}$) versus $\upsilon^{1/2}$ for 1,2-naphthoquinone-4-sodium sulfonate in pure aqueous solution is deviated from the origin, as shown from Fig. (100b). This behaviour may be attributed to adsorption on the electrode surface. The apparent diffusion coefficients of the reduced and oxidized forms (D_R and D_O) were determined from the slopes of these linear plots. The obtained values were listed in Table (52). The diffusion coefficient values indicate the partitioning of 1,2-naphthoquinone-4-sodium sulfonate between the oil droplet, surfactant film and aqueous domain.

The values of E_p and ΔE_P of micellar solutions or microemulsions have Differences which observed in Table (49-51). The changes in half-wave potential ($E_{1/2}$) are expected due to the different effects of the surfactant as local environment on the relative stabilities of the reactant and products of the electron transfer reaction. $E_{1/2}$ shifted to less negative value in the CTAB micellar solution and microemulsion as shown in Table (53).

B- Rotating disk voltammetry (RDV)

The rotating disk voltammograms were carried out successfully in CTAB, AOT and C_{18}DMB micelles and microemulsion systems as well as in pure aqueous solution using 1mM of 1,2-naphthoquinone-4-sodium sulfonate. The effect of rotation speed on the voltammograms were recorded at different speeds (250-200 RPM) . The rotating disk voltammograms were recorded at

small sweep rate (5 mV/sec) in the potential window 900 to -1000 mV. The voltammograms recorded in pure aqueous solution as well as in different micellar solutions and microemulsion media are essentially similar showing the one step reduction-plateau, as represented in Figs. (104a,105). Except, in C_{18}DMB micelle it displayed two waves, Fig. (105c). The effect of rotation speed on the voltammogram was recorded at angular velocities varying from 250 to 2000 RPM. As shown from Figs. (104, 105), on increasing the angular velocity the limiting current is increased, and a negative shift in the half-wave potential ($E_{1/2}$) (~20 mV) indicating the chemical reversibility.

The half-wave potential and the number of electrons consumed in the reduction process were determined from the logarithmic analysis of the rotating disk voltammograms of 1,2-naphthoquinone-4-sodium sulfonate in pure aqueous as well as micelles and microemulsion media at 250, 1000 and 2000 RPM. On using equation (III.3), the plots of log ($\frac{i}{i_l - i}$) versus E displayed linear correlations, Figs. (106,107,108). The slopes of these plots were listed in Table (54). The data obtained indicating the quasi-reversible electron transfer process.

On using Levich equation [133], the plots of i_l versus $\omega^{1/2}$ in all media showed linear correlations passing through the origin, Figs.(104b,109&110). This behaviour indicates that the reduction process takes place under mass transfer control. The slopes of these linear plots were used to estimate the apparent diffusion coefficients in various media, Table (52).

C- Chronocoulometry of 1,2-naphthoquinone-4-sodium sulfonate

The chronocoulometric responses of 1,2-naphthoquinone-4-sodium sulfonate were recorded in micellar solutions and microemulsion media of three different types of surfactants (CTAB, AOT and C_{18}DMB) as well as in pure aqueous solution. The chronocoulograms of 1,2-naphthoquinone-4-

sodium sulfonate in micellar solutions were recorded by stepping the potential from 1100 to -1100 mV and switched back to the original value by applying pulse width of 250 millisecond. The chronocoulograms of the forward step in these micelles and microemulsion systems were obtained by plotting the charge (Q_{tot}) versus time (t), as represented in Figs. (111a, 111c, 111e). A similar chronocoulograms were observed in microemulsion systems, Figs. (111b, 111d, 111f) and in pure aqueous solution, Fig. (112). The values of the amount of adsorbed reactant species Γ_o were listed in Table (55). And by considering that there is no alteration or negligible contribution by adsorption on Helmoholtz diffusion layer structure. Therefore, the capacitive term of charge (Q_c) for both forward and reverse reactions should be the same.

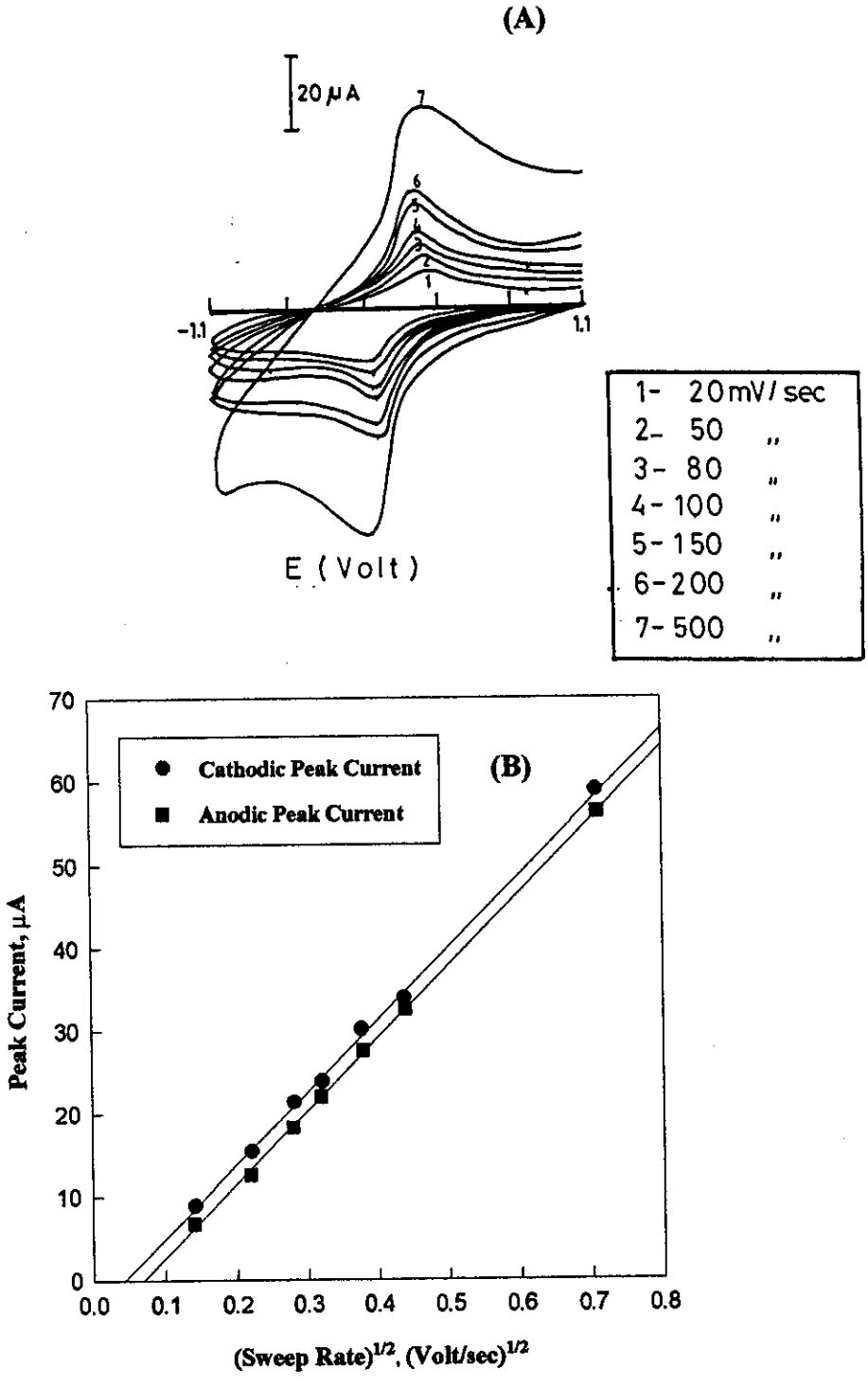

Figure100: Peak currents of 1,2-naphthoquinone-4-sodium sulfonate in aqueouse media obtained from cyclic voltammetry, (a) and its plot versus $\upsilon^{1/2}$, (b).

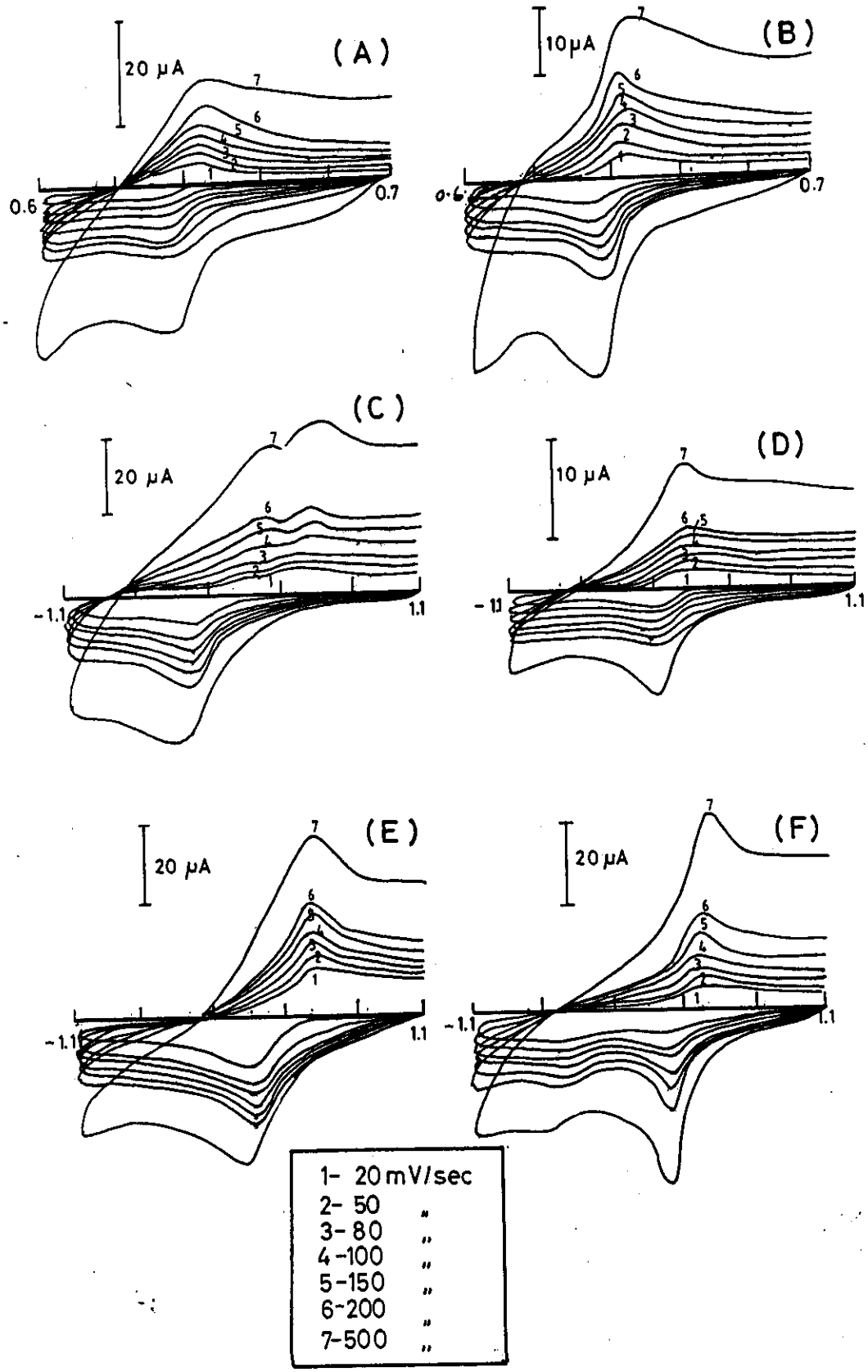

Figure 101: Cyclic voltammograms of 1,2-naphthoquinone-4-sodium sulfonate in different systems, (a) CTAB micellar solution, (b) CTAB microemulsion, (c) AOT micellar solution, (d) AOT microemulsion, (e) C_{18}DMB micellar solution, and (f) C_{18}DMB microemulsion. The sweep rates are 20, 50, 80, 100, 150, 200 and 500 mV/sec

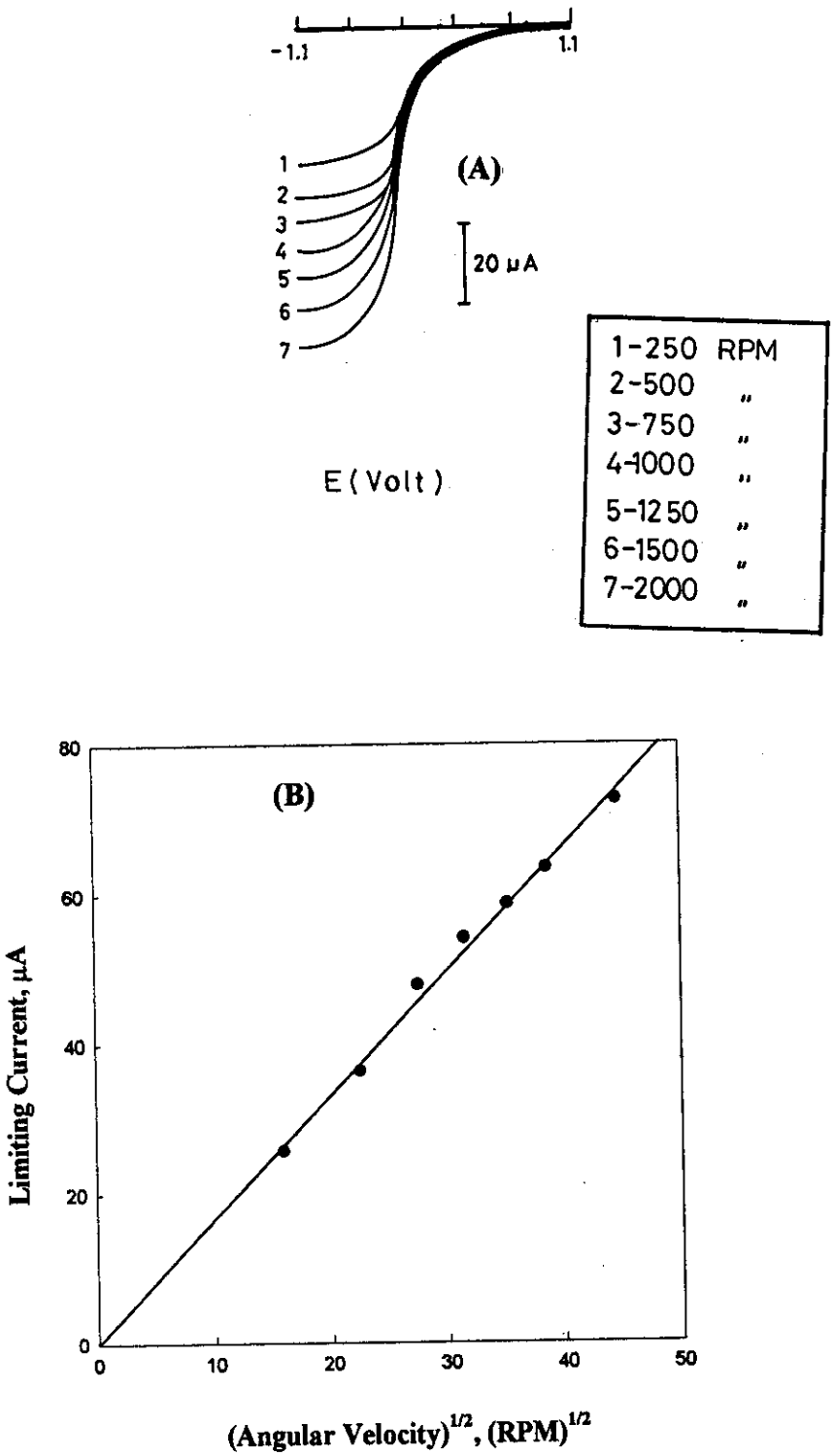

Figure 104: The effect of rotation speed of glassy carbon electrode on the linear sweep voltammogram obtained for 1,2-naphthoquinone-4-sodium sulfonate in aqueous solution, (a) and the plots of limiting current (i_l) versus square root of angular velocity ($\omega^{1/2}$), (b).

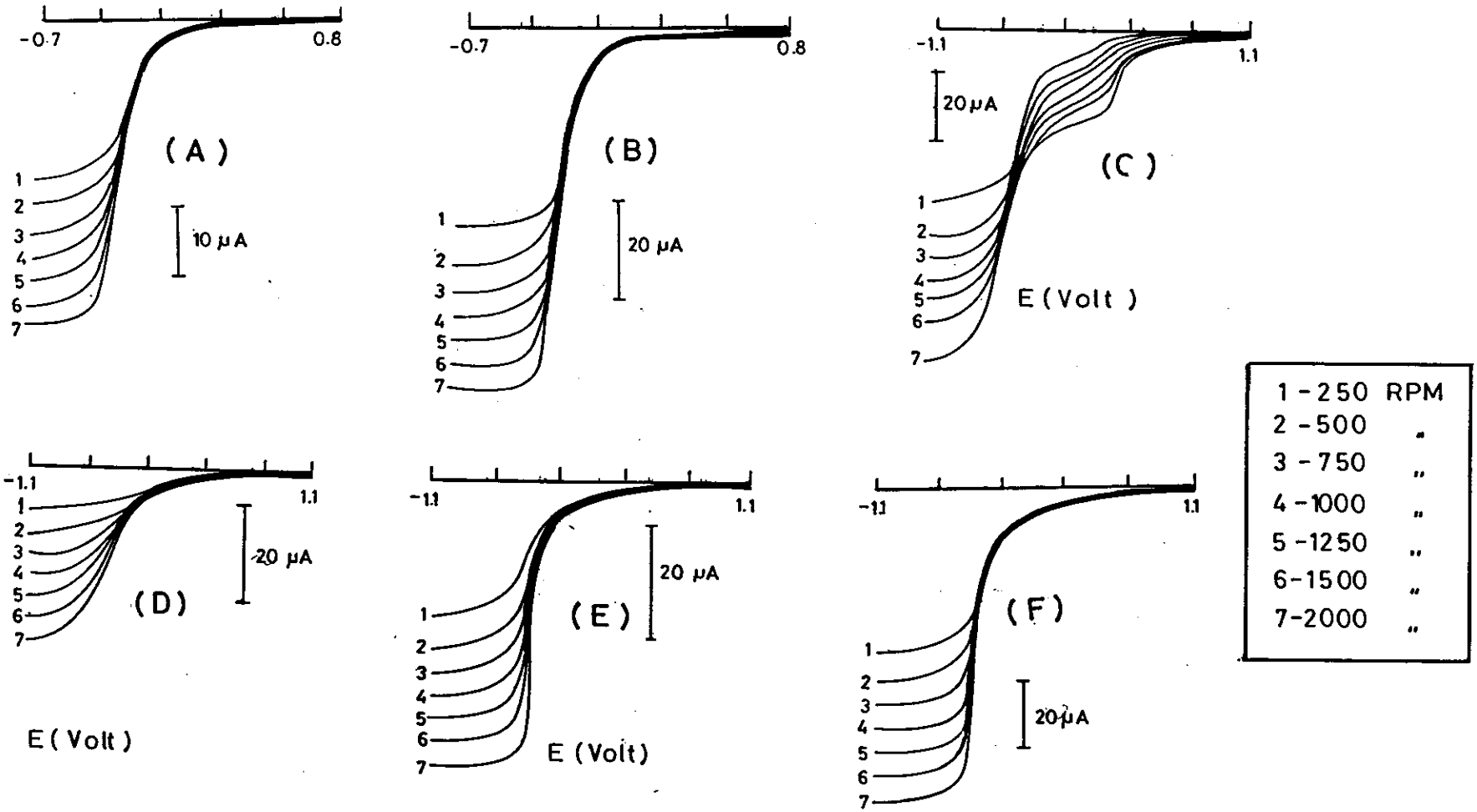

Figure 105: The effect of rotation speed of glassy carbon electrode on the linear sweep voltammograms of 1,2 naphthoquinone -4-sodium sulfonate in different systems, (a) CTAB micellar solution, (b) CTAB microemulsion, (c) AOT micellar solution, (d) AOT microemulsion, (e) C_{18}DMB micellar solution, and (f) C_{18}DMB microemulsion. The speeds are 250, 500, 750, 1000, 1250, 1500 and 2000 RPM.

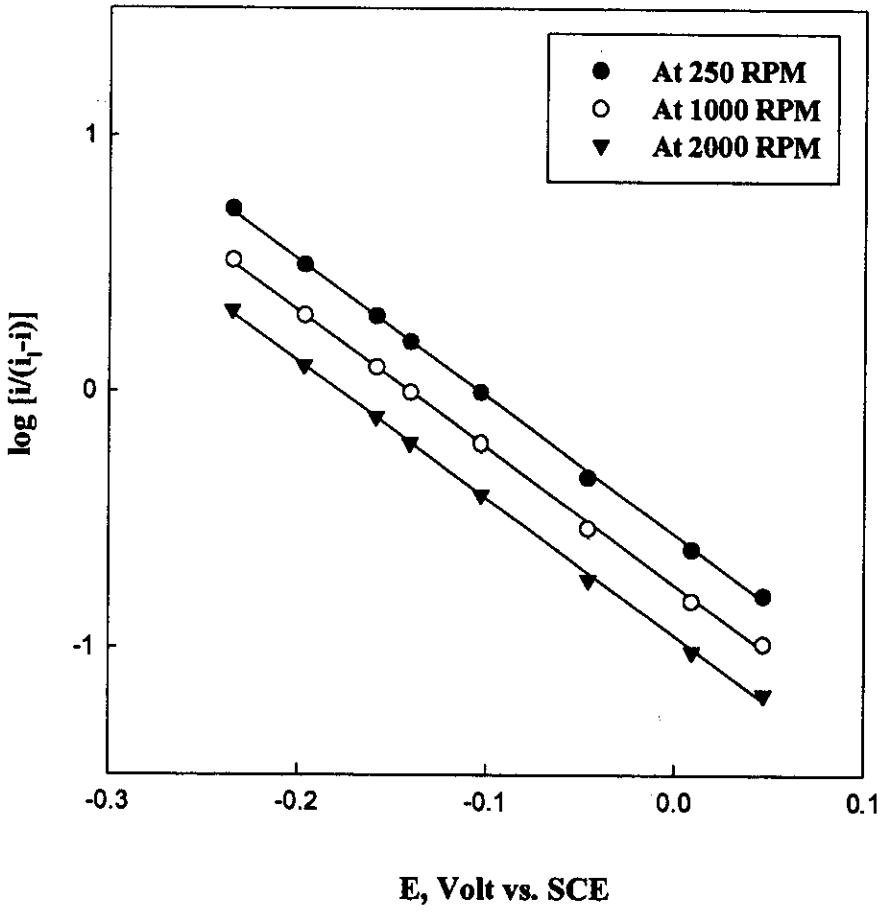

Figure 106: Logarithmic analysis of 1,2-naphthoquinone-4-sodium sulfonate in aqueous solution contanining 0.1 M NaCl at 25°C.

A- in CTAB
B- in AOT
C- in C_{18}DMB

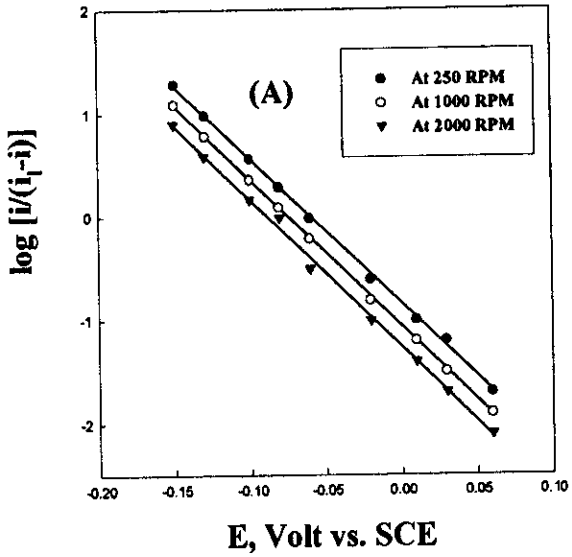

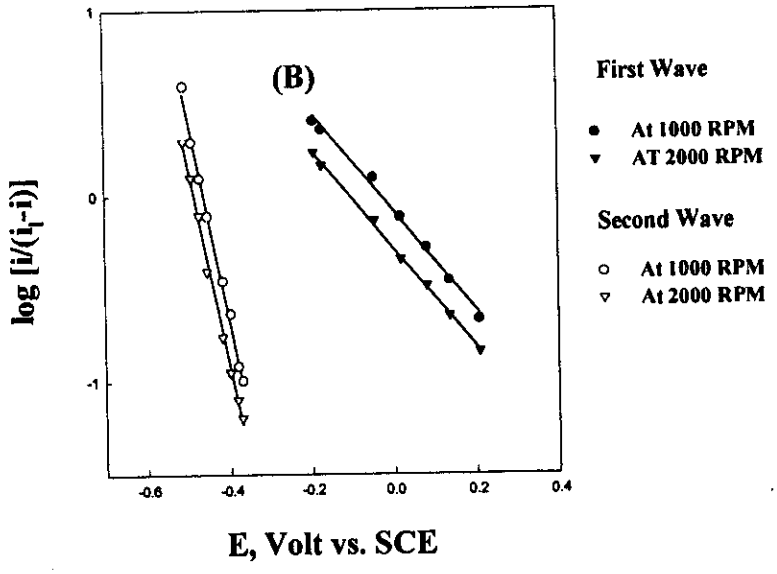

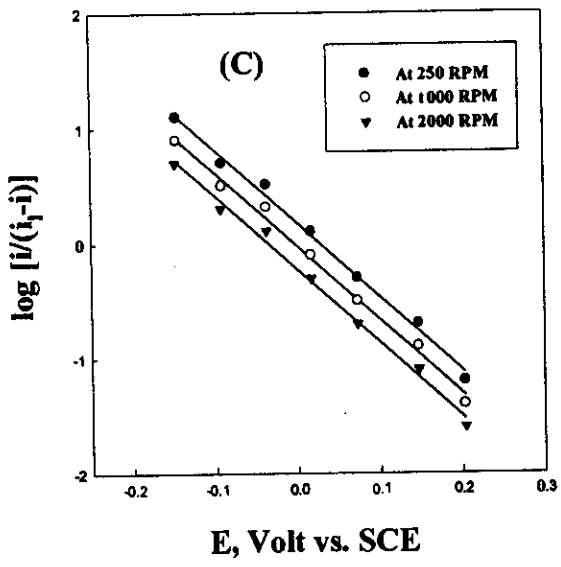

Figure 107: Logarithmic analysis of 1,2-naphthoquinone-4-sodium sulfonate in micellar solutions.

A- CTAB
B- AOT
C- C_{18}DMB

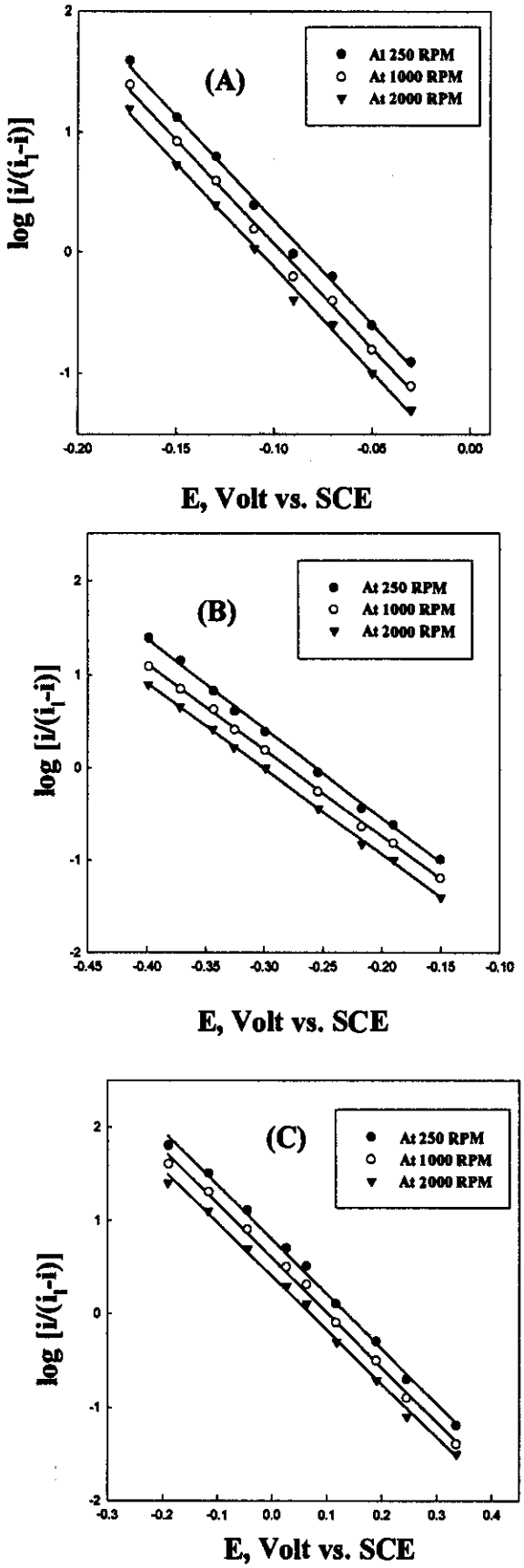

Figure 108: Logarithmic analysis of 1,2-naphthoquinone-4-sodium sulfonate in different microemulsion systems, a- CTAB, b- AOT and C_{18}DMB.

A- CTAB
B- AOT
C- C_{18}DMB

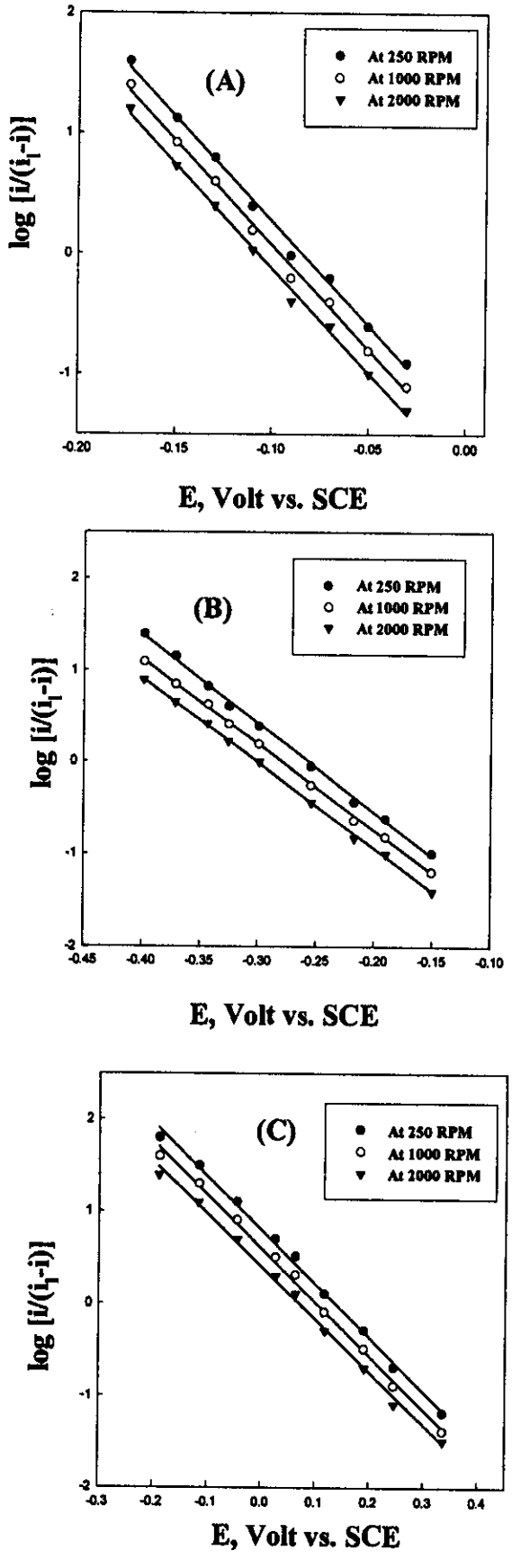

Figure 108: Logarithmic analysis of 1,2-naphthoquinone-4-sodium sulfonate in different microemulsion systems, a- CTAB, b- AOT and C_{18}DMB.

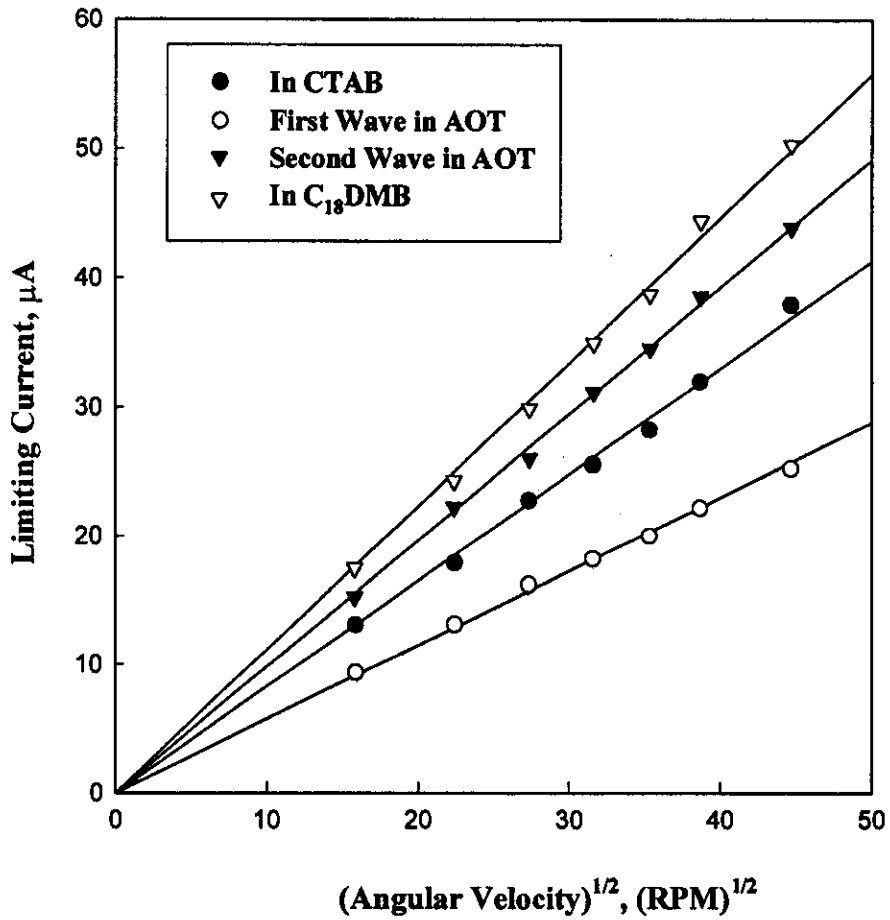

Figure 109: The plots of the limiting (i_l) versus square root of angular velocity ($\omega^{1/2}$) for 1,2-naphthoquinone-4-sodium sulfonate in differrent micellar solution.

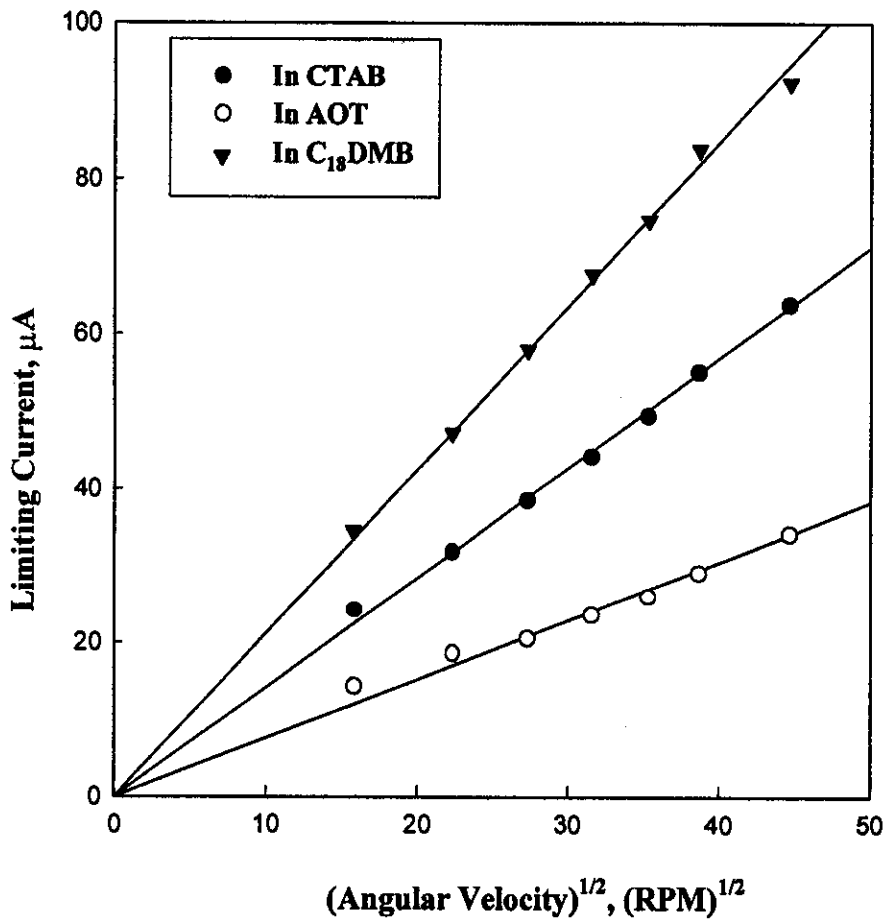

Figure 110: The plots of the limiting (i_l) versus square root of angular velocity ($\omega^{1/2}$) for 1,2-naphthoquinone-4-sodium sulfonate in microemulsion systems.

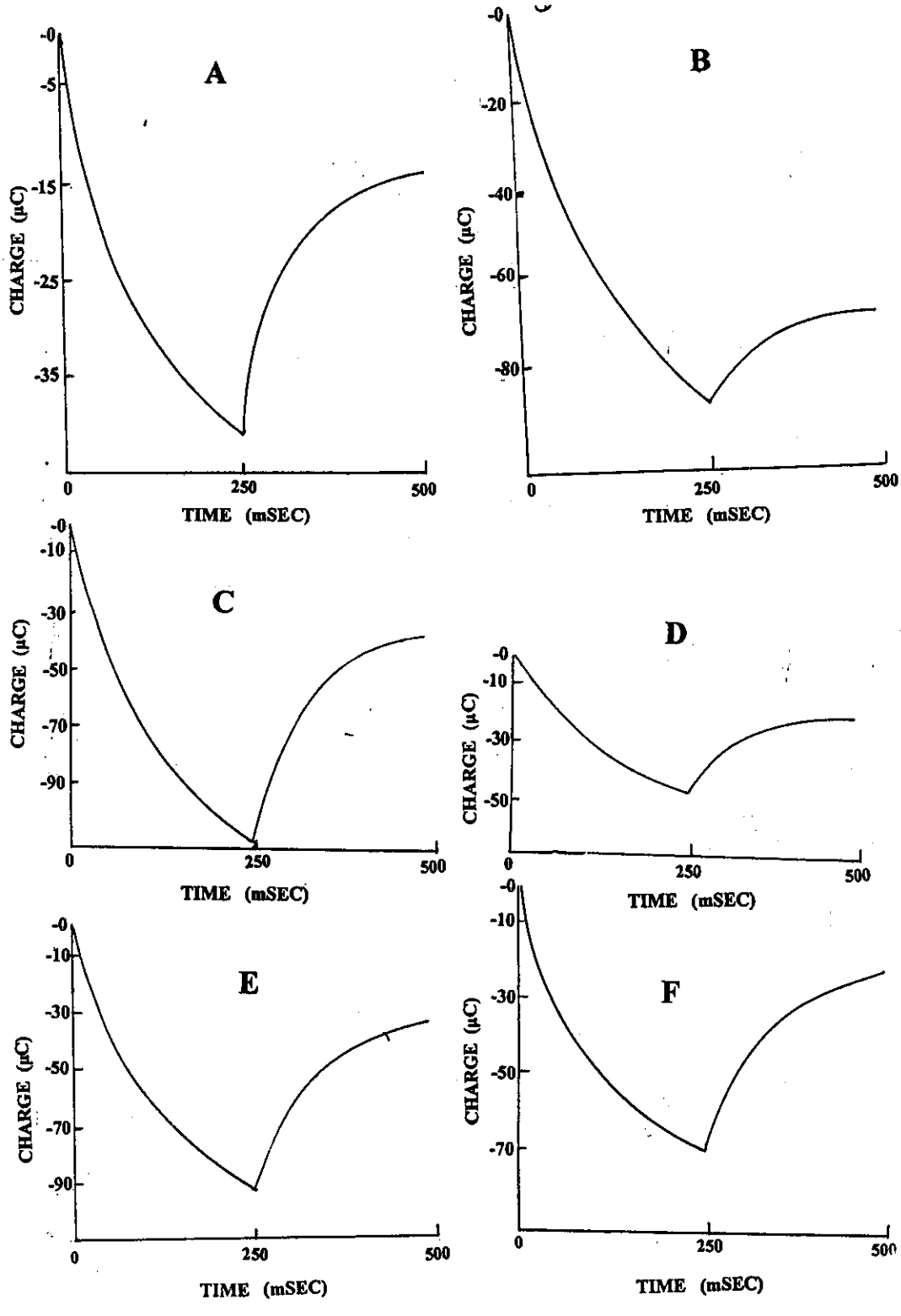

Figure 111: Chronocoulometric responses of 1,2-naphthoquinone-4-sodium sulfonate in different systems, (a) CTAB micellar solution, (b) CTAB microemulsion, (c) AOT micellar solution, (d) AOT microemulsion, (e) C_{18}DMB micellar solution, and (f) C_{18}DMB microemulsion.

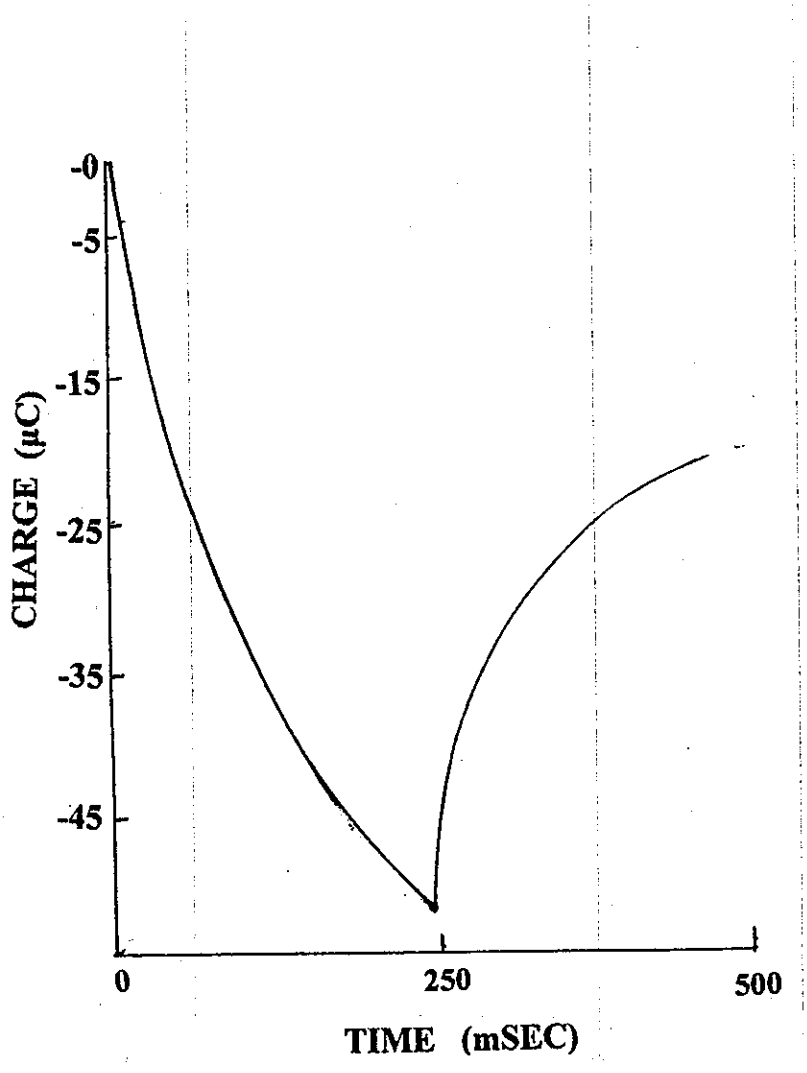

Figure 112: Chronocoulometric responses of 1,2-naphthoquinone-4-sodium sulfonate in pure aqueous solution. Charge versus time.

Table 49: Cyclic voltammetric data obtained for 1mM of 1,2-naphthoquinone-4-sodium sulfonate in pure aqueous media at 25°C.

Sweep Rate	$-E_{p,c}$	$-E_{p,a}$	$I_{p,c}$	$I_{p,a}$	$I_{p,a}/I_{p,c}$	ΔE_p
mV/sec	mV	mV	µA	µA	-	mV
20	214	46	8.75	6.75	0.771	168
50	214	46	15.20	12.50	0.822	168
80	214	44	21.25	18.25	0.858	170
100	214	44	23.75	22.00	0.926	170
150	214	43	30.00	27.50	0.916	171
200	217	43	33.75	32.50	0.962	174
500	226	34	58.75	56.30	0.958	192

Table 50: Cyclic voltammetric data obtained for 1mM of 1,2-naphthoquinone-4-sodium sulfonate in micellar solutions.

System	Sweep Rate	$-E_{p,c}$	$E_{p,a1}$	$E_{p,a2}$	$I_{p,c}$	$I_{p,a1}$	$I_{p,a2}$	$I_{p,a}/I_{p,c}$	ΔE_p
	mV/sec	mV	mV	mV	µA	µA	µA	-	mV
(A) CTAB Micellar Solution									
	20	80	-39	-	3.98	3.65	-	0.917	41
	50	90	-35	-	6.43	6.10	-	0.948	55
	80	88	-39	-	8.33	7.70	-	0.924	49
	100	86	-50	-	9.41	8.86	-	0.941	36
	150	86	-47	-	11.10	10.59	-	0.954	39
	200	86	-43	-	12.98	12.35	-	0.951	43
	500	82	-43	-	20.40	19.71	-	0.966	39
(B) AOT Micellar Solution									
	20	226	104	479	9.70	5.70	2.80	-	330
	50	227	104	479	12.85	8.57	4.28	-	331
	80	227	106	480	17.14	10.00	5.70	-	333
	100	226	106	480	20.00	11.42	7.14	-	332
	150	226	106	482	23.85	13.85	8.57	-	332
	200	228	108	482	27.14	17.14	10.00	-	336
	500	230	113	485	47.14	30.10	17.14	-	343
(C) C_{18}DMB Micellar Solution									
	20	44	186	-	9.10	7.60	-	0.835	230
	50	44	184	-	14.20	12.30	-	0.866	228
	80	42	184	-	18.50	16.80	-	0.896	228
	100	42	182	-	21.00	19.30	-	0.919	224
	150	42	180	-	25.26	23.10	-	0.914	222
	200	40	180	-	29.30	26.31	-	0.897	220
	500	71	175	-	46.80	44.60	-	0.952	246

Table 51: Cyclic voltammetric data obtained for 1mM of 1,2-naphthoquinone-4-sodium sulfonate in microemulsion systems.

System	Sweep Rate	$-E_{p,c1}$	$-E_{p,c2}$	$-E_{p,a1}$	$I_{p,c1}$	$I_{p,c2}$	$I_{p,a1}$	$I_{p,a}/I_{p,c}$	ΔE_p
	mV/sec	mV	mV	mV	µA	µA	µA	-	mV
(A) CTAB Microemulsion									
	20	126	-	87	5.17	-	4.53	0.876	39
	50	122	-	87	7.57	-	7.31	0.965	35
	80	122	-	82	9.67	-	8.87	0.917	40
	100	122	-	82	11.20	-	10.50	0.937	40
	150	122	-	74	13.17	-	12.50	0.949	48
	200	117	-	65	15.30	-	14.60	0.954	52
	500	117	-	61	24.86	-	23.93	0.962	56
(B) AOT Microemulsion									
	20	174	-	140	3.13	-	2.50	0.798	34
	50	174	-	140	4.37	-	3.75	0.858	34
	80	175	-	142	5.63	-	5.00	0.888	33
	100	175	-	144	6.25	-	5.63	0.900	31
	150	176	-	146	7.60	-	6.70	0.881	30
	200	176	-	146	8.98	-	7.70	0.851	30
	500	178	-	149	13.70	-	12.50	0.912	29
(C) C_{18}DMB Microemulsion									
	20	645	113	-276	9.47	7.30	5.90	-	-
	50	645	113	-276	11.60	11.98	10.20	-	-
	80	645	114	-276	14.70	14.98	13.98	-	-
	100	645	113	-278	15.78	17.30	15.98	-	-
	150	645	113	-279	18.90	22.40	18.98	-	-
	200	646	105	-280	20.00	25.21	22.30	-	-
	500	650	78	-285	31.50	42.10	36.98	-	-

Table 52: Diffusion coefficient values of reductant and oxidant species for 1,2-naphthoquinone-4-sodium sulfonate in different systems.

System	(CV)				(RDV)
	$D_{R1}x10^{-6}$ cm^2/sec	$D_{R2}x10^{-6}$ cm^2/sec	$D_{O1}x10^{-6}$ cm^2/sec	$D_{O2}x10^{-6}$ cm^2/sec	$Dx10^{-6}$ cm^2/sec
A- In Aqueous Solution					
	3.18	-	2.81	-	3.95
B- In CTAB Micellar Solution					
	0.36	-	0.37	-	0.33
C- In CTAB Microemulsion					
	0.45	-	0.37	-	0.77
D- In AOT Micellar Solution:					
	1.34	-	0.75	0.24	(0.19[a],0.43[b])
E- In AOT Microemulsion					
	0.13	-	0.17	-	0.29
F- In C_{18}DMB Micellar Solution					
	3.61[c]	-	3.80[c]	-	3.10[c]
G- In C_{18}DMB Microemulsion					
	0.13[c]	3.00[c]	2.46[c]	-	2.35

a,b- for first and second wave respectively.

c- Measured at 40°C.

Table 53: The half-wave potential for 1,2-naphthoquinone-4-sodium sulfonate in different systems.

System	$-E_{1/2}$(mV vs. SCE)	
	(CV)	(RDV)
A- In Aqueous Solution	129	124
B- In CTAB Micellar Solution	63	62
C- In CTAB Microemulsion	98	92
D- In AOT Micellar Solution	60	(3.6^b,436[c])
E- In AOT Microemulsion	159	264
F- In C_{18}DMB Micellar Solution	67[a]	27[a]
G-In C_{18}DMB Microemulsion	184[a]	-125[a]

b,c- for first and second wave respectively
a- Measured at 40°C.

Table 54: The slopes of the plots of log ($i/(i_l-i)$) versus E for 1,2-naphthoquinone-4-sodium sulfonate in differrent systems at 25°C.

System	Slope (V^{-1})
A- In Aqueous Solution	5.38
B- In CTAB Micellar Solution	14.32
C- In CTAB Microemulsion	17.31
D- In AOT Micellar Solution	(2.69[a],11.23[b])
E- In AOT Microemulsion	9.64
F- In C_{18}DMB Micellar Solution	6.40[c]
G-In C_{18}DMB Microemulsion	5.84[c]

a,b- For first and second wave respectively.

c- Measured at 40°C.

Table 55: Γ_o values obtained from chronocoulometric data of 1,2-naphthoquinone-4-sodium sulfonate in pure aqueous, micelles and microemulsion systems.

Systems	Γ_o **moles/cm^2**
(A) Pure Aqueous	2.08×10^{-9}
(B) CTAB Micelles	2.02×10^{-9}
(C) CTAB Microemulsion	5.92×10^{-9}
(D) AOT Micelles	8.61×10^{-9}
(E) AOT Microemulsion	2.20×10^{-9}
(F) C_{18}DMB Micelles	5.93×10^{-9}
(G) C_{18}DMB Microemulsion	3.85×10^{-9}

3.6.5 The electrode reaction mechanisms

The electrochemical behaviour of 1,4-naphthoquinone (1,4NAQ), 2-methyl-1,4-naphthoquinone (2-ME-1,4NAQ), 2-hydroxy-1,4-naphthoquinone (2-OH-1,4NAQ) and 1,2-naphthoquinone-sodium sulfonate (1,2NAQ) were recorded in micelles and microemulsion systems as well as pure aqueous solution. Three different surfactant types were used in this investigation. Cationic (cetyltrimethylammonium bromide, CTAB), anionic [bis(2-ethylhexyl) sulfosuccinate, AOT] and zwitterionic (octadecyldimethyl betaine, C_{18}DMB) model surfactants were used in this investigation.

From cyclic voltammetric studies of 1,4-naphthoquinone (1,4NAQ), only a single redox couple of peaks were observed on both the cathodic and anodic branches of sweep in micelles and microemulsion media as well as aqueous. Except in C_{18}DMB micelles it displayed two oxidation peaks of almost equal heights. The peak current ratio ($I_{p,a}/I_{p,c}$) is slightly less than unity in micelles and microemulsion systems. The voltammograms recorded at very small sweep rates showed peak potential separation ΔE_p (= $E_{p,c}$- $E_{p,a}$) is very close to 34 mV. While on increasing the sweep rate, the peak potential separation is increased from 34 to 263 mV. ΔE_p is around 90 mV in AOT microemulsion and 107 mV in AOT micelle and increased from 250 mV to 263 mV in C_{18}DMB microemulsion system, whereas, in CTAB microemulsion ΔE_p is increased up to 49 mV on increasing the sweep rate from 20 to 500 mV/sec but it is around 77 mV in CTAB micelle. These facts lead generally to the electrochemical-chemical-electrochemical (ECE) reaction nature, and the reduction of 1,4NAQ is quasi-reversible. The protonation of the anion radical generally leads to a disproportionation reaction [170,171]. Therefore the disproportionation reaction of the anionic free radical $1,4NAQ^{\cdot-}$ is favored by the decrease of the energy difference between $1,4NAQ^{\cdot-}$ and $1,4NAQ^{-}$due to hydrogen bond solvation of the carbonyl group by water molecules as

observed with anthraquinones [174,175]. The plots of the cathodic peak currents ($I_{p,c}$) as well as the anodic one ($I_{p,a}$) versus $\upsilon^{1/2}$ for 1,4-naphthoquinone (1,4NAQ) in micelles and microemulsion of different surfactant systems showed linear correlations almost passing through the origin. This behaviour confirming that the electrode reaction is mainly controlled by diffusion with slight adsorption contribution.

The cyclic voltammetric data of 2-methyl-1,4-naphthoquinone (2-ME-1,4NAQ) in pure aqueous and various surfactant systems are summarized in Tables (35-37). The peak potential separation ΔE_P ($\Delta E_P = E_{p,c} - E_{p,a}$) is very close to 30 mV at very small sweep rates in aqueous and in CTAB micellar solution. Since ΔE_P equal to 0.059/n V, the obtained data suggested that reduction of 2-methyl-1,4-naphthoquinone is chemically reversible with a net transfer of two electrons. In other media, the peak potential separation ΔE_P is increased from 113 to 258 mV, Table (36). These facts lead generally to the fact that the electrochemical-chemical-electrochemical (ECE) reaction nature. Protonation of the anion radical generally leads to a disproportionation reaction [170, 171]. The slightly smaller ΔE_P (30 mV) in CTAB micellar solutions compared to about 62 mV in microemulsions shows that the stabilization in microemulsion is less than in micellar solutions. This is because the electrostatic effects are generally less in microemulsions than in micellar solutions due to the decreased charge density on the surface of the microemulsion droplets compared to micelles.

The voltammograms of 1 mM of 2-hydroxy-1,4-naphthoquinone (2-OH-1,4NAQ) in micelles and microemulsion systems showed two cathodic peaks on the cathodic scan and two anodic peaks on the reverse scan. Whereas, except in C_{18}DMB micelles it displayed one redox peak, and in C_{18}DMB microemulsion it showed one oxidation and two reduction peaks. The voltammograms of 2-hydroxy-1,4-naphthoquinone in the corresponding pure aqueous solution containing only 0.10 M NaCl supporting electrolyte showed

a similar voltammetric response, two redox peaks. The voltammograms recorded at different sweep rates varying from 20 to 500 mV/sec are essentially similar displaying two redox peaks.

The cyclic voltammograms of 1mM of 1,2-naphthoquinone-sodium sulfonate (1,2NAQ) showed a single redox couple of peaks on the cathodic and anodic branches of sweep in all micelles and microemulsion media as well as in pure aqueous solution, except in AOT micelles it displayed two oxidation peaks of almost equal heights. Also, two reduction peaks were observed in C_{18}DMB microemulsion system. The anodic peak current, $I_{p,a}$ and the cathodic peak current, $I_{p,c}$ are slightly different as shown from Tables (49-51). The anodic to cathodic peak current ratios ($I_{p,a}/I_{p,c}$) does not exceed 0.966 in micelles and microemulsion systems. These results indicated the very weak adsorption on the electrode surface.

The rotating disk voltammograms recorded for naphthoquinones (1,4NAQ, 2-ME-1,4NAQ, 2-OH-1,4NAQ and 1,2NAQ) displayed one or two waves depending on the media and the nature of the substituents. Compounds displayed two peaks in cyclic voltammetric experiments showed two waves from rotating disk voltammetry. The voltammograms recorded at different angular velocity ranging from 250 to 2000 RPM showed a cathodic shift of half- wave potential ($E_{1/2}$) of almost about 20 mV. This behaviour confirmed that the electrode reaction process takes place completely reversible in CTAB systems and quasi-reversible in AOT and pure aqueous media. These results were found in a good agreement with those obtained from cyclic voltammetry.

Chronocoulometric studies of 1,4NAQ, 2-ME-1,4NAQ, 2-OH-1,4NAQ and 1,2NAQ were recorded in micellar solutions and microemulsion media as well as in pure aqueous solution. From chronocoulometric measurements the values of the amount of adsorbed reactant species on the electrode surface were found to be about 10^{-9} mole/cm^2 indicating a negligible adsorption on the electrode surface compared to the original solute concentration (1 mM).

Stabilizations of the free anion radical by cationic CTAB systems micelles and microemulsion was observed from the smaller peak potential separation, ΔE_P. And the predominant effect is attributed to electrostatic stabilizations of the product of the electron transfer process as observed from the same peak potential separation in both systems. Stabilizations of naphthoquinones in micelles and microemulsiopn systems takes place via hydrophobic effects as well as electrostatic effects for the reactants and products of the electron transfer process.

In view of the obtained results the electrode reaction mechanism of 1,4NAQ, 2-ME-1,4NAQ, 2-OH-1,4NAQ and 1,2NAQ at the glassy carbon electrode takes place via disproportionation reaction (equation 2.1) followed the first electron transfer. Cationic, anionic and zwitterionic surfactants affecting the disproportionation reaction to different extent as well as the effect of substituents. The proposed electrode reaction pathway of naphthoquinones could take place as following:

1.The electrode mechanism of 1,4-naphthoquinone (1,4NAQ)

$$1,4NAQ + e^- \Leftrightarrow 1,4NAQ^{-\cdot} \quad (1)$$

$$1,4NAQ^{-\cdot} + H^+ \Leftrightarrow 1,4NAQH^{\cdot} \quad (2)$$

$$2(1,4NAQ^{-\cdot}) + 2H^+ \Leftrightarrow 1,4NAQ + 1,4NAQH_2 \quad (2.1)$$

$$1,4NAQH^{-\cdot} + e^- \Leftrightarrow 1,4NAQH^- \quad (3)$$

$$1,4NAQH^- + H^+ \Leftrightarrow 1,4NAQH_2 \quad (4)$$

2.The electrode mechanism of 2-methyl-1,4-naphthoquinone (2-ME-1,4NAQ)

$$2\text{-ME-}1,4NAQ + e^- \Leftrightarrow 2\text{-ME-}1,4NAQ^{-\cdot} \quad (1)$$

$$2\text{-ME-}1,4NAQ^{-\cdot} + H^+ \Leftrightarrow 2\text{-ME-}1,4NAQH^{\cdot} \quad (2)$$

$$2(2\text{-ME-}1,4NAQ^{-\cdot}) + 2H^+ \Leftrightarrow 2\text{-ME-}1,4NAQ + 2\text{-ME-}1,4NAQH_2 \quad (2.1)$$

$$2\text{-ME-}1,4NAQH^{-\cdot} + e^- \Leftrightarrow 2\text{-ME-}1,4NAQH^- \quad (3)$$

$$2\text{-ME-1,4NAQH}^{\cdot} + H^{+} \Leftrightarrow 2\text{-ME-1,4NAQH}_2 \quad (4)$$

3.The electrode mechanism of 2-hydroxy-1,4-naphthoquinone (2-OH-1,4NAQ)

$$2\text{-OH-1,4NAQ} + e^{-} \Leftrightarrow 2\text{-OH-1,4NAQ}^{\cdot-} \quad (1)$$

$$2\text{-OH-1,4NAQ}^{\cdot-} + H^{+} \Leftrightarrow 2\text{-OH-1,4NAQH}^{\cdot} \quad (2)$$

$$2(2\text{-OH-1,4NAQ}^{\cdot-}) + 2H^{+} \Leftrightarrow 2\text{-OH-1,4NAQ} + 12\text{-OH-,4NAQH}_2 \quad (2.1)$$

$$2\text{-OH-1,4NAQH}^{\cdot} + e^{-} \Leftrightarrow 2\text{-OH-1,4NAQH}^{-} \quad (3)$$

$$2\text{-OH-1,4NAQH}^{-} + H^{+} \Leftrightarrow 2\text{-OH-1,4NAQH}_2 \quad (4)$$

4.The electrode mechanism of 1,2-naphthoquinone-sodium sulfonate (1,2NAQ)

$$1,2\text{NAQ} + e^{-} \Leftrightarrow 1,2\text{NAQ}^{\cdot-} \quad (1)$$

$$1,2\text{NAQ}^{\cdot-} + H^{+} \Leftrightarrow 1,2\text{NAQH}^{\cdot} \quad (2)$$

$$2(1,2\text{NAQ}^{\cdot-}) + 2H^{+} \Leftrightarrow 1,2\text{NAQ} + 1,2\text{NAQH}_2 \quad (2.1)$$

$$1,2\text{NAQH}^{\cdot} + e^{-} \Leftrightarrow 1,2\text{NAQH}^{-} \quad (3)$$

$$1,2\text{NAQH}^{-} + H^{+} \Leftrightarrow 1,2\text{NAQH}_2 \quad (4)$$